THE EFFECT OF COMBUSTION CHAMBER DEPOSITS ON HEAT TRANSFER AND COMBUSTION IN A HOMOGENEOUS CHARGE COMPRESSION IGNITION ENGINE

by

Orgun A. Güralp

A dissertation submitted in partial fulfillment
of the requirements for the degree of
Doctor of Philosophy
(Mechanical Engineering)
in The University of Michigan
2008

Doctoral Committee:

Professor Dionissios N. Assanis, Co-Chair
Associate Research Professor Zoran S. Filipi, Co-Chair
Professor Volker Sick
Professor James F. Driscoll
Tang-Wei Kuo, General Motors

Ailem ve askım icin

ACKNOWLEDGMENTS

I would first like to thank Prof. Zoran Filipi for all the help and guidance he has provided me in the last six years. His motivation and passion has served as an example which I have tried to follow. I would like to thank Prof. Dennis Assanis for granting me the opportunity to pursue my career goals and for the continued support he has provided for my work, as well as for what he has done to make the Autolab what it is today.

From the UM faculty, I would also like to thank Dr. George Lavoie, Prof. Volker Sick, Dr. Aristotelis Babajimopoulus, and Prof. James Driscoll. Without the help of the guys in the machine shop, Bill Kirkpatrick, John Mears, and Kent Pruss, who were always willing to drop anything to help, it would have been impossible to run the lab. Much thanks also to Kevin Morrison for his help in updating and maintaining the test cell.

I have endless thanks for the support provided by General Motors R&D Center. Tang-Wei Kuo has dedicated much of his time to provide invaluable technical support and guide the project scope, as well as help maintain a close relationship between our group and industry partner. I would also like to thank Paul Najt and Rod Rask for their continued support and assistance in this work, as well as the help provided by Nicole Wermuth.

I have to acknowledge Dr. Junseok Chang for all that he taught me during my first few years in the lab. He was my first direct mentor and taught me how to run the engine and perform proper testing. I thank Dr. Kukwon Cho and Mark Hoffman for the

assistance in this work also. I also want to thank all my friends and peers in the Autolab who have defined my experience at the University of Michigan.

Finally, the most appreciation goes to my family; Can and Ece Güralp, who have been the perfect parents, and my sisters, Çağla and Ayça. I thank Ata for being my best friend. And of course my wife Saadet, whom I met just as I began my time in Michigan and has been the most important thing in my life since.

TABLE OF CONTENTS

LIST OF FIGURES

LIST OF TABLES

LIST OF ABBREVIATIONS

A/F	Air to Fuel Ratio
ATAC	Active Thermo-Atmosphere Combustion
aTDC	After Top Dead Center
BC	Boundary Condition
BSN	Bosch Smoke Number
bTDC	Before Top Dead Center
CA	Crank Angle
CAD	Crank Angle Degree
CCD	Combustion Chamber Deposits
CFD	Computational Fluid Dynamics
CI	Compression Ignition
CIHC	Compression Ignition Homogeneous Charge
CoV	Coefficient of Variance
CP	Constant Pressure
CV	Constant Volume
DI	Direct Injection
DISI	Direct Injection Spark Ignition
GDI	Gasoline Direct Injection
EGR	Exhaust Gas Recirculation
EI	Emissions Index
EOI	End of Injection
EVC	Exhaust Valve Close
EVO	Exhaust Valve Open
FP	Fully Premixed
HC	Hydrocarbons
HCCI	Homogeneous Charge Compression Ignition
IC	Internal Combustion
ICE	Internal Combustion Engine
IMEP	Indicated Mean Effective Pressure
ISFC	Indicated Specific Fuel Consumption
IVC	Intake Valve Close
IVO	Intake Valve Open
LC	Lead Correction
LFE	Laminar Flow Element
LP	Limited Pressure
MFB	Mass Fraction Burn
MK	Modulated Kinetics
MON	Motor Octane Number
NMEP	Met Mean Effective Pressure
ORI	Octane Requirement Index

PCCI	Premixed Charge Compression Ignition
PCI	Premixed Compression Ignition
RON	Research Octane Number
RPM	Revolutions Per Minute
SCV	Swirl Control Valve
SI	Spark Ignition
SOI	Start of Injection
TC	Thermocouple
TDC	Top Dead Center
TS	Toyota-Soken
VVA	Variable Valve Acuation

ABSTRACT

Homogenous Charge Compression Ignition (HCCI) engines have the potential to achieve diesel-like fuel efficiency while virtually eliminating NOx and soot emissions. Realizing the full fuel economy potential of the gasoline HCCI engine hinges upon our ability to expand the operating range. Due to the strong dependence of HCCI combustion to in-cylinder thermal conditions, understanding the effects of changes in the thermal boundary of the combustion chamber is essential for addressing combustion stability and HCCI operating limits.

Combustion chamber deposits (CCD) are known to increase the propensity of a conventional spark-ignition engine to knock through an increase in local wall temperature, therefore it is expected they would affect the main combustion event in an HCCI engine. The objective of this work is to determine the effect of CCD on HCCI combustion. This requires a thorough understanding of the effects of deposits on heat transfer to the chamber walls.

This experimental investigation was performed using a gasoline fueled single cylinder research engine. Combustion analysis is performed based on in-cylinder pressure measurements and combustion chamber wall heat transfer effects are characterized through the use of fast response thermocouples.

Using these measurements, it was found that there is a clear relationship between instantaneous peak temperature phasing measured below the CCD layer and the layer thickness. Based on these findings, a methodology for calculating the thermal diffusivity of the deposit layer was developed, specific for HCCI engines. These measurements were also used to develop the Lead-Corrector method, which uses numerical finite-difference

based calculation of the deposit layer instantaneous surface temperature to give insight into the direct effects of CCD on chamber heat loss.

It was found that the effect of deposit formation was of a much greater magnitude on HCCI combustion than on standard combustion modes. Specifically, it was found that reduced heat loss during intake and compression resulted in earlier ignition timings while higher wall temperature swings during heat release resulted in shorter burn duration of the peripheral regions of the air/fuel charge. The heat storage effects of CCD cause the range of operability of HCCI combustion to shift downward in load value.

CHAPTER 1

INTRODUCTION AND MOTIVATION

Right now the world is facing a critical challenge related to the dependence on fossil fuels to meet global energy consumption requirements. More than 75% of world energy use is based on fossil fuels. More than half of that is supplied by oil, which is almost entirely used for transportation purposes. Furthermore, with the rate of increase in automotive use in developing countries, this consumption rate will increase up to 60% by the year 2020 [1]. Currently there are numerous avenues being investigated in an attempt to curb the use of oil through the overall increase in efficiency of vehicular powertrains in use today.

Homogeneous Charge Compression Ignition (HCCI) represents a new field in the study of internal combustion engines that has been growing at a tremendous rate in recent years and promises to be an important part of future gasoline engine technology. Currently only spark (SI) and compression (CI) ignited engines are in popular use among road-going vehicles but one major drawback of conventional SI engines is unfavorable efficiency at part-load. Consequently, technologies such as Direct Injection Spark Ignition (DISI) and HCCI hold a promise of significant efficiency improvements at low to mid-load are critical for the future of gasoline fueled engines. The main principle behind HCCI is that a homogeneous mixture of air and fuel is compressed until chamber conditions are favorable for auto-ignition. For a quick preview of HCCI, refer to Stanglmaier and Roberts [2]. Diesel-like efficiency is achieved thanks to un-throttled lean

operation with a higher effective compression ratio than with standard spark-ignited engines, while premixed lean combustion leads to low temperatures in the combustion chamber and very low NOx and soot formation.

However there are some significant obstacles facing the potential practical application of HCCI combustion. The primary challenges include the absence of a direct method to trigger auto-ignition and a limited range of operability. Initiation of combustion is dependent on thermo-kinetics thus it is very sensitive to air/fuel mixture preparation as well as in-cylinder thermal conditions. The same minimum thermal requirements limit low load operation utilizing HCCI combustion while homogeneous heat release leads to excessive pressure gradients which limit high load operation.

In light of the importance of thermal conditions to HCCI, consideration of the known influence of Combustion Chamber Deposits (CCD) on heat transfer drives the motivation for this work. The main goal of this investigation is to provide insight into the effect of CCD on combustion and heat transfer in an HCCI engine and to use that understanding towards improvement of the practical utilization of HCCI combustion.

1.1 Project Introduction

The main objective of this investigation is to fully understand the interactions of combustion chamber deposits with HCCI combustion and to determine if a greater understanding of the mechanisms by which CCD's affect on combustion can be utilized to further our ability to control an HCCI engine. Specifically, the effect of CCD on the HCCI operating range, performance, and emissions will be studied.

There is a large collection of work and references regarding HCCI, most of which has been produced within the last decade. Published work topics range from pure theoretical studies of the fundamentals of auto-ignition chemistry [3,4] to surveys into the practical application of an HCCI engine it an automobile [5]. There is also a separate but

quite substantial amount of work concerning internal combustion engine (ICE) deposits. It has been an issue ever since 4-stroke engines became the mainstream of power generation for cars and trucks, with published work dating back several decades [6]. But since HCCI is a relatively new field, there has been little to no research dedicated to addressing the interplay between deposit formation and their effect on HCCI combustion. One challenge of this work will be to relate known features of the effect of CCD on ICE's to HCCI combustion by making connections through other common threads. For instance, the significance of in-cylinder heat transfer to both topics cannot be overstated [7, 8].

This introductory chapter will start off with a review of the HCCI process, how it works, its benefits, and its downsides. This is then followed by a survey of relevant literature regarding HCCI and specific topics related to this work, including engine heat transfer. The second main section of this introductory chapter will cover combustion chamber deposits. A review of CCD formation mechanisms and the main effects on spark ignition and compression ignition (CI) engines will be provided. This will also be followed by a survey of related literature in critical topics such as thermal and physical properties and their effect on in-cylinder heat transfer.

1.2 HCCI Background

Homogeneous charge compression ignition has been a subject of research for more than 20 years. However, it's in the last 5-10 years that efforts at making it a viable option for automotive applications have really accelerated. The reason for this is the potential of HCCI combustion to solve, or at the least, ease many issues that the internal combustion engine has been facing in recent times, by combining the best features of CI and SI engines, in terms of efficiency and emissions.

For many years, spark-ignition gasoline and compression-ignition diesel engines have been the most commonly used source of propulsion for automotive use. Though they both work well, they also have downsides. With increasingly stringent emissions regulations worldwide and tightening fuel economy standards, improvements and alternatives to these power sources are being thoroughly investigated. In particular, it is critical to improve fuel efficiency of SI engines which are using the throttle for load control, and to address the NOx and particulate emissions challenge of diesel-type CI engines. There are only a few original alternatives, such as the fuel cell, but their first practical applications seem to be 10-15 years away and the viable solutions for economic production of hydrogen are yet to be seen. Hence, further development of the internal combustion engine concept and their integration with hybrid powertrains are a research priority. The utilization of HCCI is considered the main route in extending the usefulness of internal combustion engines.

1.2.1 HCCI Principle Overview

While SI gasoline engines are capable of high power density and low emissions (with 3-way catalyst), their fuel economy is relatively inferior, particularly at part load. Diesel (CI) engines are capable of higher thermal efficiencies than SI engines, but new emissions regulations on the horizon may soon pose a hurdle for expanding the use of these engines in the marketplace, particularly in regards to emissions of nitrous oxides (NO_x) and soot particulates. HCCI combustion serves as an alternative and/or supplement to the SI and CI combustion cycles promising to decrease the aforementioned NOx and soot emission challenges while maintaining the higher thermal efficiencies of the CI engine cycle.

Homogenous charge compression ignition operation can be viewed as a hybrid between spark-ignition and compression-ignition operation. However, care must be taken

in this view because, in actuality, HCCI is fundamentally different from either conventional form of combustion. In a pure HCCI engine, fuel is premixed with air during introduction into the combustion chamber, so that near the end of the compression stroke the chamber contents consist of a 'homogenous' mixture of fuel and air, just as in an SI engine. However this is where the similarities end. Unlike SI, where there is a spark to trigger ignition, and CI, where high pressure fuel is injected at a specific time late in compression, HCCI does not rely on a discrete event to control the onset of combustion. The initiation of combustion is controlled by chemical kinetics. Basically, ignition will occur once conditions in the combustion chamber are conducive to auto-ignition; these being mainly temperature, effective equivalence ratio, and degree of mixing [9]. In addition to not being able to directly control combustion initiation, the duration and rate of heat release are also controlled by air and fuel mixture conditions. HCCI is characterized by a rapid burn process in which all chamber contents react at almost the same moment, releasing heat relatively uniformly throughout the whole mixture, as described by Onishi et al. [10] and depicted in Figure 1.1.

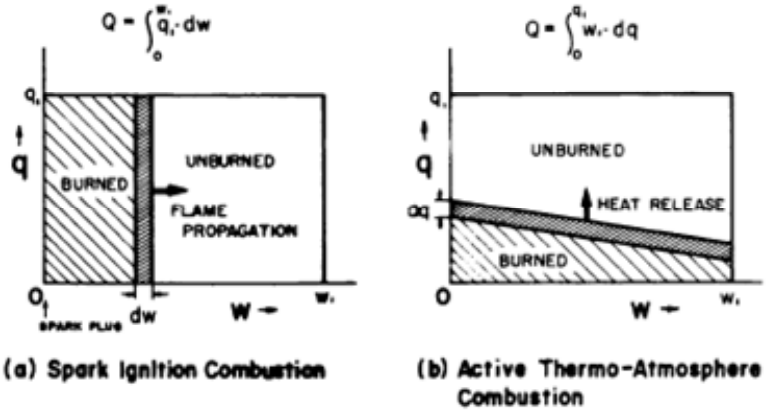

Figure 1.1 – Depiction of uniform heat release associated with HCCI-type combustion [10]

In practical terms, HCCI combustion is split into two general categories. 'Pure' HCCI relies on high, diesel-like compression ratios to auto-ignite lean air/fuel mixture, resulting in extremely short burn durations and high peak cylinder pressure [11]. While the more practical and widely used version of gasoline HCCI relies on more moderate compression ratios, like those in conventional SI engines, combined with high internal residual rates, used for the extra thermal energy to promote auto-ignition [12]. The high degree of residual retention is typically accomplished through negative valve overlap or exhaust re-induction (rebreathing).

There is another variation of HCCI, known as 'diesel HCCI', or 'premixed compression ignition' (PCI), among others, which is a form of compression ignition which relies on certain characteristics of auto-ignition combustion to control burn rates and improve emissions in engines using diesel-type fuel. This includes features such as early injection timings to enhance mixing and high residual rates to extend ignition delay. Since the work in this investigation is performed using gasoline fueled HCCI combustion, there will be minimal further reference to PCI combustion. For further information look to Ryan et al. [13], Takeda et al. [14], Suzuki et al. [15-17], Gray and Ryan [18], Mase et al. [19], Akagawa et al. [20], and Kalghatgi et al. [21].

Benefits of HCCI towards Efficiency and Emissions

There are a few apparent benefits to HCCI combustion, the main ones being increased thermal efficiency and lowered production of harmful emissions. Increased thermal efficiency from HCCI combustion is due to a few inherent characteristics. They are (1) the ability to operate without a throttle (2) the ability to operate at lean air/fuel ratios (3) the resemblance to constant volume combustion and (4) the potential for application of increased compression ratios.

Probably the greatest gains in efficiency are realized from HCCI's ability to operate without a throttle. Since spark ignition engines require stoichiometric mixtures, they must use a throttle to operate at part load conditions. This is simple and effective yet it results in significant pumping losses, which ultimately leads to a lower total net work for the cycle [22]. As already mentioned, HCCI is capable of operating at lean air-fuel ratios. In order to reduce work output of the engine for part load conditions, it is a simple matter of adding less fuel mass per cycle, much like a diesel fueled CI engine. This way the mixture equivalence ratio and thus the load is controlled by the injected fuel quantity. Since there is no throttling of the intake air required, there are no pumping losses. Net work output does not suffer and so fuel efficiency will benefit, particularly at low and mid load. Figure 1.2 is a comparison of measured cylinder pressure for premixed SI, stratified late-injection SI, and premixed HCCI combustion. It is clear from the plot that throttled operation significantly hurts net work output.

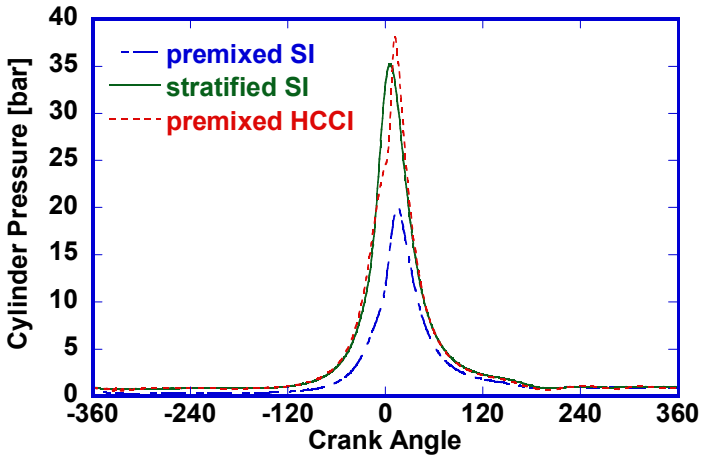

	Fueling rate [mg/cycle]	PMEP [kPa]	EI NO [g/kg]	Thermal Efficiency
Premixed SI	12.3	60.6	19.3	30.9 %
Stratified SI	11.0	16.3	32.2	36.6 %
Premixed HCCI	11.0	13.4	1.4	41.0 %

Figure 1.2 – Comparison of cylinder pressure for premixed SI, stratified SI, and premixed HCCI combustion

The ability to operate with lean air-fuel ratios also results in improved thermal efficiency because of lower overall combustion gas temperatures and thus higher ratio of gas specific heats. Spark ignition engines, whether premixed or stratified, rely on a stoichiometric mixture near the spark plug electrode in order for ignition to occur. But since HCCI combustion is initiated by auto-ignition there is no requirement for stoichiometric mixtures at any time or locale in the chamber. The potential for auto-ignition to occur, or the 'burning limits', is decided by a few other parameters that are a function of the preparation of the air/ fuel mixture, the dominating two being temperature and species concentration, as outlined by Najt and Foster [23]. Taking into consideration all the different parameters of operation, such as EGR rates, compression ratio, intake

temperature, equivalence ratio, and fuel type, they all will have some form of influence on charge temperature and species concentration, and thus the chemical kinetics of the process [10,24-28]. This ability to operate lean is what leads to improved thermal efficiencies in comparison to that of typical SI operation.

The third characteristic of HCCI combustion that provides means of increased thermal efficiency is the high rate of heat release. Typically thermodynamic analysis of a spark ignition engine cycle is based on the constant volume (CV) approximation for heat release. Specifically this means that all of the heat that is to be added in the form of fuel is added instantaneously at top dead center (TDC). However in a real SI engine, combustion usually takes up to 40-60 crank angle degrees (CAD) for 10-90% combustion duration [29]. These figures also apply to CI engines, whose profiles of heat release more closely match a constant pressure (CP) or limited-pressure (LP) approximation. In either case the actual duration of heat release is much longer for SI or CI combustion then it is typical for HCCI. As depicted in Figure 1.3, from a comparison of two similar load points taken for SI and HCCI combustion in the same engine, the equivalent period for HCCI can last on the order of only 10-15 CAD. This equates to a substantially higher rate of heat release and is much closer to the CV approximation then either of the standard combustion modes. This form of the pressure-volume relationship additionally contributes to the gains in fuel conversion efficiency that HCCI is capable of.

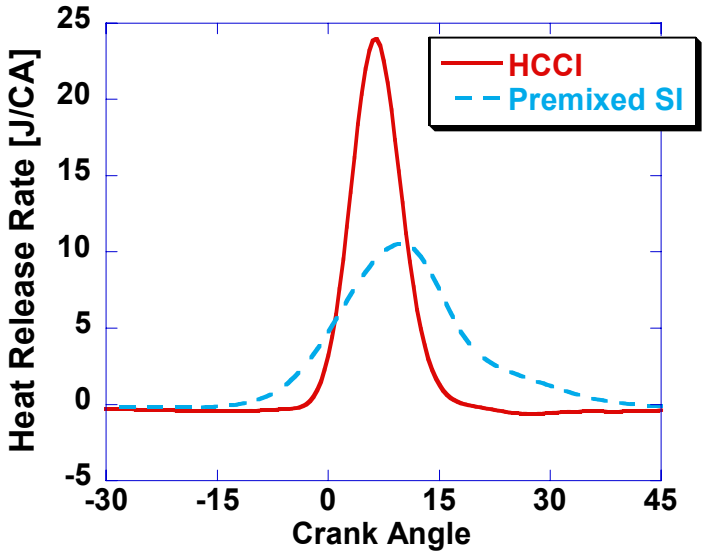

Figure 1.3 – A comparison of representative heat release rates comparing premixed spark-ignition to homogeneous charge compression ignition combustion taken from the same engine

It is commonly known that increased compression ratio results in increased thermal efficiency. However the limit of maximum operable compression ratio is probably the largest obstacle concerning the fuel efficiency of an SI engine. The potential for spark-knock sets an upper limit to compression ratios that a gasoline engine can safely operate at, so they are typically limited to ratios of about 10:1-12:1. This is fundamentally due to the minimum time it takes for flame propagation to complete the path from the spark plug to the end gas region, before the onset of auto-ignition. But because HCCI has no real 'flame', ignition occurs at multiple sites in the chamber simultaneously and the burn is completed almost homogeneously in a very short relative time-span. So HCCI engine operation can be viewed as "controlled knock". In fact, a high compression ratio is beneficial in ensuring favorable thermal conditions in the combustion chamber close to TDC compression.

In addition to the gains in efficiency that are realized with HCCI combustion, there are great benefits in regards to emissions. Specifically, there are much reduced amounts of both NO_x and particulate emissions [30-32].

Since SI engines operate at stoichiometric air/fuel ratios, combustion temperatures are typically high. The formation of NO_x emissions are a function of the temperature controlled Zeldovich mechanism, nitrous oxide emissions will thus be high [33]. Since HCCI is intended to be run at lean air to fuel ratios, overall combustion temperatures are lower. Additionally, the air/fuel mixture is homogenously prepared, so there are no ultra-rich regions of fuel due to mixture stratification. Because of this, NOx formation from HCCI is essentially non-existent, as outlined by Christensen et al. [34]. The homogenous mixture also stops the formation of soot particulates from being formed, another characteristic of CI, particularly under higher load conditions [35].

Downsides of HCCI

In addition to significant benefits of the HCCI concept, there are also some inherent problems. These problems create major research challenges that have to be addressed in order to make HCCI a more viable option for production engine use. The major issues are control of combustion timing, emissions, and range of load operability, which in particular will be a focus of the work in this investigation.

The very nature of HCCI presents a problem in regards to control of the combustion process. As mentioned earlier, there is no discrete event which triggers the initiation of combustion. The auto-ignition of combustion is controlled by the chemical kinetics of the air/fuel mixture, along the guidelines of the three main temperature regimes for hydrocarbon oxidation, as outlined by Najt and Foster [23] and Zheng et al. [36]. Auto-ignition can occur only if the right proportions of air and fuel are present, and there is enough thermal energy present in the mixture at the right time.

There are numerous methods which are used to provide the required energy for combustion, some of which include increasing compression ratio, intake charge heating, and extra amounts of internal residual [37,38]. There are a few methods which have been tried to accurately control residual; Allen and Law [39] outline the application of some of them attainable using VVA technology. It is also important to mention that a greater understanding of the thermal environment is a definite pre-requisite for better control of the combustion process, and that is one of the main motivating factors for this investigation.

The lean operation of HCCI, which allows its high levels of thermal efficiency, also leads to higher hydrocarbon (HC) and carbon monoxide (CO) emissions. Because of overall lower flame temperatures in the chamber, bulk quenching from heat transfer to the walls can cause combustion efficiency to suffer [10,11,40,]. A characteristic of lower overall core gas temperatures is that thermal boundary layer thicknesses are much greater, so there is now a greater area close to the surface in which incomplete oxidation of hydrocarbon fuels is likely. This means that HC and CO emissions from an HCCI operated engine tend to be higher than in a conventionally operated SI engine.

Probably the most critical obstacle facing HCCI combustion is its limited range of operability. Reliable and safe operation has only been possible at lower to medium load levels [11]. There are a few main reasons for this. Because the whole fuel/air mixture burns ‘simultaneously’, HCCI combustion is associated with shorter burn durations and rapid pressure rise rates [41-43]. These can easily reach knock-like levels at loads that would be considered mid-range for other combustion modes [44]. In order to prevent potentially destructive operation and excess noise, operation must be limited to medium loads. At the other end of the spectrum, extremely low loads can be problematic as well. Because of the thermal energy requirements for promotion of auto-ignition, the use of extra amounts of residual is common. As loads decrease, less fueling is required and the overall thermal state of the chamber is lowered. This combined with high rates of exhaust

recirculation acting as a diluent will likely lead to unstable operation and eventually to a misfire condition [45]. This results in a low flammability limit that is too high to allow idle operation. A pair of 'maps' of these operability limits are shown below as depicted by Noguchi [24] and Zhao et al. [46].

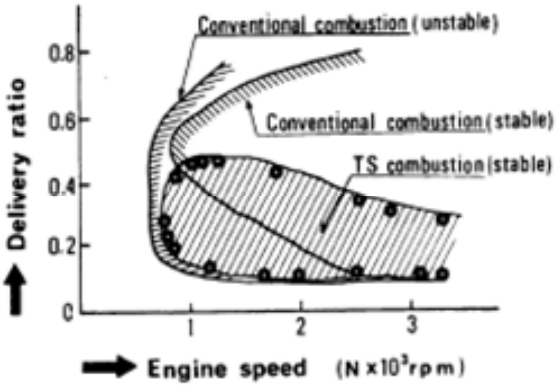

Figure 1.4 – Noguchi et al. are the first to describe the comparative range of speed-load operability possible with 'TS Combustion', in a 2-stoke engine [24]

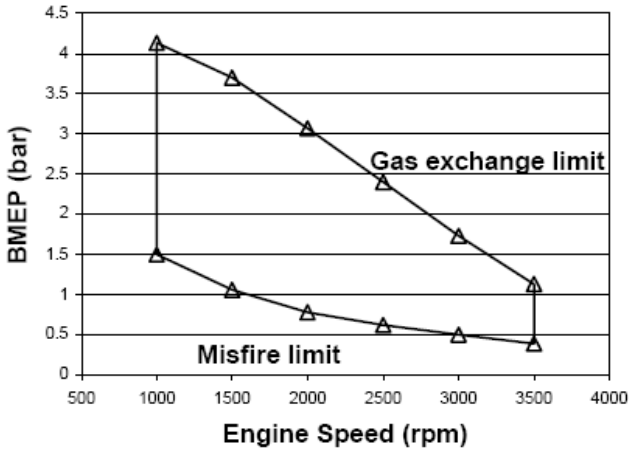

Figure 1.5 – Zhao et al. explored the limits of HCCI operability [46]

This limited operability range is currently the main deterrent for applying HCCI to production vehicles. As listed above there are many benefits to using the HCCI concept, but if it can only be applied to a small part of the driving cycle, then its impact on vehicle fuel economy is diminished. Most likely, if it is applied to an automotive engine, it would be combined with another combustion mode, such as direct injection spark ignition (DISI) gasoline, in a 'dual-mode' engine. HCCI would be utilized during mid-load operation and then engine operation would switch over to DISI at idle and high load. Nonetheless, the further the limits of operability can be extended, the greater the benefits to efficiency and emissions can be taken advantage of. Furthermore, the challenges presented by mode transitions between SI and HCCI are reduced. It is the goal of this investigation to provide insight which will help to extend these limits, specifically the low load limit.

1.2.2 Survey of HCCI Research

There has been a considerable amount of work done concerning HCCI as a potential new technology for internal combustion engines. Early focus was on understanding the fundamental characteristics and mechanisms most important for HCCI. The fundamental advantages of the concept were confirmed and the challenges defined. The field is maturing and issues critical for future practical application of HCCI are moving to the center stage. This includes control of the combustion event and expansion of the HCCI range. Some of this work has been outlined below. Additionally, since it is the most relevant to the subject matter of the forthcoming work, the importance of heat transfer to HCCI is discussed as well.

Initial Investigations into HCCI

The earliest instances of experimentally operating under auto-ignition combustion were accomplished on 2-stroke engines. Noguchi et al. [24] began with attempts to find methods of increasing the efficiency and decreasing HC emissions of a 2-stroke engine, especially at part load conditions, and it turned into the realization of a new operating regime. They called this self-ignited combustion, "TS (Toyota-Soken) combustion". The main findings include the existence of numerous self-ignition sites with reactions spreading rapidly in all directions, different than that of a single propagating flame in SI combustion. In a study of the detection of radicals throughout the cycle, it was found consistently that the formation of CHO, HO_2, and O preceded ignition and served as 'ignition kernels' for TS combustion. This was immediately followed by the production of the OH, hydroxyl radical. This is contrary to a typical SI engine in which existence of all the radicals can be detected simultaneously in the flame front.

Onishi et al. [10] described their new lean 2-stroke combustion process as "Active Thermo-Atmosphere Combustion" (ATAC). They also recorded an increase in efficiency and reduced exhaust emissions in their experimental 2-stroke engine. This was accompanied by smooth, relatively quite combustion. It had stable cycle-to-cycle operation and operated without the use of a sparkplug. In their experiments they also found that reactions begin from several different points and occur simultaneously. Some important factors that must be considered for proper operation are the homogeneity of the air/fuel mixture in the cylinder, the proper control of residual gases, and adequate temperature in the combustion chamber.

Najt and Foster [23], at the University of Wisconsin, performed pioneering experimental testing using a 4-stroke engine operating in 'CIHC' combustion. Part of their goal was to understand the chemical kinetics involved in the onset of combustion, with some focus on characterization of heat release rates. They confirmed that chemical

kinetics was the driving mechanism behind HCCI combustion, mostly affected by charge temperature and species concentrations. Parameters such as compression ratio, equivalence ratio, engine speed, EGR, and fuel type all affect the required 'ignition energy'. EGR was found to have a two-fold influence. In addition to increasing the intake charge temperature, it increases the concentration of active reaction sites. They also found that the ignition process could be broken down into two main temperature regimes. There is a low temperature (<950K) ignition process where fuel reacts with oxygen molecules from air, and the high temperature (>1000) energy release process where the reaction is characterized by the thermal breakdown of fuel.

Thring [45], at the Southwest Research Institute, focused his work on investigating what operable regimes would be useful and possible for HCCI operation to be effective. He found that for stable operation, relatively high amounts of EGR and high intake temperatures were required. As far as limits of operability, three 'boundaries' were found. The misfire limit occurred with excessively lean mixtures or high EGR, the power limit was reached with excessively rich mixtures and high EGR, and the knock limit was reached when combustion consisted of severely high heat release rates – high load and high F/A ratio. These limits are depicted in Figure 1.6.

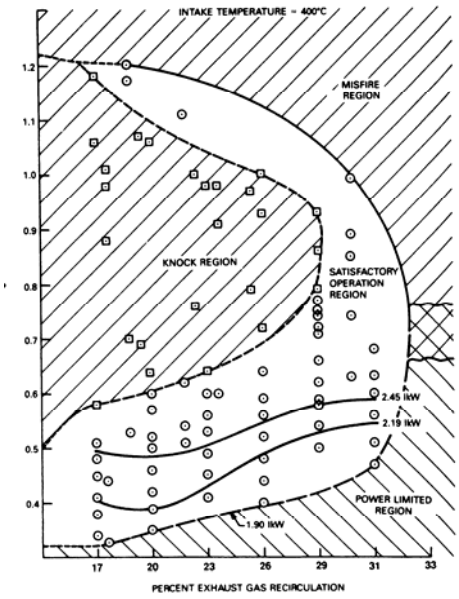

Figure 1.6 – A plot depicting the operational limits of stable HCCI combustion [45]

A group from Lund, which has since provided a continuous stream of HCCI related papers, documented a study to visualize the combustion process in an HCCI operated engine [47]. Their main focus was to understand the flame structure and its behavior. Their major conclusion, which supports findings discussed previously, was that the combustion process consisted of two halves, the first being a cool flame which precedes the main heat release. Though this only applies when certain fuels are used, specifically n-heptane, or 'diesel-like' fuels. This does not apply to gasoline or similar fuels, such as iso-octane.

Challenges Related to Practical Application of HCCI

There have since been several studies that show that increasingly more groups are investigating HCCI as a viable option for possible future use. Some of them, such as Toyota [30], looked into the possible benefits of Premixed-Charge Compression Ignition (PCCI) and found the low NOx emission benefits and ability to run lean operating points

in order to achieve higher thermal efficiencies. In trying to understand the combustion mechanism through shadow imagery of the event, it was concluded that there are multiple ignition sites and no propagating flame. Also confirming previous findings by others, a study on the effect of intake air heating was performed and it was found that elevated intake temperatures managed to extend the lean limit of combustion while also advancing the phasing and increasing the maximum gas temperatures and thus NOx emissions.

Ryan et al. [13] also studied the operational range of HCCI while comparing its performance to conventional engines. HCCI solves CI engines' problems of NOx emissions while not increasing particulates. Because of the lack of a propagating flame, compression ratio limiting knock is not an issue, permitting the potential for increased efficiency. Of additional interest are empirical correlations that were devised to predict ignition delay, based indirectly on parameters such as EGR, equivalence ratio, and intake temperature. It was determined that EGR had the greatest effect on the beginning of ignition and this effect was primarily thermal and not as a diluent. Christensen et al. [40] published further work regarding the operable range and limits of HCCI and the practicality of its usefulness.

Many have looked into the effects of the use of different fuels for combustion, such as described by Pucher et al. [48]. This work includes information on what the current operating regimes of HCCI are and how they can be extended through the use of EGR and other fuels such as methanol. Others work regarding different fuels include Christensen et al. [40], Chen et al. [49], Aroonsrisopon et al. [50], Shibata et al. [51], and Kalghatgi [52].

Christensen et al. [53] also tried to increase the performance potential of HCCI while avoiding its potentially inherent destructively severe pressure rises by forced induction. It was found that supercharging at different rates effectively increases IMEP, if inlet air temperature is adjusted accordingly in such a way that less is required at higher boost. It was also found, with regards to different fuels, that the lower the octane rating,

the more difficult it was to control ignition delay. In fact, it depended more on this then on air to fuel ratio, which had a greater influence on combustion rates than anything else. As far as emissions, an attempt was made to separate the influence of crevice flow and bulk quenching on hydrocarbon production. This was successfully done using two different compression ratios.

There has also been work done to understand charge control in order to better control the auto-ignition process. Christensen and Johansson [54] compared a piston with a square bowl and high squish area to a flat piston in order to study the effect of high turbulence levels on HCCI combustion. They found that heat release was delayed and the duration extended with the square bowl piston. This was attributed to factors including changes in heat transfer, combustion efficiency, and in-cylinder residual rates. Flowers et al. [55] found that in-cylinder fuel stratification leading up to ignition resulted in increased heat release rates, indicating the process was dictated by the higher equivalence ratio and temperature regions. They also found that HC and CO emissions were reduced with stratification and that up to a point, NOx emissions where increased, as would be expected.

Finally, to mention a few alternative uses for HCCI, Mitsubishi, one of the pioneers of Gasoline Direct Injection (GDI) technology, came up with their version of HCCI they called ’Pre-mixed Compression-Ignited Combustion’ or PCI for use with diesel fuel [56]. Some of their studies focused on decreasing the high amounts of hydrocarbon emissions usually associated with HCCI. There was work done on post oxidizing catalyst and a detailed study of different injector nozzle configurations and their effect. Hydrocarbon production was substantially effected by such things as the degree of fuel jet spray penetration, possible impingement, and dispersion throughout the air charge. Sandia National Laboratories tried a different application of HCCI then as a power source for an automobile [57]. They used a double ended free piston with a linear

alternator to generate electricity. They claimed that under homogenous charge compression ignition they achieved thermal efficiencies of up to 56%.

HCCI and Heat Transfer

The premise for this investigation is that in-cylinder heat transfer has a tremendous influence on HCCI combustion performance. This point is exemplified by what is depicted in Figure 1.7 below; a plot of HCCI heat release rates for varying coolant temperatures. Only 15°C produces a very tangible change in the burn rate. Regardless of the mechanism, any insight into the relationship between chamber thermal conditions and combustion are of great importance.

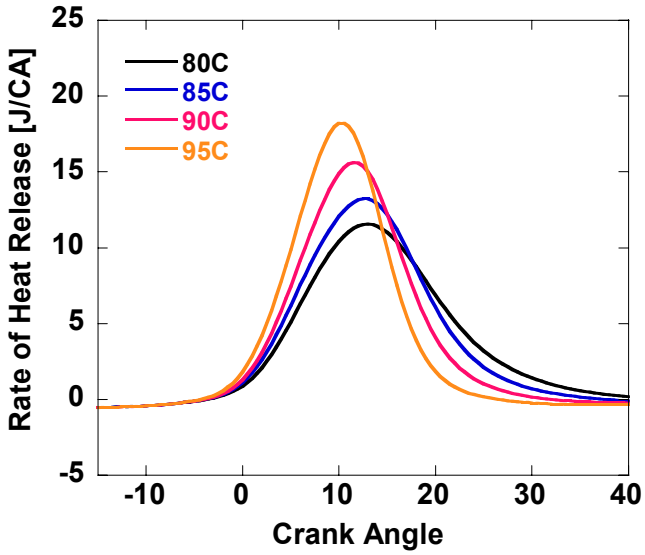

Figure 1.7 – HCCI heat release rate versus coolant temperature

Sjöberg and Dec [11] performed experimental testing, supported by computational work, for the purpose of using thermal effects to tame the high heat release rates associated with 'pure' HCCI combustion. Simply retarding combustion is not an ideal option because combustion stability deteriorates the farther into the expansion stroke heat release occurs. It was found that as load (fueling rate) was increased the

engine's sensitivity to combustion phasing was diminished. This is because of higher average wall temperatures, associated with higher loads, having a greater influence on the progression of reactions than the conditions leading up to ignition. It was also found that HCCI combustion was so sensitive to thermal conditions that a natural instability is introduced based on cycle-to-cycle changes in wall temperature. If one cycle burns early than the higher peak heat release rates for that cycle will increase wall temperatures causing the next cycle to burn earlier as well. The opposite holds true for a retarded cycle, which causes a decrease in wall temperature which is proliferated in the next cycle and so on. The main conclusion of their work was that heat release rates could be tamed by promoting thermal stratification of the chamber contents through decreased coolant temperature and increased levels of swirl; with only a small decrease in thermal efficiency with no loss in combustion stability. The greatest benefit of this smoothing of peak heat release rates is that higher loads can be achieved for a given engine under HCCI operation.

Kong et al. [25], at the University of Wisconsin, looked in depth at the actual combustion mechanism, through the use of computational fluid dynamics, by assigning time constants to the different mechanisms that could possibly affect combustion rates. These included a laminar characteristic time, a turbulent one, and an ignition time. They decided that combustion was controlled by chemical kinetics up to the point of ignition, after which it is controlled by turbulent mixing and it was this addition of the turbulence effect that set this work apart. As far as temperature effects, it was determined that higher inlet temperatures triggered ignition earlier but also leads to higher heat flux which also delays ignition. So these two effects are always competing with each other. It was added that increasing turbulence through a shrouded valve delayed ignition because of increased heat flux. The same conclusion was reached in regards to the level of swirl and its effect on ignition. While the indirect effect of turbulence through heat transfer seems to be very

plausible, the more direct effect suggested remains controversial and is a subject matter vigorously debated today.

Christensen et al. also looked into the possible use of water injection to curb NOx emissions [34]. It was found that water can be used to delay the phasing of ignition and combustion much like using lower intake temperatures does, by increasing the thermal capacity of the intake charge during compression. However, due to a decrease in combustion efficiency from the resulting low temperature and lean mixture, any possible gains in indicated efficiency were lost. They also devised a well thought out investigation on EGR and how it affects heat release phasing and rates [41]. While the typical intent of adding recycled exhaust gas is to lower combustion temperatures by diluting the intake mixture, which it does in HCCI operation by curbing combustion rates and limiting excessive pressure rise rates, it can serve another purpose. Exhaust gas is at an elevated temperature and when added to the intake as in-cylinder residual, it can raise the overall temperature leading the way to accelerating the rates of chemical reactions which are highly temperature dependent.

Chang [58] performed a focused investigation on characterization of heat transfer mechanisms and trends in a single-cylinder HCCI engine. Using head and piston surface fast response thermocouples, the effect on local heat transfer was examined and compared to combustion performance and emissions. This was performed rigorously for different tests, comparing the effects of several operating parameters, such as engine speed, equivalence ratio, load, intake air temperature, in-cylinder swirl, and injection timing. Based on these results it was shown that for premixed operation cases there was a small enough variance in local heat flux that a correlation for global heat transfer could be developed. This was done based on the previously developed modified Woschni correlation.

1.3 Combustion Chamber Deposits Background

'Deposits' can include any number of materials, excess, or residue that is gradually grown or accumulated on critical parts of an internal combustion engine. The three main varieties of engine deposits are mainly categorized according to their location in the engine [59]. They are the fuel system, which includes carburetors and fuel injectors, the intake system, which includes the intake ports and manifold, and the combustion chamber. In all three cases the composition and then subsequent effect that the deposit has on the operation of an engine can vary greatly in many different aspects. The focus of this work is on combustion chamber deposits (CCD) because these have the most direct influence on combustion and emissions formation. Also, the problems of fuel injector and intake port deposits are already better understood and controllable through the use of fuel additives and proper engine component design. The next sections will cover a general overview of CCD: its formation and effects, the strong relationship between CCD and heat transfer, and finally a prelude to the potential effects of deposits on HCCI combustion.

1.3.1 CCD Overview

There has been considerable work done in the field of conventional internal combustion engines regarding deposits. For a quick review on general subject matter related to engine deposits, not just those inside the combustion chamber see Kalghatgi [59]. The next subsections provide a review of some issues which may be directly related to objectives of this work.

Formation Parameters of Combustion Chamber Deposits

In general terms, combustion chamber deposits are formed from the condensation of fuel (or oil) on the surface. As expected, gas and surface temperature and fuel

composition are very influential in dictating the rate and type of CCD formation. The source of this fuel can vary. It can be left-over unburned fuel following combustion, extra fuel mass escaping from chamber crevice volumes, or it could be accumulated from direct injection fuel spray plumes, as in a diesel CI or a gasoline DISI engine.

Probably the most important factor to consider when tracking the growth patterns of CCD are chamber surface temperatures, as confirmed and outlined by Cheng [8]. Deposit growth is promoted at lower temperatures. As the surface temperature is increased, deposit growth rates decrease up to a critical temperature of about 310 °C, above which no deposits will form. It was found that the most effective way to control CCD growth was by varying coolant temperature, and thus the metal wall surface temperature. Furthermore, it was found that depending on the range of surface temperatures in which the deposits were formed, the physical characteristics varied; dark and sooty for low temperatures and hard, thin, and lighter colored for high temperatures.

Nakic et al. [60] confirmed the strong dependence on surface temperature as well as the critical temperature leading to termination of CCD formation. This was done by using ceramic caps of varying thickness attached to a piston crown to change the effective surface temperature and track CCD growth rates with in-piston fast-response thermocouples. Secondarily, the effect of different types of fuels on CCD formation was studied. They found that, regarding the type of hydrocarbon molecules, the boiling point of the fuel was a good indicator for its tendency to result in deposit formation. Because of a greater chance of condensation, higher boiling point fuels, like aromatics (toluene and xylene) led to greater rates of formation then lower boiling point fuels like iso-octane, which is a saturated paraffin.

Kalghatgi et al. [61] outlined the gradual process of CCD formation evolution in a combustion chamber, based on changing wall temperatures. When the chamber is clean CCD formation is the fastest and directly dictated by combustion parameters and their effect on wall surface thermal conditions. As deposits grow they act as a thermal

insulator, decreasing the rate of local heat flux. This in turn increases chamber surface temperatures which are now effectively the surface of the deposit material. But as the surface temperatures increase, deposit growth rates decrease. Eventually, an equilibrium corresponding with the previously mentioned critical surface temperature is reached, and deposits no longer grow.

Cheng [62] extended knowledge of CCD formation tendencies by performing an exhaustive investigation into the effect of varying different operating parameters for a direct injection SI engine on the rate and types of deposit formation. While surface temperature is still the main parameter, it is shown how factors such as spark timing, equivalence ratio, and fuel type are important. It is argued that the most important thing to consider for these factors is how they in turn affect surface temperatures. In addition, some interesting points are made regarding direct injection gasoline engines and mixture formation peculiarities. Depending on the nature of the fuel spray into the chamber, deposit material can be cleaned from some surfaces while accelerated growth can be seen in others because of lean operation modes resulting in lower overall combustion temperatures, promoting fuel condensation.

The Effect of CCD on Combustion in SI and CI engines

As shown in the previous sub-section, deposits have a significant effect on heat transfer in the chamber. However understanding the details of how this effect varies under different modes of combustion, for example SI versus CI versus HCCI, and then how it varies further at different operating conditions has proven to be a challenge. This is primarily because in addition to the thermal effect of CCD on combustion, in many instances there is potential for an additional physical influence as well due to absorption of fuel or gases in porosities, etc. This is especially true in diesel engines where there is a potential for fuel spray plumes to impact deposits on the piston and walls. Additionally,

just the long-term accumulation of deposits in the engine is enough to have a significant effect on compression ratio, regardless of combustion type.

Ishii et al. [63] have made many efforts to better understand heat transfer mechanisms in ICE's so it is natural for them to perform a study on deposits. They confirmed, through the use of fast response combustion chamber surface heat flux probes that peak temperature levels to the metal below a layer of deposit material decreases. Thus there is a gradual decrease in the cycle average temperature with the formation of CCD. Additionally, peak heat flux levels also decrease with deposit layers but the cycle net heat transfer out of the chamber does not change much for the cycle. Woschni [64] also shows a trend countering the expected for a diesel engine. He suggests that the thermal storage capacity of soot and deposit on the wall of the chamber will cause the flame to burn closer to the present thermal boundary layer and actually increase heat transfer to the wall, though this finding still remains controversial.

LaVigne et al. [65] show that it is oversimplified to look at CCD as a homogenous layer of insulating quality. They claim that the effective porosity of the material is a dominant characteristic which controls the rates of heat transfer at the surface, suggesting that indeed conduction is the major mode of heat transfer related to deposits. Tree, Wiczynski, and Yonushonus [66] extended this line of reasoning by claiming that the porous characteristics of the CCD layer actually interacted with fuel spray in a diesel engine. This was causing the duration of heat release to increase and indicated specific fuel consumption (ISFC) suffered as a result. Additionally, they pointed out that surface roughness inherent in the material affected local air flow and mixing. They then tested these hypotheses by studying the changes in combustion with pistons coated with various materials like zirconia, which is a ceramic with similar thermal properties of deposit material [67]. By varying other physical properties such as surface roughness and porosity, they showed that a change in heat transfer was not the only factor influencing combustion.

1.3.2 CCD and Heat Transfer

Regardless of the different forms of influence that combustion chamber deposits have on engine operation, its thermal effect is most dominant. In order to ultimately quantify and assess the impact of CCD on engine parameters, there must be a thorough understanding of the heat transfer processes involved, and in accordance a significant effort has been put forth by the petroleum and engine community to accomplish this, at least in the context of conventional engines.

Thermal and Physical Properties of CCD

The specific properties of deposit material in the chamber are important for their effects on in-cylinder processes. Whether they are thermal or some other physical properties, it is worthwhile trying to experimentally determine the CCD properties as a function of different operating modes and conditions. There have been a number of attempts in conventional engines, as documented below, but none have so far been performed in an HCCI engine.

Probably the most popular method for trying to determine the thermal properties of deposits is through the use of chamber surface thermocouples. Overbye et al. [68] performed one of the first in-depth studies regarding experimental in-cylinder crank angle resolved surface temperature measurements in a spark ignited engine. The work was split among general in-cylinder heat transfer and heat transfer affected by combustion chamber deposits, with the latter subject matter providing the most useful insight. They tracked parameters such as cycle temperature swing, temperature gradients, and cycle averaged temperature trends, with different degrees of CCD formation. They also devised methods for estimating the thermal properties of CCD as well as the effective surface temperature of the deposit layer itself, though many approximations were required.

Anderson [69] focused on radiometric measurements to determine the thermal conductivity and diffusivity of CCD. He used a two stroke SI engine with optical access and surface mounted fast response thermocouples to measure the steady heat flux through the deposit layer and determine a conductivity range. To determine the effective thermal diffusivity, the ignition was cut and the temperature decay at the surface of the deposit layer was tracked. These values were then related to the cycle temperature swing and deposit layer thickness at the sampled chamber location. In addition to temperature measurements, Nishiwaki and Hafnan [70] also used infrared radiometry on probes with deposit material growth on them, which were removed from the engine. Not only did they calculate values of the same relevant properties, but also tracked the changes in these properties as a function of different operating conditions, such as equivalence ratio, load, speed, and fuel oil content.

Anderson et al. [71] attempted to indirectly determine quantitative values for conductivity, diffusivity, and heat capacity through temperature measurements below and on the surface of the deposit layer. They found that not only do the properties change as the thickness changes, but this occurs in a non-linear manner, such that their effect on unsteady heat transfer is quite significant. Additionally the porous volumes found in the material presented the potential for intra-material heat transfer through convection and radiation, which complicates the ability to fully understand the important heat transfer mechanisms.

Hopwood et al. [72] devised one of the most practical methods for estimating the thermal properties of chamber deposits. Like others, they relied on instantaneous chamber surface temperature measurements. They tracked the changes in the signal phasing as deposits material formed on its surface. Combining this with thickness measurements of the deposits material, they were able to calculate the effective thermal diffusivity. This procedure actually is quite practical for our experimental setup and will be discussed in more detail later.

CCD and HCCI

The previous sections covered the major topics that relate to combustion chamber deposits in either SI or CI engines. The key to making progress in the work related to HCCI will be leverage findings from previous investigations of CCD in conventional engines as useful guidance in developing plans for this investigation.

Hayes [73] combined experimental and modeling work to estimate the effect of combustion chamber deposits on the octane requirement increase (ORI) in a single cylinder SI engine. He used in-cylinder thermocouples to estimate the thermal properties of deposits at different locations in the chamber and then applied them to the wall boundary conditions in a two-zone cycle simulation to determine the sensitivity of burned and unburned gas temperatures to deposit thicknesses and varying conductivity and thermal diffusivity. This is relatable to the work presented here in the light that HCCI combustion and spark knock share the same fundamental auto-ignition kinetics.

Woschni [64] tried to better understand CI 'adiabatic engines'. This concept is something attempted by many before. The idea is that if enough of a thermal barrier is put at the chamber walls, usually in the form of ceramic coatings, then the subsequent reduction in heat loss will allow containing more energy in the chamber, thus producing more work and increasing combustion efficiency. This is also quite relevant to HCCI combustion since it is so dependent on thermal conditions in the chamber. Intuitively, decreasing heat loss can only help combustion performance. Unfortunately, just as Woschni found, there are enough other parameters affected by changes in heat transfer, such as flame dynamics and volumetric efficiency, that it is difficult to make a definitive conclusion about the general benefits of thermal coatings, especially in diesel engines.

Similarly, Hultqvist et al. [74], tried to utilize insulating and catalytic coatings on the chamber walls of an HCCI engine in an attempt to see if the added heat insulation could decrease hydrocarbon emissions. As stated earlier, HC emissions are prevalent in

HCCI engines because of the thicker than normal thermal boundary layers from ultra-lean combustion. In some cases the added thermal resistance was helpful, but it turned out that the physical properties of the utilized ceramic coatings also affected combustion in other ways because of physical surface/fuel interactions.

Due to HCCI engines' sensitivity to thermal boundary conditions it can be hypothesized that CCD will have a significant effect on ignition and combustion. While there is a considerable amount of work published related to deposits in SI and CI engines and their effects on conventional combustion modes, it is apparent that the effects of deposits on HCCI combustion are potentially much more direct and significant and thus merit in-depth investigation. For example, in an SI engine, combustion chamber deposits are noted for causing an increase of the fuel octane requirements, i.e. making an engine more prone to knock under extreme conditions. This happens because deposit material causes an increase in instantaneous local surface temperatures due to its thermal conductivity being significantly lower than steel (or aluminum), hence enhancing the rates of pre-ignition reactions in the end gas. Considering that ignition and combustion in HCCI are driven by chemical kinetics and that these processes are often referred to as "controlled knock", it is not difficult to see that deposits could have a major role in the *normal* HCCI burning process, rather than just *extremes*. Yet no previously published accounts of work related to HCCI and CCD were found, even though this new form of combustion has started receiving wide-spread attention recently.

1.4 Project Direction and Objectives

As outlined earlier in this chapter, one of the issues critical for the overall fuel economy benefits of the HCCI concept, as well as the robustness of its practical implementation, is the speed/load window of safe operation. Because of its high rates of heat release, high load leads to "ringing" or "knocking". Hence, the high load limit is

established to prevent damage to engine components. At very low loads, misfire occurs due to a high degree of dilution, and low in-cylinder gas temperatures insufficient for initiation and sustaining the pre-ignition and bulk-burning reactions. A practical engine would hence be dual-mode, operating as an SI engine at extremely low or very high loads. While the thermal efficiency of the HCCI operating mode can be up to 50% higher than that of an SI cycle for the same load, the ultimate benefit in terms of the *vehicle fuel economy* will depend on how many engine operating points fall into the HCCI window during a typical driving schedule. Consequently, expanding the limits of HCCI operation is of tremendous importance for the success of future practical implementations of this promising concept. One of the main objectives of this work is to understand and characterize the mechanisms and magnitude of the effect of CCD on HCCI combustion, in order to provide the knowledge base for developing strategies for expanding the HCCI operating range. The primary benefit is expected in guiding techniques for moving the low-load limit downward, closer to idle, since CCD in principle enhances burn rates. In addition, understanding the effects of deposits and possible similarities with other means of altering the thermal conditions in the chamber could also benefit efforts to move the high-load limit upwards. In other words, understanding how the effect of deposits can be countered would reduce the danger of ringing at higher relative loads.

An additional challenge related to developing dual mode (SI+HCCI) engines are load transients and mode transitions. Moving from a high-load SI operating point to a low load HCCI operating point poses a control challenge, in particular because the thermal boundary conditions will be much different at that instant compared to a steady condition [75]. Managing the mode transitions and hot-to-cold and cold-to-hot transients under realistic, in-vehicle conditions will be greatly aided by a thorough understanding of the impact of deposits on HCCI engine and the way they can be correlated to other parameters influencing in-cylinder thermal conditions.

Research Objectives

The research questions to be answered start with understanding the dynamics of deposit formation and chamber 'conditioning' in a gasoline HCCI engine. Then a characterization of the effects of combustion chamber deposits on HCCI combustion will be developed, including both qualitative and quantitative assessment of combustion results obtained. Once the general nature of the thermal influence of CCD is determined, it will be compared to other factors characteristic of HCCI combustion, such as effects of charge temperature versus wall temperatures changes. Further in-depth analysis will attempt to understand spatial variations of deposit coverage and the resulting effects on combustion, such as deposits on the head versus the piston surfaces. Once the general influence of deposits on HCCI combustion is determined, a more detailed breakdown of the specific mechanism of the interactions between the deposit layer and HCCI operation will be performed, with emphasis placed on quantifying the dynamics imposed on thermal conditions responsible for the recorded changes in combustion and emissions. Specifically, is the deposit layer's influence only insulating in nature or is there a transient effect on wall temperature and heat flux responsible for its effects? Additionally, any other insight regarding determination of CCD thermal properties and other relevant characteristics of the layer that aid this effort, including development of methodologies to do so, will be performed as well.

The approach will rely on a unique combination of experimental methods utilized on a single-cylinder gasoline HCCI engine setup in the University of Michigan Automotive Laboratory. The engine is fully instrumented for pressure based combustion diagnostics and complete emissions measurements. The experimental techniques also include instantaneous surface temperature and heat flux measurements, as well as CCD thickness measurements at discrete points in time via removable probes or when the engine is disassembled. An additional goal of this work is related to development and

refinement of dedicated experimental techniques suited for CCD studies. A combination of instantaneous surface temperature measurements and CCD thickness measurements is expected to provide an extensive set of data pertaining to deposit properties, which could in turn allow development of a methodology for in-situ, real-time tracking of deposit growth based only on crank-angle resolved surface temperature measurements. Insights gained with this type of methodology could shed light on the correlation between different HCCI operating conditions and deposit growth, as well as on local phenomena and spatial variations.

The next two chapters outline the experimental setup and data analysis procedures used for this work as well as a description of the in-cylinder heat flux probes which are central to the planned engine experiments. This is followed by a chapter reviewing initial work illustrating the preliminary mapping of deposit formation in the HCCI engine during the so called passive CCD formation test. Chapter 5 is an in-depth look at temperature and heat flux measurements taken from the chamber which characterize deposits and their effects on wall temperature and heat flux as well as a review of the methods used to calculate the thermal properties of deposit layer in the engine. Chapter 6 and 7 are an outline and results of the developed Lead-Corrector method for calculating the surface temperature profile of the in-cylinder deposit layer. Chapter 8 is a discussion of the effect of CCD on the operability limits of HCCI combustion and the last chapter provides a summary of conclusions and an outline of future work.

CHAPTER 2

EXPERIMENTAL SETUP

The emphasis in this investigation is primarily on experimental measurements. A correctly set up engine and test cell with proper data acquisition system is thus required for obtaining accurate and reliable data. This chapter consists of a description of the engine, with sub-systems, the test cell and dynamometer, and specifics on the fast-response thermocouples used throughout testing.

2.1 Engine

This investigation is part of the General Motors Collaborative Research Lab in the W.E. Lay Auto Lab at the University of Michigan, Ann Arbor.

2.1.1 Engine General

The engine's crankcase is a Ricardo L850 Hydra single-cylinder intended for 4-stroke gasoline operation. The research-type single-cylinder head provided by General Motors is a belt driven double overhead cam with dual intake and exhaust valves. The general cylinder dimensions are based on the GM 2.2 liter Quad 4 engine. Figure 2.1 is a 3D view of the piston which is also based on general dimensions of that same engine. It is all aluminum and is similar to the piston used for the previous gasoline direct injection research performed with this engine [76], with the exception of a much shallower piston bowl. Table 2.1 lists the main geometric dimensions of the engine.

Figure 2.1 - Unigraphics model of GM MD-4 piston

Table 2.1 - Major Engine Dimensions

Bore	86.0 mm
Stroke	94.6 mm
Connecting Rod Length	152.2 mm
Compression Ratio	12.5:1

The shape and dimensions of the combustion chamber as defined by the piston and head are depicted in Figure 2.2. Also shown are the locations for the injector, spark plug, in-cylinder pressure transducer, and two head-mounted heat flux probes. On the piston, the locations of eight fast-response thermocouples are marked, but these will be indicated more clearly in the latter part of this section.

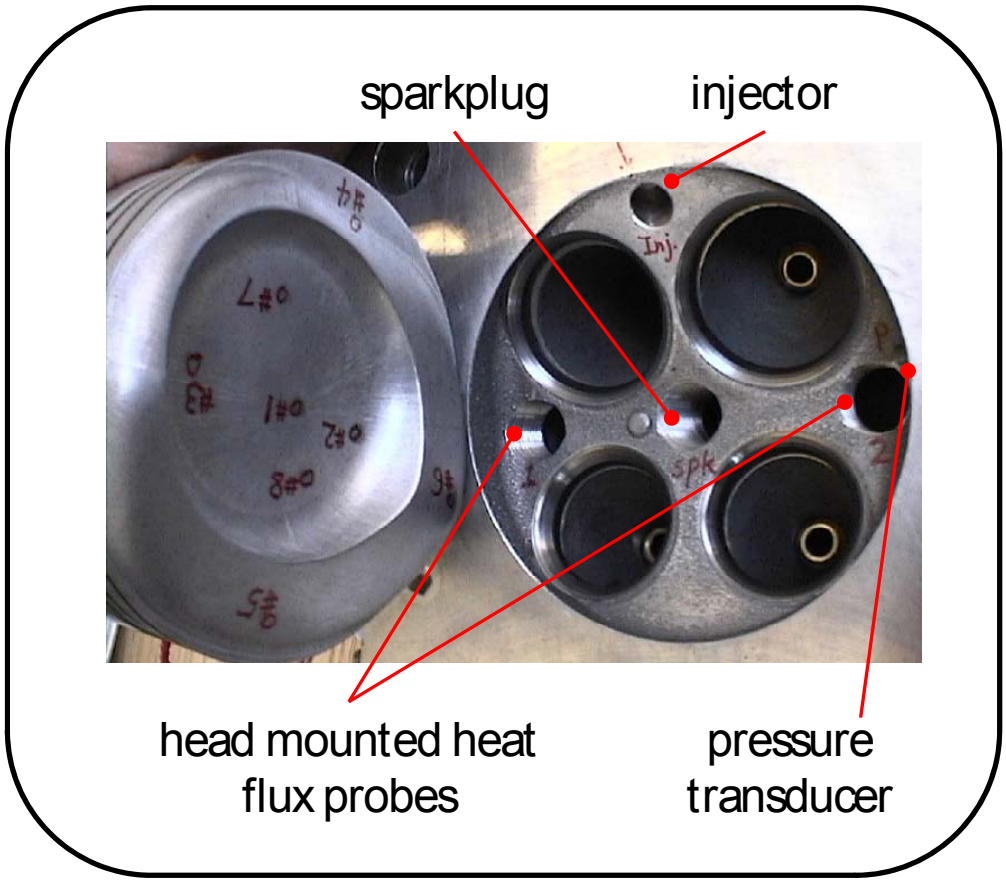

Figure 2.2 - Piston and Head surfaces, indicating locations of spark plug, injector, pressure transducer, and two head mounted heat flux probes

2.1.2 Engine Sub-Systems

A schematic of the engine and sub-systems is shown in Figure 2.3, as taken from Chang [58] and modified for the changes relevant to this investigation.

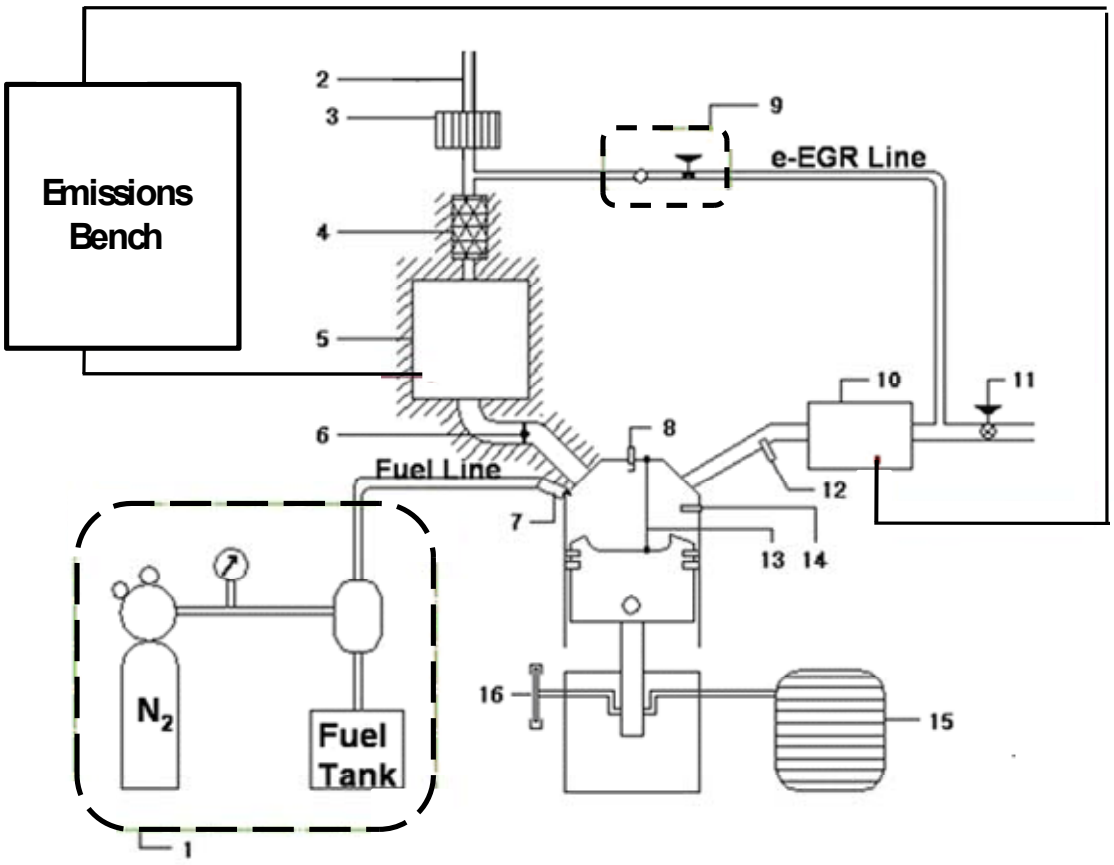

Figure 2.3 – Schematic of Engine and Subsystems, including fuel system, intake, and exhaust. The components are labeled in Table 2.2

Table 2.2 - Component labels of engine schematic in Figure 2.3

1	High Pressure Fuel Supply	9	EGR Valve
2	Regulated and Filtered Shop Air	10	Exhaust Canister
3	Laminar Flow Meter	11	Exhaust Line Gate Valve
4	Intake Circular Heater	12	UEGO Sensor
5	Intake Canister	13	Heat Flux Sensors
6	Intake Swirl Throttle Valve	14	Pressure Transducer
7	Injector	15	Hydraulic Dynamometer
8	Spark Plug	16	Crank Angle Encoder

Intake System

The intake system consists primarily of a main runner and two plenum heaters attached in series between the main air source and the intake ports of the head. In addition there are a few crucial sections that provide either control or measurement of the air, including pressures and temperatures. The intake air is supplied by a critical flow orifice system. A high pressure air supply is filtered and regulated down to pressures pertinent to engine operation, with further fine adjustment for use during testing to maintain desired air flow rates. A laminar flow element (LFE), which determines air mass flow through differential pressure measurement across an orifice, is used to measure flow rates during operation, though emissions measurements are ultimately used for final data analysis.

Following the LFE is a section of heated intake piping. Heat is supplied through a resistance heater which is precisely controlled during motoring and firing operation. Standard procedure for HCCI operation is to heat the air to 90° Celsius. But for some tests this temperature is varied, as will be explained in detail later. Following the heater, the air passes into a large plenum which serves to dampen pressure fluctuations. Every section of intake from the heater to the port is insulated to minimize heat loss.

The intake runner's main function is to direct air into each of the two intake ports in the cylinder head. But it is also where the swirl control valve (SCV) is located. It consists of a butterfly valve leading to the tangential port of the head, which provides a way to vary the degree of air motion in the cylinder. The valve can be adjusted between 20° (fully closed) and 90° (fully open) at infinite adjustability. In general, as the valve is closed, more of the intake air is directed through the 'straight-through' inlet port, compared to the tangential port, resulting in an increase in levels of swirl for in-cylinder motion.

Exhaust System

The exhaust system consists mainly of a long section of piping, highlighted by an exhaust plenum with pressure and emission sample line taps as well as a probe for an AVL smoke meter. In addition, there are two gate valves in series at the end of the main exhaust line to control back-pressure. This is important for maintaining consistent pressures across the exhaust port, specifically relevant for the re-breathing exhaust scheme this engine uses to promote HCCI combustion. There is also an external unheated exhaust gas recirculation (EGR) line. This is routed from the main exhaust line just after the plenum with two manual control valves, for precise control, which feeds back into the intake. This EGR serves a different purpose from the 'internal EGR' that the re-breathing scheme of the engine provides. As EGR is customarily utilized, it dilutes the intake charge and effectively decreases the total quantity of combustible mixture while also adding to the thermal mass. This can be used during HCCI operation to slow down run off combustion, limit excessive pressure rise rates, and lower overall combustion temperatures.

Exhaust Gas Re-breathing

The valve-train consists of two fixed-timing camshafts operating two intake and two exhaust valves. However, for this setup the exhaust cam can be described as a 're-breathing' exhaust camshaft. This is because it actually has two lobes per valve on it. In addition to the typical exhaust lobe there is a shorter duration 're-breathing' lobe, with shorter lift, that opens the exhaust valves for part of the intake stroke. A chart depicting the re-breathing exhaust event in relation to the normal intake and exhaust events is included in Figure 2.4. This allows for fresh, still hot, exhaust gas to re-enter the combustion chamber, directly from the exhaust port along with the intake air. It serves to introduce high levels of hot, high quality internal residual directly back into the chamber.

Since this engine has a moderate compression ratio, gas temperatures at the end of compression would not be sufficient without the re-introduction of high temperature residual to permit auto-ignition of the fuel-air mixture [77,78].

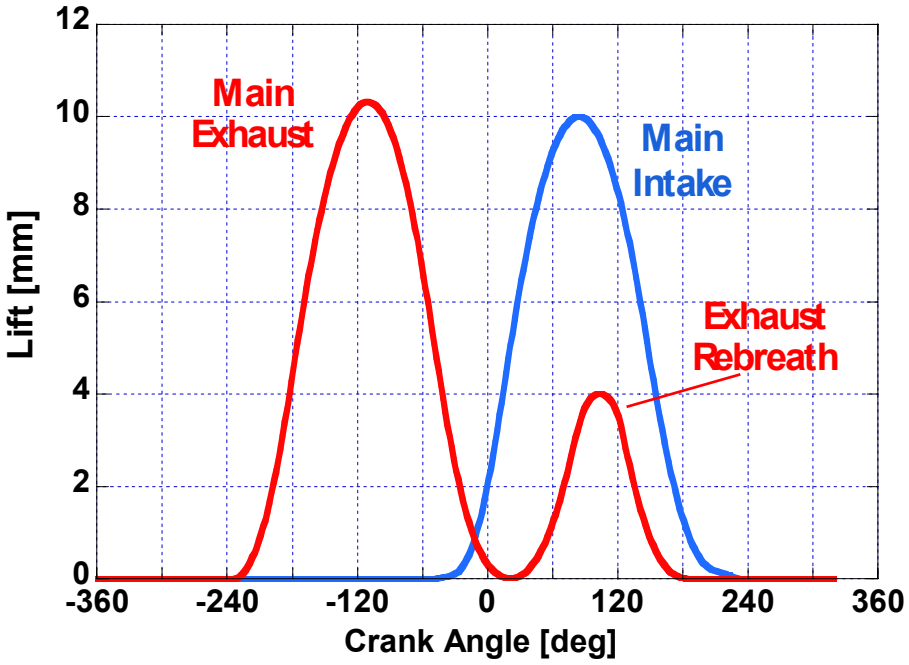

Figure 2.4 – Camshaft timing profiles, with exhaust re-breath event indicated

Ignition System

There is an ignition system in place for this engine which is used strictly for initiating HCCI operation. Since hot residual charge is required for auto-ignition to occur, a number of fired cycles are needed before the engine is able to operate in HCCI mode. Due to the high levels of residual used in this engine, it does not take long before HCCI is able to sustain itself and the spark plug is no longer needed. Timing and dwell of spark is controlled by the GM provided PCESC Setpoint Controller. For reference, even though it is not required to sustain HCCI, the spark is left on throughout testing. Back to back comparison of HCCI operation, with and without spark, have been performed and if the

engine is operating within the predefined stability limit, a coefficient of variance (CoV) of IMEP ≤ 3.0, then there is no measureable effect on combustion.

2.1.3 Fuel System

For this engine setup, the air-fuel mixture may be prepared through two different methods, direct injection (DI) and fully premixed (FP) preparation. All of the testing for this investigation was completed with DI operation, so no explanation of the fully premixed fuel circuit will be given.

Direct Injection

The fuel injection system consists of a Bosch single nozzle injector with 70° spray cone and 20° offset, which is side mounted in the combustion chamber. For most operation the injector is oriented so that the center of the spray cone is directed at the spark plug location, which is at the center of the bore. Figure 2.5 depicts the orientation of the spray pattern in the chamber.

The fuel system is operated at 10.5 MPa and injection timing and duration are electronically controlled by a PCESC Engine Setpoint Controller and Bosch driver. An elaborate system is required to pressurize the fuel system to the required pressure. It basically consists of a bladder-type accumulator pressurized by nitrogen. Regulating the pressure of nitrogen allows control of the fuel injection pressure. For more specific information please refer to Lee, 2001 [76].

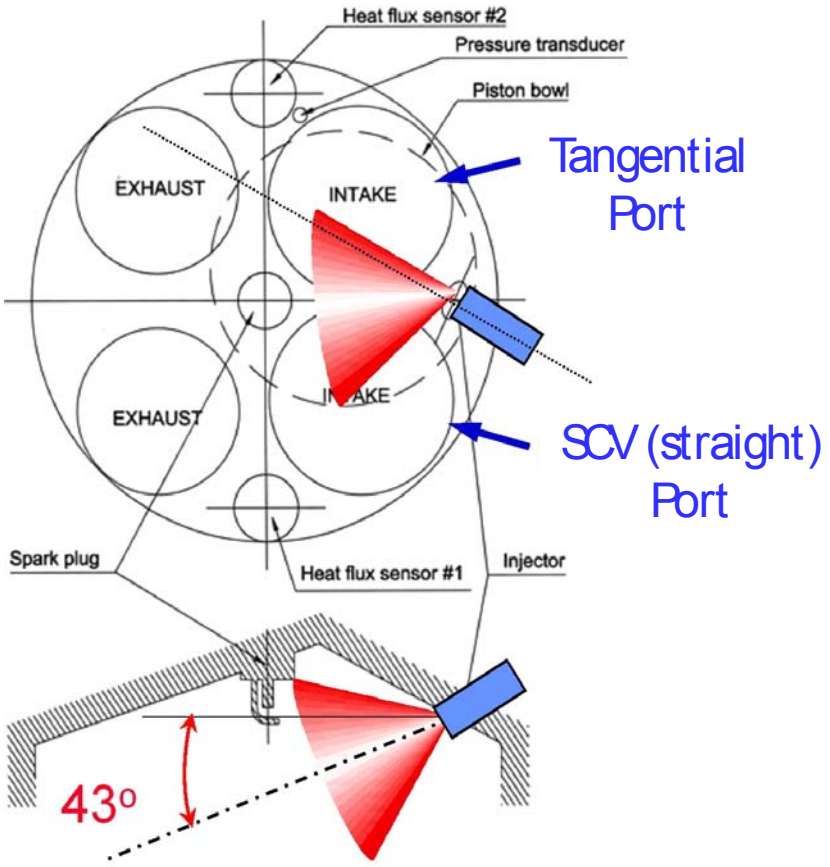

Figure 2.5 – Top and side view diagrams of injector mounting and spray pattern of fuel stream and normal injector orientation

Fuel

The fuel used is a specially prepared control blend from Chevron-Phillips intended for engine testing. It is very similar to typical pump fuel and is used for control and consistency across testing. This is especially critical for this investigation because of the dependence of CCD formation and properties on fuel. Details are listed in Table 2.3.

Table 2.3 - Chevron Phillips RD387 Control Fuel Properties

Specific Gravity	0.7373
Carbon [wt%]	85.56
Hydrogen [wt%]	13.64
Oxygen [wt%]	0.0
Hydrocarbon Types [Vol %]	73.4 % Saturates 22.5 % Aromatics 4.1 % Olefins
RON	90.8
MON	83.4
Pump Octane No.	87.1
Lower Heating Value	44.37 MJ/kg
Higher Heating Value	47.26 MJ/kg
Stoichiometric A/F	14.6415

Since in-cylinder deposit formation rates are so dependent on fuel type and composition, it is crucial to note that in addition to the fuel specification used for this testing an additive is used as well for the purpose of keeping the fuel injector tip clean. The additive used is Techron, manufactured by Chevron-Phillips as a fuel system cleaner. It primarily contains solvents and is used to ensure steady and consistent fuel distribution from the injector nozzle. It is used for all testing except for one exception. This will be explained in detail when required.

2.2 Test Cell

The test cell supports all systems which are required for experimental testing with the single-cylinder engine, including instrumentation and a dedicated hydraulic

dynamometer. All data acquisition is maintained in the adjacent control room in addition to other instrumentation.

2.2.1 Engine Dynamometer

The engine dynamometer is a MICRO-DYN computer controlled hydrostatic dynamometer, designed and built by Electro-Mechanical Associates. It consists mainly of an electrically powered hydraulic pump with pressure relief and control valves. In accordance with the parameters set by the controller, these valves maintain a pressure potential across a second pump which is directly mounted to the flywheel of the engine. With a positive potential across this pump, the dynamometer is capable of applying torque to the engine in order to motor it. Conversely, with a negative pressure drop, the dynamometer switches to a mode of absorbing load from the engine when it is firing.

2.2.2 External Systems

Both coolant and oil systems are maintained externally from the engine crankcases and plumbing of each is such that desired temperatures and pressures/flow rates are achieved and then pumped into the crankcase and head as required. Since the engine, especially in HCCI operation, is not capable of a cold start and does not produce enough heat itself to maintain required block temperatures, both the oil and coolant systems must be heated and primed in advance of engine operation. Basically both subsystems consist of a pump, heater, cooler, and filter as necessary. Cooling of both oil and water is accomplished by liquid-liquid heat exchangers in which one liquid is the medium to be cooled and the other is building supply water.

2.2.3 Emissions Measurements

For exhaust emissions data, a Horriba emissions analyzer bench is set up for accurate steady-state measurement of O_2, CO_2, CO, HC's, and NO_x. These are not only useful for direct characterization of combustion at different operation regimes but also crucial for determination of mixture air-fuel ratio. Additionally there is a means to measure CO_2 from the intake stream for calculation of external EGR fraction but this is seldom used in the operation of our HCCI engine.

Figure 2.6 − Horriba emissions bench used throughout testing for analysis of engine out emissions and determination of operating air/fuel ratio

As a supplementary means to measure air-fuel ratio, an ETAS Wideband Lambda Meter is utilized. This allows us to monitor engine air-fuel ratio in real time while testing is being done. This is one of the main control parameters for operation of the engine and one of the most valuable. The wideband oxygen sensor probe is installed in the exhaust line just before the plenum.

For the measurement of particulate emissions, an AVL 415S Variable Sampling Smoke Meter with a 4210 Instrument Controller is used. It works by passing a stream of raw undiluted exhaust gas through a segment of white filter paper which traps particulate on one surface. After a given preset volume of gas passes through the paper, a calibrated light source is shined onto it and the change in reflectivity in comparison to a clean segment of paper is recorded. This measurement can be correlated to a Bosch Smoke Number (BSN), which is a commonly used quantification of particulate emissions, mostly used for the testing of compression ignition engines. It is shown in Figure 2.7.

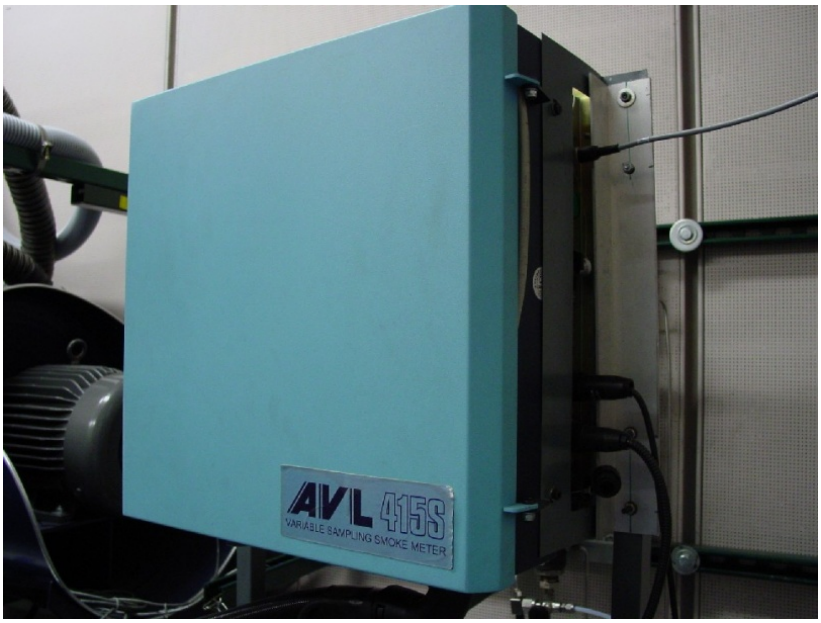

Figure 2.7 – AVL 415S Variable Sampling Smoke Meter

2.3 Heat Flux Probes and Telemetry System

The ability to acquire instantaneous in-cylinder local temperature and heat flux measurements is a major advantage for this investigation. Previously, a telemetry system had been developed [79] for the specific purpose of research regarding the thermal characterization of this engine and the development of an HCCI specific global heat transfer correlation [58].

The telemetry system is built with the purpose of allowing reliable and consistent transmission of temperature measurements by custom made probes by Medtherm Corporation. A schematic of one probe is shown in Figure 2.8. These probes consist of two co-axial J-type thermocouple junctions each, one located at the surface, flush with the chamber wall when installed, and the other is located 4mm back and is needed for steady heat flux calculations. *Note that the second junction is not shown on in the figure.* A coaxial thermocouple (TC) probe consists of a thin wire of one TC material (Iron) coated with ceramic insulation of high dielectric strength, swaged securely in a tube of a second TC material (Constantan). The surface TC 'sliver' junction is formed by mechanically cold-forming (scraping) 1~2 microns thickness of one TC element over the sensing end of the probe, forming a metallurgical bond of the two TC elements. Because the junctions are so thin, their response time is on the order of a few microseconds and for the purpose of thermal measurements in an engine operating at no greater than 3000rpm, they are considered *instantaneous*.

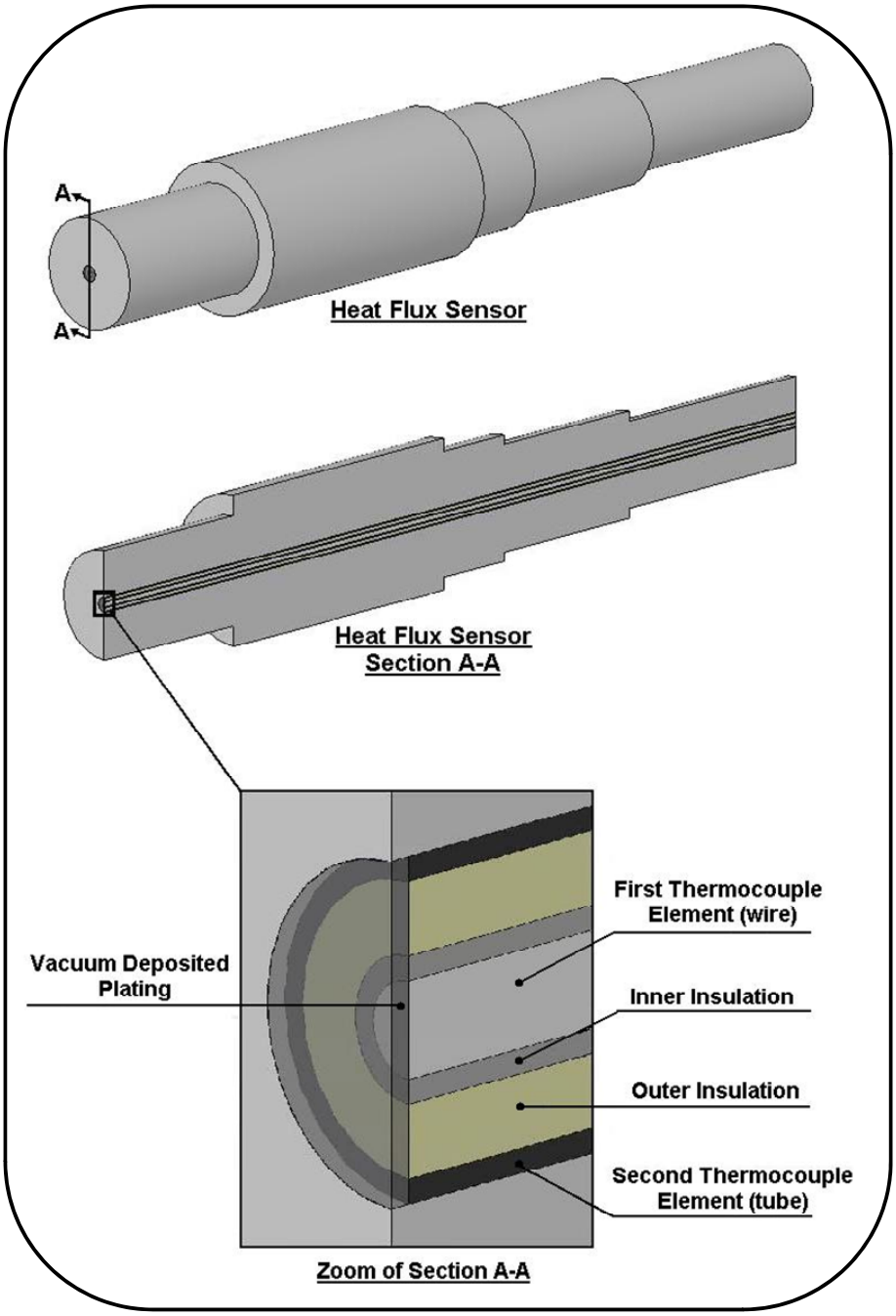

Figure 2.8 – Medtherm co-axial temperature probe as used at two locations in the head. Thermocouples of similar design are located at eight points in the piston top.

Two of these probes are located in the head, flush with the combustion chamber, as shown in Figure 2.9. The diameter of the probe tip is 6mm, though the actual junction diameter is much smaller, as is demonstrated by the drawing above.

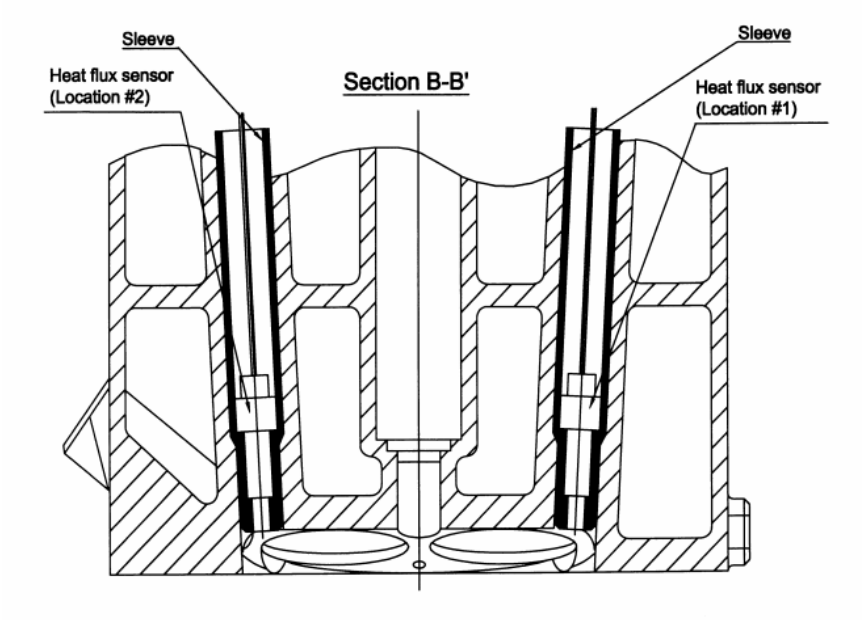

Figure 2.9 – Cross section of head, indicating the mounting locations of the sleeves which hold two fast-response temperature probes flush with the combustion chamber surface

Figure 2.10 is a picture of the mechanical linkage and instrumented piston which contains eight more probes. The linkage was custom developed in-house specifically for this engine and obtaining the signals from the piston mounted thermocouples [79]. Others have used a similar telemetry for measurements from the piston [80,81]. The locations are indicated in the picture of the piston on the right. In this case, there are not separate probes inserted in the piston face. The indicated locations on the piston below are only junctions inserted directly into the piston material.

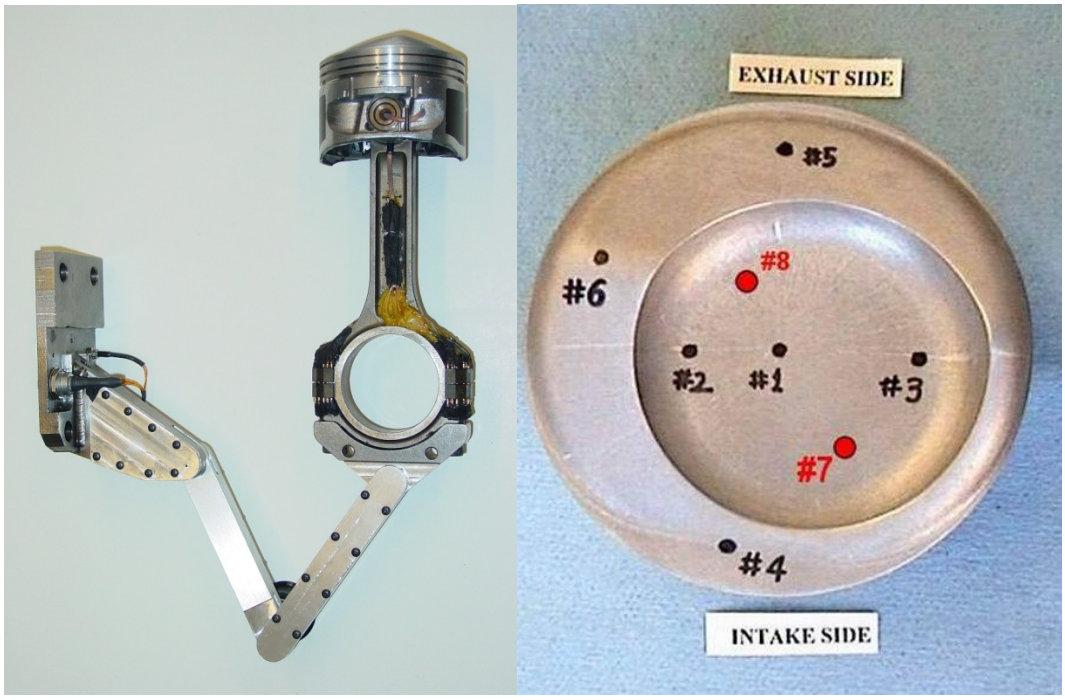

Figure 2.10 – Mechanical telemetry system for fast-response thermocouples located in the crown of the piston, with the specific locations shown on the right.

These measurements will be invaluable for fully understanding local thermal conditions in the chamber and allow the tracking of spatial variations of wall heat flux trends as combustion chamber deposits are formed. These measurements will also be utilized to calculate the thermal properties of the deposit layer and to numerically determine the apparent layer surface temperatures. Measurements will be routinely taken from the probes in the head and limited specific testing will include measurements from the piston top. It should be noted that while there are eight probe locations in the piston, measurements from locations P2 and P3 are not available in this work due to the obtained signals being excessively noisy during testing. This is likely due to partial failure of some of the wiring for those thermocouples.

Probes of these types have been used extensively in the past for similar heat transfer studies [82-85]. Woschni used measurements of this type while formulating his much used global heat transfer correlation [86]. The Musashi Institute of Technology in

Japan carried out extensive investigations specifically on instantaneous piston measurements [87]. They performed a study into the ideal design of quick response surface thermocouples, e.g. they optimized the thickness and diameter of the vacuum-deposited junction in their coaxial thermocouples for accurate measurements. It was concluded that the thermal properties of the materials used in the construction of the thermocouple should as closely match those of the material they are embedded in. Assanis and Badillo performed a similar study and found comparable results [82]. Nakic et al. [60] and Assanis and Friedman [88] show work done on the analysis of piston surface measurements in a diesel engine and even track the changes in heat flux as CCD are formed in the chamber.

2.4 Deposit Thickness Measurement

One goal of this work is to quantify CCD formation levels and correlate that to the changes in combustion that are recorded. Based on the work of Hopwood et al. [72], a Fischer Dualscope was used for specific quantification of deposit levels for this investigation. It is a hand-held device that is capable of measuring the thickness of various types of coatings on different substrate materials. A photo of the device and a diagram depicting its operating principles is included in Figure 2.11. The principle of operation is based on measuring the strength of an induced magnetic field on the substrate material of the sample. The strength depends on the distance from the substrate, which happens to be the thickness of the coating. For this investigation two different probes were obtained. One for measurements on the aluminum combustion chamber surfaces (non-ferrous) and one for measurements directly on the face of the steel heat flux probes (ferrous). The manufacturer stated accuracy of the device is ±5% [89].

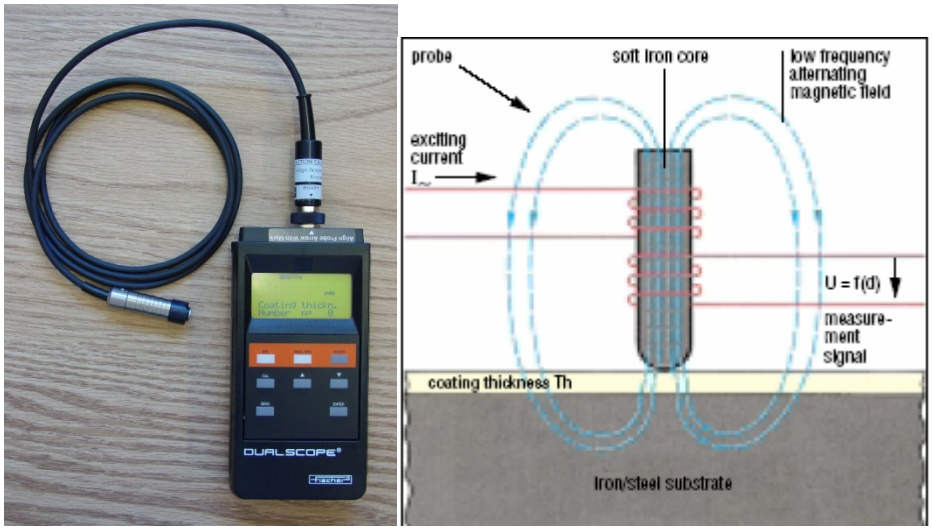

Figure 2.11 – Fischer Dualscope and a diagram depicting working principles [89]

CHAPTER 3

DATA PROCESSING AND ANALYSIS

3.1 General

The electric signals received from the data acquisition system are what data analysis is ultimately based on. These signals must be recorded as either time based or crank angle based measurements, depending on the measurement type. Then the signals are converted to meaningful units based on previous calibration of the measuring device in question. This converted data can include temperatures, pressure, exhaust emissions gas fraction, and engine speed, to name just a few. These measurements are then combined using basic principles of engine dynamics and thermodynamics to calculate performance parameters and other useful formulations to describe and characterize engine operation for a particular data set. In this chapter, the processing and formulation for heat release calculations and surface temperature and heat flux measurements will be the main focus.

3.1.1 Data Acquisition Systems

The engine in this investigation is fully instrumented so that detailed analysis of all aspects of operation can be studied. There are two main systems which are utilized for conditioning, displaying, and recording of the data required for complete analysis.

Time Averaged Data

There are extensive 'slow' time averaged data streams which are primarily used for characterizing the operating point, calculating emissions, and also to supplement heat release calculations offline. Some of the most critical are intake manifold pressure, intake air temperature, exhaust temperature, coolant and oil temperatures, fuel flow rate, and exhaust emission measurements, which include CO_2, CO, O_2, UHC, and NO_x. This is handled by a PC-based Labview data acquisition program.

Crank-Angle Resolved Data

There are also a few channels of 'fast' crank angle resolved measurements that are required. The most critical for this investigation are cylinder pressure and heat flux probe temperature signals. The pressure transducer used is a Kistler model 6125A, used with a flame guard for all testing. The heat flux probes are those mentioned in the previous chapter, made by Medtherm Corporation. Because the output of the actual sensors is in millivolts, the signals must be amplified then read in by the data acquisition system. For the transducer signals, the voltages must be converted to real dynamic pressures within the high speed data acquisition system based on previous calibration results. A similar conversion is actually done for the thermocouples by post processing algorithms performed offline. All crank-angle resolved measurements are handled by an AVL IndiSet 620 signal acquisition and conditioning system with IndiCom 1.6 software used for real-time display and recording of data streams. All data is taken at a resolution of one half crank angle resolution.

3.2 Heat Release Analysis

Proper heat release analysis performed on the recorded data is absolutely critical for accurate quantification and characterization of the combustion process. All

calculations are based around the cylinder pressure measurement so proper calibration and referencing of the pressure transducer must be performed before any measurements can be taken.

There are many variations and customizations that can be included in combustion heat release calculations and this case is not an exception. All combustion modes, engines, and analysis requirements call for a tailoring of the computations in order to extract the most useful and relevant information as possible. This is one reason Matlab was used for the software development, because changes and modifications can readily be made to suit the analysis. In our case, the general approach to model setup for the heat release code is structured by algorithms set forth by Gatowski et al [90], but a few other published works were also consulted [29,91-93]. General Motors' in-house software analysis tools are similarly based on this as well. Since this work is supported by and performed in order to supplement similar work by researchers at General Motors R&D, it seemed fitting to match their methods as closely as possible.

3.2.1 Governing Equations

The model for which the heat release computations are based on is derived from energy conservation of a single zone approximation of the composition of the combustion chamber with a linear correlation for gas ratio of specific heats (gamma) as a function of charge temperature. This way the composition of the combustion chamber is considered homogeneous, of which the overall properties change as burning proceeds. This greatly simplifies computation and may even be closer to real effects considering the fact that HCCI is combustion of premixed fuel and air and there is no propagating flame, in the typical context of the phrase. As indicated in equation (3.1), the main contributing terms are internal energy of the control mass, work, heat transfer, and mass flow.

$$\frac{dQ_{ch}}{dt} = \frac{dU_{cv}}{dt} + \frac{dW_{cv}}{dt} + \frac{dQ_{loss}}{dt} + \sum h \frac{dm_{flow}}{dt} \tag{3.1}$$

Now each term in this equation can be expanded and re-written in terms applicable to a system of an internal combustion engine. The term on the left represents the chemical heat release from the fuel as a function of the other terms in the formulation. The first term on the right of equation (3.1) represents internal energy and accounts for the total energy content of the air/fuel/exhaust mixture in the cylinder. It is described by the average charge temperature and average specific heat representation of chamber contents.

$$\frac{dU_{cv}}{dt} = mC_v \frac{dT}{dt} = \frac{1}{\gamma - 1}\left[V\frac{dP}{dt} + P\frac{dV}{dt}\right] \tag{3.2}$$

The cylinder content average gas temperature is re-formulated as pressure based on the ideal gas law. The second term on the right of equation (3.1) represents work done on the piston by gas pressure; it is described in equation (3.3).

$$\frac{dW_{cv}}{dt} = P\frac{dV}{dt} \tag{3.3}$$

Equations (3.2) and (3.3) can be substituted into the original governing equation (3.1) and simplified for the result below:

$$\frac{dQ_{ch}}{dt} = \left(\frac{1}{\gamma - 1}\right)\left[V\frac{dP}{dt} + \gamma P\frac{dV}{dt}\right] + \frac{dQ_{loss}}{dt} + \sum h\frac{dm_{flow}}{dt} \tag{3.4}$$

The last term above represents mass flows into and out of the control volume. Since heat release analysis is performed during the close portion of the cycle (while the valves are closed) the only source for this term is crevice-flow or blow-by. These are treated as negligible, so the term including enthalpy flows is neglected. This particular investigation looks at the data in a primarily qualitative manner and since this term accounts for such a small portion of the total chemical heat release it can be ignored.

The third term on the right of equation (3.1) represents energy loss from the chamber in the form of heat transfer.

$$\frac{dQ_{loss}}{dt} = hA_s\frac{dT}{dt} \tag{3.5}$$

The temperature difference is taken as that being between the gas and the average chamber surface temperature. The surface temperature average is estimated based on our heat flux probe measurements. There are numerous ways to handle the convection term. Typically it is done by applying an empirical correlation to represent the convective coefficient term, 'h'. In this case it will be through the use of the heat transfer correlation developed through previous work at the University of Michigan and published by Chang et al. [94]. It is a development of Woschni's global heat transfer correlation for specific application to HCCI engines. Its general form is as follows:

$$h(t) = \alpha_{scaling} L(t)^{-0.2} p(t)^{0.8} T(t)^{-0.73} v_{tuned}(t)^{0.8} \tag{3.6}$$

$$v_{tuned}(t) = C_1 \overline{S}_p + \frac{C_2}{6} \frac{V_d T_r}{p_r V_r} (p - p_{mot}) \tag{3.7}$$

The respective variables are h [W/m^{2}K], L [m], p [kPa], T [K], v [m/s], S_p [m/s], V_d [m^3], T_r [K], V_r [m^3], and p_{mot} [kPa]. For the constants, α = 11.1, C_1 = 2.28 (for compression and expansion strokes), and C_2 = 0.00324 m/sK. In this case, L represents the instantaneous chamber height.

Equation (3.5) is substituted into (3.4) and we end up with the final formulation for heat release. It is important to mention that the 'α' term in equation (3.6) is used for scaling of the overall heat transfer term and is used to ensure that the total cycle integrated heat release matches the total chemical energy content of the fuel used for the cycle, though a value of 11.1 has been used with success for this work.

A note should be made regarding gas properties, specifically the ratio of specific heats, or gamma, γ. The true value of gamma is a strong function of temperature and composition and the since the accuracy of heat release analysis is so sensitive to the value used for γ it is important to estimate it correctly. Due to the unique operating parameters required for HCCI, which includes a lean air/fuel mixture and a high amount of residuals, previously proposed correlations for SI engine conditions are not suitable for HCCI application. The following 3rd degree polynomial was developed, as a function of temperature [K], based on a chemical equilibrium program using 14 species and is suitable within the range of air/fuel ratios used for testing in this work [94].

$$\gamma = -9.967x10^{-12}T^3 + 6.207x10^{-8}T^2 - 1.436x10^{-4}T + 1.396 \tag{3.8}$$

3.2.2 Pressure Measurements and Processing

Apart from the governing relations required for the calculation of heat release rate, mass fraction burned, etc., there are many other sub routines that need to be performed for successful and accurate completion of the desired calculations.

First of all, before any of the real computation is performed, filtering of the pressure signal must be completed. Due to various effects such as mechanical noise, electrical noise, and circumstances derived from the resolution of the encoder and transducer combination, extra effects which are not real can be picked up in the pressure trace. These include spikes, discontinuities, and cyclic variations about an average point. Some of this is already dampened out once cycles for a particular point are averaged together, but final filtering insures that the influence of these on final calculations will be minimal.

Also crucial for accurate pressure traces is 'pegging' of the pressure signal for a particular cycle. Since a piezoelectric pressure transducer works on the principle of measurement of dynamic pressures, the absolute values of the recorded pressure trace must be offset to match a known absolute pressure that there is confidence in. In this case time averaged pressure readings from the intake manifold are used. This recorded pressure is matched to the in-cylinder pressure at BDC of the intake stroke. The offset of these two measurements is used to offset the rest of the in-cylinder pressure data.

One final important aspect that needs to be included in the discussion of proper calculation of cycle heat release is residual and how it is calculated. Typically, this only involves exhaust residual that left in the cylinder following the blow-down period of the cycle, but due to the exhaust re-breathing scheme in place for this engine, similar methods need to be applied to determine how much more residual is introduced into the chamber during the exhaust valve open period of the intake stroke. In order to do this, the mass in the cylinder after the intake valves closes is assumed to be comprised only of

intake air and of exhaust residual. The contribution of each to the total mass is calculated by considering the partial pressures through the use of their properties based on the ideal gas law. The amount of residual mass left in the cylinder at the end of the intake process is equated by:

$$m_{residual} = \frac{P_{residual} V_{IVC}}{R T_{residual}} = \frac{V_{IVC}}{R T_{residual}} \left(P_{IVC} - P_{\text{int}} \right) \tag{3.9}$$

$$P_{\text{int}\,ake} = \frac{m_{\text{int}} R T_{\text{int}}}{V_{IVC}} \tag{3.10}$$

Where the subscript '*IVC',* indicates the crank-angle at which the intake valve closes, and the residual properties are assigned those of the exhaust gas.

3.3 Temperature and Heat Flux Analysis

This section will outline the steps that are used to convert the raw voltage signal from the heat flux probes to the final temperature curves shown in the upcoming figures.

3.3.1 Temperature Data Acquisition

As has been mentioned before, the heat flux probes used in the piston and in the head consist of two J-type thermocouple junctions. One is located at the surface of the probe and the other 'backside' junction is four millimeters below it. The two wire types that J-type thermocouples consist of are iron and constantan. Because these wires are so thin and sensitive, it is ideal to minimize the length for which they are used. As described before, they only need to be used until the point of the cold temperature reference point, and this location differs for probes in either the head or piston.

In the case of the piston, there are thermistors attached to the back of the piston. These provide absolute temperature measurements based on a negative temperature coefficient of resistance [95]. The thermistors are physically mounted on an 'isothermal plate', in the back of the piston, which is where the J-type thermocouple wires terminate. Thus the temperatures measured in the piston are the relative difference between that piston surface location and the isothermal plate. From that point on, normal stainless steel wires are used to transmit the signal to the data acquisition computer through the mechanical linkage then eventually to the signal conditioning channels in the AVL IndiSet system. This path includes a set of connectors for switching the wires over to co-axial type for shielding and then an amplifier for applying a gain to the signal so that it reads in volts instead of milli-volts. A schematic of the circuit is shown in Figure 3.1. It is now simply a matter of using the typical conversion equations to get temperatures from those voltages.

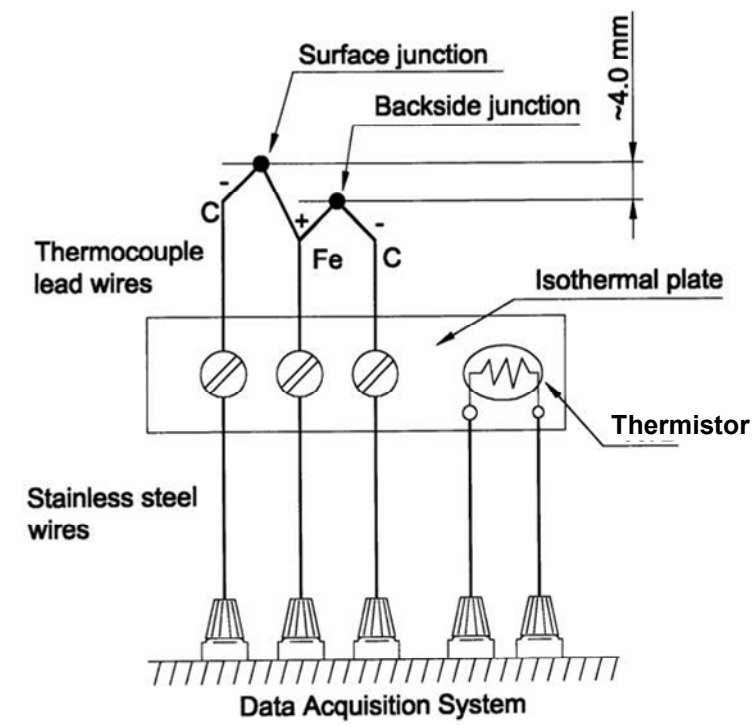

Figure 3.1 – Representational schematic of wiring required for piston surface temperature measurements. This includes at each measurement location two junctions and necessary thermocouple wiring to back of piston where isothermal plate and reference thermistor are located [96]. The mechanical linkage is not depicted.

The probes used in the head are a little simpler. The thermocouple wiring is routed all the way out of the top of the engine through custom metal sleeves to an ice box. This serves as a 'cold' junction. Thus the temperature measurements from the head are direct measurements on a 0°C reference. From the ice box, shielded co-axial cable carries the signal to the DAQ system, where it is again amplified.

3.3.2 Temperature and Heat Flux Calculations

In order to effectively use the temperature data obtained from the thermocouples it must be put into a form in which it can easily be manipulated. The file that is generated

by our data acquisition system software is setup to record crank-angle based voltage readings for each location at each one half crank angle. Therefore there are 1440 data points for each thermocouple per cycle. The preliminary steps are to average 100 cycles, then to convert the voltages to real temperatures based on the polynomial correlation for a J-type thermocouple. The measurements are adjusted according to the pertinent cold junction reference temperature.

Following is a short review of the methods required to calculate heat flux through the wall of the combustion chamber based on measurements taken with our heat flux probes. This requires both the surface junction as well as the backside junction that is located 4mm below the surface [97].

The basis of this method for determining heat flux is dependent on a few assumptions. As is indicated in the governing equation (equation 3.11), the system is simplified as one-dimensional unsteady heat conduction. Heat transfer can be assumed to be one dimensional, normal to the chamber surface because the front-side and back-side junctions are so close to each other. The temperature measurements from the two junctions each make up a boundary condition for the problem, as listed in equation (3.12). In the equations, 'T_s' indicates the measured temperature at the probe's surface junction and 'T_b' indicates the measured temperature at the backside junction. It is critical to mention that the backside junction is far enough below the surface that it always measures a steady temperature, as depicted in Figure 3.2.

$$\frac{\partial T}{\partial t} = \alpha \frac{\partial^2 T}{\partial x^2} \tag{3.11}$$

$$\begin{aligned} T(0,t) &= T_s(t) \\ T(\delta,t) &= T_b(\delta) \end{aligned} \tag{3.12}$$

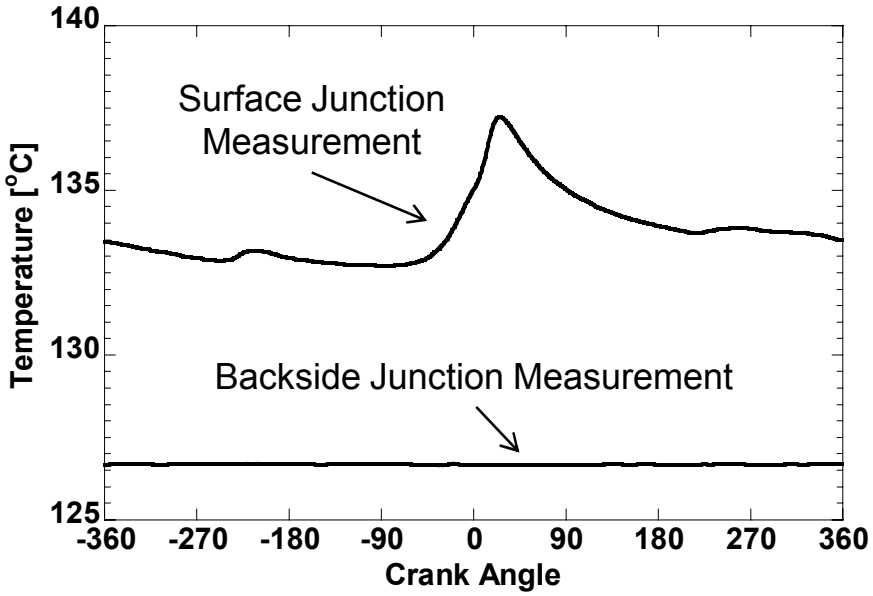

Figure 3.2 – Sample experimental temperature measurements taken from one of the head mounted heat flux probes, consisting of surface and backside junctions measurements

Applying the boundary conditions, the one-dimensional transient heat equation can be put into the following form:

$$T(x) = \frac{x}{2\alpha}\frac{\partial T}{\partial t}(x-\delta) + \left(\frac{x}{\delta}\right)(T_b - T_s) + T_s \tag{3.13}$$

Substituting the spatial derivative of (3.12) into the common relation for heat flux,

$$q'' = -k\frac{\partial T}{\partial x} \tag{3.14}$$

results in an equation for heat flux which is a function of 'x' (depth into surface) and the time derivative of temperature. Immediately, any term with 'x' goes away since we are seeking the heat flux at the surface (x=0). But the time derivative term is a little

more involved. Now the temperature data, which is currently a discrete set of points at every half crank-angle, must be represented in a form which will allow us to eventually take the time derivative of it in order to fit into the heat equation. This is most suitably done by representing it as a Fourier series:

$$T_s(t) = \overline{T_w}(0) + \sum_{n=1}^{N} \left(A_n \cos n\omega t + B_n \sin n\omega t \right) \tag{3.15}$$

After substituting back into the heat flux equation, the final form of heat flux is shown in equation 3.16. Thermal conductivity of the metal probe is represented by 'k' in the equation.

$$q_s(t) = -k \frac{\partial T}{\partial x}(0,t) = \frac{k}{\delta}\left[\overline{T_w}(0) - T(\delta)\right] + k \sum_{n=1}^{N} \sqrt{\frac{n\omega}{2\alpha}} \left[A \left(\cos n\omega t - \sin n\omega t \right) + B_n \left(\sin n\omega t + \cos n\omega t \right) \right] \tag{3.16}$$

Figure 3.3 is a sample plot of heat flux calculated from the temperature profiles shown earlier.

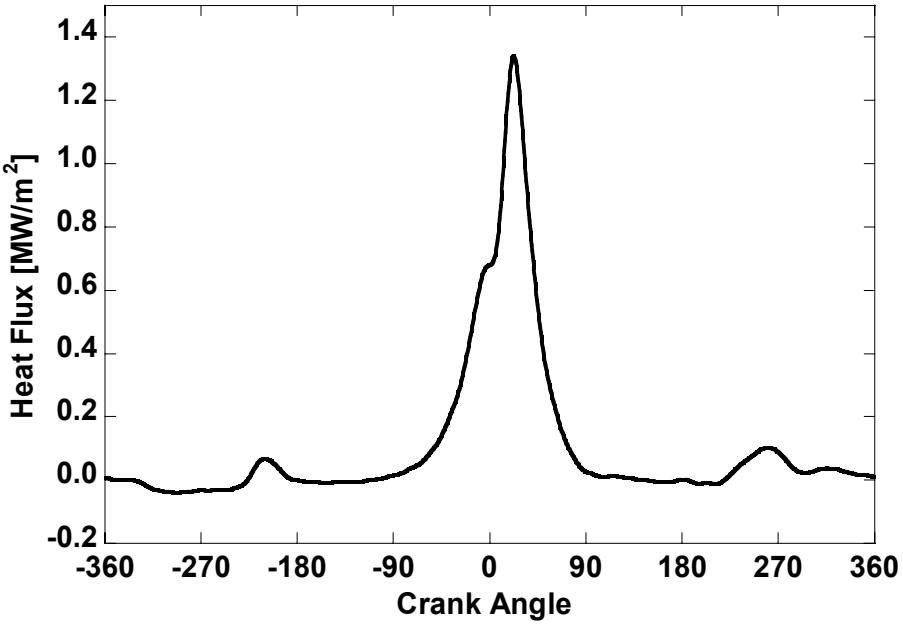

Figure 3.3 - Sample calculated surface heat flux profile from head mounted heat flux probes

Once testing is performed, the data is post-processed into meaningful and useful results, based on the algorithm described above. More on how the use of heat flux measurements will be utilized to aid in the study of the effect of CCD on HCCI combustion will be discussed in upcoming chapters.

3.3.3 Accuracy of Thermal Measurements

Quantifying the relative error and certainty of temperature and heat flux measurements is crucial to this work because a large amount of the deposit properties analysis is based on these measurements. Also, in a later chapter, some numerical methods are developed and their accuracy will depend on the certainty of measurements discussed here.

The ISA standards for a J-type thermocouple, which are met by Medtherm corporation, the manufactures of the probes, lists a maximum error of 2.2°C or 0.75%,

whichever is greater. Since temperature measurements from the chamber rarely exceed 150°C, the former is considered the limit, which results in a maximum relative error for temperature measurements of 1.5% [98].

There are two facets to the accuracy of heat flux measurements. The first is the error due to inaccuracy of the temperature measurement propagating through the heat flux calculation and its affect on the final value. The second is the error due to the time response of the thermocouple junction itself.

Based on the procedure discussed above, a few calculations are required using the temperature measurements in order to get a heat flux. Any error associated with the temperatures will also be present to some degree in the heat flux as well. While it would make sense to quantify this error propagation based on the computations involved, since a fast fourier transform is used to represent the temperature profile for the purpose of heat flux calculations the actual experimental uncertainty associated with the thermocouples would no longer apply.

Instead, ensuring that the calculated heat flux profiles are accurate comes down to choosing a correct harmonic number for the Fourier series representation, as indicated by 'n' in equation 3.15. This is the number of sinusoidal modes used to represent the original data. For all of the results in this work, a harmonic number, n=40, was used to represent the surface temperature profile. It is clear from Figure 3.4, with data taken at 0.5°CA increments, that a harmonic number greater than n=30 does not results in significant additional accuracy when compared to the original measured temperature profile.

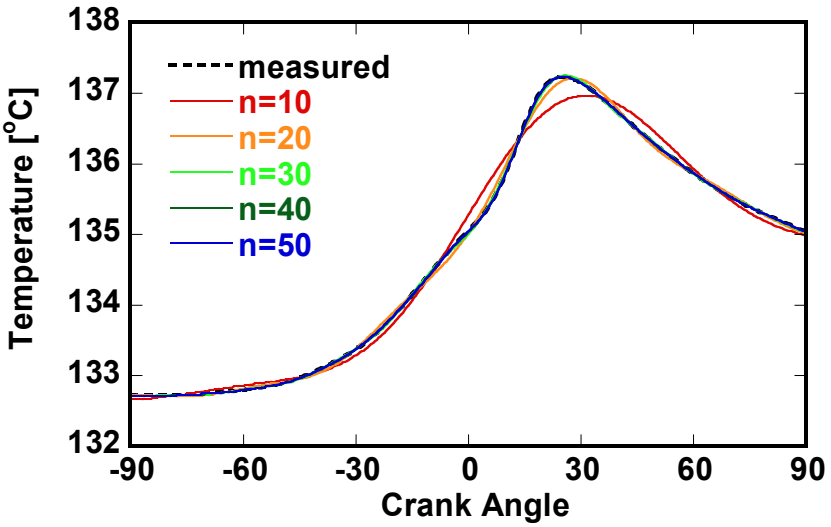

Figure 3.4 – Comparison of harmonic number value used for Fourier series representation of surface temperature measurements

The second potential source of error relates to the response time of the thermocouple junction. Due to the derivative term, the accuracy of the heat flux calculation is greatly dependent on the transient response of the measuring probes. The manufacturer of the heat flux probes states a response time of less than 10 microseconds for the sliver junctions used for these thermocouple [99]. This response time is the theoretical time required for ~63% of a measurable step change in surface temperature to occur. At a maximum speed of 2000rpm and 0.5 crank angle resolution, 42 microseconds pass between measurement points. Based on a time constant of the junction of 10 microseconds, 40 microseconds are required to reach 98.2% of a step change in temperature, providing an error of less than 2%.

It is also important to mention that Chang [58] has shown that performing these calculations on data representing the average of angle-resolved temperature for several cycles is representative of performing the heat flux calculations on each individual cycle and then averaging them. This is a procedure that is adhered to for all the data presented in this work, except when noted otherwise.

CHAPTER 4

THE EFFECT OF CCD ON HCCI

4.1 Introduction

The goal of this work is to understand how the thermal influence of combustion chamber deposits can be utilized to expand of the operating range of HCCI combustion. In order to do this, two main objectives must first be met; tracking deposit formation trends in an HCCI engine and determining the sensitivity of HCCI combustion to CCD. This requires testing that demonstrates the differences in combustion between a clean engine and one with deposits coating the chamber. This will involve a long-term test that tracks the effects of CCD on combustion. The test will start with a clean engine. One baseline HCCI operating point is maintained for the duration of the test during which gradual combustion chamber deposit formation will occur. Combustion parameters, including heat release rates and emissions will be tracked for the duration and compared to the case of a clean engine.

This chapter will begin by detailing the specifics of the test procedure and measurements taken throughout the test. Then a review of the effects of the gradual formation of deposits in the engine will be given. This includes the effects on HCCI burn rates and emissions. Next, a comparison of the effect of CCD on combustion with that of intake and coolant temperature changes will be discussed. Finally, how the formation levels of combustion chamber deposits are quantified will be shown. During this testing, combustion chamber surface temperatures are taken using the fast response heat flux probes discussed in the previous chapter. These measurements will be utilized to get

insight into the properties of deposit material; however these results will be discussed in the next chapter.

4.2 Experiment Procedure

4.2.1 Test Procedure - 'Passive' Conditioning

The goal of this testing is to determine the net effect of naturally formed combustion chamber deposits on HCCI combustion. A carefully controlled test procedure is established in order to methodically track changes in combustion parameters and quantify the sensitivity of HCCI combustion to varying levels of deposit growth. Determining when CCD formation rates in the chamber will reach an equilibrium point, i.e. after how many hours of HCCI operation will the chamber become *fully conditioned*, is of high interest as well.

This test procedure is specifically referred to as 'passive conditioning' because the deposits created throughout the test are formed by natural means. Nothing is done to accelerate their formation rates. Later on, in following chapters, an 'aggressive conditioning' procedure will be discussed. This is a specific set of operating parameters that is developed to simulate the long-term formation of natural combustion chamber deposits. This is intended to shorten the time required to achieve a *conditioned* combustion chamber. This will be discussed further in a later chapter.

This whole test procedure was repeated twice to ensure that the procedure would be repeatable. There is always going to be a degree of variability when testing involves deposit formation, but overall results and trends were very consistent.

Experimental Approach

Combustion chamber deposit formation is affected by a range of factors, i.e. mixture preparation, fuel properties, combustion chamber design, wall temperatures, etc.

Various ways of creating favorable conditions for ignition in the HCCI engine, e.g. high compression ratio, retention or re-induction of residual, can be additional influencing factors. There is no previously published work involving both HCCI and CCD and hence no base for hypothesizing about the magnitude of CCD effects on combustion. However, initial work hinted at a strong influence of deposits on combustion in this specific engine [79], and that was utilized to develop a procedure for systematic evaluation reported here.

The test starts with a completely clean 'unconditioned' combustion chamber. The engine operates at a standard representative operating point, listed in Table 4.1, which is considered to be a medium load point for HCCI operation in this engine. The duration of the test consists of running at this same point as CCD accumulates over time. Changes in combustion and heat flux are tracked at regular intervals by way of in-cylinder pressure measurements and heat flux measurements, respectively. This is continued until there is no longer any appreciable change with further engine operation. At this point the chamber is considered 'conditioned' and the test is concluded.

Table 4.1 – Passive Conditioning Operating Parameters

Engine Speed	**2000 rpm**
Load	**11 mg/cycle**
Air/Fuel Ratio	**20:1**
Injection Timing	**EOI 318 °bTDC**
Swirl Control Valve	**Fully Open (minimum swirl)**
Intake Air Temperature	**90°C**
Oil/Coolant Temperature	**95°C**

The engine did not run continuously for the extent of the test since the size of the fuel accumulator limits operation to 2 hours at a time. However, the test procedure

ensured that restarts did not significantly affect the CCD formation rates. At the beginning of every new test cycle the combustion parameters were compared to those measured right before the end of the previous cycle to verify consistency.

CCD Growth and Stabilization

As discussed in chapter 1, changing in-cylinder thermal conditions, specifically anything affecting wall temperatures, in combination with fuel component boiling points, will eventually lead to the stabilization of deposit growth rates. As outlined by Kalghatgi et al. [61], when the chamber is clean, for given operating conditions, CCD formation is the fastest and directly dictated by combustion parameters and their effect on surface thermal conditions. As deposits grow they act as a thermal insulator, dampening and decreasing the rate of local heat flux. This in turn increases chamber surface temperatures and reduces deposit growth rates. Eventually, an equilibrium corresponding with the previously mentioned critical surface temperature is reached, and no additional deposits form. One of the objectives of this testing is to quantify the differences in combustion between a clean engine and one at which combustion formation has stabilize, in addition to understanding the relative amount of time required for stabilization.

It is important to note that this testing is performed at one constant operating point. It is likely that the idea of a ‘stabilized’ state of deposit formation is irrelevant in a real engine that sees a wide range of operating conditions. Furthermore, the time required for stabilization may differ depending on the operating point used, even for continuous testing, as performed here.

4.2.2 Testing Hardware

This test utilizes the engine setup discussed previously in chapter 2. All relevant measurements, including crank-angle based cylinder pressure and temperatures, all time-averaged, and emissions are recorded at regular intervals.

In order to quantify CCD formation levels, the Fischer Dualscope described in Chapter 2 will be used as well. Throughout the duration of testing, the heat flux probes are removed from the head every 4 hours to measure the thickness of the deposit coating formation on their tip, above the thermocouples junction. This served as a rough indication of the overall relative level of in-cylinder deposit levels as the test progressed. When testing was completed, the head was removed and a more thorough set of thickness measurements was taken on all head and piston surfaces.

4.3 Results

4.3.1 Combustion and Emissions Results

The duration of the test was 40 hours. After approximately 34 hours there were no longer any measureable changes in combustion and heat flux measurements and it was concluded that the deposits levels reached equilibrium. Additionally, by the end of 40 hours, the speed of combustion had increased enough to be close to the engine's knock limit.

Figure 4.1 through Figure 4.3 show the evolution of several key combustion performance parameters as a function of engine operation time. Figure 4.4 shows heat release results for every ten hours of engine operation.

Figure 4.1 and Figure 4.2 show the evolution of 10-90% burn duration, ignition timing, represented by 10% mass fraction burned (CA10), and peak pressure (Pmax). There is a significant change in combustion from simply running the engine for several hours. In general, combustion occurs faster and closer to TDC as chamber conditioning

progresses. Burn duration decreases by about 5 crank angle (CA) degrees, and CA10 advances by about 2.5 degrees CA. Changes slow down and tail off in the last 10 hours of the test. Cylinder peak pressure ultimately increases from 35 bar for the clean chamber to 43 bar for the conditioned.

Figure 4.2 also shows combustion stability through coefficient of variance of mean effective pressure (CoV). The cycle to cycle variability decreases significantly throughout the duration of testing. This is important when considering load operability limits and is thought to be primarily related to the advancing combustion phasing. Figure 4.3 shows the changes in NOx and HC emissions throughout the testing. As expected from the increase in peak burn rates, nitrous oxide emissions increase significantly while unburned hydrocarbon emissions decrease. It is speculated that the deposits on the chamber walls raise instantaneous wall temperatures enough to reduce the 'flame' quenching near the wall and in the crevices. The trend of carbon monoxide emissions follows that of HC emissions. There were essentially no smoke emissions throughout the test.

Figure 4.4 shows the results of cycle heat release analysis performed on the pressure data throughout the 40 hours. They are very consistent with combustion performance results. Starting from the clean case, heat release rates increase in a gradual manner during the first 30 hours of operation. Ignition timing is advancing, although not very rapidly, and duration of heat release is shortening. In summary, peak heat release rates increase from about 18 joules per crank angle to about 27, a roughly 50% increase.

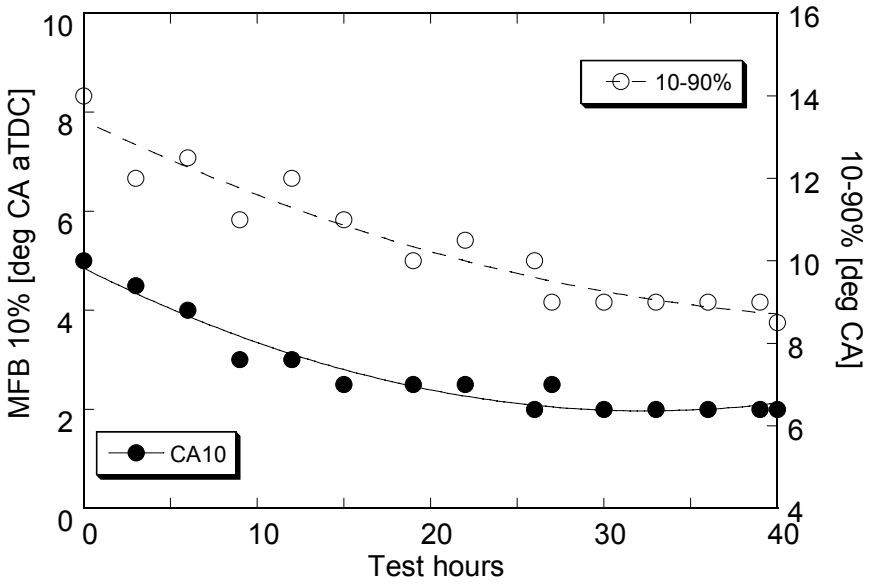

Figure 4.1 – Evolution of 10-90% Burn Duration and Ignition Timing

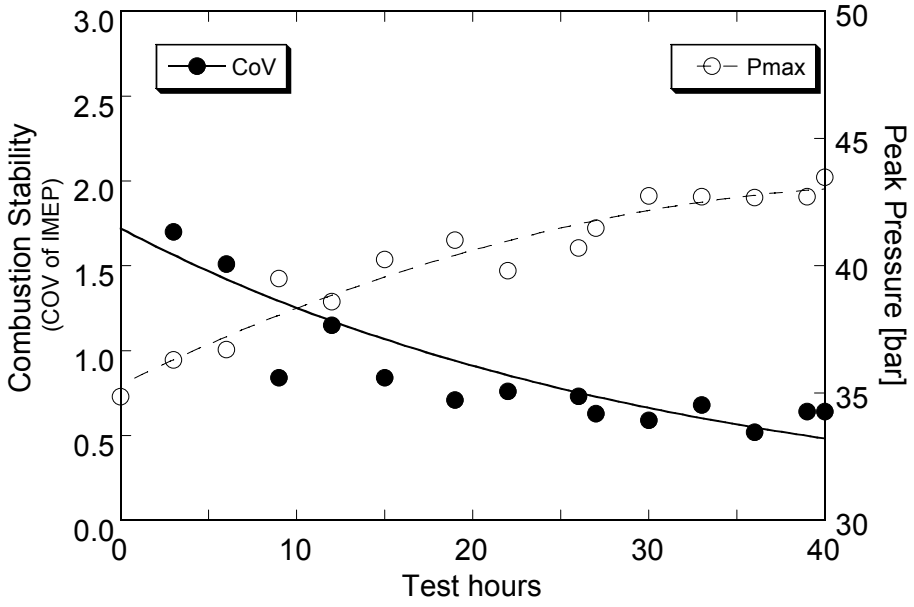

Figure 4.2 – Evolution of Combustion Stability and Peak Cycle Cylinder Pressure

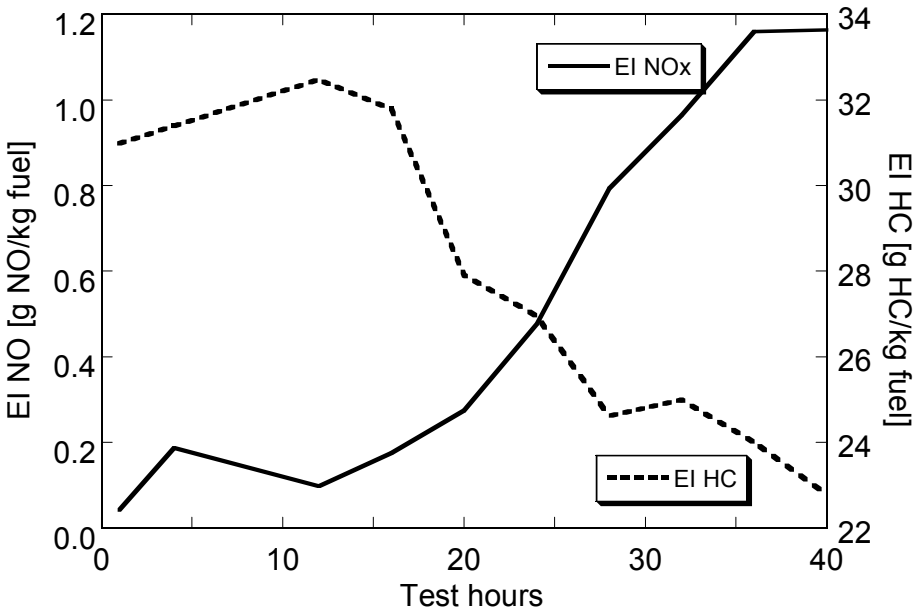

Figure 4.3 – Evolution of NOx and HC Emissions Indexes

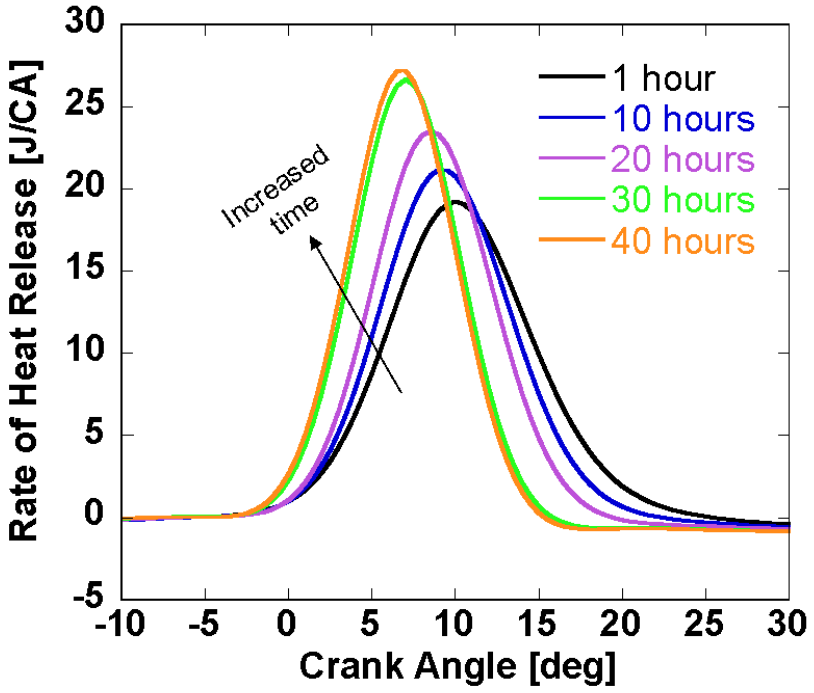

Figure 4.4 – Evolution of Heat Release Rates during the 40 hour conditioning test at 10 hours intervals

It is worth pointing out that while the formation of a CCD layer on the surfaces of the combustion chamber will reduce the clearance volume and thus increase the effective compression ratio, this is not nearly enough to account for the changes in burn rates observed during these tests. Based on sample deposit layer thickness measurements taken from this engine, calculations indicate that even the most extensive degree of deposit coverage in the chamber would only increase the compression ratio a negligible amount.

4.4 Analogy of CCD effects with other thermal parameters

4.4.1 HCCI sensitivity to thermal conditions

A unique way of extracting insight about the nature of thermal effects, including deposits, on combustion is to examine the spread of individual cycles at different operating instances. When measurements are taken at a particular operating point, 100 successive cycles are typically recorded. As has been done in the previous sections, it is common to only look at the average of all cycles. However, assessing the spread of individual cycles reveals trends that are otherwise lost after averaging. An assessment of the characteristics of individual cycles is the basis for this section on HCCI thermal effects.

There have been several experimental as well as numerical studies focused at understanding the sensitivity of HCCI to thermal conditions, some of which were already mentioned in Chapter 1 [27,43,94,100]. Sensitivity of HCCI combustion parameters and local heat flux to variations in both coolant and intake temperature investigated by Chang et al. [7] is of particular interest for the present study. Specifically, the nature of changes in near wall thermal conditions versus core gas temperatures was compared. Just five degree changes in each (coolant and intake temperatures) have a significant influence on both ignition and phasing. However, the nature of the impact of intake charge temperature vs. coolant (wall) temperature is very different. As taken from a *clean* engine

and seen in Figure 4.5, examining individual cycles shows a very close correlation between burn duration and ignition timing, when intake temperature is varied. The high coefficient of correlation (R^2=0.92) confirms that all cycles follow the trend closely throughout the range of intake temperatures. The same was reported by Sjöberg et al. [11]. In contrast, Figure 4.6 shows stratified layering of data points corresponding to different coolant temperatures, i.e. the increasing coolant temperature causes burn duration to decrease more than what would be expected strictly from changes in ignition phasing. The resulting coefficient of correlation for all points is much lower (R^2=0.722). These differences illustrate the special nature of the wall temperature effect on the total heat release event. While intake temperature has direct impact on core gas temperature and thus ignition, the coolant temperature variations affect near-wall regions and bulk burning (50-90% MFB). In this light, it seems that CCD could potentially have high a impact on bulk burning as well, due to their effect on dynamic variations of surface thermal conditions.

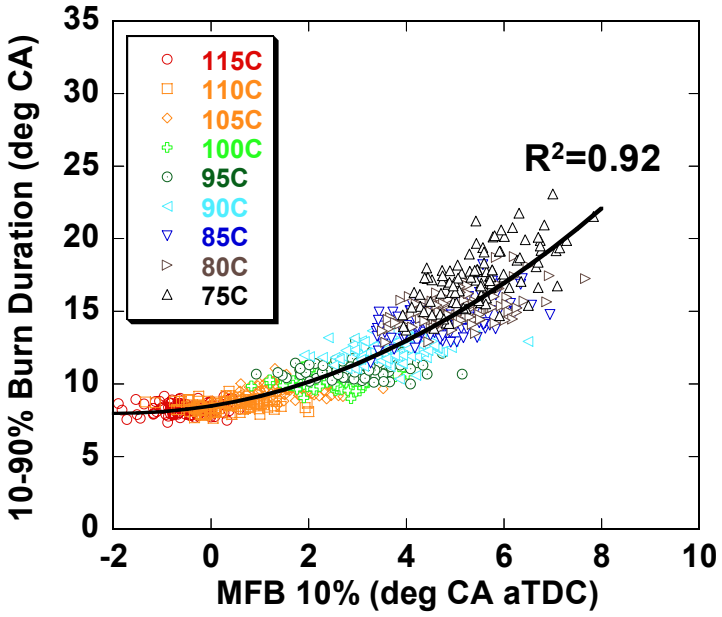

Figure 4.5 – Burn Duration versus ignition timing at varying intake charge temperatures, individual cycles [7]

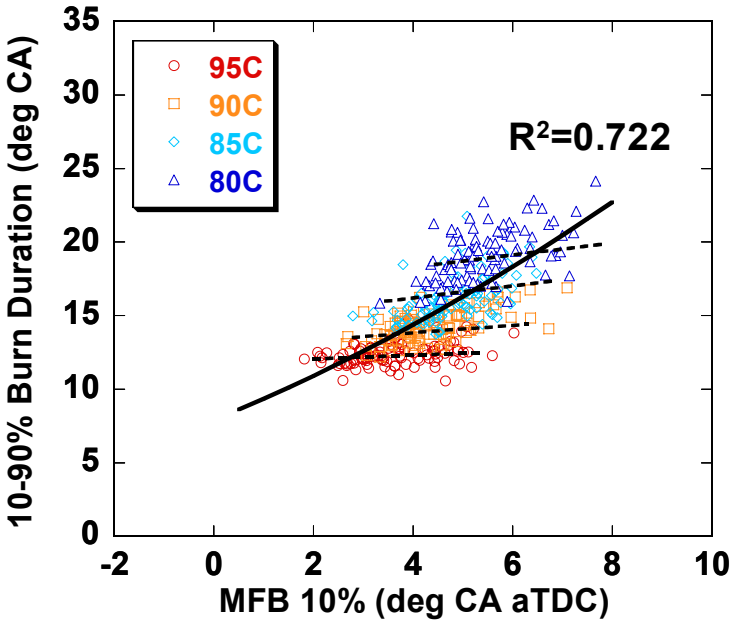

Figure 4.6 – Burn duration versus ignition timing at varying coolant temperatures, individual cycles [7]

4.4.2 Comparison of Effects of CCD to Intake and Coolant Temperature

Figure 4.7 shows scatter plots of 10-90% burn duration versus 10% MFB, at different intervals of conditioning throughout the 40 hour test. It can be seen that each set of points obtained at ten hour intervals moves to the left and down, thus indicating an advance in ignition timing and an increase in the rate of burning. However, the correlation between the ignition timing and burn duration is relatively weak, just as it was in the case of varying wall temperature. The distribution of points around the regression line and the calculated coefficient of correlation resemble results in Figure 4.6. The implication of this is that again the reduction of burn duration is not just a function of advancing ignition. In summary, CCD affect ignition due to the variations in heat transfer during intake/compression, but also produce an additional strong effect on bulk burning due to altered near-wall boundary conditions, surface temperature, and heat flux.

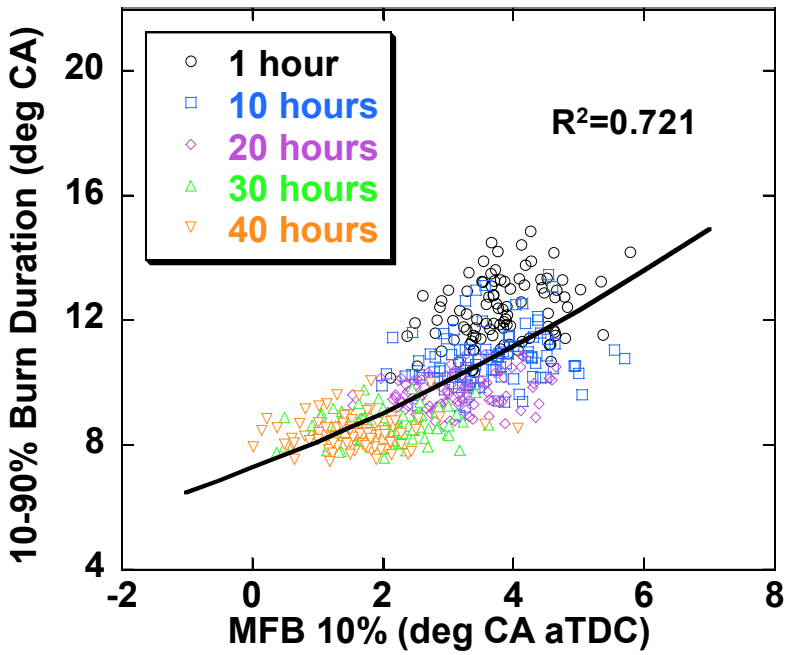

Figure 4.7 – Correlation between 10-90% Burn Duration and Ignition (MFB 10%) measurements obtained at 10 hour intervals. Every set of points contains 100 cycles

4.5 Quantification of Deposit Formation Levels

Using the Fischer Dualscope, detailed measurements of CCD thicknesses were taken at multiple locations on the piston and head surfaces after completion of passive conditioning. The measured values in *micrometers* are indicated on photographs of the piston top and the cylinder head shown in Figure 4.8 and Figure 4.9, respectively. Photos allow detection of spray direction, since impinging fuel cleans the piston bowl and the edge of one of the intake valves. The highest thicknesses are seen around the periphery, since this is where average temperatures are lower, promoting accelerated CCD formation. In particular, the thickest deposit layer is found on the edge of the piston bowl. As the fuel film forms and moves towards the bowl's edge it cools these surfaces and provides plenty of fuel in liquid form for the bowl lip. The surfaces of all four valves are virtually clean. The temperatures on these surfaces appear to be higher than the maximum for any CCD layer to form.

Another significant point is that the piston bowl remained almost completely clean. This is obviously due to washing from the fuel spray. These types of qualitative findings are confirmed by Cheng [62] and other works [101,102], where some points are made regarding direct injection gasoline engines and mixture formation peculiarities as a result of injector spray patterns.

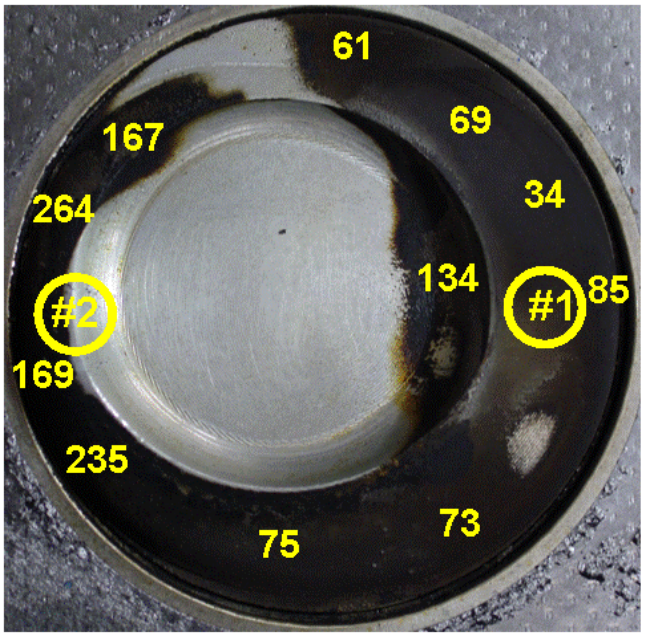

Figure 4.8 – Deposit layer thicknesses [µm] on piston after 40 hours of testing

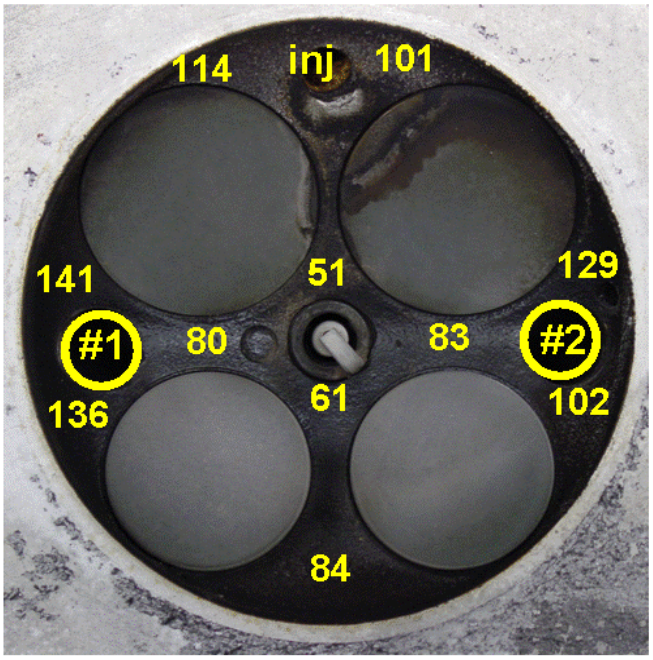

Figure 4.9 – Deposit layer thicknesses [µm] on the head surface after 40 hours of testing

4.6 Chapter Summary and Conclusions

For this testing, the engine was operated over an extended period of time to allow the buildup of deposits and assessment of their effect on HCCI combustion. Burn rates became significantly faster as the test progressed. Thus the main combustion event in an HCCI engine is very sensitive to the presence of a deposit layer on the combustion chamber surface. Full conditioning of combustion chamber walls was achieved in forty hours, as there were no further variations of combustion after that period of time. Peak heat release rates increased 50% by the end of conditioning.

The analysis of individual cycles recorded during the combustion chamber was used to explore the nature of the CCD effect on HCCI combustion. When a correlation between ignition timing and burn duration is examined for a large number of cycles, groups of points corresponding to different instants in the test are staggered, suggesting that burn rates change more than what would be expected based solely on ignition phasing. This is in contrast to the effect of increased intake temperatures, where the correlation between ignition timing and combustion duration is very strong. This leads to a conclusion that deposits affect bulk burning near the wall more than the core gas temperature at the end of compression. Consequently, the thermal capacity of deposits and temperature swings at the surface are potentially more relevant than global reduction of heat loss due to their insulating characteristics.

Even though deposit formation rates stabilized after 40 hours for this testing it is not to say that it would have not been possible for further deposit formation to occur. At other operating points, likely lower load points, with varying injection timings and amounts, with different coolant controlled wall temperatures; it is likely that further increase of deposits coverage would occur. Conversely, it is also possible that CCD levels in the engine could decrease at a higher load or wall temperatures, in affect burn off deposit material.

With that said, it is possible that CCD levels stabilized not only because of higher peak wall temperatures but also because of the changes incurred in combustion. As the test progressed, burn rates increased, resulting in higher peak cycle gas temperatures. This served as an additional factor influencing deposit formation along with the changing thermal conditions on the chamber walls. Compared to HCCI, the effect on heat release rates in SI and CI engines is much less, as demonstrated in this chapter. In the case of those engines, deposit formation rates eventually decrease solely from wall temperatures effects due to CCD insulation. This is a much different problem for HCCI compared to SI and CI because there is such as strong coupling between the formation of CCD and overall combustion characteristics.

Regardless, it is difficult to attribute the stabilization of deposits levels solely to wall temperature effects. As found by many before, including Nakic et al. [60], the minimum surface temperature to prevent deposit formation is about 310°C. There is no chance that the deposits layer surfaces are reaching that high of a temperature even after 40 hours of testing (this will be confirmed). There are other additional factors to consider. This engine operates with high levels of residual, about 45%, and at very lean air to fuel mixtures. Combine these facts with the stronger combustion as a function of CCD formation and it is highly likely that deposit growth will be limited, *at this operating point.*

What is important to take away from this testing is the thermal nature of the effect of deposits on HCCI. Also, that there is clearly a very strong coupling between combustion and deposit affected wall temperatures. How the deposits form and at what rate are only secondary to what implications they have on HCCI operation. In a practical dual-mode engine, it is likely that more CCD will form during the SI portion of operation than HCCI, due to the higher fueling rates and the likelihood of cold starts occurring under SI operation. But once transition to HCCI mode occurs, combustion will be affected by the present in-cylinder deposits. Regardless, the influence on HCCI burn rates

is much greater than ever encountered before with other typical modes of operation. It is enough of an effect that control schemes would have to be implemented in order to compensate.

This test was run over 40 hours, but that is not to say the effect of deposits will evolve and change over only long-term operation only. In just minutes, from a cold start, transitioning to high load highway operation, back to stop and go city traffic driving, the relative magnitudes of deposit levels can vary greatly. Thus the effects will have to be compensated for on the same order time scale.

CHAPTER 5

THERMAL PROPERTIES OF CCD

5.1 Introduction

Heat transfer is critical for all forms of internal combustion. It has a significant impact on gas exchange and filling of a cylinder with fresh charge, on the conditions at the end of compression but prior to ignition, on combustion and emissions formation, and finally there is a cumulative effect on heat rejection and thermal efficiency. As shown by Chang et al. [7] the effect on ignition/combustion is more profound in the case of an HCCI engine. For decades there have been numerous investigations aimed at accurately characterizing the physics behind heat transfer in engines, many of which have relied heavily on experimental work to understand details of in-cylinder processes, like Enomoto [87,103], Cho [96], Alkidas [97,104], and Hayes [105]. Developing fundamental insight and a large amount of experimental data enabled capturing of relevant physics with empirical models. Some fundamental work has been aimed at developing empirical models which represent the relevant physics, such as Woschni [64], Chang [94], Annand [106], and Hohenberg [107]. The experimental techniques typically rely on *instantaneous* combustion chamber surface measurements, similar to those used for this work.

Understanding the mechanisms responsible for the strong impact of deposits on HCCI combustion requires additional information about in-cylinder processes. This chapter provides insight into the effect that deposits have on chamber surface temperature

and heat flux. It is these changes that will ultimately characterize the direct thermal influence on ignition and combustion. While physical effects imparted by the deposit layer's rough, porous surface may be present as well, they are expected to be secondary to thermal effects [62,66,71,73].

5.1.1 Focus of this chapter

There are three main objectives of this chapter. The first is to characterize the effect of local deposit formation on in-cylinder temperature and heat flux measurements. This includes understanding the effect of increasing deposit thickness and potential changes in the CCD layer thermal properties on heat transfer. In this case, it will be shown there is a strong correlation between measured temperature phasing and deposit layer thickness. Furthermore, it turns out that it will be possible in the future to use instantaneous temperature measurements to track local CCD growth rates 'in-situ'.

The second objective is the development of a methodology to simulate the long-term deposit conditioning procedure from Chapter 4 in a shorter engine operating time. The previous 'passive conditioning' procedure required 40 hours to stabilize deposit formation levels in the engine. For future testing it would be impractical to repeat this every time. Therefore an 'aggressive conditioning' procedure was developed which consists of a particular set of operating points and engine parameters. With these settings, in just two hours a chamber is coated with 'deposits', and 'conditioning' is reproduced with almost the same effects on HCCI combustion as with the previous 40 hour test. Of course, it is of primary importance to confirm that the effects of these 'deposits' on measured temperature, heat flux, and combustion match those of naturally formed (or passively formed) deposits.

The third objective is to extend the analysis of the measured temperature profile below the CCD layer in order to calculate thermal properties of the deposit material itself.

Specifically, it is possible to determine the effective thermal diffusivity value of the deposit layer as a function of thickness, based on variations of the measured instantaneous temperature profile.

This chapter begins with discussion of initial measurements to demonstrate the capabilities of the fast-response heat flux measurements. Then previous work relevant for utilization of thermal measurements for deposits characterization is reviewed. Following this, measurements taken with the probes underneath the growing CCD layer are shown, followed by the analysis of the relationship found between deposit growth levels and characteristics of instantaneous temperature profiles. The accelerated 'aggressive conditioning' method to simulate long-term deposit formation is explained next, followed by a comparison of the effect of natural 'passive' deposits and 'aggressive' deposits on measured instantaneous chamber temperatures. The findings are subsequently used to develop the method for calculating the thermal diffusivity of the deposit layer.

5.2 Sample Instantaneous Surface Temperature and Heat Flux Measurements

In this section sample surface temperature and heat flux measurements taken in a clean engine are shown in order to examine their general characteristics. The piston and head surface probes used in this investigation are referred to as *fast-response thermocouples* or *heat flux probes* interchangeably throughout the text.

This section contains some sample temperature and heat flux measurements taken from all of the piston and head locations in the chamber. In Figure 5.1 and Figure 5.2, temperature and heat flux measurements taken from all the head and piston thermocouple (TC) locations in the engine are shown, while Figure 5.3 provides an illustration of the thermocouple probe locations on the piston. These are taken with a clean chamber at the baseline operating point of 2000 rpm, 11 mg fuel per cycle, and an air to fuel ratio of 20:1. A review of the methods required to calculate heat flux through the wall of the

combustion chamber based temperature measurements was given in Chapter 3. Due to degradation of the signal wires for piston probes P2 and P3, results pertaining to those two locations are excluded.

In general, measured wall temperatures are much lower than those typically measured in an SI engine [96,97,104] due to the overall lower combustion temperatures from HCCI combustion. All piston temperatures are at least 5° higher than those in the head, due to the direct influence of coolant on the head surfaces. This is confirmed by the higher peak heat flux levels from the two head probes. Furthermore, the temperatures at locations in the piston bowl are, in general, higher than those on the periphery of the piston due to their proximity to the main combustion event and a longer path for heat conduction through the piston crown. It is quite evident from both the temperature and heat flux profiles that, due to its location at the front of the piston bowl and close to the injector tip, probe P7 is directly affected by the fuel spray early in the intake stroke, as is probe P1 to a lesser degree. A dip of the signal right after TDC intake (~-300 deg CA) is clear indication of intense cooling due to impinging high pressure spray.

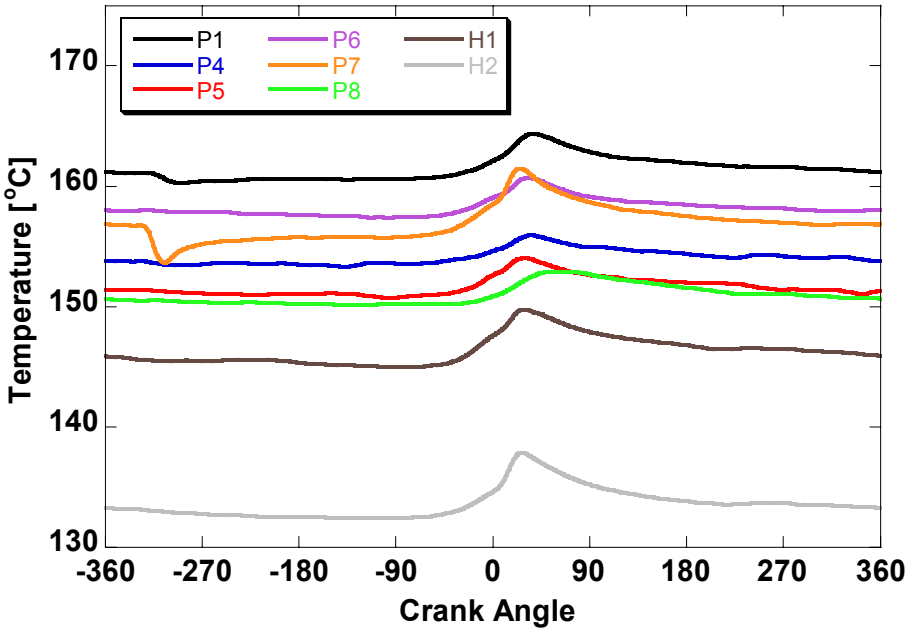

Figure 5.1 – A plot of sample temperature measurements taken from locations in the piston and head. The operating point is at 2000 rpm, 11mg fuel/cycle, A/F 20:1

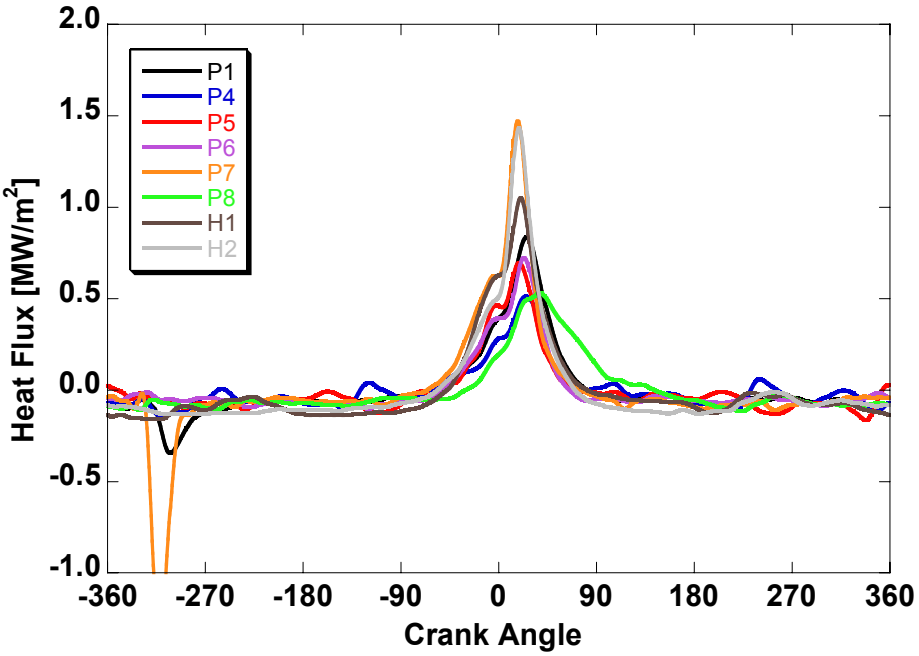

Figure 5.2 – A plot of sample heat fluxes taken from locations in the piston and head. The operating point is at 2000 rpm, 11mg fuel/cycle, A/F 20:1

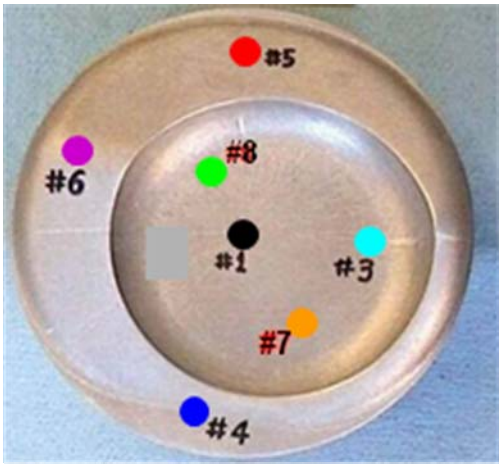

Figure 5.3 – Heat Flux Probe locations in Instrumented Piston

5.3 Background

The ability to measure instantaneous combustion chamber surface temperature is a critical dimension to this investigation. In previous investigations, similar thermocouple probes have been used to characterize the heat transfer characteristics and thermal sensitivity of this engine under HCCI operating conditions [7,58,94]. Objectives of this investigation dictate focus on the changes of instantaneous surface temperature profiles on the metal surface due to the deposits being accumulated on top of the TC junctions. Since the probes located in the head are removable, they also serve as coupons for measuring deposit thicknesses at regular intervals during combustion chamber conditioning. As mentioned previously, the probes consist of a coaxial type junction and were selected for this work because of their accuracy and reliability demonstrated from the previous heat transfer studies performed on the same engine [58,96]. As will be shown in this chapter, instantaneous temperature measurements not only allow characterization of in-cylinder thermal effects, but can also provide significant insight into combustion chamber deposit formation and properties.

Overbye et al. [68] were one of the first to perform an extensive characterization of the effects of combustion chamber deposits on in-cylinder temperature measurements in an SI engine. They relied on fast-response thermocouples, similar to those used in this work, to take surface temperature measurements at three locations in the chamber of a CFR engine, using various types of fuels. The probes used consisted of a vacuum deposited junction at its surface, flush with the combustion chamber wall. A backside junction on the coolant side wall surface provided a backside steady temperature profile for heat flux calculations. The total work was split into measurements taken with a clean engine and those taken with deposit material covering the thermocouple junctions. With a clean engine, the cycle total temperature swing versus pressure swing was analyzed across different operating points. The surface temperature profiles from the thermocouples at each location in the chamber were compared. Finally, the authors attempted to develop an empirical heat transfer correlation, *h*, based on their measurements, but found it difficult to develop one that was accurate across a broad range of operating conditions.

The section of work regarding CCD consisted of the investigation of various measureable parameters that could be correlated to deposit formation levels over the thermocouples. Some of these parameters included the changing slope of the measured temperature curve at the time of flame front arrival, cycle total temperature swing, time-averaged temperature, and phase shift of the temperature profile. Finally, the same set of measurements was used to determine deposit thermal properties. One-dimensional thermal circuit analysis was used to obtain a thermal conductivity, based on cycle averaged gas and wall temperatures below the deposit layer. Thermal diffusivity of the layer was estimated based on transient temperature measurements and measurement of the deposit thickness under a microscope. The calculated values for the deposit thermal conductivity and diffusivity, respectively, were 0.1 to 0.38 W/mK and 1.5e-6 m^2/s.

Some of these methods were attempted with the data collected in this work; however there were issues with some of the results. They require several assumptions regarding the boundary conditions used for the calculations, including gas temperatures and global convection coefficients for the entire cycle. Also, the results turned out to be very sensitive to the accuracy of average temperature measurements and deposit layer thicknesses. Thus, it is very difficult to get consistent deposit properties using these methods.

Anderson [69] combined radiometric measurements in an engine with optical access to obtain deposit surface temperatures. A 2-stroke single cylinder gasoline SI engine was instrumented with a fast response thermocouple, with both surface and backside junction. It was mounted in the head at a location directly opposite the port for optical access. A radiometer was designed which could provide accurate deposit surface temperature based on infrared radiation. Great effort was made to ensure minimal interference at the wavelengths used from the combustion reactants/products in the relevant temperature range. Steady deposit surface temperature radiometric measurements were combined with average deposit/wall interface temperatures to calculate the CCD thermal conductivity. The thermal diffusivity could not be calculated with transient measurements during firing operation because of excessive interference. Instead, after firing at steady conditions, ignition was cut and the transient decay response of the thermocouple temperature measurement over a few cycles was tracked. Numerical methods were then used to calculate an effective diffusivity, based on one-dimensional transient heat diffusion.

Infrared measurements indicated that maximum temperature swings at the deposit surface were nearly 200 K compared to about 15 K in a clean engine. Calculated deposit thermal conductivities ranged from 0.38 to 0.5 W/mK and thermal diffusivity is ~0.3e-7 m^2/s. Subsequent work focused on similar measurements to study deposit layer heat flux dynamics as a function of variable thermal conductivity [71]. It was found that not only

do the properties change as the thickness changes, but they change in a non-linear manner, such that their effect on unsteady heat transfer is quite significant. Additionally the porous volumes found in the material presented the potential for intra-material heat transfer through convection and radiation, which complicates the ability to fully understand the heat transfer mechanisms and the dynamic behavior of the CCD layer.

Hayes [73] utilized laser-pulse techniques to determine CCD thermal properties in a spark-ignition engine. His work was related to the octane requirement increase (ORI) associated with deposit formation in engines. After a period of forming deposits over fast-response thermocouples mounted in the chamber surface over 250 hour tests, the probes were removed from the engine. To determine the thermal diffusivity, a laser pulse was applied to the deposit surface while front and backside temperatures measurements (from beneath the deposit layer) were compared to the analytically calculated temperature profile on a clean probe. Steady laser illumination was used to calculate thermal properties. Tracking the time-averaged measured front and backside junction temperatures as the deposit layer was heated by the laser provided a thermal conductivity. The gradual increase in temperatures allowed calculation of the diffusivity, similarly to the methods used previously by Anderson, where decaying temperatures where tracked in an engine after the ignition is cut. Calculated CCD thermal diffusivity ranged from ~0.6e-7 to 4e-7 m^2/s and thermal conductivity from 0.14 to 1.0 W/mK. The properties calculated for the deposit, combined with measured thicknesses, were utilized in a two-zone cycle simulation and a knock model by Douaud and Eyzat [108]. Compared to the case of a clean combustion chamber, the calculations were able to determine the potential octane requirement increase with different fuels, due to the effect of deposits in the end gas region.

The results obtained by the last two researchers are very useful and the methods used were very thorough. However the setups used, specifically providing optical access to the combustion chamber and the utilization of laser diagnostics, is not practical to

implement. One goal of the current work is to develop methodologies and measurable correlations that are practical and easier to implement.

Hopwood et al. [72] developed a technique to calculate the deposit layer thermal diffusivity based on the decay of the temperature signal measured below the deposit layer. Their approach provides a foundation for the work presented in this chapter. Modifications were necessary to address the specific goals of the HCCI study. All previous investigations were carried out in SI engines, and they suggested CCD properties varying in a wide range. The goal here is to fully characterize CCD's formed in the HCCI engine and determine the CCD properties relevant for gasoline HCCI operation.

5.4 Experimental Results from Head Mounted Heat Flux Probes

Due to the length of the test, for the 40 hour passive conditioning, only the two head mounted heat flux probes were utilized; the wiring for the instrumented piston would likely not last that long. The head probes were extremely useful for tracking the effect of a CCD layer over time. It is critical to note that the heat flux probes in this engine are mounted flush with the metal surface of the combustion chamber. As deposits grow, they form a thermal barrier on top of the probe. Therefore, measurements do not reflect conditions at the gas-surface interface; rather they are indicative of conditions below the deposit layer, as depicted in Figure 5.4. This enables characterizing the effect of CCD on heat transfer and subsequent evaluation of deposit properties.

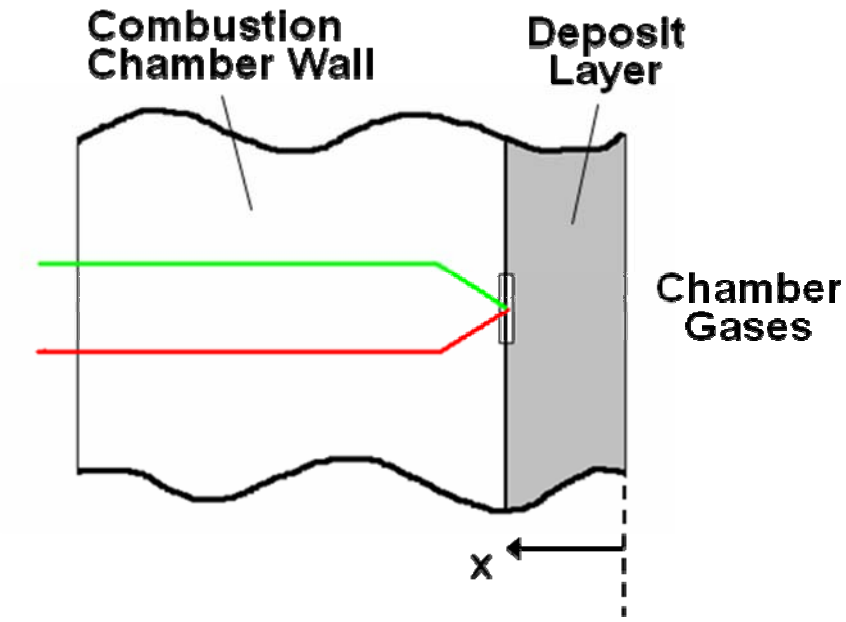

Figure 5.4 – As the deposit layer thickens, the thermocouple junction gradually becomes shielded from the combustion chamber gases

5.4.1 Surface Temperature and Heat Flux Evolution

Figure 5.5 shows a plot of the measured temperature profile at head location #2, shown at ten hour intervals throughout the passive conditioning tests. Therefore this plot characterizes variations of a temperature profile below a gradually thickening deposit layer. As the deposit layer grows, the fast response surface thermocouple is being insulated from the high temperatures of combustion, as depicted in Figure 5.4. This causes a slight decrease in the measured cycle average temperature. The degree of average temperature decrease is limited because as deposits form, higher peak combustion rates intensify the heat flux at the gas-deposit interface and offset the influence of the deposit layer. Perhaps more importantly, the shape of the temperature swing changes, particularly during the heat release portion of the cycle. The overall phasing of the temperature profile becomes retarded as the test progresses. These characteristic changes are consistent with findings by other researchers [71,72], except

for the additional effect of CCD on burn rates in HCCI that is not present in conventional engines.

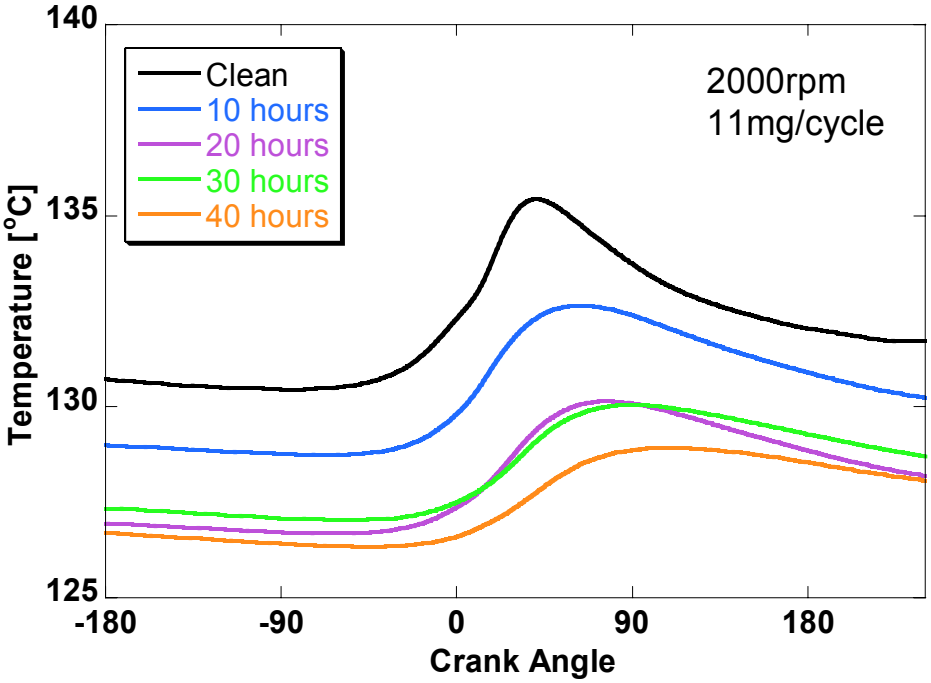

Figure 5.5 – Evolution of measured temperature profile at CCD/metal interface as the deposit thickness increases throughout the 40 hour passive conditioning test

The calculated heat flux profiles at the same location are shown in Figure 5.6. At the beginning of the test, it is easy to see the heat flux profile phasing closely follows heat release in the chamber. As hours accumulate and deposit material thickens, the peak measured levels decrease and the phasing becomes more and more retarded. Again, the relative change in phasing is even greater than the graph indicates, since burn rates accelerated significantly as the chamber was conditioned.

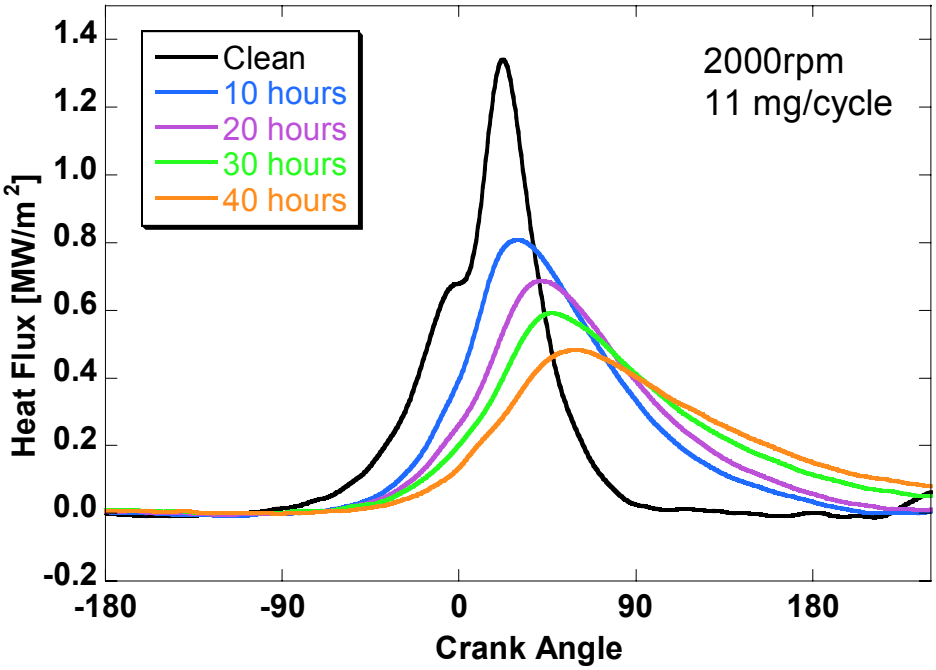

Figure 5.6 - Evolution of measured heat flux profile at CCD/metal interface as the deposit thickness increases throughout the 40 hour passive conditioning test

There is one other interesting finding regarding the cumulative effect of heat flux changes. Figure 5.7 shows a bar graph of the cycle integrated heat fluxes plotted in Figure 5.6. Considering conservation of energy, it can be assumed that the cycle integrated heat flux, or *heat loss*, at the bottom of the deposit layer, is equal to the heat loss at the surface of the deposit. Interestingly, even though there is a significant decrease in measured peak heat flux levels, the total heat loss at the head location does not change very much over the 40 hours. Ishii et al. had similar findings [63]. As the deposit layer thickened, the measured temperature and heat flux profiles at the wall became smoother and more profiled. But the cycle average temperature and the net heat loss changed little. This will be explored further in later chapters and will help us understand the mechanism responsible for the variation of combustion with CCD growth.

All of the trends described in this section apply to the other head probe as well.

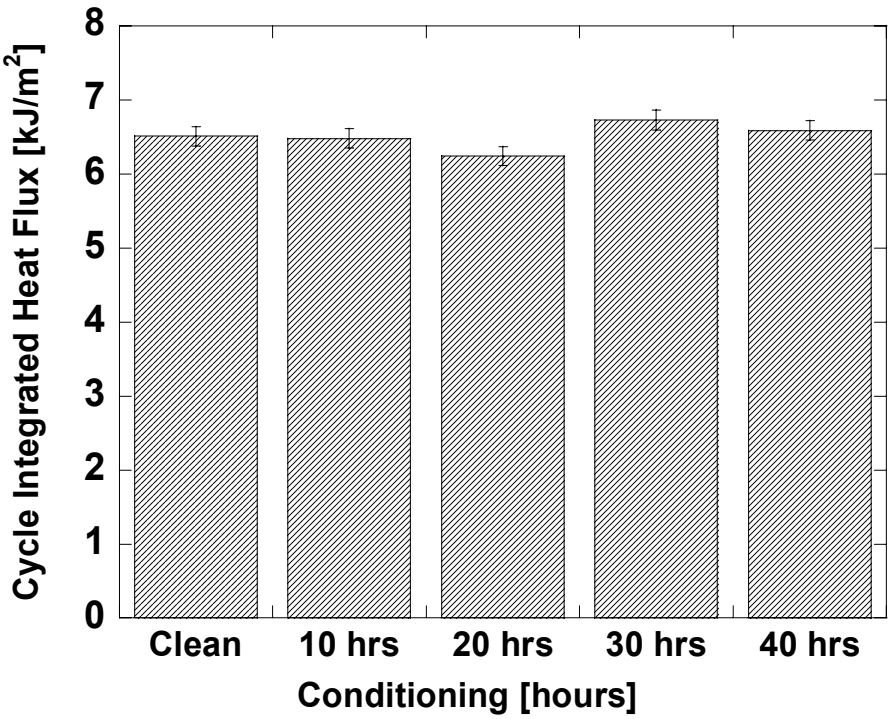

Figure 5.7 – Graph of cycle integrated measured heat flux at head probe location at different intervals during the passive conditioning process

5.4.2 Thermal Characteristics of Naturally Formed CCD's (Passive Conditioning)

As just indicated, there is a strong sensitivity of measured instantaneous surface temperature and heat flux to CCD formed above. So, if a correlation can be established between temperature measurements using fast response TC's and CCD growth, it could be a basis for a technique for in-situ tracking of CCD formation. In other words, deposit thickness could be estimated without stopping the engine and taking it apart. Several parameters were considered, including peak cycle temperature, peak heat flux, cycle integrated heat flux, in addition to parameters tried by previous investigators, such as Overbye [68]. But when applied, they were found to be inconsistent at different locations in the chamber or did not provide enough sensitivity to deposit thickness levels to be useful. It was finally determined that there is a very strong correlation between CCD thickness and peak surface temperature phasing.

Figure 5.8 is a graphical depiction of the phasing variation, $\Delta\Theta_{T\max}$, for the case of 30 hours. This parameter, which is the change in measured cycle peak temperature phasing, is plotted against local CCD layer thickness for both thermocouple locations in the head in Figure 5.9. These are measurements taken throughout the 40 hour passive conditioning test. The heat flux probes in the head were removed at regular intervals and the Fisher Dualscope was used to measure the deposit thickness over the junction.

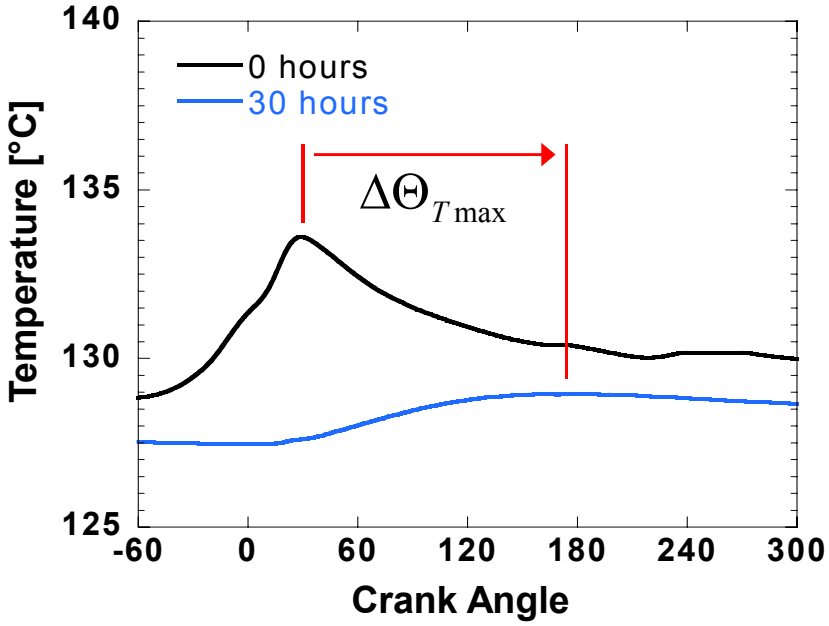

Figure 5.8 - An example measurement of the peak temperature phasing change for the case of the deposit layer after 30 hours of operation

It is clear that the same relationship between phasing change and thickness exists at both head locations. Hence, even though the deposits grow at different rates at two locations, their properties seem to be equally closely correlated with thickness.

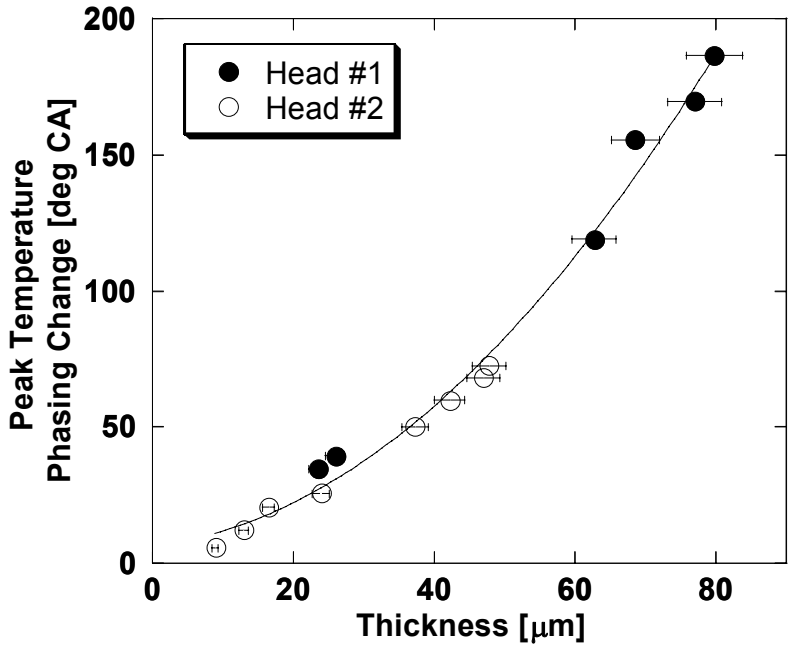

Figure 5.9 – A plot of the change in phasing of cycle peak temperature as the deposit layer thickness over the thermocouple increases.

The physical reasoning for the strong correlation is consistent with the case of the measured temperature profile below any thickening layer, or specifically heat diffusion into a semi-infinite surface. The measured general surface temperature profile is a product of the main heat release event in the combustion chamber. As the deposit grows, or the TC junction gets deeper and deeper below the layer, the time for the heat flux from combustion to propagate towards the junction increases, hence the delay in phasing. It turns out that the slope of the correlation in Figure 5.9 is a function of the thermal properties of the insulating layer. Consequently, the analytical methodology of Hopwood et al. [72] for determining the thermal diffusivity of deposit materials could be applied and will be utilized in the next section. The technique was originally applied to an SI engine, but results shown in Figure 5.9 encourage its application to an HCCI engine as well.

5.5 Aggressive Conditioning

As shown in Chapter 4, 40 hours were required to stabilize deposit formation levels in the HCCI engine at the chosen operating point. Throughout the test, temperature measurements were taken regularly from the two head mounted heat flux probes. This allowed the determination of the correlation shown on Figure 5.9, but does this hold for all locations in the chamber, specifically the piston? We have the capability of additional measurements at several locations in the piston as well, but this requires the use of the mechanical linkage system described in Chapter 2. The problem is that the wires in the linkage would usually wear out and break before the test could be completed; they usually last only about 20 hours. Furthermore, it was determined to be quite impractical to operate the engine for 40 hours every time a conditioned chamber was required, so it was decided that it would be advantageous if a method could be developed to accelerate *conditioning* of the combustion chamber.

5.5.1 Aggressive Conditioning Procedure

After lengthy exploratory experimentation on the engine, an *aggressive conditioning* methodology was devised which allowed us to simulate the 40 hours of passive conditioning in just 2-3 hours, while still running in HCCI mode. This required two main stages: 1) *smoke production* and 2) *stabilization*.

Smoke Production Stage

In the *smoke production* stage, the intent is to operate the engine in such a manner that smoke is produced during combustion, which happens to be quite difficult for an HCCI engine. The basic premise of the HCCI process is that spontaneous reactions in the mixture at multiple locations in the chamber will keep combustion in the low-temperature regime without any rich pocket capable of producing particulate. Hence certain

irregularities had to be intentionally created in order to create smoke. The fuel injector was rotated in such a manner that the offset injector nozzle hole was pointed as directly at the piston as possible, about 90° counter-clockwise from typical conditions, as depicted in Figure 5.10. Injection timing was advanced to SOI 350 bTDC (just after gas exchange TDC) so that the piston was close to the injection spray cone. The final requirement for smoke production is to operate using fuel without Techron additive. As discussed in Chapter 2, an additive made by Chevron-Phillips is normally mixed into our fuel supply in order to keep the injection system clean. It was found that smoke production was achieved easier without this additive in the fuel.

One to two hours of operation in this manner were required before the engine would start producing smoke, but once the smoke started appearing in the exhaust the concentration would slowly increase to peak smoke levels of about BSN 1.5-1.7. The stabilization of smoke levels required about 30 minutes after smoke production first started. During this time, heat release phasing kept advancing significantly due to the insulating effects of the soot/deposit coating the chamber walls. The inspection of the deposit layer, revealed a fluffy, sooty material that easily flaked off. It *did not* physically resemble naturally formed deposit material observed in previous tests.

It is thought that with TDC injection timing and a rotated injector, the fuel spray directly impinges on the piston face, likely pooling. Initially a thin resin-like layer forms (determined from inspection) which serves as a ‘holder’ for successive fuel spray plumes. Gradually a thick enough layer forms and traps fuel on the piston top for a longer time, which results in compositional stratification of charge and some smoke producing combustion, possibly even localized flames.

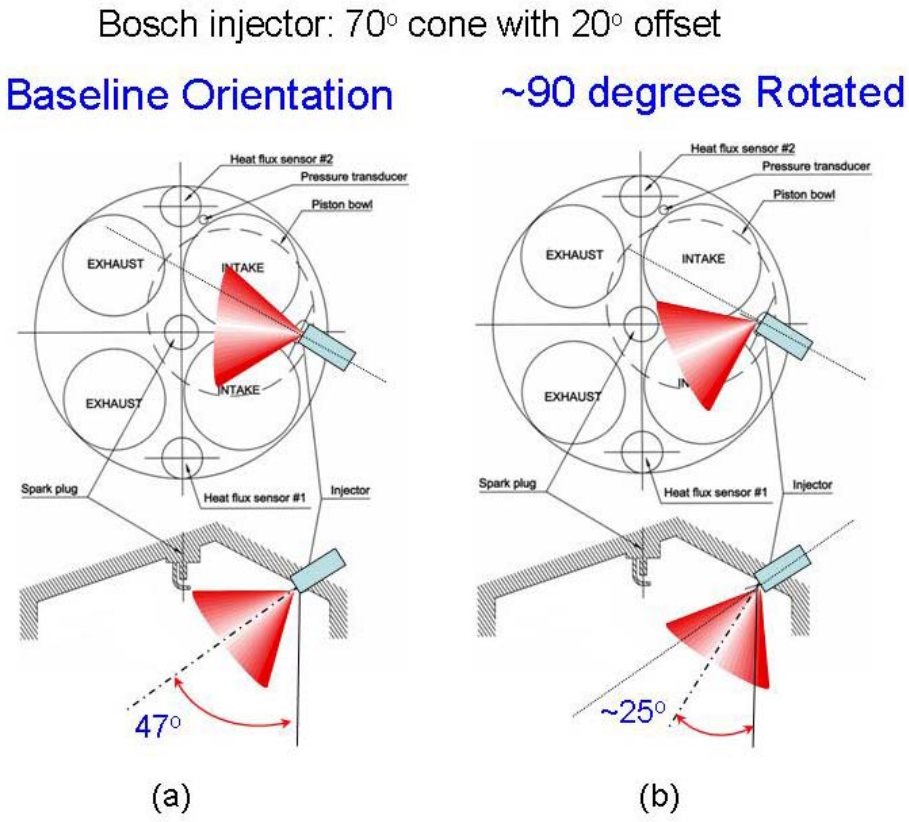

Figure 5.10 – The injector orientation and spray targeting: (a) The baseline orientation of the injector, roughly pointed at the spark plug (b) rotated injector aimed at the piston for maximizing impingement and smoke production.

Stabilization Stage

In the *stabilization* stage of aggressive conditioning the injector is rotated back to its default orientation and the engine is run for about 2 hours at its regular operating point (2000 rpm, 11mg/cycle, SOI 333 bTDC). During this time the sooty material covering the walls is 'baked' into a form that very closely resembles deposit material formed naturally. The complete process, including 'conditioning' and 'stabilization' is qualitatively depicted in Figure 5.11.

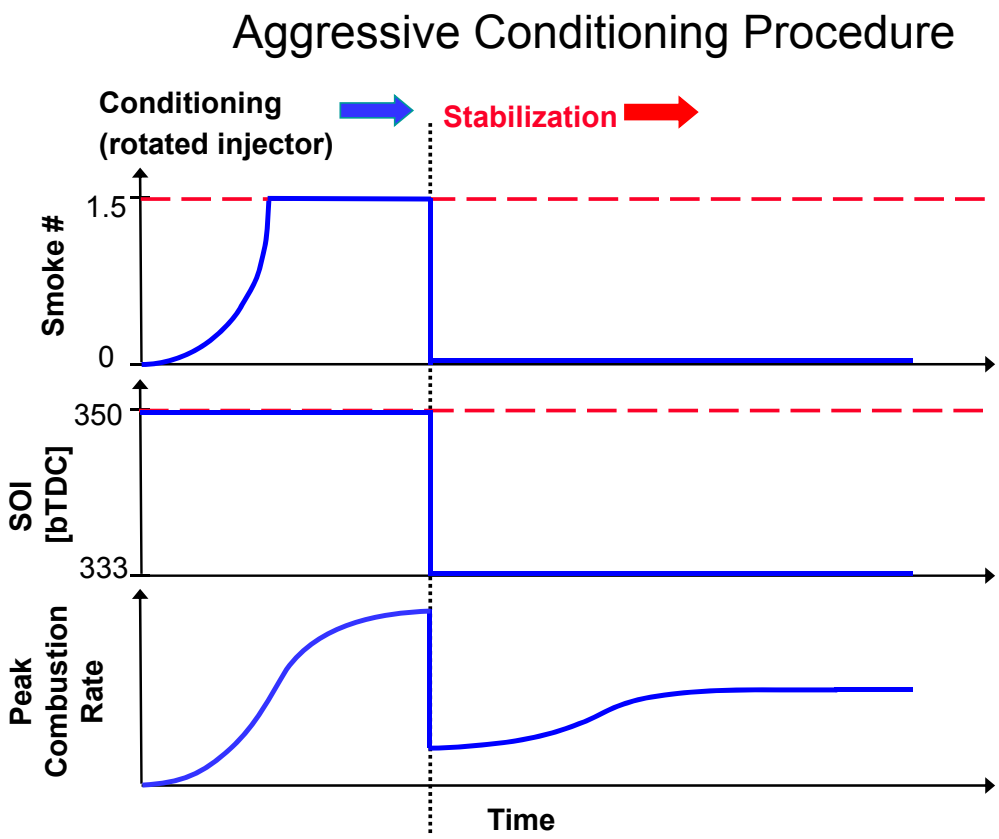

Figure 5.11 – Qualitative illustration of the aggressive conditioning procedure which shows the relative smoke #, injection timing, and combustion rates associated with 'conditioning' and 'stabilization' stages

The advanced burn rates at the end of the stabilization phase resemble those at the end of 40 hours of passive conditioning, as shown in Figure 5.12. Most importantly, Figure 5.13 shows that the correlation between peak temperature phasing change and deposit thickness is maintained for these deposits formed with smoky combustion. The thickness of the deposit layer on the head probes is significantly less than in the passive testing even though the changes in burn rates from a clean engine are similar. This point will be explained in the next section.

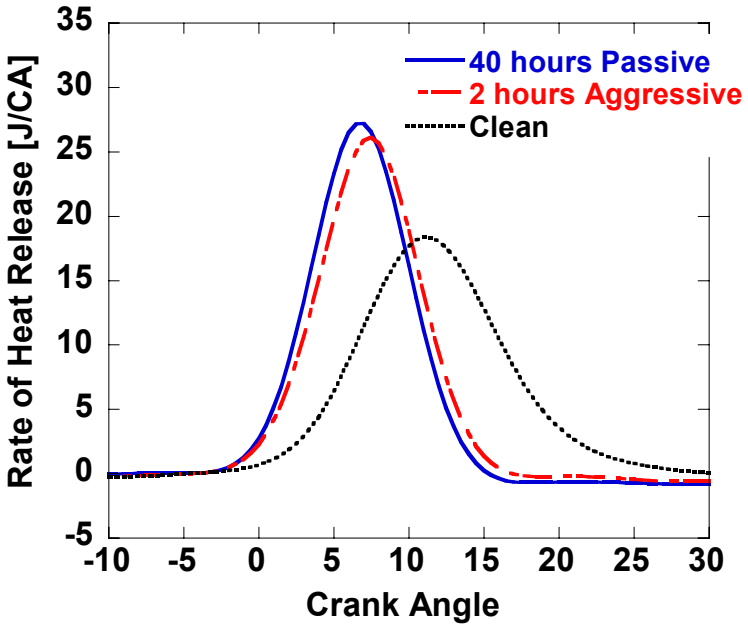

Figure 5.12 – Heat Release Rate changes due to chamber conditioning by two different methods; Passive and Aggressive

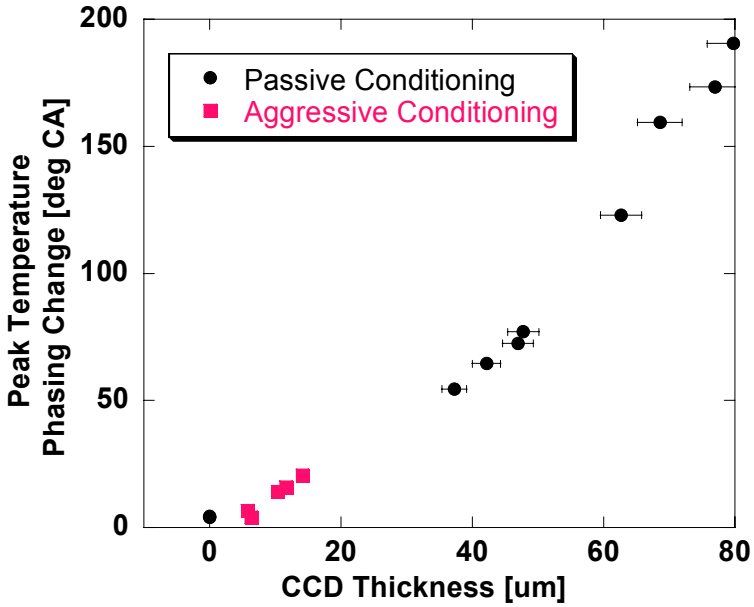

Figure 5.13 – The effect of deposits from both passive and aggressive conditioning on the phasing of measured peak surface temperature

We now have a procedure that can be used to simulate the changes in combustion recorded during our original 40 hour test in a shorter time, so that our instrumented piston measurements can be utilized for studies of CCD formation on the piston top. Again the deposit thickness on the head probes is less than seen before, but total accumulation of CCD material in the engine has resulted in similar combustion changes.

5.5.2 Spatial Variations

Figure 5.13 suggests that there must be differences in the nature of deposit coverage between the passive and aggressive conditioning methods. The thermal effect of the deposit layer on measured temperatures as a function of thickness is the same for the two cases but the actual thicknesses are at the two measured head locations are quite different for the 'fully conditioned' instances achieved with each methodology; less than 20 microns in the aggressive conditioning case, but 50 and 80 microns for the two head probes at the end of 40 hours of passive conditioning. And yet the burn rates were very similar to one another in both instances.

Figure 5.14 shows local CCD thicknesses measured after full 'passive' and 'aggressive' conditioning. The photographs indicate clear differences in the coverage of deposit material on the piston and head surfaces. The main difference is in the coverage on the piston bowl. In the passive conditioning case, the directly injected fuel spray (with Techron additive) keeps the piston bowl mostly clean. In the aggressively conditioned case, deposit coverage is formed from smoke production coating the chamber, so every surface, including the bowl, is covered. The only surfaces that stay clean in both cases are the valves. In the pictures they may look 'dirty' but the thickness of the CCD layer is negligible. This is due to the much higher temperatures that the valves operate at compared to the rest of the chamber.

Another observation is that the local thicknesses tend to be greater in the passive conditioning case than the aggressive case, especially on the head surface. The obvious question is how was the same acceleration of burn rates achieved with thinner coating deposited using the aggressive procedure? It seems that since the total area of coverage of the deposits from aggressive conditioning is greater, and it includes the piston bowl, less deposit material thickness is required to have the same net influence on HCCI combustion. The region of coverage may be important for considering the nature of the effect of deposits on combustion. For example, do deposits in the bowl have the same sort of effect as deposits on the periphery of the chamber? Is there a difference in contribution to the changes in burn rates from the piston and head? These are potentially interesting topics for future work in this field.

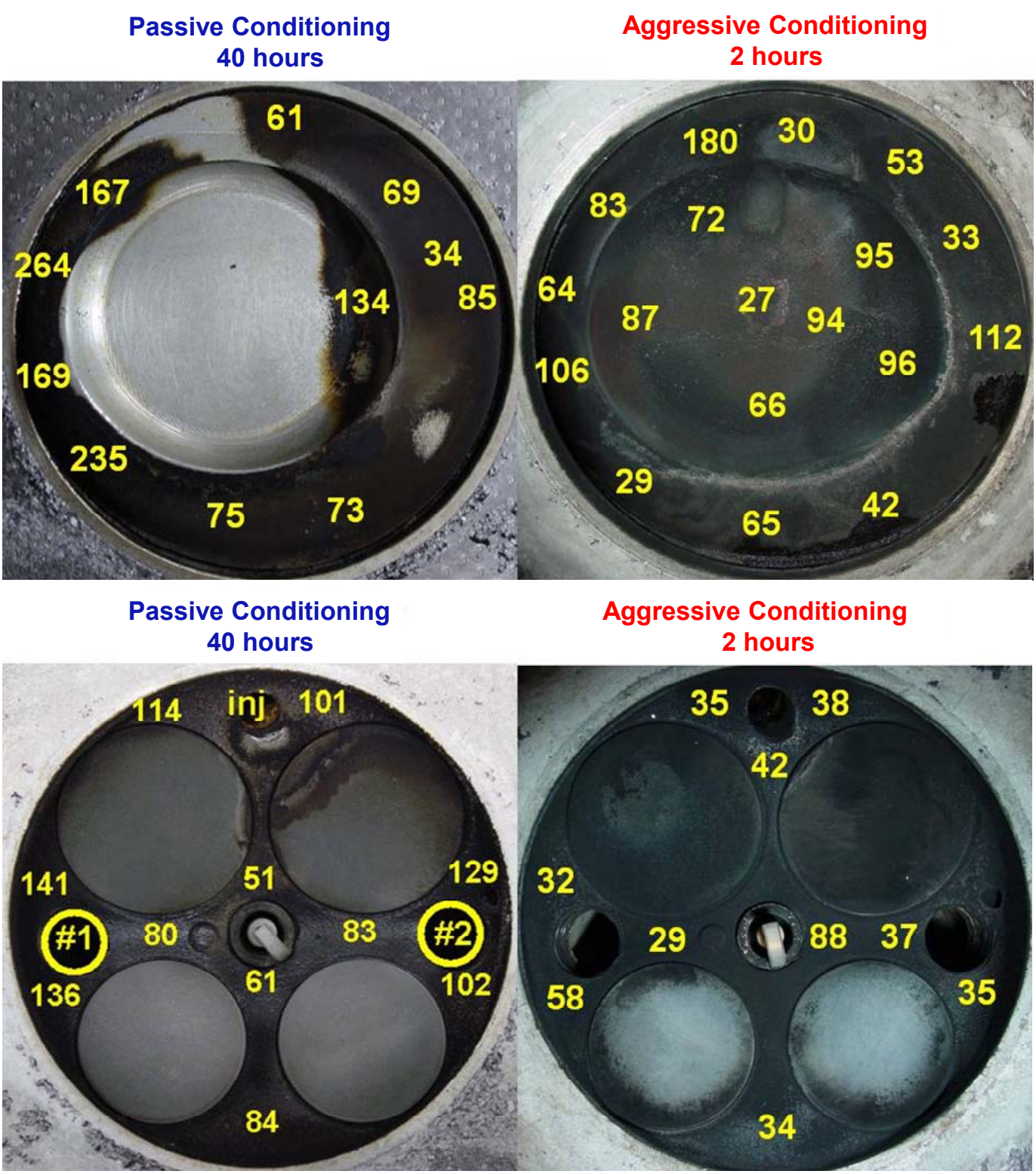

Figure 5.14 – CCD layer thickness on piston and head surfaces measured at the end of passive and aggressive conditoning

5.6 Experimental Results obtained with Piston Mounted Heat Flux Probes

Having developed the aggressive conditioning procedure, it was possible to take temperature measurements on the piston top. This will significantly increase the data set given the six thermocouples mounted on the piston. The aggressive conditioning procedure resulted in the burn rate changes already depicted in Figure 5.12. The burn rates at the end of conditioning achieved with either method match each other closely.

5.6.1 Temperature and Heat Flux measurements

Figure 5.15 and 5.16 show the changes in measured temperatures and heat fluxes at the piston locations in the clean and conditioned cases. The characteristic changes in profiles are consistent with those recorded in the head probes during the 40 hour passive conditioning test. The temperatures indicate a flattening of the profile and a delay in overall phasing. It is important to note that the cycle averaged temperatures at every location are higher by at least 5°C in the conditioned case compared to the clean. Generally speaking, wall temperatures are higher in the conditioned case and this is attributed to the faster observed burn rates observed with deposit coverage. Another point of interest is that the peak heat flux at some locations does not decrease as much as would be expected with a deposit layer. In fact, the peak heat flux at location P5 increases with deposits. This is again attributable to increase burn rates with deposits and a possibility of having a very thin layer of CCD at that location.

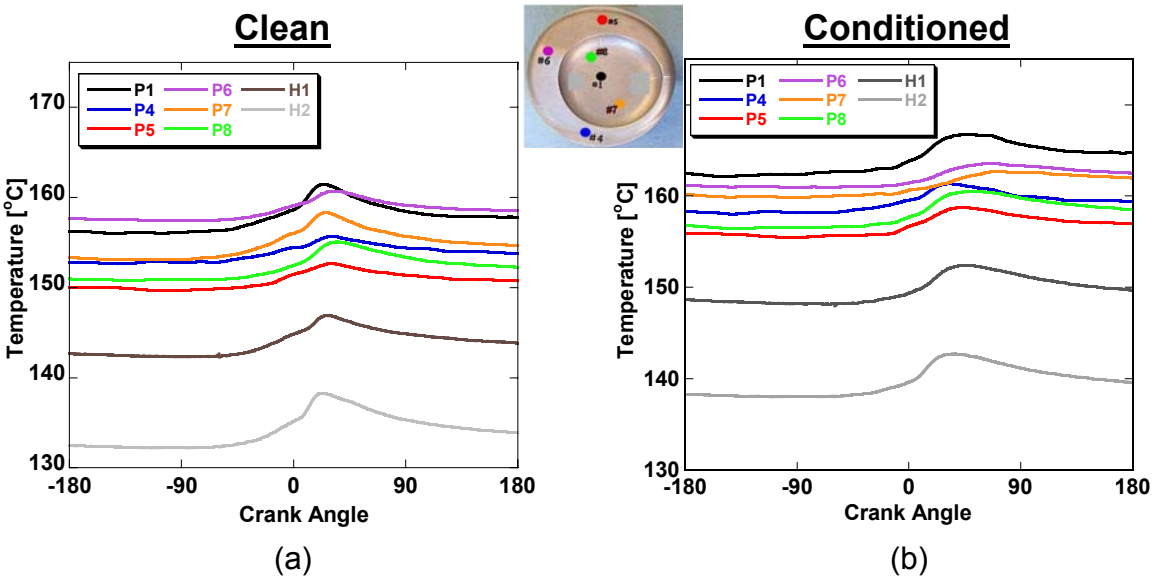

Figure 5.15 – Measured temperature at locations in the piston and head of: a) clean chamber, and b) conditioned chamber.

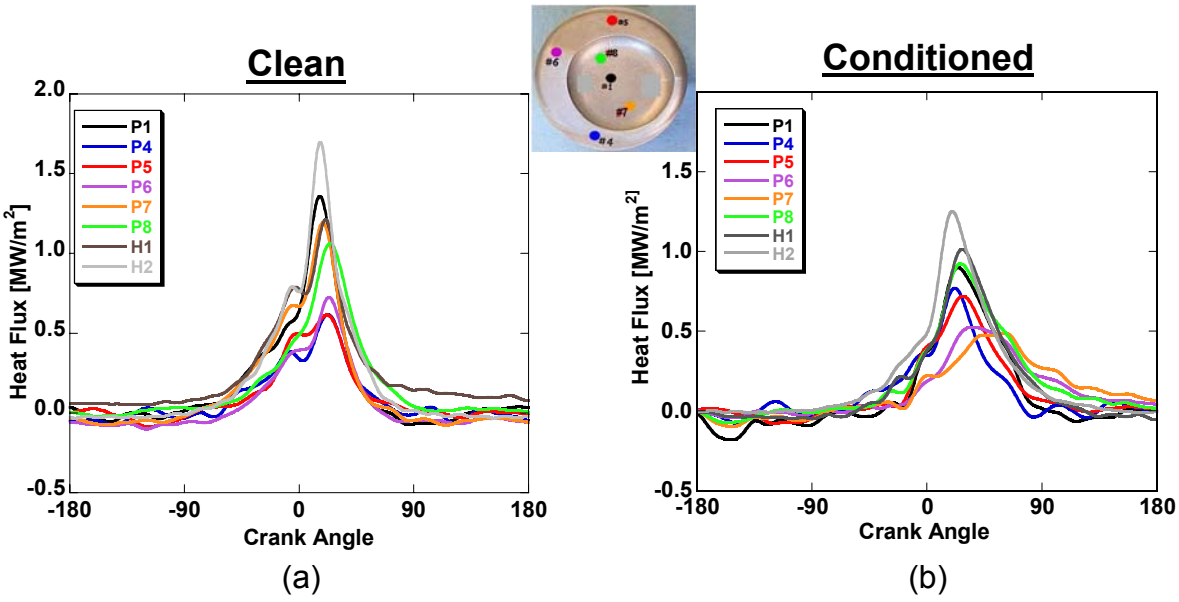

Figure 5.16 - Measured heat flux at locations in the piston and head of: a) clean chamber, and b) conditioned chamber.

Modified Procedure for HCCI investigations

The procedure described by Hopwood et al. [72] requires a direct comparison of surface temperature profiles between the temperature measurements with a clean probe, and measurements with a probe covered with a deposit layer. For an SI engine, such as in Hopwood's work, a direct comparison was indeed possible. However, for the case of an HCCI engine, it was evident that the procedure had to be modified, because of the strong coupling between wall temperatures and HCCI combustion. Heat release advances significantly with deposits growth, as shown in Chapter 4. As the phasing of combustion advances, so does the surface temperature profile, thus distorting the calculations based on the assumption that thermocouple signal phasing depends only on the thermal properties of the CCD layer covering the junction. Hence, it is necessary to remove the effect of higher, advanced combustion rates. For an HCCI engine, the easiest way to do this is by reducing intake temperature until the original phasing of combustion with a clean chamber is replicated. At that point, the measured surface temperatures are affected only by the deposit layer and proper application of the methodology can be accomplished.

The intake temperature had to be varied by different amounts as the testing progressed, due to increased degree of chamber conditioning. By the end of chamber conditioning, a T_{intake} reduction of 20° from the original 90°C was required to match the combustion rates of a clean chamber, as shown in Figure 5.17. This reduced intake temperature operation was maintained for a short interval, long enough to record combustion data, before the engine was to be stopped for deposit probe thickness measurements. Otherwise T_{intake} was maintained at 90°C for the duration of all testing.

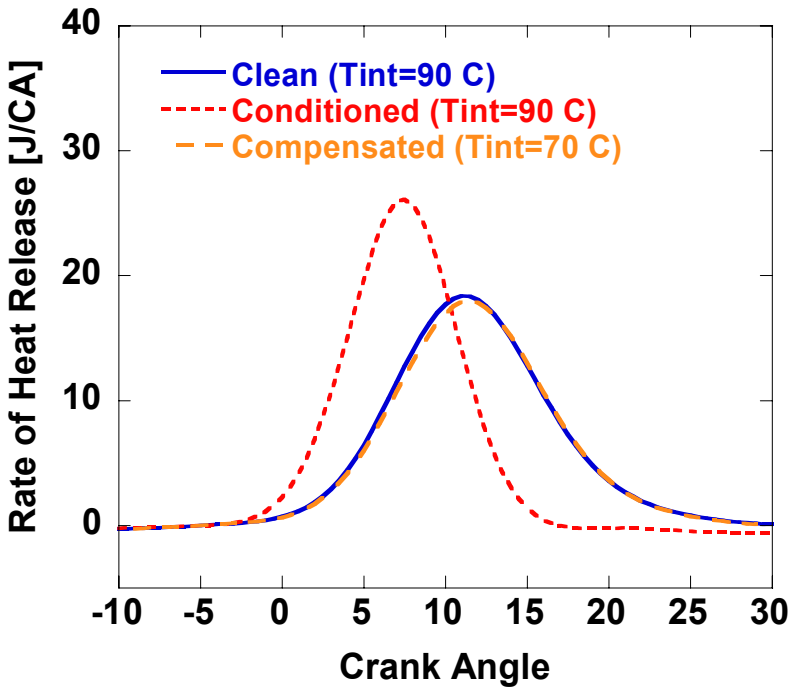

Figure 5.17 – Comparison of net heat release rate, obtained in the clean and conditioned chamber with baseline intake temperature (90°C) and in the conditioned chamber with reduced intake temperature (70°C)

Figure 5.18 and 5.19 show a comparison of the piston temperatures and heat fluxes obtained for a clean chamber compared to the conditioned chamber, with fully matched burn rates in both cases. It is clear that in every location the peak heat flux is lower with deposit coverage, as expected. Additionally, the cycle average temperature at every location is reduced from the clean case because with matched burn rates the only differences are now due strictly to the insulating effects of a deposit layer.

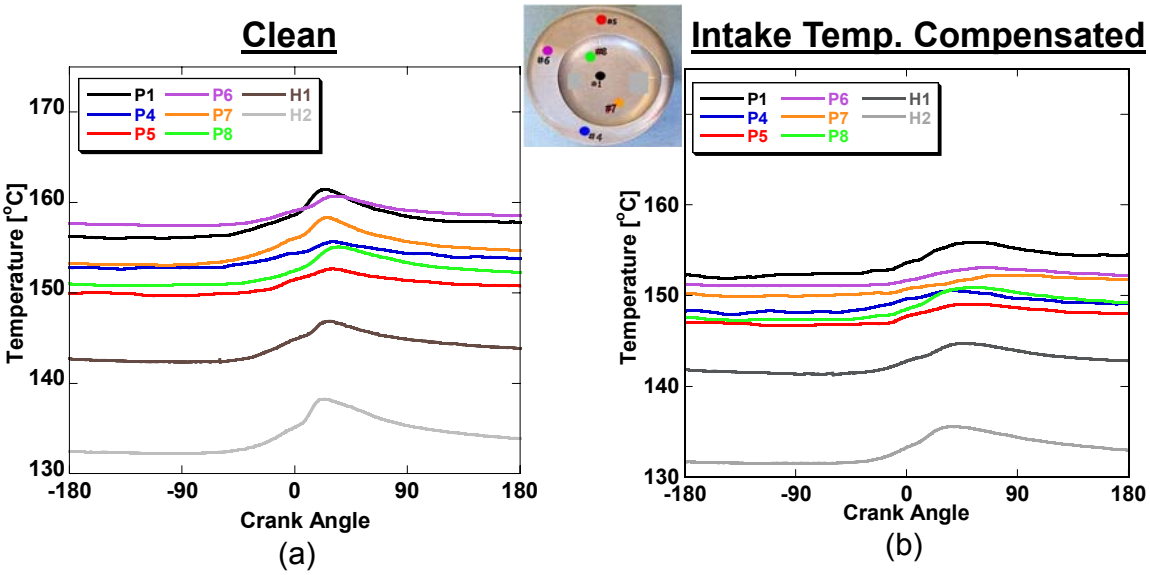

Figure 5.18 - Measured temperature at locations in the piston and head of: a) clean chamber, and b) conditioned chamber with reduced intake temperature so that burn rates match.

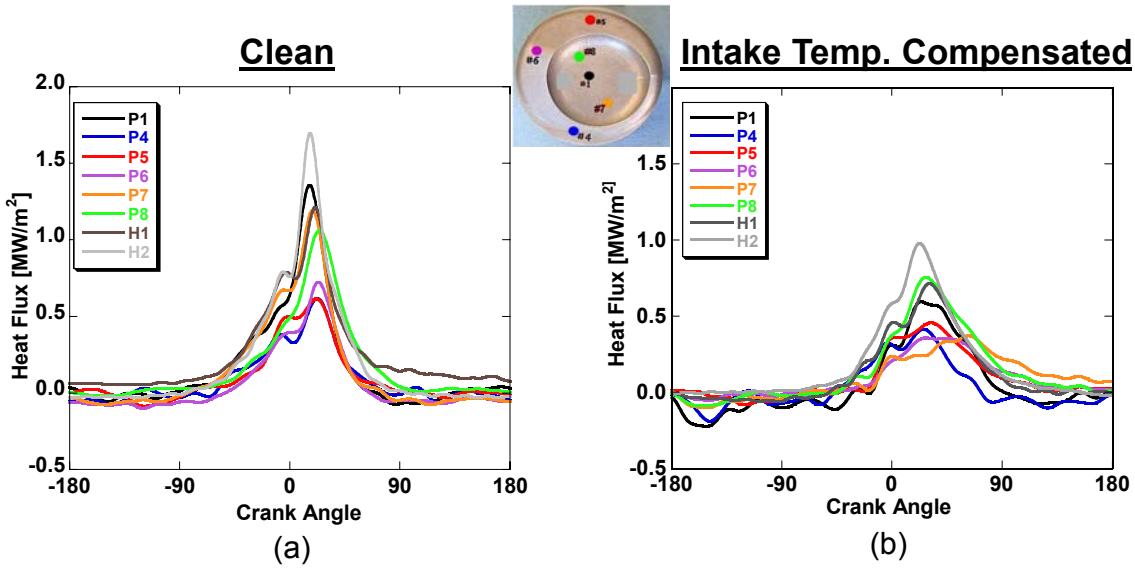

Figure 5.19– Measured heat flux at locations in the piston and head of: a) clean chamber, and b) conditioned chamber with reduced intake temperature so that burn rates match.

5.6.2 Comparison of Head and Probe deposits on Temperature Phasing

Figure 5.20 is a plot of the change of the peak temperature phasing of locations on the head and the piston for both passive and aggressive conditioning cases. As discussed previously, this data is obtained with reduced intake temperatures so that burn rates are the same for all cases. First, as shown before, it is clear that the temperature phasing of the data from the head probes follow the same correlation whether they are from passive conditioning or aggressive. This indicates that the effective deposit thermal properties for the two conditioning types as a function of thickness are similar. Second, the plot shows that deposit material from the piston follows a slightly different trend from that of the head. The fact that all head data is similar indicates that deposits on the piston have a different net effect on heat diffusion through the layer, and it is the local conditions (perhaps surface temperature) that cause the difference rather than the method of deposit formation.

It is apparent that deposits on the piston do not have the same effect on temperature phasing for a given thickness as deposits on the head. In general there is less of a change in temperature phasing for a given layer thickness, suggesting piston deposits to be more conducive to heat flow than head deposits. This could be due to the higher average temperatures of the piston resulting in differences in specific properties such as composition, density, but also morphology. Even though the data from the head in both cases of passive conditioning and aggressive conditioning follow the same trend, it is still possible that the aggressive conditioning procedure had an effect on piston CCD. In particular, the intense fuel impingement on the piston, and sooty combustion could affect the morphology, but this was impossible to verify with diagnostic techniques available for this study.

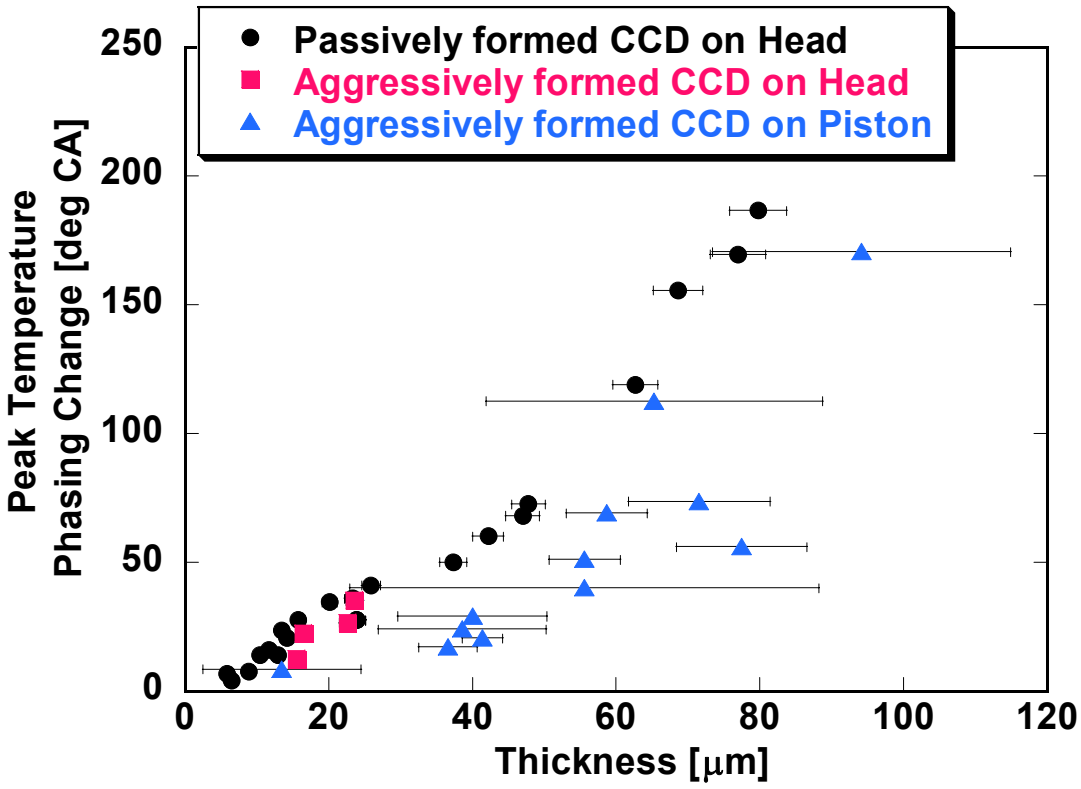

Figure 5.20 – Comparison of the cycle peak surface temperature phasing obtained from the piston top and two head locations as a function of deposit thickness

Previously, the thickness measurements from the head probes were plotted with an indicated 5% error. But for Figure 5.20, the error bars indicate one standard deviation of the measurements instead. Whenever thickness measurements are made, multiple samples are taken. Measuring thicknesses on the head probes is easy because the tips of the probes are flat, but those taken from the piston are more difficult because of the curved and irregular surfaces. For this reason Figure 5.20 shows the standard deviation of measurements and indicates that there is a greater degree of uncertainty in the case of measurements from the piston top. Assessing accuracy of these measurements is critical for issues discussed in the next section.

5.6.3 Tracking CCD formation levels *In-Situ*

The data in Figure 5.20, in addition to providing insight into the thermal effects of deposits, can serve another useful purpose. With data spanning a CCD layer thickness from zero to 100 microns, on both the head and piston surfaces, it is evident that this plot can actually be used to estimate the degree of deposit coverage based solely on instantaneous temperature measurements taken during engine operation. Normally, determining how much deposit material has formed in the chamber at a specific location requires the heat flux probes to be removed from the head, or in the case of the piston, the head must be removed to gain access. Using the correlation from Figure 5.20 enables estimating CCD thickness while the engine runs at the pertinent operating point, as long as burn rates are adjusted to ensure equal dynamic boundary conditions. Based on the correlation between cycle peak temperature phasing and thickness, a simple inspection of the data can indicate the thickness of material at every location where surface temperature is measured. This can be useful for research testing and exploration of spatial variations or fuel effects, but there is also the potential to apply this technique for development of future HCCI control schemes capable of compensating for the effects of CCD.

5.7 Calculation of CCD Thermal Diffusivity

It was already shown that the variations in peak surface temperature phasing can enable in-situ estimates of CCD thickness. In addition, this data can be used for calculating thermal diffusivity of the deposit material by applying one-dimensional heat diffusion analysis. Thermal diffusivity, or the ratio of conductivity to capacitance, dictates the transient response of the material in question. How quickly does it diffuse heat versus store it, and thus increase in temperature? It is expected that the thermal diffusivity of the deposit layer is much lower than that of the metal wall. This slows

down heat conductance, shifting it to storage in the local layer instead. This causes an increase in instantaneous temperature compared to clean metal and is presumed to be one of the main factors contributing to the influence of deposits on HCCI combustion.

5.7.1 Techniques for Calculating Thermal Diffusivity

The objective of this part of the study is to determine the thermal diffusivity of the deposit layer. In section 5.3, previous work carried out in conventional engines was described. Hopwood et al. [72] devised one of the most practical methods for estimating the thermal properties of chamber deposits. Like others, they relied on instantaneous chamber surface temperature measurements. The changes in the signal phasing were tracked as deposit material formed on its surface. Combining this with thickness measurements of the deposits material, they were able to calculate the effective thermal diffusivity. This procedure is deemed applicable to our experimental setup. Temperature measurements with a deposit layer on the two heat flux probes and the piston have already confirmed a strong correlation between CCD thickness and surface temperature phasing, thus promising success in using the same data for diffusivity calculations.

Hopwood et al. used in-cylinder temperature measurements and combined them with intermittent deposit thickness measurements over the tip of the probe. They then demonstrated how through the application of unsteady heat conduction analysis, a formula can be derived for determining thermal diffusivity (α) in units of m^2/s. The formulation is based on the solution for the periodic temperature cycle at any depth in a surface. The main governing equations are listed below but for a more detailed derivation please refer to the Appendix.

Similar to the procedure for calculation of heat flux with fast response thermocouple measurements, begin with the one dimensional transient heat diffusion equation.

$$\frac{\partial^2 T(x,t)}{\partial x^2} = \frac{1}{\alpha}\frac{\partial T(x,t)}{\partial t} \tag{5.1}$$

This can be solved by separation of variables to get the solution of general form.

$$\begin{aligned} T(x,t) = {} & D_1 e^{\alpha\lambda t + xi\sqrt{\lambda}} + D_2 e^{\alpha\lambda t - xi\sqrt{\lambda}} + D_3 e^{\alpha\lambda t + x\sqrt{\lambda}} + D_4 e^{\alpha\lambda t - x\sqrt{\lambda}} \\ & + D_5 e^{-\alpha\lambda t + xi\sqrt{\lambda}} + D_6 e^{-\alpha\lambda t - xi\sqrt{\lambda}} + D_7 e^{-\alpha\lambda t + x\sqrt{\lambda}} + D_8 e^{-\alpha\lambda t - x\sqrt{\lambda}} \end{aligned} \tag{5.2}$$

Combine with a Fourier series representation of the surface temperature measurement.

$$T(0,t) = \sum_{n=1}^{\infty} \left\{ a_n \cos(n\omega_0 t) + b_n \sin(n\omega_0 t) \right\} \tag{5.3}$$

An expression for the periodic temperature cycle at any depth, x, from the surface of a semi-infinite solid can be derived.

$$\begin{aligned} T(x,t) = {} & \frac{a_0}{2} + \sum_{n=1}^{\infty} e^{-\left(x\sqrt{\frac{n\omega_0}{2\alpha}}\right)} \left[a_n \cos\left(n\omega_0 t - x\sqrt{\frac{n\omega_0}{2\alpha}} \right) \right] \\ & + \sum_{n=1}^{\infty} e^{-\left(x\sqrt{\frac{n\omega_0}{2\alpha}}\right)} \left[b_n \sin\left(n\omega_0 t - x\sqrt{\frac{n\omega_0}{2\alpha}} \right) \right] \end{aligned} \tag{5.4}$$

Since absolute temperature values are not important, only the relative phasing, the a_0 term, which represents the average temperature, can be eliminated. Then approximate the surface temperature profile by a trigonometric series and substitute.

$$T(x,t) = 2\exp\left(-x\sqrt{\frac{\pi}{\alpha t_0}}\right)\cos\left(\frac{2\pi\left(t-\frac{t_0}{12}\right)}{t_0} - x\sqrt{\frac{\pi}{\alpha t_0}}\right) - \exp\left(-x\sqrt{\frac{2\pi}{\alpha t_0}}\right)\sin\left(\frac{4\pi\left(t-\frac{t_0}{12}\right)}{t_0} - x\sqrt{\frac{2\pi}{\alpha t_0}}\right) \tag{5.5}$$

Then take the time derivative and set to zero (for the peak temperature). Combine similar terms and simplify:

$$t_{peak} = \Delta t = x\frac{\left(1+\sqrt{2}\right)}{6}\sqrt{\frac{t_0}{\pi\alpha}} \tag{5.6}$$

Rearranging for the final formula:

$$\alpha = \left(\frac{x}{\Delta t}\frac{\left(1+\sqrt{2}\right)}{6}\right)^2 \frac{t_0}{\pi} \tag{5.7}$$

Where x is the thickness of the deposit layer (meters), t_0 is the duration of an engine cycle (seconds), and Δt is the change in peak temperature phasing (seconds), as previously illustrated in Figure 5.8.

While the analytical formulation used on the data taken in this work is that developed by Hopwood et al., the application for the special case of HCCI combustion is

different. As mentioned previously, the measured peak temperature phasing is not only a function of the properties of the deposit layer above, as in the case of an SI engine, but is also affected by changes in combustion phasing due to the strong sensitivity of HCCI to changes in thermal conditions. For that reason the utilization of the methodology for determination of thermal diffusivity must be modified as described if it is to be used in an HCCI engine.

5.7.2 Results from Head and Piston

Based on the experimental temperature measurements shown in section 5.6 regarding the phasing of the peak temperature of the cycle, the data has been re-plotted in Figure 5.21, with a separate 3rd degree polynomial trendline representing the data from the head and piston, respectively. The trendline is set with an intercept that intersects the origin of the plot, as would physically be the case with no deposit layer thickness. It should be noted that no differentiation has been made between passively and aggressively formed deposits.

Thermal diffusivity values determined using the described technique are plotted in Figure 5.22. The formula for thermal diffusivity was applied using the polynomial in Figure 5.21 in order to reduce noise. This was useful particularly in the lower end of the deposit thickness range, where the changes in peak temperature phasing are very small, thus increasing relative error. Short intervals measured with half crank angle degree resolution make calculation of thermal diffusivity extremely sensitive to the time interval expressed in seconds, and using a curve fit proved to be very effective for removing the noise stemming from the limited resolution of measurements.

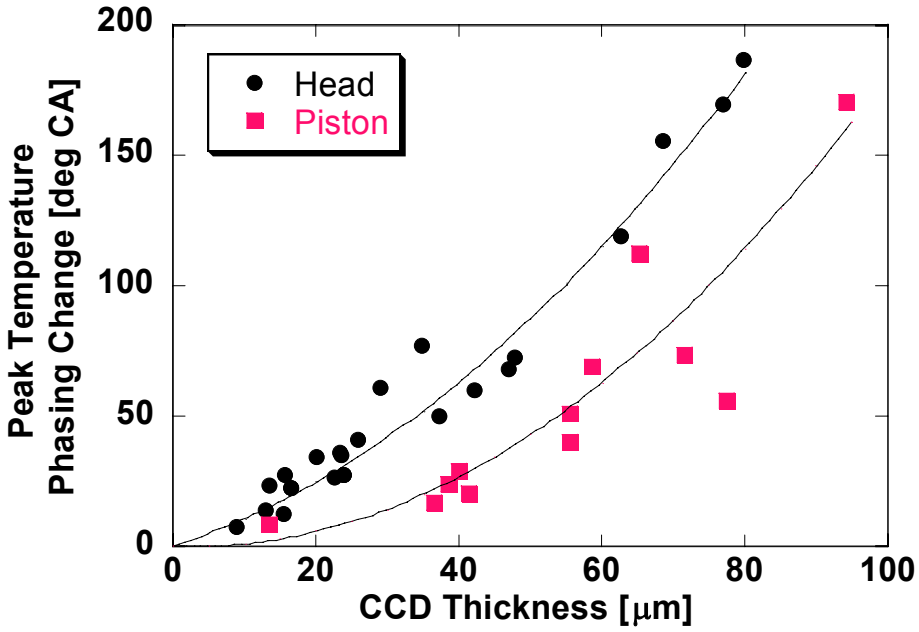

Figure 5.21 – A plot of all data from head and piston with polynomial trendline

It is very important to mention that these calculated values of diffusivity do not represent the deposit material itself. It is an 'effective' thermal diffusivity of the entire deposit layer. The measured temperature profile below the deposit layer is affected by everything above it, which is an inhomogeneous layer of fuel and oil based condensates highly porous in nature [59]. The calculated diffusivity is a net representative value of this layer. Furthermore, Figure 5.22 shows that the calculated diffusivity value is changing as a function of thickness. The porosity fraction as well as morphology at different depths into the deposit layer is likely changing more than the relative contribution from variations in different hydrocarbon molecules.

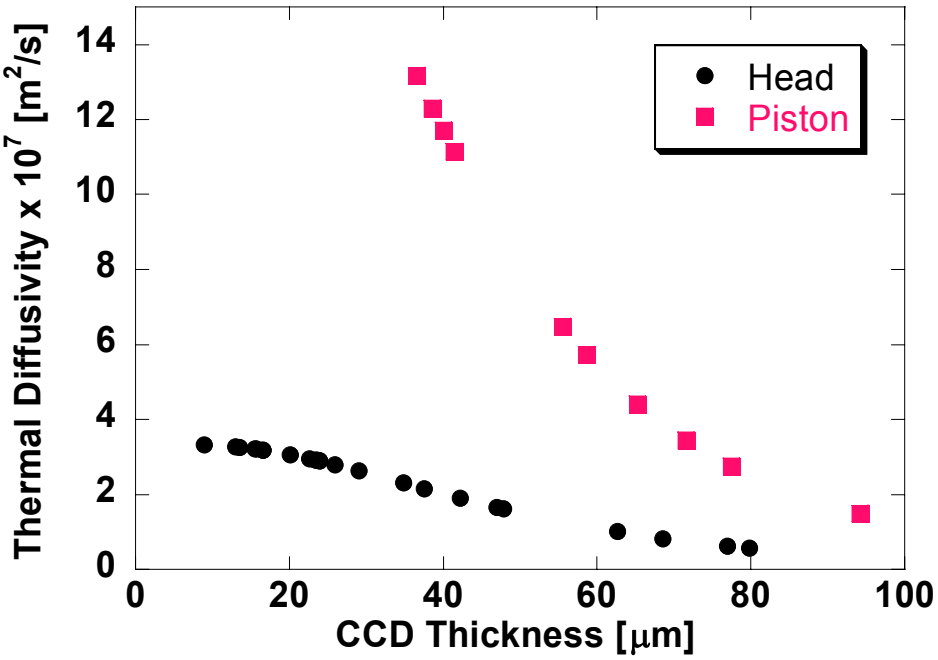

Figure 5.22 – Calculated thermal diffusvity of deposit layer on head and piston as a function of thickness

For both the head and piston the calculated values of thermal diffusivity are a strong function of thickness, but more so for the piston. In general, thicker layers of material have a lower 'effective' thermal diffusivity. The range of thermal diffusivity values throughout the testing falls between $0.8x10^{-7}$ - $1.5x10^{-6}$ m^2/s. This is a few orders of magnitude less than the diffusivity values for aluminum of about $1x10^{-4}$ m^2/s [109]. Interestingly, even though the HCCI combustion process is very different, the results in Figure 5.22 matched relatively closely those published for an SI engine [72], as well as CI engines [68,69,73].

A large difference in the calculated thermal diffusivity values between the head and piston are observed for thin deposits. Based on the values shown in Figure 5.21 at the initial stages of deposit formation on the piston, there was not a great change in measured temperature phasing as a function of thickness. This indicates that the deposit layer had minimal influence on heat diffusion, thus the effective diffusivity values are much higher.

In fact the diffusivity value of the thinnest deposit sample taken from the piston is omitted from the plot because its value is so high (~2.5×10^{-6} m^2/s).

These results indicate first that that the properties of the deposit change greatly with thickness. This is likely due to a mix of contributions including changing composition, porosity, and morphology. Recall that the surface temperature of the layer will change as it thickens, thus causing different components of the condensing fuel to contribute to layer formation. Second, the effective thermal influence of the deposit layer is different for the piston and the head. This could be due to the varying average temperature levels that each exists at during operating or it could be due to varying physical interaction with the fuel spray, among other possibilities.

5.8 Summary and Conclusions

In this chapter it was demonstrated how crank-angle resolved temperature and heat flux measurements from the head and piston surfaces can be used to gain insight into combustion chamber deposit formation. The general characteristics of the change in temperature profiles as a function of deposit layer thickness were shown, as well as a method for estimating the thickness of local deposit layers *in-situ*. Finally, the measured temperature profiles were used to analytically calculate the effective thermal diffusivity of the deposit layer, which will be utilized in the next steps of this work.

As a useful tool for future testing, a methodology for producing a conditioned combustion chamber in a much shorter time than the 40 hours required for doing it naturally was developed. It was shown that the effective CCD thermal influence on peak surface temperature phasing with these aggressively formed deposits was similar to passively conditioned natural deposits, at least on the cylinder head.

Nevertheless, considering the differences in the two methods of chamber conditioning, it would be difficult to argue that the final deposits in both cases are

absolutely the same material, same density, same molecular content, etc. In passive conditioning, the deposit is formed by the gradual accumulation of condensed unburned fuel on the chamber walls. In aggressive conditioning the conditioning starts with deposition of the sooty layer and subsequent "baking". Therefore, there are larger differences between the CCD layer formed naturally or aggressively in the early stages than at the end of conditioning.

In addition, we need to consider that not even all naturally formed deposits are going to be the same, from operating point to operating point, from engine to engine. For example, cold starts and high load operation will result in different types of deposit material, with different molecular, thermal, and physical properties. Obviously, being able to account for different types of possible deposit material would not be possible. With that in mind, aggressive conditioning is a way to produce a chamber coating which happens to have similar properties as natural deposits and can be done in just a few hours.

However, for the purpose of this work, the most important outcome is that CCD in either case produces a significant effect on HCCI combustion and that surface temperature measurements can provide insight about the nature of this effect. The fact that these materials are likely different is not really important. The goal is to understand the effects on wall heat transfer that any given material could have and what is the mechanism of its effect on HCCI combustion. Are we able to develop methods to quantify the thermal or physical effects of this coating material and account for the measured differences in burn rates, therefore, separating this from possible fuel absorption effects? That is the intent of the work in the following chapters.

CHAPTER 6

ESTIMATING THE CCD LAYER SURFACE TEMPERATURE

6.1 Introduction

So far, quantified CCD layer formation in the combustion chamber has been shown to have a significant effect on HCCI burn rates, as described in Chapter 4. Through measurements using heat flux probes in the head and piston, it has been shown that temperature and heat flux characteristics at the chamber wall change as the deposit layer thickens. It is concluded that it is these changes in heat transfer at the chamber wall surfaces could be a strong factor for what cause the changes in combustion.

However, in order to accurately understand what the specific effects of the deposit layer are leading up to and during combustion, one must know the temperature and heat flux history at the CCD layer surface where it interacts with the contents of the chamber. Currently heat flux probe measurements provide temperature and heat flux profiles throughout the cycle at the bottom of the CCD layer, at the CCD/metal wall interface, but there is no practical way to measure these parameters at the surface of the deposit. However, knowing the temperature profile on top of the CCD layer would be an invaluable contribution to our understanding of the mechanism responsible for variations of HCCI combustion in a conditioned chamber. In addition, this information would be useful to the computational fluid dynamics community as it would provide realistic boundary conditions for detailed in-cylinder calculations. Therefore, the objective of this

chapter is to develop a methodology for calculating the CCD surface temperature. It will use the temperature profile that is measured at the bottom of the layer and the thermal properties of the deposit material calculated in Chapter 5.

This methodology, the development of which is one of the significant contributions of this work, is referred to as the 'Lead-Corrector' (LC) method. The procedure is based on the analysis of one-dimensional heat diffusion, and the solution hinges upon the availability of wall thermocouple measurements, known deposit layer thickness, and thermal properties. However, one boundary condition is still missing and an iterative technique was necessary to eventually converge on the CCD top surface temperature.

The following section starts with background info on previous work by other investigators related to CCD surface temperature. Then the LC methodology is described in detail, as well as its validation using measurements in a clean engine. Finally, results obtained from the head heat flux measurements using the LC method are presented and discussed.

6.2 Background

There have been a few previously documented attempts at calculating or measuring the surface temperature of deposit layers and ceramic coatings. While they each provide useful insight, there are deficiencies or other aspects that require development of a methodology suitable for the study at hand.

6.2.1 Approach

The governing equation which dictates the thermal history in the deposit layer is represented by the one-dimensional transient heat diffusion equation.

$$\frac{\partial T}{\partial t} = \alpha \frac{\partial^2 T}{\partial x^2} \tag{6.1}$$

It is assumed that the deposit layer is thin enough so that heat diffusion into the layer is one-dimensional. The calculations required to solve this equation are straight-forward using finite-difference techniques, provided there are sufficient boundary conditions (BC's). However, in this case the main output of the calculation will be the 'boundary condition' at the top surface. The temperature measurements on the metal surface serve as one boundary condition in the x-direction at the bottom of the CCD layer. The LC method is centered on determining the second boundary condition and will be described in the latter part of this section, after considering previous work published by others.

6.2.2 Previous Work

As already mentioned, Anderson [69] used an optical technique to directly measure the surface of temperature of the deposit layer. A 2-stroke single cylinder gasoline engine was instrumented with a fast response thermocouple, with both surface and backside junction. It was mounted in the head in such a manner that directly opposing it was located a port for optical access. A radiometer was designed which could provide accurate deposit surface temperature based on infrared radiation. However this requires optical access to the engine's combustion chamber and this is not practical for our current setup.

Hayes [73] combined calculated CCD thermal properties with known thicknesses in a two-zone SI cycle simulation. So deposit surface temperature was estimated based on a calculated gas temperature history and a convective heat transfer correlation. Since coolant temperature was known, wall temperatures and thus also deposit layer

temperatures could be inferred. This was ultimately used to estimate octane requirement increase due to deposit coverage in the end-gas region.

Deficiencies with Previous Methodologies

There are a couple specific problems with these previous methods. In it, calculations rely on a calculated total gas mixture average temperature and an empirical global heat transfer correlation (for example, Woschni) to calculate the total heat flux to the chamber wall and thus the wall temperature. The current work will be based on wall temperature measurements at several specific locations in the chamber, where temperature profiles will be specific to the region of the head or piston where the measurement is being made. Assuming an average gas temperature for the completer chamber contents neglects any form of thermal stratification and it has been shown that there is definitely some stratification effect for the relatively dilute mixtures used for HCCI combustion and direct injection of fuel into a confined space of a relatively small combustion chamber. In particular, the thermal stratification between the core gas and the cooler boundary layer near the walls is relevant for all aspects of HCCI combustion and heat transfer [110]. Mixture preparation is a factor too, and Chang shows clearly that for direct injection operation, local heat loss can vary greatly throughout the chamber [58]. The assumption of uniform gas temperature would create uncertainties for the accuracy of the final solution.

In order to avoid any assumptions about gas-side heat flux to the wall, calculation of CCD surface temperature should be based strictly on measured results. That is one of the advantages of the LC-method. All that is required to determine the temperature profile of the deposit layer is the measured CCD layer/metal wall interface temperature, the thickness of the layer, and the thermal properties of the layer, the determination of which was reviewed in the previous chapter.

6.3 Lead- Corrector Methodology

In general, the Lead-Corrector method applies the predictor-corrector idea for determining the temperature profile of the surface of the CCD layer. Once found, this surface temperature, along with the measured heat flux profile at the bottom of the deposit layer as two boundary conditions, it is possible to calculate the temperature gradients anywhere in the deposit layer, thus heat flux can be calculated anywhere in the layer, including the surface. It is applied at every location where a fast-response thermocouple is located in the chamber. The thermal properties used in the calculations are those determined for the deposit layer as described in the previous chapter. For the analysis used in this chapter, the model setup, and the calculations used see the Appendix.

6.3.1 General Methodology

Figure 6.1 illustrates a schematic of the grid used to represent the deposit layer and how the boundary conditions are applied. The bottom of the layer boundary condition is the *heat flux* that is measured by our fast response thermocouples. This is the heat flux into the metal wall from the bottom of the CCD layer. The top of the layer BC is the temperature which we are trying to ultimately determine. The method that will be used to actually get this temperature starts off by simply guessing the surface temperature profile. This becomes the temporary top boundary condition of the deposit layer. The two spatial boundary conditions are now a guessed temperature at the top of the layer and a measured heat flux at the bottom.

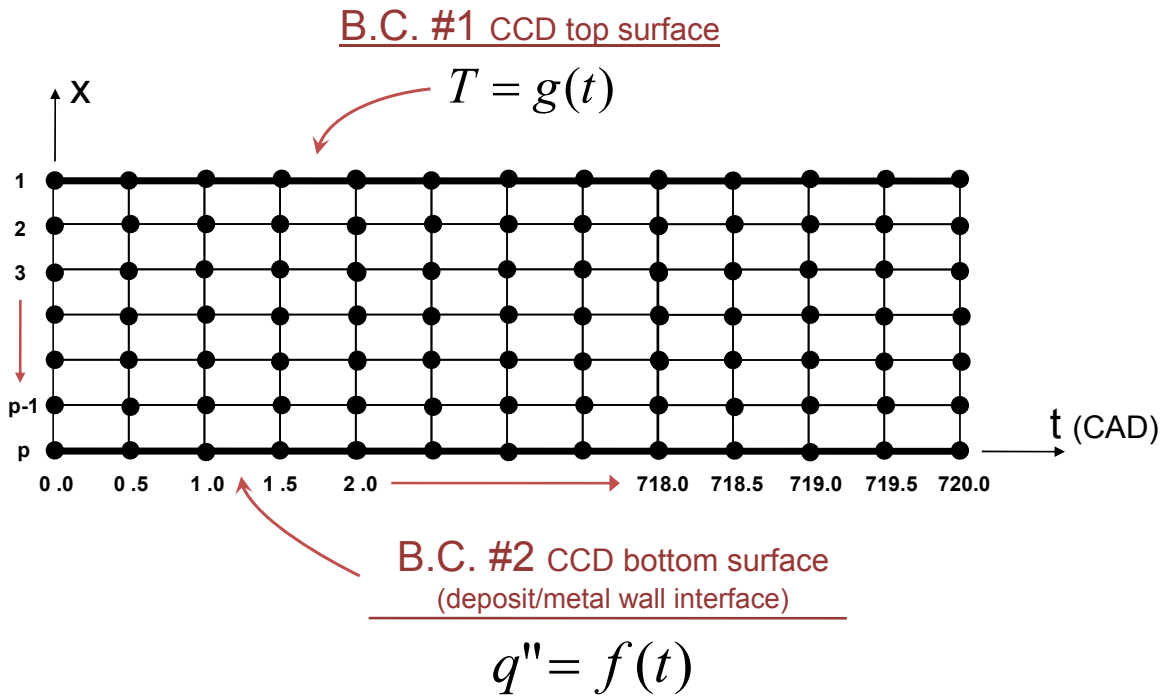

Figure 6.1 – Schematic of the finite element grid representing the CCD layer in the Lead-Corrector methodology. The bottom surface boundary condition is the experimentally measured heat flux profile, while the top surface boundary condition is the output of the iterative calculation procedure.

Equations 6.2 through 6.4 represent the basic finite-difference equations used to calculate the temperature gradients in the grid depicted in Figure 6.1. For a detailed derivation refer to the Appendix.

Equation 6.2 is the center-difference implicit representation of temperatures for every internal node depicted in Figure 6.1, based on the governing equation for transient heat diffusion.

$$\frac{\partial T}{\partial t} = \alpha \frac{\partial^2 T}{\partial x^2} \tag{6.1}$$

$$T_i^t = -rT_{i-1}^{t+1} + (1+2r)T_i^{t+1} - rT_{i+1}^{t+1} \tag{6.2}$$

where, $r = \dfrac{\alpha \Delta t}{\Delta x^2}$ and i = 1→ p-1

A similar formulation for the application of the heat flux boundary condition is applied for the nodes at the bottom of the CCD layer.

$$q_m'' + \frac{\partial T}{\partial t} = \alpha \frac{\partial^2 T}{\partial x^2} \tag{6.3}$$

$$T_p^t = (1+2r)T_p^{t+1} - 2rT_{p-1}^{t+1} - 2rb_{q''} \tag{6.4}$$

where $b_{q''} = \dfrac{\Delta x}{k} q_m''(t)$

Also required for the solution is an initial condition. Since this is an iterative procedure, it is possible to make the initial condition, in this case, the first time-step at 0 crank angles, to be equal to the last time-step, at 720 crank angles. From this model setup, temperature gradients, such as the ones in Figure 6.2, can be produced. This demonstrates the calculated temperatures gradients at an intermediate iteration before complete convergence of the solution.

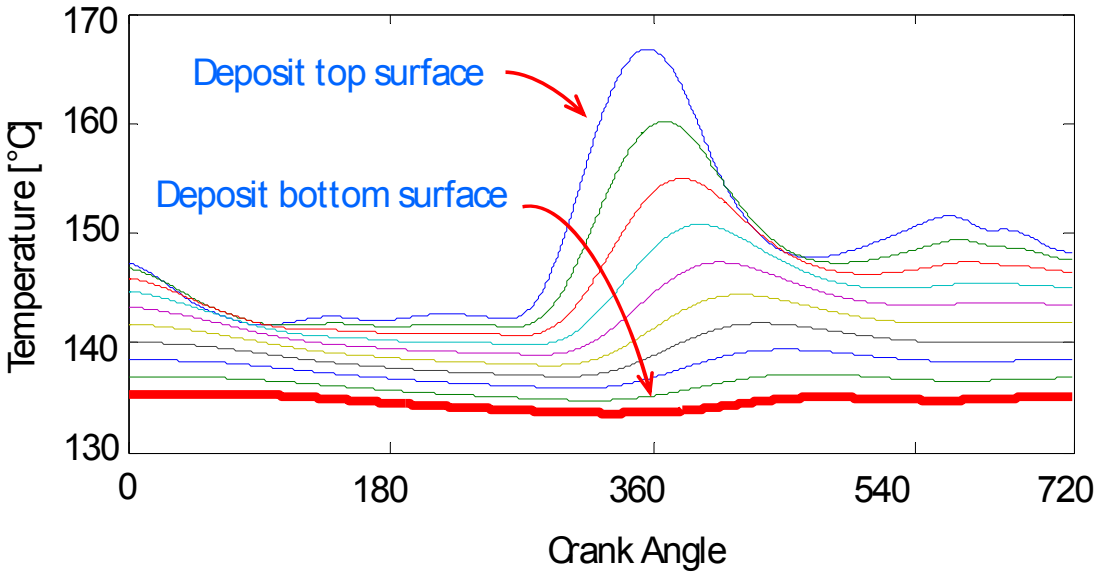

Figure 6.2 – This is a depiction of the calculated temperature profiles at even-spaced intervals within the deposit layer. These particular temperature gradients were calculated at an intermediate iteration before final convergence of the temperature solution. The thick profile at the bottom of the layer is directly compared to the actual experimental temperature measurement at the metal wall surface.

Of course, temperature gradients include a calculated temperature profile at the bottom of the deposit layer, as indicated by the bold red profile. This calculated profile is derived from the estimated temperature profile at the top of the CCD layer, which diffuses down to the bottom, as dictated by the one-dimensional transient diffusion equation shown before. The rate of diffusion is dictated by the measured heat flux at the bottom. If the guessed temperature profile at the top is incorrect, then of course the calculated profile at the bottom will be incorrect. This can be determined by performing a direct comparison between the calculated bottom layer temperature and the measurements obtained by the heat flux probe in the metal, as demonstrated in Figure 6.3. Recall that the *heat flux* at the metal wall was used to calculate the temperature

gradients. The measured *temperature* is thus used as a check, for determining the error of the current iteration.

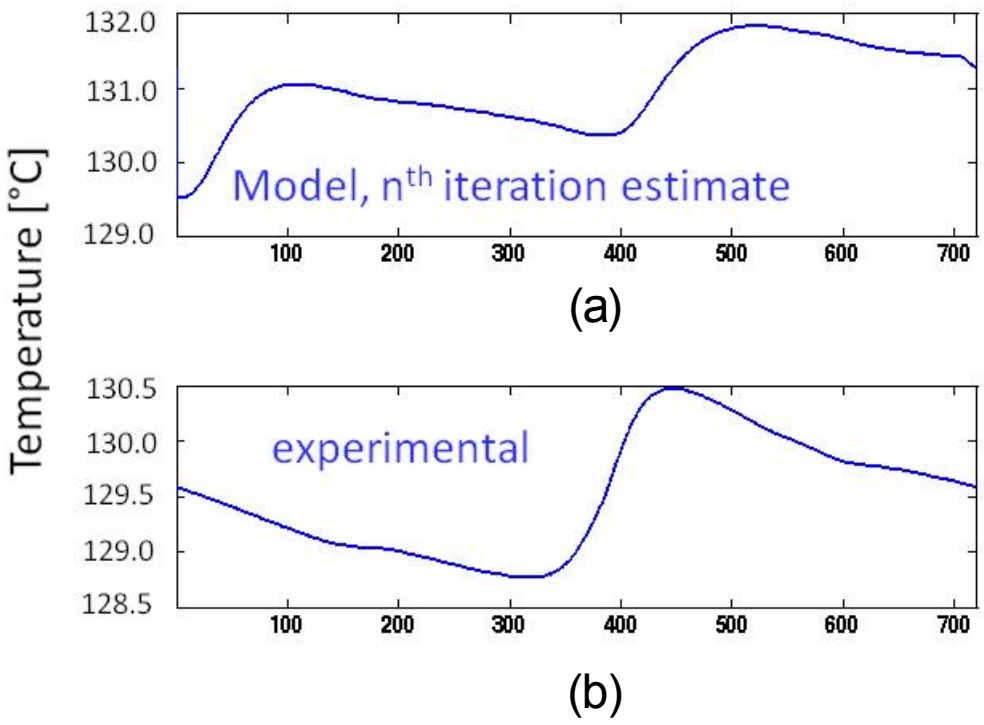

Figure 6.3 – An example of the comparison of the temperature profile at the bottom of the deposit layer at an intermediate iteration in the solution process: a)The calculated temperature profile at this iteration, (the thick line in Figure 6.2) and b) the experimentally measured temperature profile.

The actual data arrays of the calculated and the measured temperature profiles are compared and the difference between each at every half crank-angle (resolution of the measured data) results in an *error* array. This error array is multiplied by a factor, typically a value much less than one, to ensure stability and eventual convergence, and subtracted from the originally estimated surface temperature profile. Then temperature gradients throughout the layer are re-calculated and the process is repeated until the bottom layer temperature converges to the measured at the same location. The complete

process is depicted in Figure 6.4. The step regarding the correction scheme will be explained in further detail.

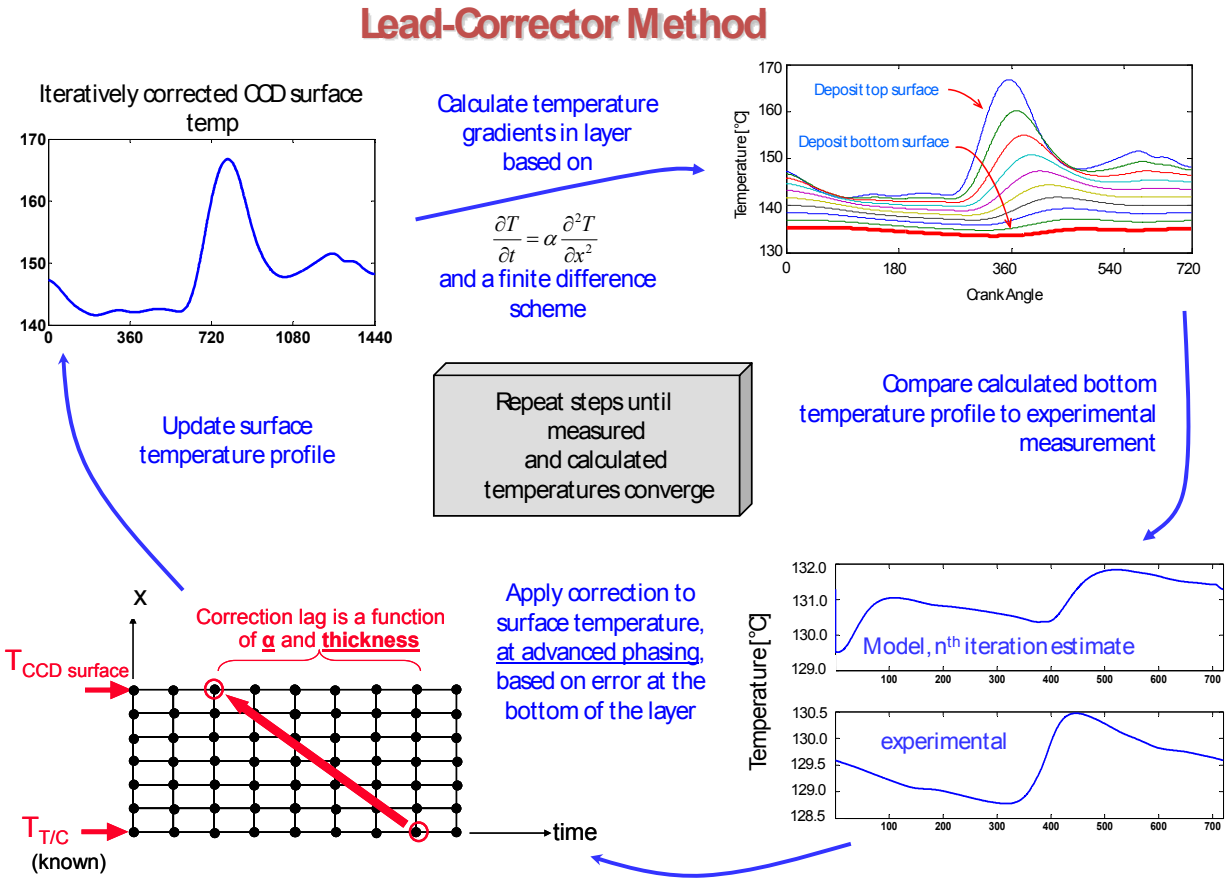

Figure 6.4 – This schematic depiction of the Lead-Corrector method. The major steps include estimation of layer surface temperature profile, calculation of layer temperature gradients, comparison of calculated temperature profile at the bottom of the layer, and then correction of the surface temperature estimate.

The method is based on the fact that if the calculated bottom layer temperature is higher than the measured temperature at any point in the cycle, then the estimated temperature at those same crank-angles is too high, and vice versa if the calculated is lower than the measured at a particular crank angle. If this prediction-correction process

is repeated, eventually the CCD top surface temperature profile will be shaped such that it results in realistic estimates of profiles at any depth and a satisfactory match between predictions and measurements at the bottom of the layer. An example of the typical calculated temperature profile gradients in the CCD layer (converged) is shown in Figure 6.5.

It should be noted that the crank-angle reference is shown two different ways in these plots. In some cases the crank-angle scale starts at 0 and ends at 720 due to the actual referencing in the code. Final results are shown in the range -360 to 360 degrees in order to match the crank-angle reference to future combustion data.

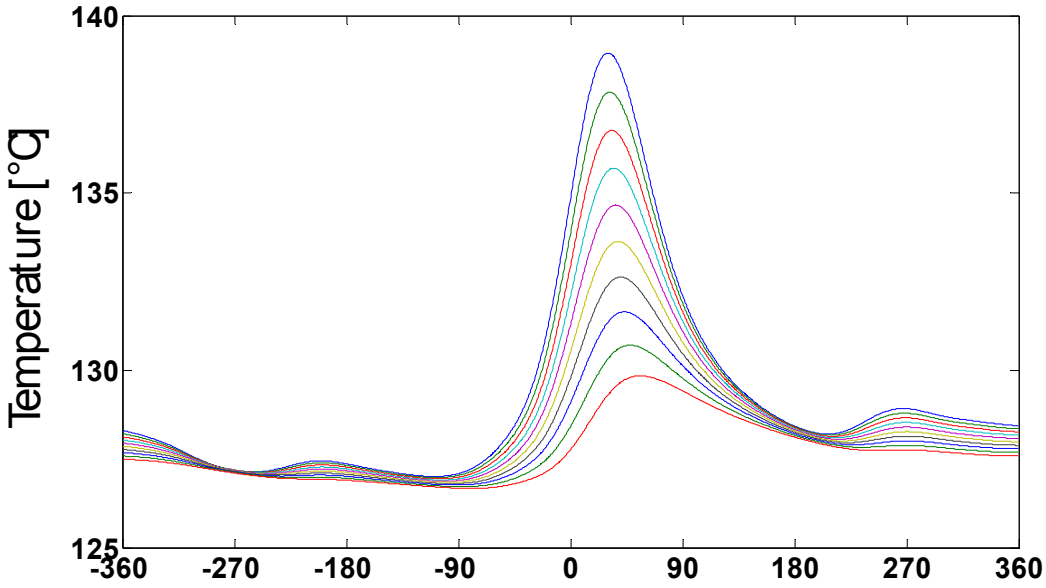

Figure 6.5 – An example of typical temperature profiles at even-spaced depths within the deposit layer after solution convergence.

It is worth noting that the accuracy of the *initial* guess for the temperature profile at the CCD surface is not really important. Assuming the correction shift factor is small enough to keep the process stable, a solution will converge eventually. The only factor

that is affected by the initial guess is the number of iterations it will take for the solution to finally converge. Typical computation time on a desktop PC for the temperature gradients at one probe locations is 5 minutes.

Lead-Correction

An important point needs to be made regarding the correction portion of the LC methodology. As stated above, after each cycle of calculations of temperature gradients in the deposit layer, the error in the bottom surface temperature profile is found. This is then used to directly apply a correction shift to every point in the guessed CCD top surface temperature profile before starting the next iteration. The actual crank angle value of the particular correction shift, relative to the phasing of the error, determines whether the solution will ever converge.

As stated before, this is a heat diffusion problem. A temperature spike at the surface of the deposit layer from heat release near TDC will be measured at the bottom of the deposit layer at a later point in the cycle, perhaps 30 crank angle degrees later. This value can vary greatly depending on the thickness and properties of the deposit layer. For this reason, when the correction array is applied to the surface temperature profile, the phasing at which the correction is applied is advanced relative to the measured error crank angle; hence the name *Lead*-Correction. Figure 6.6 illustrates the phasing shift of the applied correction.

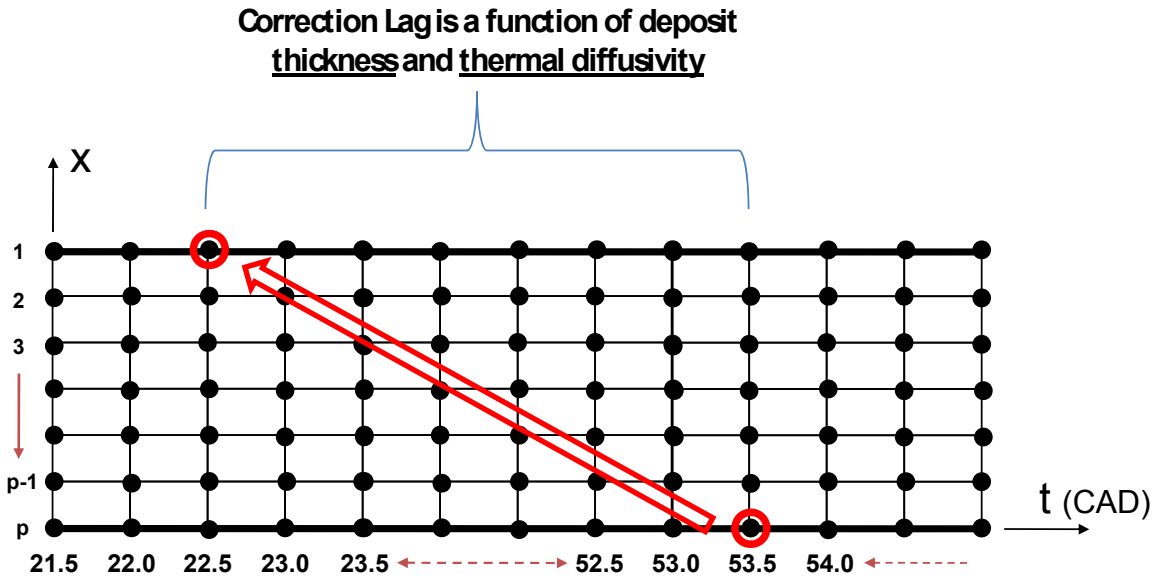

Figure 6.6 – The 'lead-correction' aspect of the methodology. The surface temperature guess at each temporal node is adjusted based on the error calculated at each node at the bottom. The correction is derived from the error and applied with advanced phasing. The phasing is amount a function of total layer thickness and thermal diffusivity.

The amount by which to advance the application of the correction array is determined by trial and error. It varies between probe locations, depending on the local CCD layer thickness and thermal diffusivity. Recall that in the previous chapter, the method for calculating the deposit thermal diffusivity required the phasing shift of the measured cycle peak temperature between a clean probe and one covered with deposit material. This same phasing shift at each particular location can also be used as an estimate for the amount of phasing advance that is required for the correction, though it is not exact because difference in combustion rates will change the value.

Model Setup, Calculations, and Convergence

The calculations used for the LC-method are performed in a program written in Matlab. The base for the calculation of the temperature gradients in the deposit layer is an

implicit finite-difference scheme with relevant boundary conditions. Further details of the code and the finite-difference scheme setup are included in the Appendix.

The main body of the program consists of a loop which repeats the layer temperature calculations, error determination, and correction steps until convergence of the calculated and measured temperature at the bottom of the layer is attained. The criteria for convergence were set such that the maximum error at any crank angle was not greater than 0.1 degrees Celsius. This may seem like an extremely low error limit but one must realize that this error is magnified at the surface of the deposit. It was found that a maximum error of less than 0.1 degrees did not give appreciable improvement in final results and computation time was kept reasonable.

6.3.2 Model Assumptions

There are a few significant assumptions being made in order to complete the calculations required for this methodology.

Thermal Conductivity

The first is regarding the thermal conductivity of the layer itself. Chapter 5 discusses the methodology used to determine the thermal diffusivity of the deposit layer as a function of thickness and this will be required for the main governing equations used in these calculations. In addition, an effective deposit layer thermal *conductivity* is required. While determining these values requires a special setup and was not in the scope of this work, the conductivity estimates are provided in the work published by others [68,69,73]. Specifically, a thermal conductivity value of 1.5 W/mK will be used throughout. This value is on the high end of what previous researchers have found. It is preferred to error on the side of underestimating the thermal influence of the deposit

material rather than over-estimating, so that we do not attribute more thermal influence on the part of the CCD layer than possible.

The use of a higher biased thermal conductivity value will have the effect of underestimating the calculated peak temperature levels at the deposit surface, as shown in Figure 6.7. This is a plot of the calculated temperature profile at the surface of a 50μm deposit layer on one of the head mounted probes. Clearly the cycle temperature swing is very sensitive to the conductivity value used. While this larger temperature swing will decrease peak heat flux at the surface of the deposit, Figure 6.8 shows that it is not as great of an effect as expected. More importantly, for future analysis into transient thermal effects, varying thermal conductivity has no effect on the phasing of peak heat loss. This is more dependent on the thermal capacitance of the deposit material, thus diffusivity values have a greater affect on phasing. It is also important to note that the integrated cycle heat loss is the same for all values of thermal conductivity. As mentioned previously, the measured heat flux at the bottom of the deposit layer serves as a constraint for the total heat loss of the cycle.

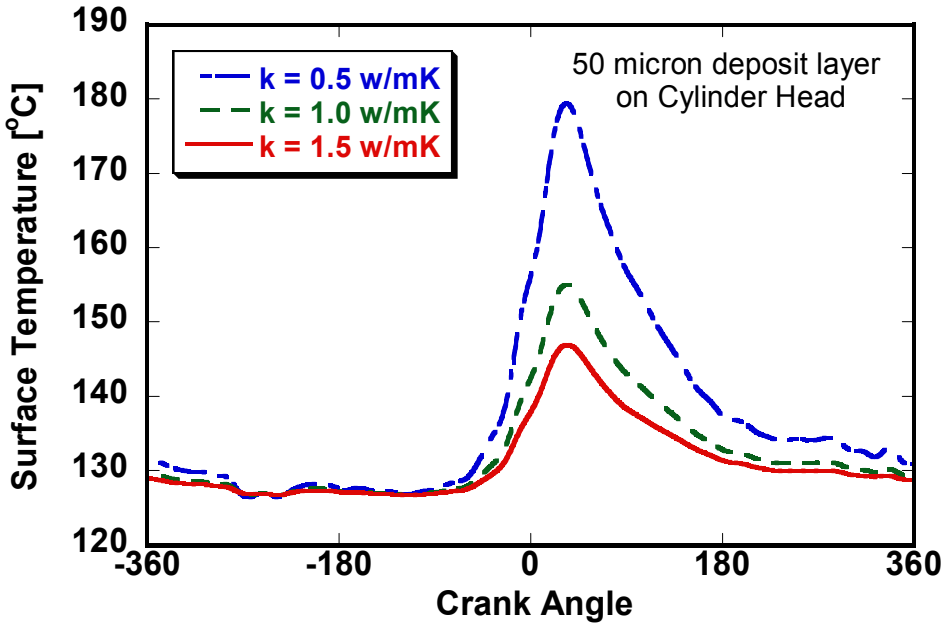

Figure 6.7 – The effect of thermal conductivity values on calculated deposit layer surface temperature using the LC method

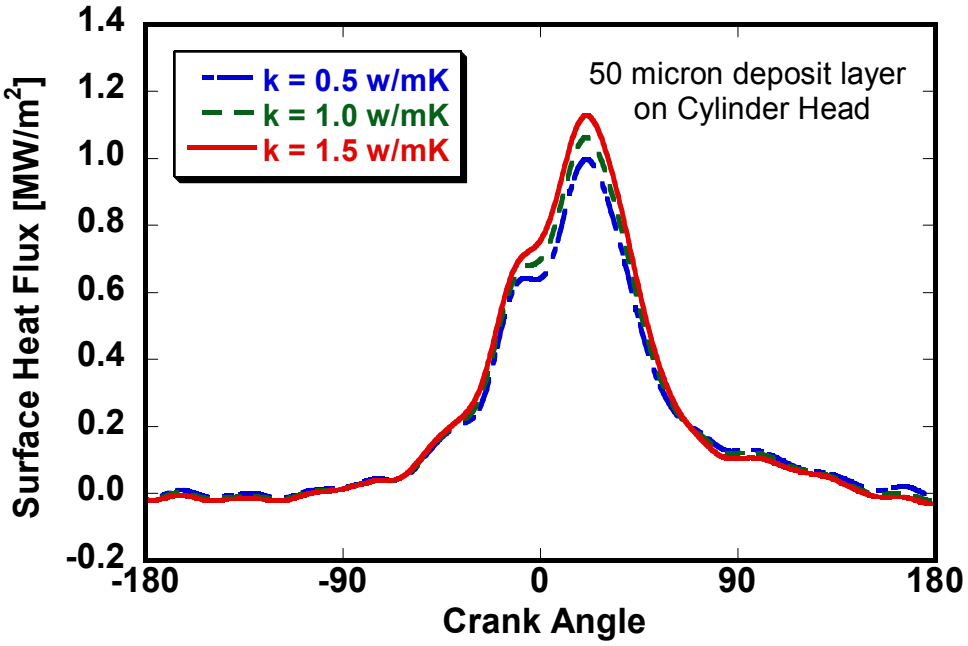

Figure 6.8 – The effect on calculated deposit layer surface heat flux for the temperature profiles shown in Figure 6.7

Other Assumptions

The next assumption is that the measured wall surface temperature from the heat flux probe is equal to the temperature at the bottom of the deposit layer. Essentially we are assuming zero contact resistance between the metal wall and deposit layer. It is easy enough to introduce a contact resistance, but deciding on the value to use is difficult. There is no previous experimental work in this area. This assumption also means that heat flux at the bottom of the deposit layer is equal to heat flux at the metal wall surface. Some trial values of contact resistance pertaining to similar problems were introduced in the solution for a trial run and it was found to have a small but still measurable effect. It would be a much smaller effect than those for varying values of thermal conductivity. Because any value of contact resistance would have the effect of increasing the deposit surface temperature further, no matter how little, it was decided to ignore it. As already discussed, it is preferred to error on the side of underestimating the thermal influence of the deposit material rather than over-estimating.

The final assumption is that the CCD layer is treated as isotropic. Specifically, the property values used will apply at every depth of the layer. In reality, the composition and morphology might change with depth. However, the calculated thermal diffusivity values are based on the net effect of the complete layer on measured temperature profiles, so they are handled as such.

6.4 LC- Methodology Validation

It was found that applying the LC-method at every thermocouple location in the combustion chamber gave very reasonable results. But how can it be ensured that these results are accurate? A method was devised for validation of the LC-methodology, using measurements from a clean heat flux probe located in the head of the engine.

This section will demonstrate how a validation case was produced so that the LC methodology could be tested. This was done by making a simulated 'deposit' layer of which the temperature gradients throughout the thickness were already known. Then using the same parameters we would start with in the case of a real deposit, namely the bottom surface heat flux and temperature, the top surface temperature profile (of this simulated layer) was calculated using the LC-method, then compared to the known temperature profile.

6.4.1 Simulated Deposit Layer Setup

The validation case 'deposit' layer is simulated using measurements from a clean heat flux probe. Recall that these probes consist of two thermocouple junctions. One is located at the surface, flush with the chamber wall and exposed to the chamber gases, and a second one is located 4mm beneath the surface, which is combined with the surface junction for wall heat flux calculations. Sample measurements from a clean head heat flux probe are shown in Figure 6.9, for both junctions. Note that the backside junction is far enough below the surface that fluctuations from transient heat flux at the surface do not reach it, so it just measures a constant temperature throughout the cycle.

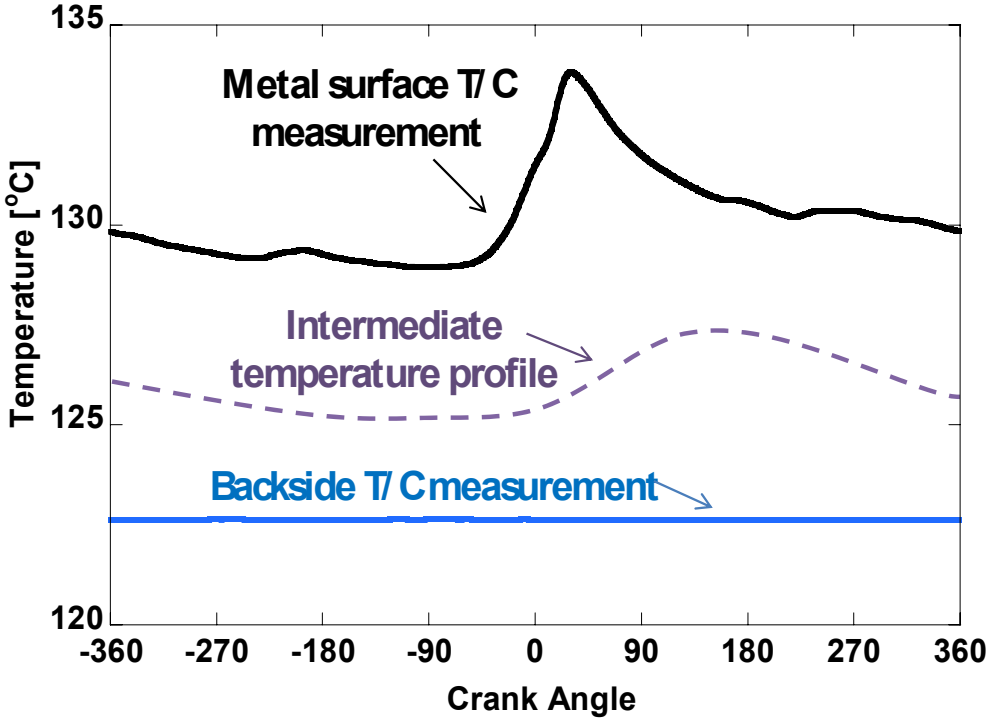

Figure 6.9 – Instantaneous temperature measured at the surface of the clean probe, and at a depth of 4mm below surface. A temperature profile at an intermediate depth into the heat flux probe is required for validation of the LC method.

For validation, the LC-method will be used to try and calculate the measured surface temperature using a temperature profile from below the surface, so the simulated layer will be an aluminum 'deposit' layer. While the flat backside temperature measurement would not work as a sample input to back-calculate the surface profile, a temperature curve somewhere in between would be viable. This sample curve is depicted in Figure 6.9 as the drawn-in dashed purple line.

In order to produce this actual curve, the front and backside temperature measurements were used to calculate the temperature gradient solution within the metal of a clean heat flux probe, as shown below in Figure 6.10. The calculation was performed using the same governing equations as those used for the LC methodology itself, with the two measured temperature profiles serving as the two x-direction boundary conditions.

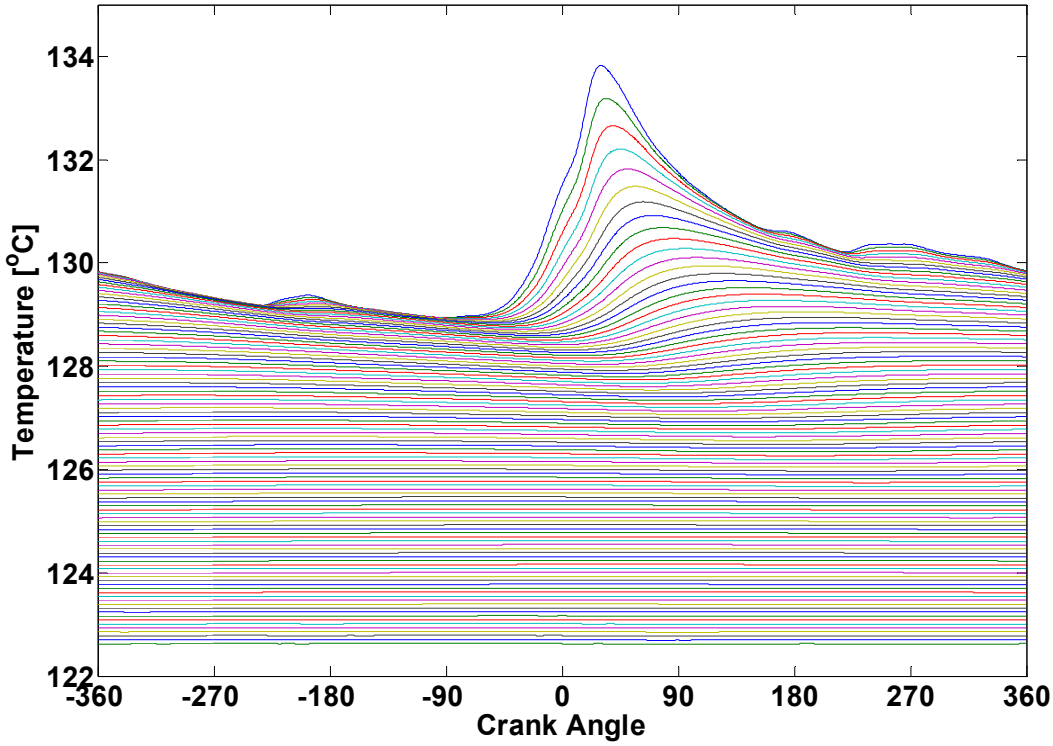

Figure 6.10 – A plot of the 100 evenly spaced calculated temperature profiles in a heat flux probe based on clean probe measurements from the engine under HCCI operation.

The 4mm distance between the two temperature boundary conditions was divided into 100 equal thickness layers. As depicted by the thicker profile in Figure 6.11, a gradient profile was initially chosen at a depth of 400 microns, the tenth calculated layer.

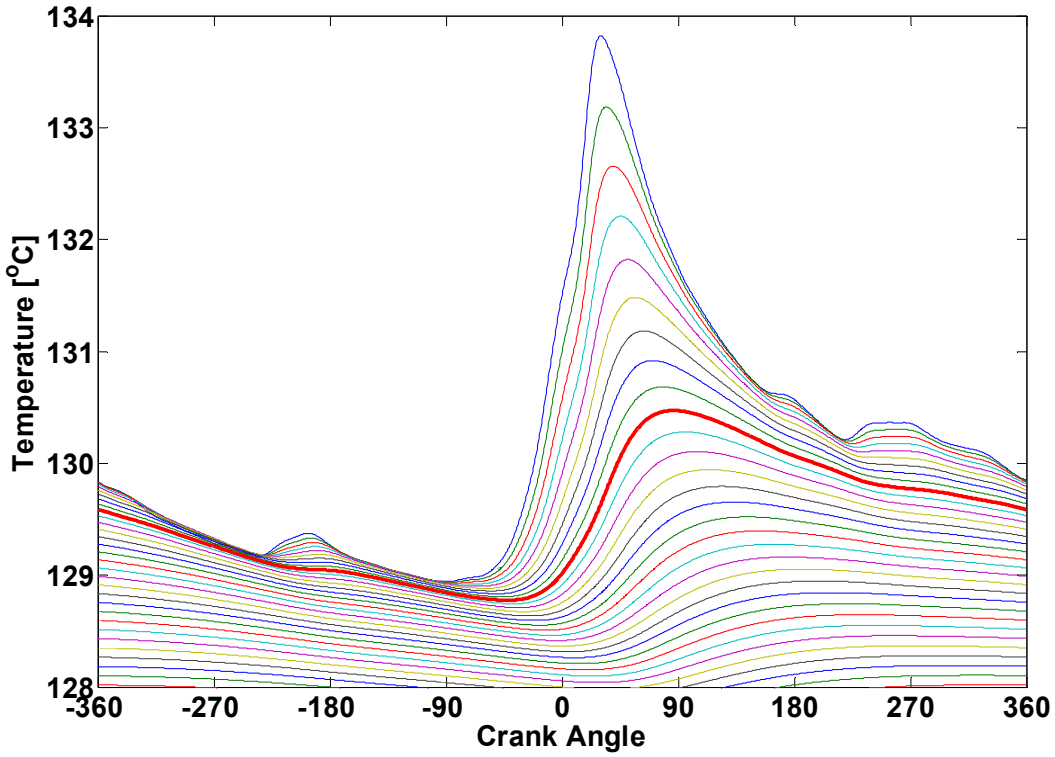

Figure 6.11 – A closer look of the surface temperature profiles of Figure 6.10. The highlighted 10th layer will be used as a 'bottom of layer' temperature profile for a sample 'deposit' of the same thermal properties as aluminum, for validation.

This layer will now be treated as if it was an experimental temperature measurement taken during engine operation. It would be the hypothetical temperature measurement taken below a 'deposit' layer of thickness 400 microns, with the thermal properties of aluminum. It is straightforward to also calculate the heat flux profile at this depth into the probe. Figure 6.12 shows the simulated below layer experimental temperatures and heat flux profiles which will be used with the LC-method to test if it is capable of calculating the surface temperature profile of this aluminum 'deposit' layer. Since this surface temperature profile is measured, and shown in Figure 6.13 (top curve) with the simulated bottom layer temperature (bottom curve), a direct comparison can be made to determine if the LC-method provides accurate results. Note that the shapes of the

simulated bottom of the layer profiles in Figure 6.12, look very similar to actual temperature and heat flux measurements at the bottom of a real deposit layer, such as those in Figure 5.5 and 5.6.

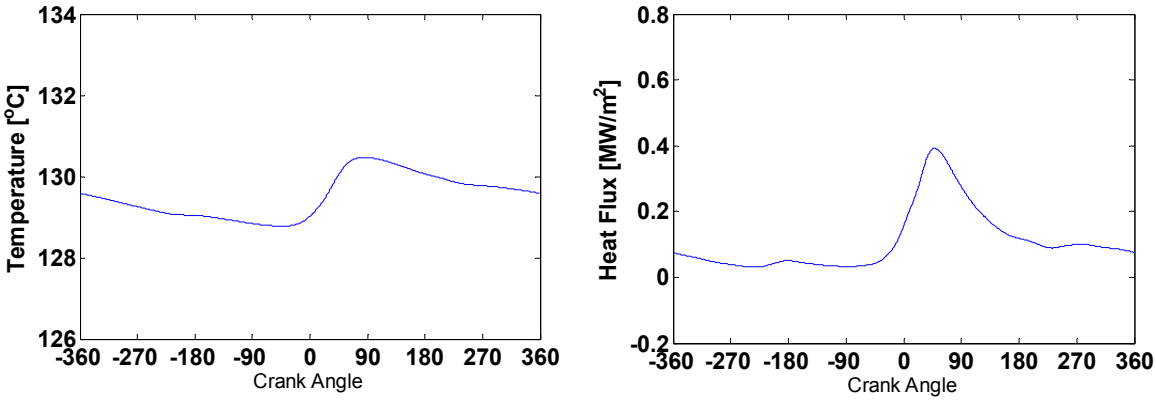

Figure 6.12 – These are the calculated 'bottom of layer' temperature and heat flux profiles to be used for validation of the Lead-Corrector method.

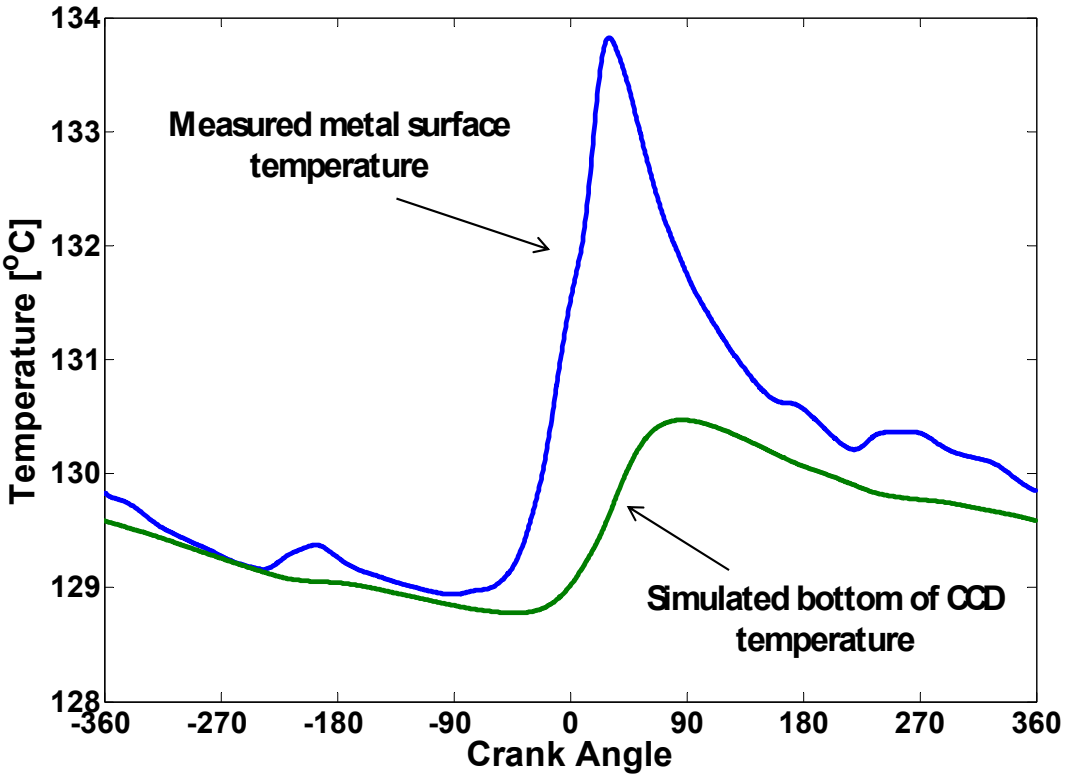

Figure 6.13 – The 'bottom of layer' temperature profile is to be used as boundary condition in the Lead-Corrector method to reproduce the actual measured (metal) surface temperature profile.

6.4.2 Validation Results

Figure 6.14 shows the results of using the LC methodology on the parameters explained in the previous section. The narrow-dashed curve is our simulated temperature measurement at the bottom of the layer, the wide-dashed curve is the temperature profile calculated using the LC-method, and the solid line is the actual measured surface temperature profile.

It is clear that the actual experimental measurement and the calculated profile are very close. The LC-method was successful in using the 'measured' bottom of the deposit layer temperature and heat flux (not shown) to determine the layer top surface

temperature. It is convincing to see that starting with such as simple shape, at the bottom of the 'deposit' layer, so many details of the surface profile could be restored through the LC method. A closer look shows that these details, such as the temperature bumps at -180° and near +270°, are still present in the bottom-of-layer profile as subtle changes in slope that are magnified as you get closer to the surface.

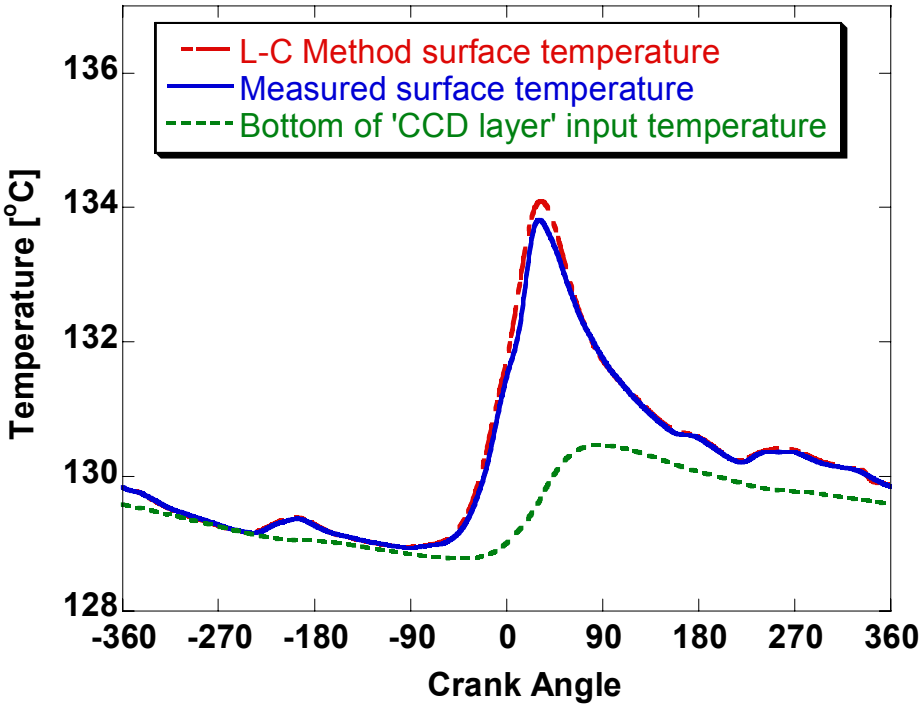

Figure 6.14 – The results of the validation attempt of the Lead-Corrector method. The 'bottom of layer' temperature profile was used to calculated the surface temperature profile. The solid line is the actual measured temperature profile at the surface of the probe, indicated close agreement.

Note that the thickness of the simulated deposit layer was 400 microns, whereas the thickness of actual deposit layers in the engine never exceeds 100 microns. Thermal properties must be taken into consideration. The thermal conductivity and diffusivity values of the simulated aluminum layer are much greater than the real CCD layer, as

indicated in Table 6.1. Thus, the penetration depth of surface heat flux transients will be much greater for the aluminum 'deposit'.

Table 6.1 – Comparison of Thermal Properties of Aluminum and CCD [109]

	Aluminum	**CCD**
Thermal Conductivity, k [W/mK]	175	~1.5
Thermal Capacity, ρC_p [J/m^{3}K]	2.4 x 10^6	~7.5 x 10^6
Thermal Diffusivity, α [m^2/s]	7.3 x 10^{-5}	1.0 → 14 x 10^{-7}

6.4.3 Accuracy of Lead-Correction Method versus Deposit Thickness

It is presumed that, for a layer's given thermal properties, the thicker the deposit, the more difficult it will be to accurately calculate the surface temperature. A parameter must be devised, which includes thermal properties and thickness, which can predict how accurate the surface temperature results will be for a given deposit.

The parameter used to quantify the possible accuracy for a deposit is the 'Layer Fourier Number'.

$$Fo = \frac{\alpha t}{L^2} \tag{6.5}$$

It is used as a dimensionless time for classic transient heat conduction problems regarding thermal non equilibrium between a surface and its interior, as well as determines stability for explicit finite different methods [113].

For the case of the LC-method it will be used to characterize the transient conduction resistance for a given deposit layer. 'L' describes the deposit layer thickness,

'α' is the thermal diffusivity of the deposit material, and't' is the characteristic time, *in milliseconds*, which is a function of engine speed and measurement increment resolution. By inspection it is clear that thicker deposits with lower thermal diffusivity make it more difficult to get accurate results. Both factors are consistent with the ability of the experimental temperature profile measurement at the bottom of the deposit layer to pick up the penetration of the heat flux transients at the surface. The thicker and more thermally resistive the layer, the more dampened the temperature profile signal will be once it reaches the heat flux probe at the back of the deposit layer, and the harder it will be to reproduce the temperature profile at the gas-side surface of the layer.

Figure 6.10 showed 100 layers of temperature gradients in a clean heat flux profile. For the above validation case, the 10^{th} layer at 400 microns was used and gave good results. What happens if a deeper layer is used, e.g. a thicker deposit? Figure 6.15 below is a plot of different 'deposit' thicknesses used with the LC-method to calculate the surface temperature.

It is clear that as the simulated deposit gets thicker, the calculation accuracy suffers. Enough of the original surface temperature profile characteristics are dampened out that the LC-method cannot reproduce the surface temperature profile. Going forward, based on these results, if a deposit layer's Fourier number is greater than 1.0 than it can be considered that the LC-method is suitable for accurate surface temperature calculation. All results in this Chapter and the next pertain to Fourier numbers greater than 1.0.

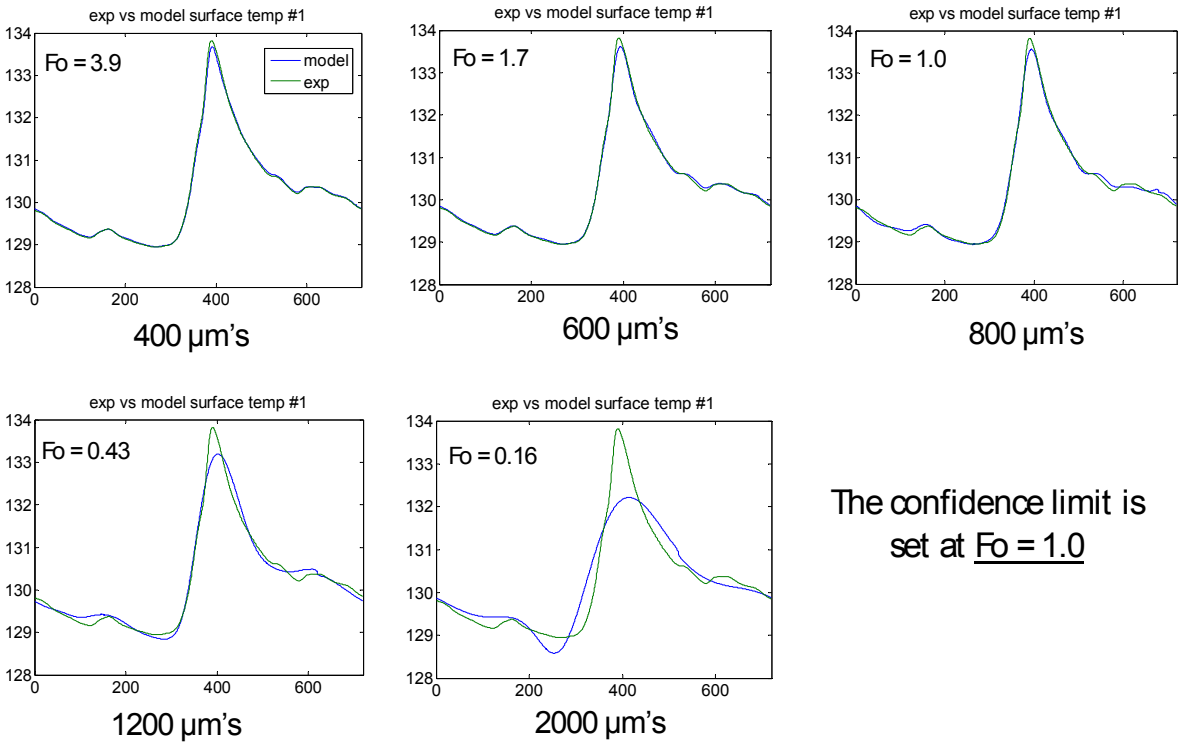

Figure 6.15 – Each plot is a comparison of the heat flux probe surface temperature profile with the calculated temperature profile using the Lead-Corrector method. Each plot is based on a 'bottom of the layer' temperature profile at varying depths. As the thickness of the 'deposit layer' increases, the ability to accurately calculate the surface temperature profile diminishes.

6.5 Sample Results

A quick illustration of some initial results from one of the head mounted heat flux probes are shown here. More results and in-depth analysis is given in the next chapter, using both head and piston probe locations.

6.5.1 Initial Results for CCD on the Cylinder Head

Figure 6.16 is a plot of the calculated CCD layer surface temperature on a head mounted heat flux probe at two different thicknesses compared to the measured surface temperature on a clean probe. It is clear that deposits have a significant effect on the temperature at the 'wall'/gas interface. The main effect is on the temperature swing. In the clean case (red), the maximum temperature swing is about 5°C. But for the thickest deposit layer case of 50 microns, the temperature swing is about 20°C. As will be shown, this can have a significant effect on local peak heat flux levels. It is thought that these higher wall temperatures during heat release are responsible for less heat loss and thus higher burn rates for combustion chambers covered in CCD.

Another point to consider is that the cycle average temperature does not change very much. This will be looked at more closely in the next Chapter.

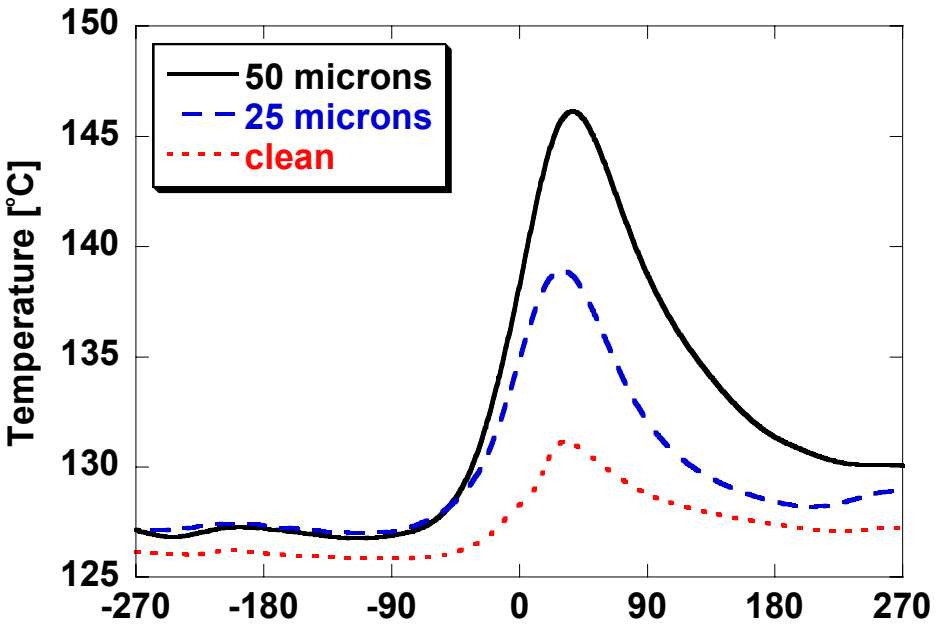

Figure 6.16 – These are sample results of the Lead-Corrector method. The experimentally measured surface temperature of a clean probe in the head is compared to the calculated deposit layer surface temperature at thicknesses of 25 and 50 microns.

6.6 Chapter Conclusions

This chapter introduced the Lead-Correction Method for calculating the surface temperature profile of a deposit layer. The advantage of the LC-method is that the calculations can be made based solely on experimental measurements. All that is required are the measured temperature and heat flux profiles at the bottom of the deposit layer, at the metal wall surface, and the correct thermal properties of the deposit material itself, which are obtained from experimental measurements. There are no assumptions or generalities made regarding local gas temperatures and heat transfer coefficients, which can vary locally due to in-cylinder stratification.

The methodology was validated using clean heat flux probe measurements and analyzing a contrived ‘aluminum layer’ on the head surface.

The sample results shown for the single head mounted heat flux probe indicate that with 50μms deposit coverage the cycle temperature swing at the surface increase from about 5°C in a clean engine to at least 20°C with deposits. This change in peak temperature swing can have a significant effect on heat loss rates during the heat release portion of the combustion cycle. This will be studied more in depth in the next chapter, using measurements obtained on both the cylinder head and the piston.

CHAPTER 7

THE EFFECT OF A DEPOSIT LAYER ON COMBUSTION CHAMBER SURFACE HEAT LOSS

7.1 Introduction

The previous chapter introduced the Lead-Correction (LC) method specifically developed for approximating the gas-side surface temperature profile of the deposit layer in the combustion chamber. It is based on experimental temperature and heat flux measurements taken *below* the deposit layer and a known deposit layer thickness.

Based on sample results from measurements taken from one of the head probes, it is clear that the magnitude of temperature swing during the cycle varies significantly as the deposit layer thickness increases. The cycle temperature swing measured on a clean head probe is 5°C. With a 50μm layer of deposit, the temperature swing increase to 20°C. It will be shown in this chapter that this is transient change in temperature at the gas-deposit layer interface is sufficient to affect the heat flux from the gas to the wall is affected.

In this chapter the LC method will be applied to temperature measurements taken from several locations in the piston with a deposit layer on it. The change in cycle heat flux will be studied and then compared to the heat flux at the same locations with a clean combustion chamber. This provides insight into the nature of the effect of combustion chamber deposits on HCCI combustion that has been demonstrated in chapter 4.

7.2 Lead-Correction Method Results

This section will start off with an in-depth comparison of the calculated temperature gradients from a head probe with two different deposit layer thicknesses. Then CCD surface temperature profiles from the piston will be examined for the effect of deposit coatings at different locations.

Results obtained from the Cylinder Head Surface

Figure 7.1 below is a plot of the temperature profile on the surface of deposit layers of 25 and 50 microns as calculated by the LC method. This is the same plot shown at the end of the previous Chapter. As already indicated, the cycle temperature swing quadruples between the 50 micron deposit layer and the clean probe. The next section regarding temperature gradients is based on these temperature profiles.

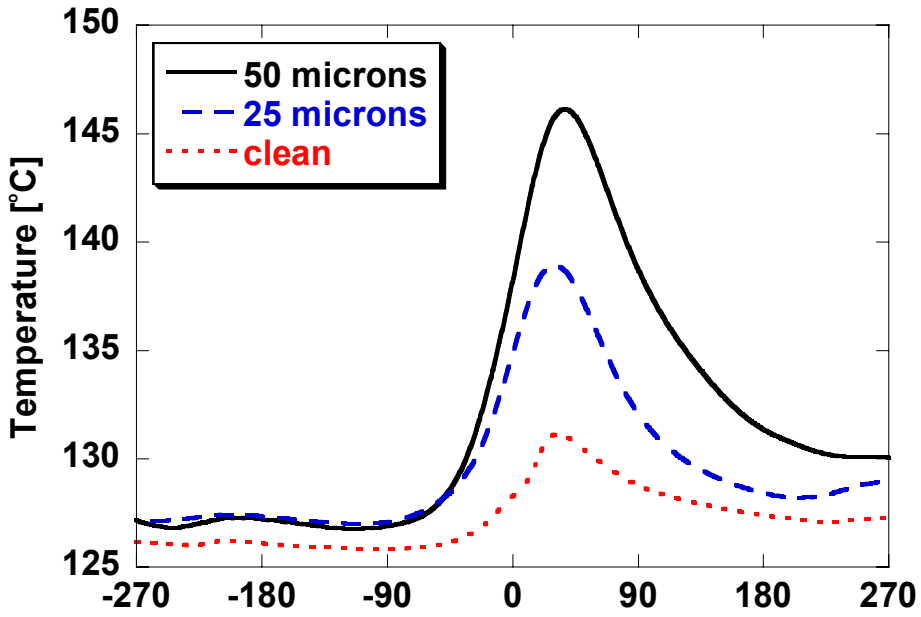

Figure 7.1 – Comparison of the measured temperature profile of a clean heat flux probe located in the head to the calculated deposit surface temperature at two different thicknesses.

Temperature Gradients

Figure 7.2 and Figure 7.3 show calculated temperature gradients within the clean heat flux probe. Figure 7.4 and Figure 7.5 show calculated temperature gradients throughout the CCD layer for the 50μm thickness case. Studying these gradients helps us understand heat flow within the deposit layer/heat flux probe. The gradients are plotted at regular intervals with all plots indicating a total depth of 50μm for both cases.

The major features of the surface temperature profile in both cases are dictated by the combustion process. At different depths into the metal of deposit layer (depending on the case) the overall shape does not change very much. But it is clear that there is increased dampening of the signal with depth and the phasing of the overall profile is retarded from the surface layer. In general, the farther apart the profile lines are, the higher in magnitude the heat flux is at that point. So it is actually possible to track the main heat flux event (from heat release) as it penetrates down into the layer within the first 90 crank angles after combustion TDC.

It can also be seen that during the intake stroke and early in the compression stroke the temperature profiles are closer together within the CCD layer than within the metal wall of the clean chamber, indicating less heat flux into the wall. The second Figure in each pair is a magnified look at this portion of the cycle. It is evident that not only is there less heat flux into the deposit layer than the clean metal wall but there is actually a greater amount of heat flux reversal between -300° to -200° interval. This is indicated by the surface profile being overlapped by profiles that are from below the surface. This will result in heating of the cool intake charge by the chamber walls. Heat flux curves for these cases will be shown later in this chapter.

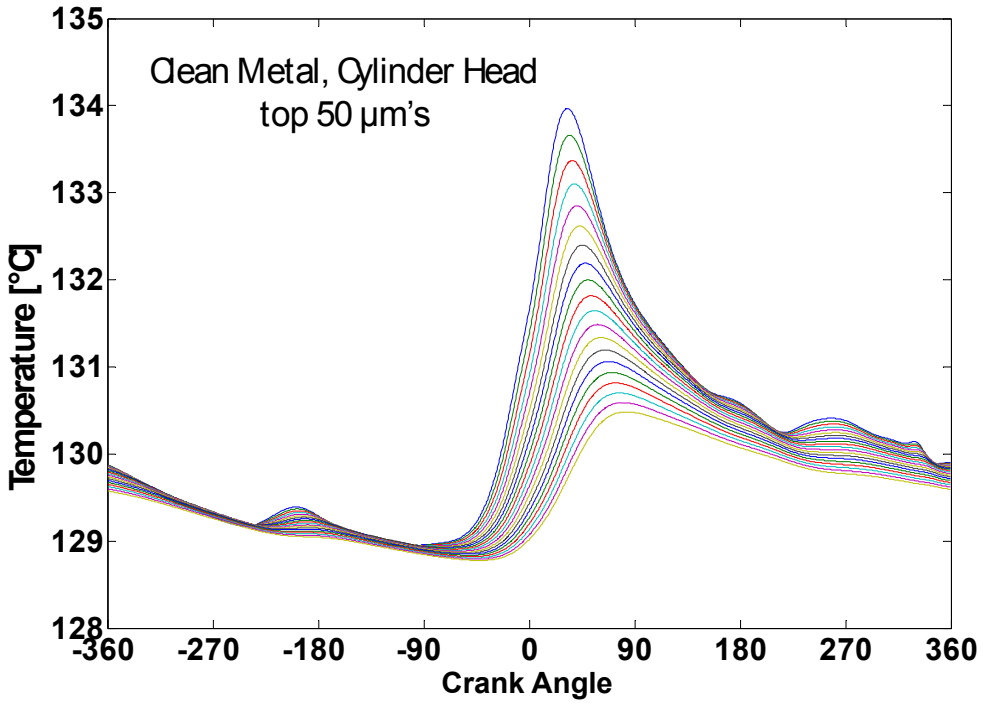

Figure 7.2 – Calculated temperature gradients at even depth intervals down from the surface of a clean heat flux probe.

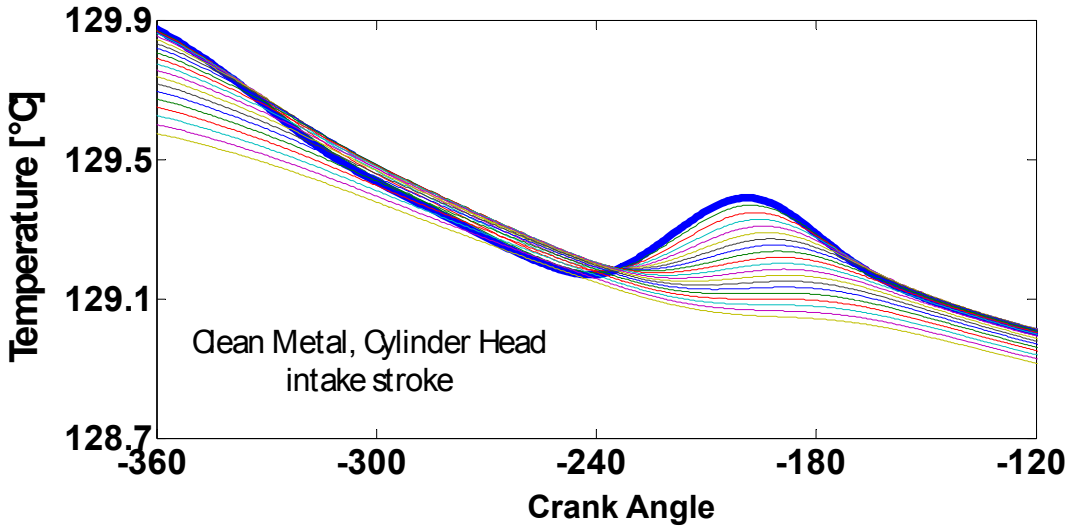

Figure 7.3 – A close-up of the intake portion of the temperature profiles at even depth intervals for a clean heat flux probe, showing heat flux reversal. The bold line is the clean surface temperature profile.

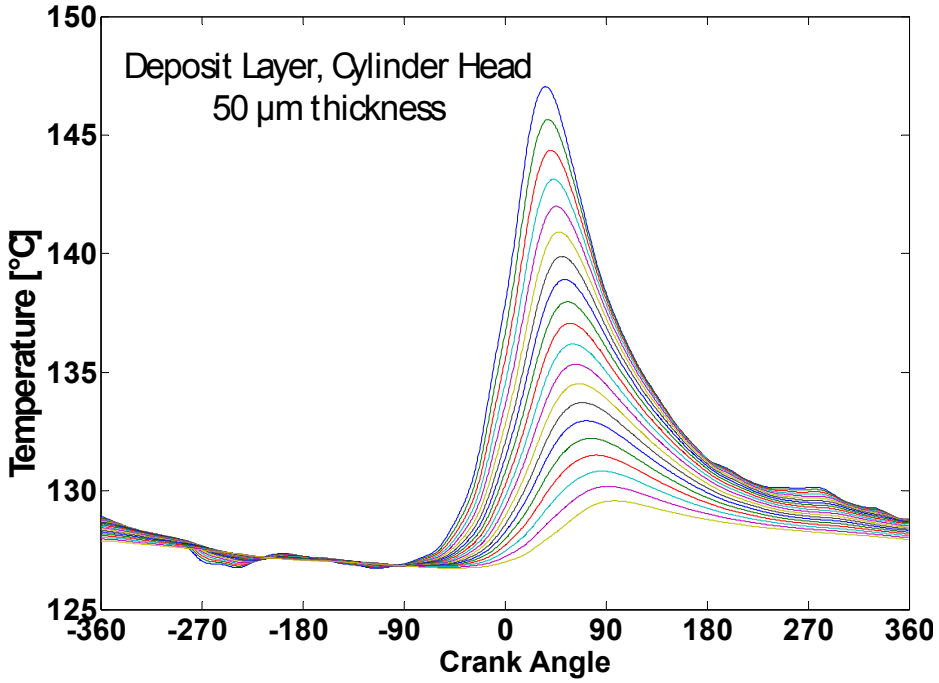

Figure 7.4 – Calculated temperature gradients at even depth intervals down from the surface of a 50 microns thick deposit layer.

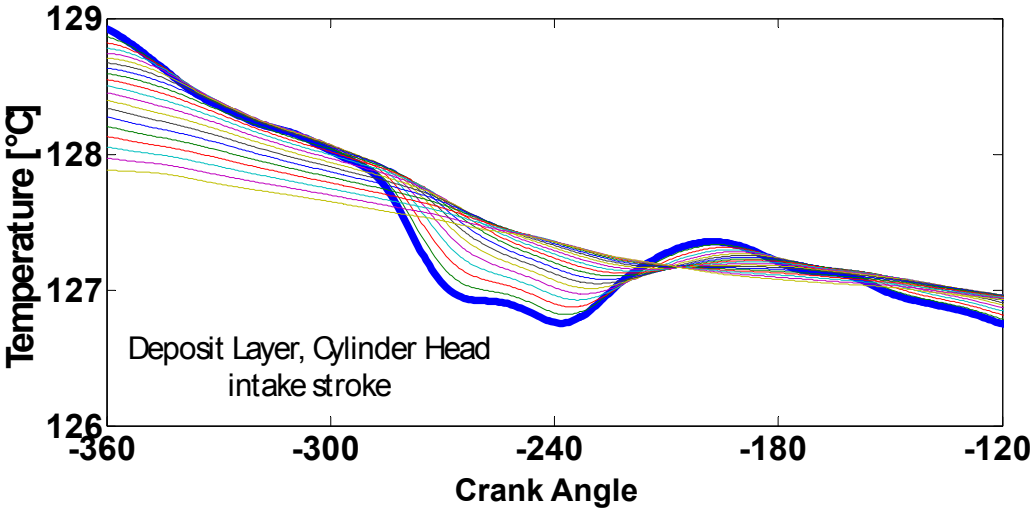

Figure 7.5 – A close-up plot of the intake portion of the temperature profiles at even depth intervals into a 50 micron thick deposit layer, showing heat flux reversal. The amount of heat flux reversal is much greater than in the case of the clean probe, shown in Figure 7.3.

7.2.2 Results from the Piston

The previous section demonstrated the nature of the changes in wall heat flux imposed by an insulating deposit layer on one of the head-side mounted heat flux probes. This section will look at similar results from several probe locations in the piston. First, temperature measurements from a clean chamber will be shown, followed by the calculated surface temperature profiles of a conditioned piston. Then comparative surface heat flux profiles from a few locations will be examined.

Surface Temperature

Figure 7.6 is a plot of the temperature profiles from the piston while the combustion chamber is clean. This same plot was shown previously in Chapter 5. As in the previous head probe measurements, the temperature swing at every location is no greater than 5°C while the probe is clean. Figure 7.7 is a plot of the calculated surface temperature profiles at the end of chamber conditioning, as calculated by the Lead-Correction method. This shows the actual temperature profile at the CCD layer/gas interface. In this case the burn rates are higher than in the clean chamber case, due to the effect of deposits on HCCI combustion demonstrated earlier. Consistent with the previous results from the head probe, the cycle temperature swing is much higher at the 'wall'/gas interface with a conditioned combustion chamber than in the clean case.

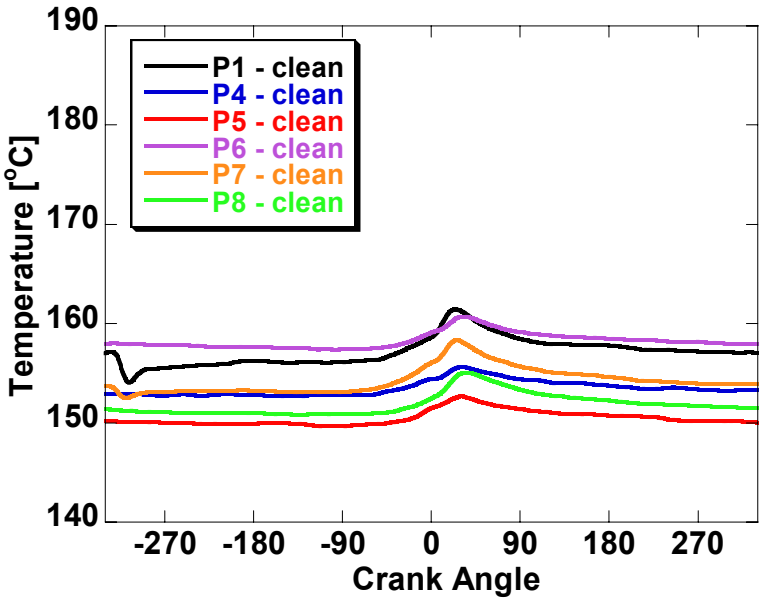

Figure 7.6 – Measured temperature profiles from six locations of a clean piston.

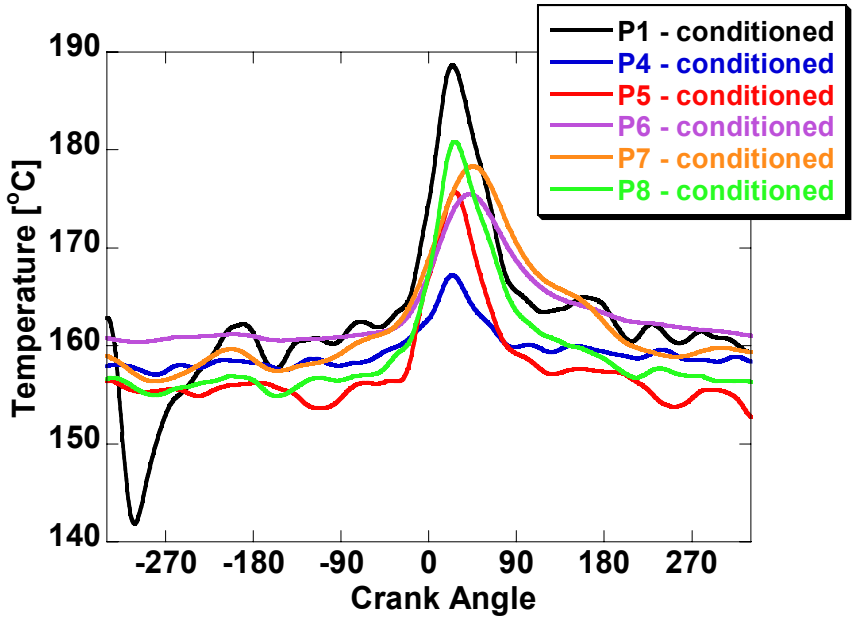

Figure 7.7 – Calculated deposit surface temperature profiles for six locations on the piston in a conditioned combustion chamber. The calculations are based on the Lead-Correction method.

For a better direct comparison, the burn rates for each case should match, because of the direct influence that heat release phasing and magnitude has on gas temperatures and thus wall temperature profiles. With burn rates compensated it is possible to single out the effect of the deposits on temperature and heat flux without any influence from varying heat release rates. As done before, the intake temperature was lowered until the phasing of 50% MFB in the conditioned chamber matched that of the clean chamber, thus the burn rate and gas temperature during heat release were much closer together, so that overall heat loss levels were comparable, as confirmed in previously.

Figure 7.8 is a plot of the calculated surface temperature profiles with a conditioned chamber but with intake temperature lowered from 90°C to 70°C so that burn rates match those of a clean chamber. Though the temperature swing at each location is not as great as in Figure 7.7 with faster burn rates, they are still on the order of 10-15 °C, compared to the clean case of about 5°C for most locations. This indicates again that there is a thermal effect imposed by the deposit layer which causes a greater surface temperature swing than with a clean wall. Also, the fact that in the intake temperature had to be reduced for combustion timing to match confirms the significance of the transient CCD response for HCCI combustion.

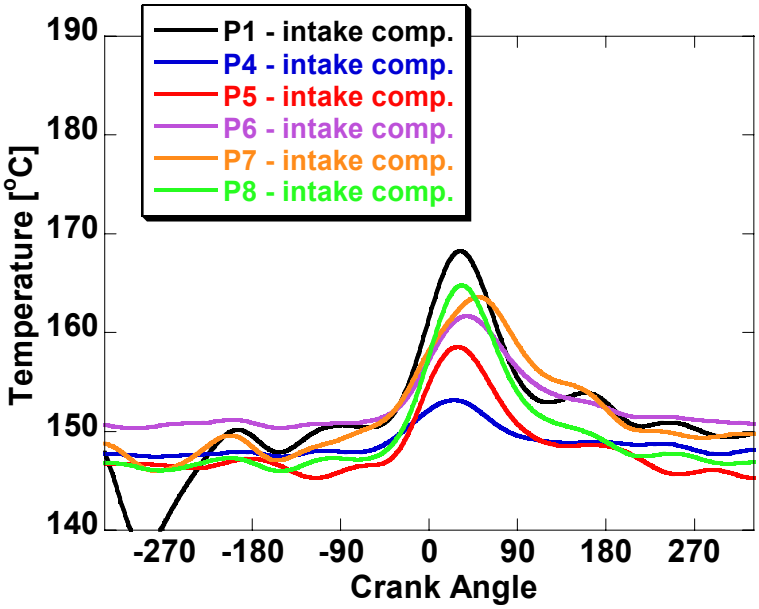

Figure 7.8 – Calculated deposit surface temperature profiles for six locations on the piston in a conditioned combustion chamber. In this case the intake temperature has been decreased until the HCCI burn rates match those of a clean chamber.

Surface Heat Flux

Figure 7.9 through 7.11 are the heat flux profiles at the gas/surface interface for a few locations on the piston for the clean chamber versus conditioned. The profiles from the clean engine are based on direct measurements from the engine and the profiles for the conditioned chamber are based on the calculated temperature gradients at the surface of the deposit layer. All results are obtained with same burn rates, i.e. the results from the conditioned chamber were obtained in the engine operating with reduced intake temperature. The local deposit layer thickness is indicated on each plot.

In every case shown, the peak cycle heat flux during heat release is reduced for the case with CCD coverage. The thermally resistive properties of the deposits cause the higher temperature swings, as shown by the temperature curves, which reduces the local heat flux levels. In a couple of the locations, specifically, P1 and P8, the heat flux

throughout most of the cycle is lower with deposit coverage. For example, a negative absolute heat flux magnitude during the first 180 degrees of the cycle indicates heat transfer from the wall to the intake charge, which will increase the gas temperature at intake valve closure. This offsets the impact of reduced intake temperature so that ignition occurs at roughly the same timing as in a clean chamber, leading to overall similar burn rates. In locations P1 and P5 it is possible to see clearly that there is less heat loss during compression, which will also affect the ignition timing.

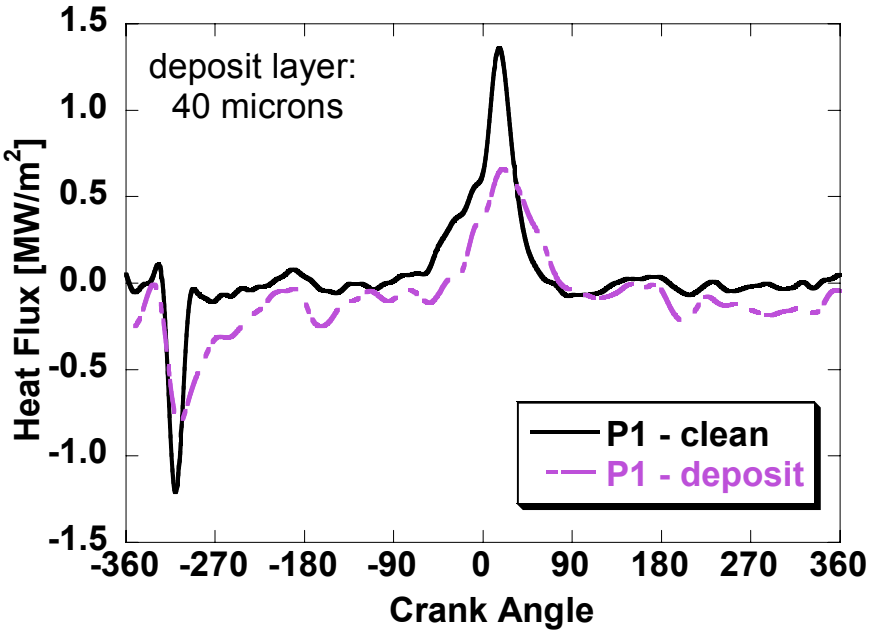

Figure 7.9 – Measured clean piston heat flux profile compared to the calculated deposit surface heat flux profile at probe location #1.

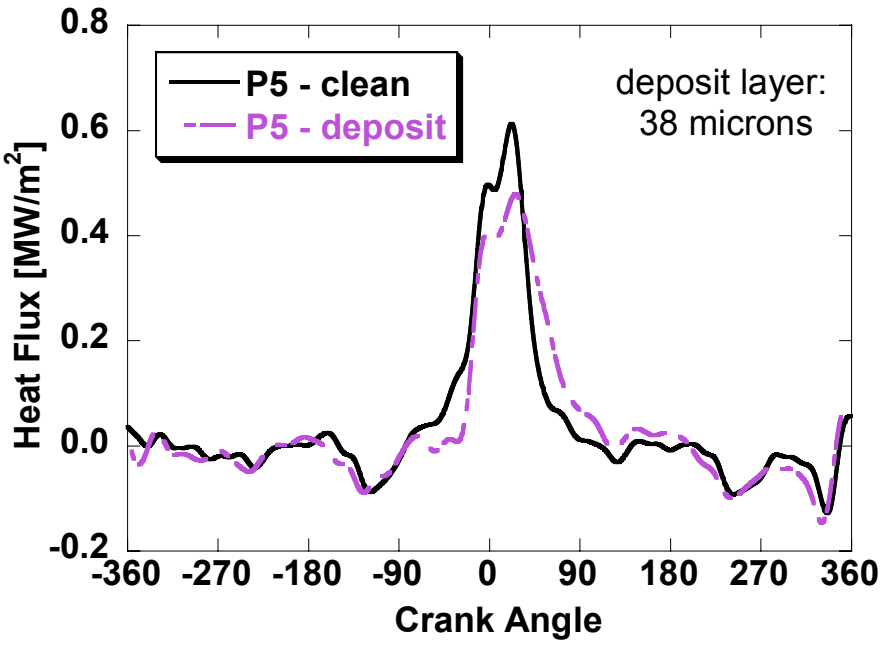

Figure 7.10 – Measured clean piston heat flux profile compared to the calculated deposit surface heat flux profile at probe location #5.

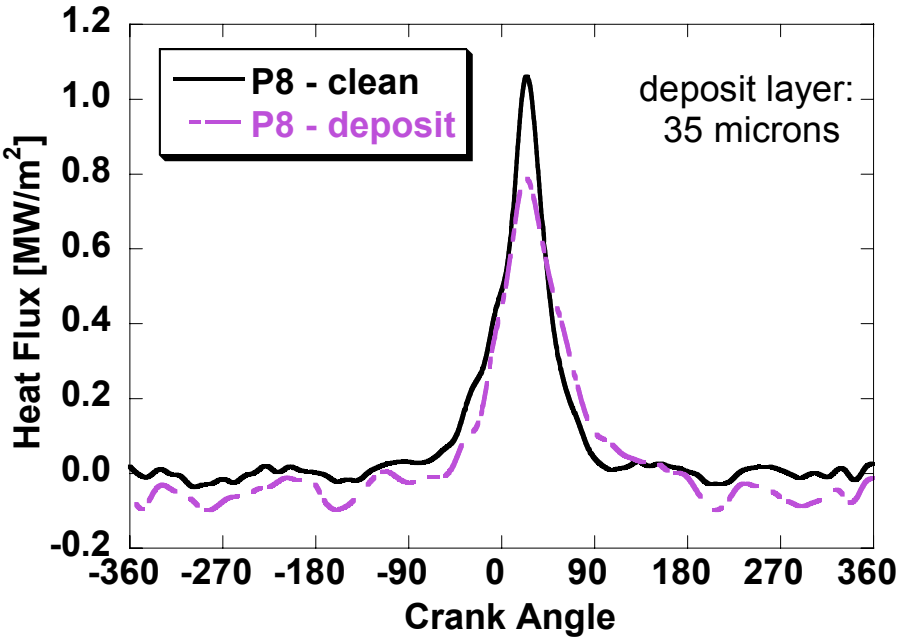

Figure 7.11 – Measured clean piston heat flux profile compared to the calculated deposit surface heat flux profile at probe location #8.

Discussion of CCD Surface Heat Flux

It is apparent from the results shown so far in this chapter that a deposit layer covering the metal walls of the head and piston has an effect on the local heat flux levels out of the chamber. Not only are the peak heat flux levels during the heat release portion of the cycle affected, but also throughout the entire cycle, including the intake and compression strokes. Reduced heat flux to the walls during actual combustion would explain the documented changes in burn duration, especially the bulk burn period, which also affects hydrocarbon emissions. But for combustion phasing to be as advanced as it is, the ignition point would have to occur earlier. Intake charge heating from the deposit level as well as reduced heat loss during the compression stroke would explain this.

It must now be determined whether these calculated changes in heat flux are enough to consider them responsible for the effect of CCD's on HCCI combustion, demonstrated in Chapter 4.

7.3 Quantification of Heat Flux Changes due to CCD Coverage

The previous section demonstrated how the calculated CCD layer surface temperatures could be used to understand what changes the deposit layer imposed on surface thermal interactions. Based on the results shown in Chapter 4 it is clear that deposit layer formation in the combustion chamber has a significant effect on HCCI combustion. This section will demonstrate the nature of the effect of the changes in chamber surface heat flux and how that causes the changes recorded in combustion.

7.3.1 Combustion

Figure 7.12 below is a plot of the heat release rate curves for the data points described in the previous section of this chapter. These will be the cases for comparison of heat flux in this section as well. The solid curve depicts the calculated heat release rate

with a clean combustion chamber at the baseline operating point of 2000rpm and 11 mg fuel/cycle. The dotted curve depicts the heat release rate after the chamber has been 'conditioned' at the same operating point; it is completely covered by a layer of deposits. The dashed curve is a plot of the 'compensated' case, with heat release rate matching the clean engine. Thus, the intake temperature was reduced from 90°C to 70°C to 'compensate' for the combustion chamber deposits.

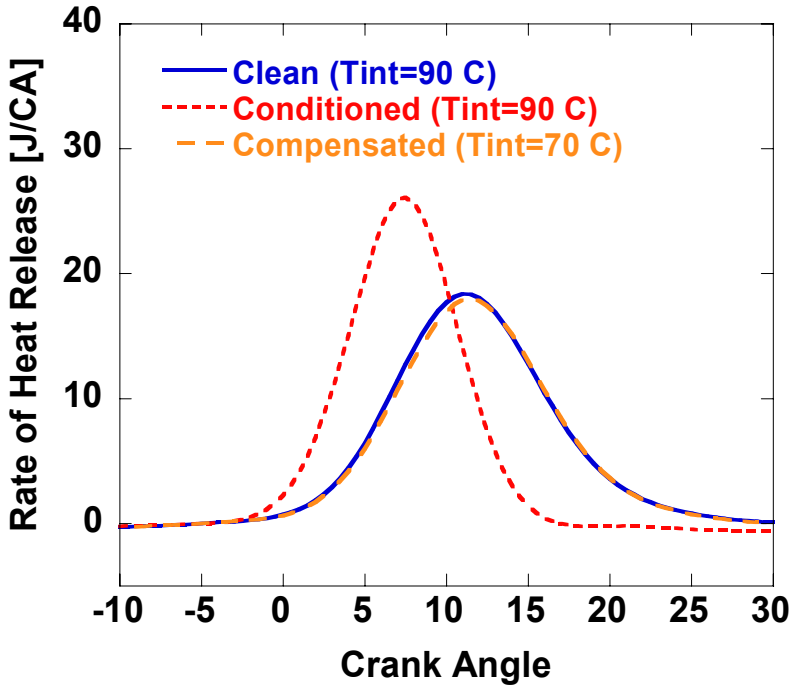

Figure 7.12 – Heat release rates for the three cases considered in this discussion. The solid is for a clean chamber, the dotted is for a conditioned chamber, and the dashed is for the same conditioned chamber, but the intake temperature has been reduced from 90°C to 70°C so that the original clean chamber heat release is repeated.

The purpose of studying the 'compensated' case is in order to single out the effect of CCD on combustion. In the 'conditioned' case, the thermal effects of the deposits causes ignition to advance and burn rates to increase, as quantified below in Table 7.1. The higher burn rates result in higher cycle peak gas temperatures and thus higher rates

of heat loss to the walls, regardless of the deposit layer. Because HCCI combustion is so dependent on the effects of deposits, it is easier to quantify their effects when the changes in combustion are eliminated. With the reduced intake temperature case, since cycle heat release rates are matched, any changes in wall heat flux, emissions, etc. will be due only to the deposit layer itself.

Table 7.1 – Comparison of a few key operating parameters

2000rpm, 11mg/cycle	CLEAN	CONDITIONED	COMPENSATED
T_{intake} [°C]	90	90	70
CA10 (°aTDC)	6.7	2.8	5.8
CA50 (°aTDC)	12.3	7.3	12.0
Burn Duration (°CA)	16.6	9.2	15.3
Peak HRR (J/CA)	18.0	25.8	18.0
IMEP (kPa)	361	363	353
$T_{exhaust}$ [°C]	726	712	726
EI HC (g/kg fuel)	32.3	22.3	34.3
EI NOx (g/kg fuel)	0.16	0.62	0.24

7.3.2 Averaging Heat Fluxes

As shown previously, temperature measurements were taken in the combustion chamber at a total of eight different locations, two on the head side and six on the piston. Instead of comparing every individual location it will be easier to group the locations into sections of the chamber. Of course the most straight-forward way to do this is to group

them into head locations and piston locations. The six piston locations are then further split into the three probes from the bowl and the three located on the periphery of the bowl. The local thickness of the deposit layer at each probe location is listed in Table 7.2.

Table 7.2 – Table of the local deposit layer thickness at each probe location

Probe #	**P1**	**P4**	**P5**	**P6**	**P7**	**P8**	**H1**	**H2**
CCD thickness [µm]	40.0	13.5	38.6	47.5	55.6	36.6	16.5	15.5

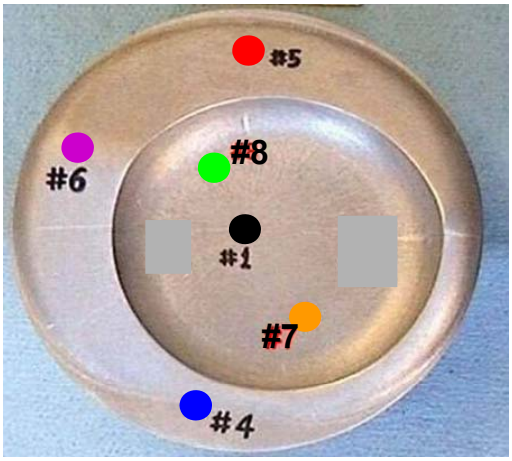

In the rest of this section, as before, for the case of the clean chamber, the *clean* heat flux profiles used are direct measurements from the engine. The conditioned cases are calculated deposit layer surface heat flux as a result of applying the LC method to temperature measurements taken below the deposit layer.

Because of the number of probe locations in the chamber to consider, for the purposes of comparison between the clean and conditioned cases, the heat flux profiles from certain locations will be grouped together and a representative heat flux profile will be used for each case of chamber state. This will be done by performing a weighted average of the heat flux profiles depending on their location and the surface area represented by them. The total combustion chamber surface will be split into two main parts, the head and the piston surfaces. The piston will then be further split into the

locations in the bowl (probes P1, P7, and P8) and those on the periphery of the crown (probes P4, P5, and P6). Table 7.3 lists the surface areas represented by each section of the chamber and the percentage of the total chamber surface area.

Table 7.3 – Surface area percentage of each region of the combustion chamber

Location	**Piston Bowl**	**Piston Crown**	**Piston Total**	**Head Total**	**Chamber Total**
Surface area (cm^2)	30.6	39.4	70	67.9	137.9
Percent of total chamber surface area [%]	22.2	28.6	50.8	49.2	100

Piston Average Heat Flux

Figure 7.13 is a plot of the average heat flux for the six probe locations in the piston for the three cases of chamber state (clean, conditioned, and compensated). It is clear that in both cases with deposit coverage, regardless of the burn rate, the peak surface heat flux level is less than the clean case. In the 'compensated' case, with reduced intake temperature, the peak heat flux is only a little more than half that of the clean case. This will have a significant effect on combustion during the heat release portion of the cycle, especially when considering the importance of thermal conditions for HCCI. Also, for both cases with deposits, the heat flux during intake and compression is lower than the clean case. For the conditioned case with 90°C intake, this leads to advanced ignition timing, as was indicated in Table 7.1. For the conditioned case with 70°C intake temperature, the ignition timing is similar to the clean case, so the further reduction in heat flux during intake (actually charge heating) compensates for the cooler intake charge temperature so that the ignition timing matches the clean case.

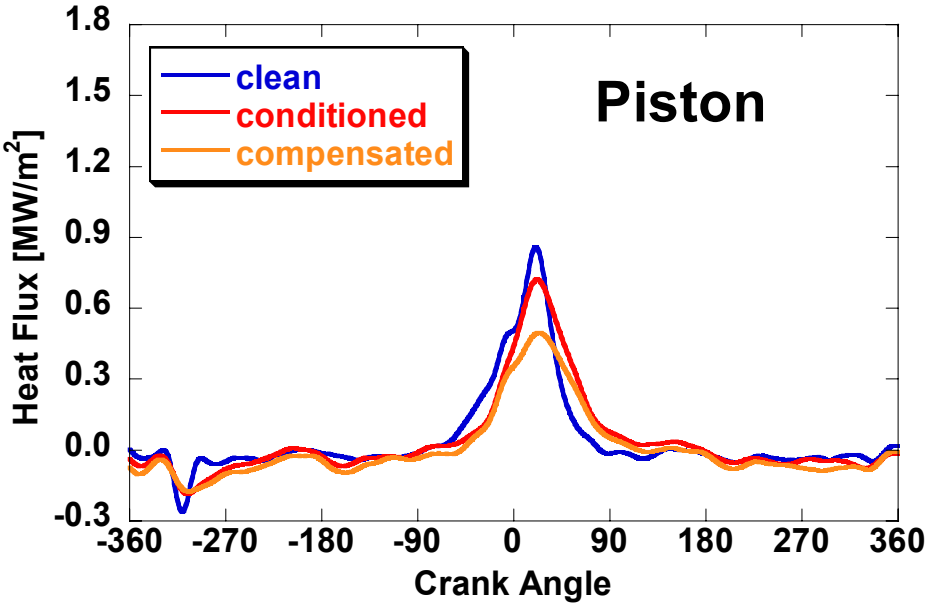

Figure 7.13 – Average heat flux profile representing all probe locations in the piston.

Another important point to confirm is that with CCD coverage, there is higher heat flux levels during the latter part of heat release compared to the clean case. The reduction in heat flux during compression and the early part of heat release causes the surface temperature swing to increase, as shown in the previous chapter, storing thermal energy in the deposit surface only to have it finally diffuse out of the chamber during the latter parts of heat release. This is consistent with the faster bulk burn and lower HC emission associated with a conditioned combustion chamber, as described in Chapter 4.

Bowl versus Crown Heat Flux

Figure 7.14 shows the plots of the average heat flux profiles representing the three probes in each of the piston bowl and crown. Since the main characteristics of heat flux are so different between the piston bowl and the periphery of the crown, these plots are actually more representative of the actual local heat transfer changes. As would be expected, the peak heat flux levels in the bowl are actually very high, while the levels are

much lower around the periphery, where combustion is not able to penetrate as close to the cool walls due to in-cylinder thermal stratification.

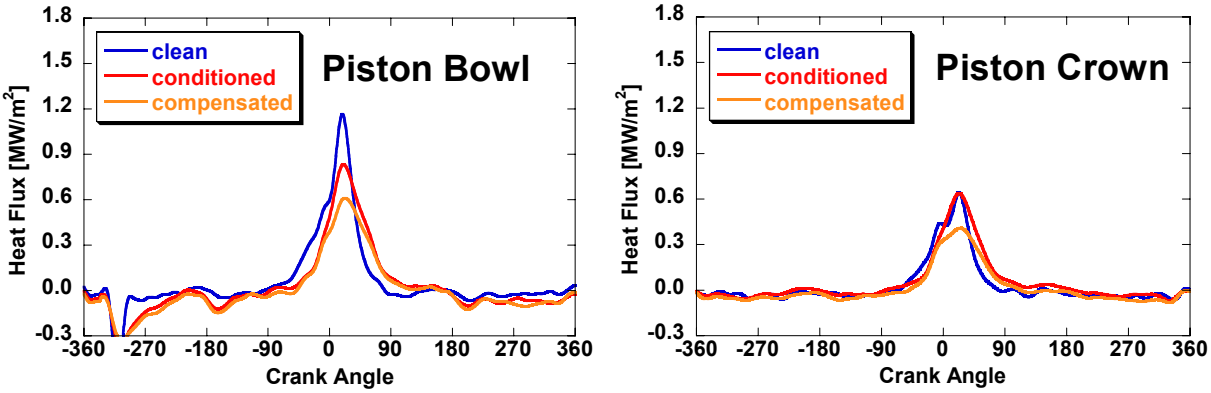

Figure 7.14 – Average heat flux profile representing all probe locations in the piston bowl and crown separately. The bowl represents piston locations P1, P7, and P8. The crown represents piston locations P4, P5, and P6.

In the plot of locations from the piston bowl, the effect of the deposit layer on the fuel impingement is clear, at about -330° CA. The total heat flux is similar as the clean case, but is a longer event. This indicates possible pooling of the fuel into the deposit layer until it evaporates later into the intake stroke.

It is also interesting to note that even though the burn rates for the respective cycles are quite different, the average peak heat flux rates on the periphery of the piston crown between the clean and conditioned cases does not changes much. This would indicate that burning around the periphery of the piston has increased enough with respect to the rest of the chamber that the thermal effects of the deposits are not enough to offset the increased burn rates, like at the other locations. This is shown most clearly in the case of piston location P5 shown in Figure 7.15 below. Even with the deposit layer, the peak heat flux levels are higher than with a clean surface.

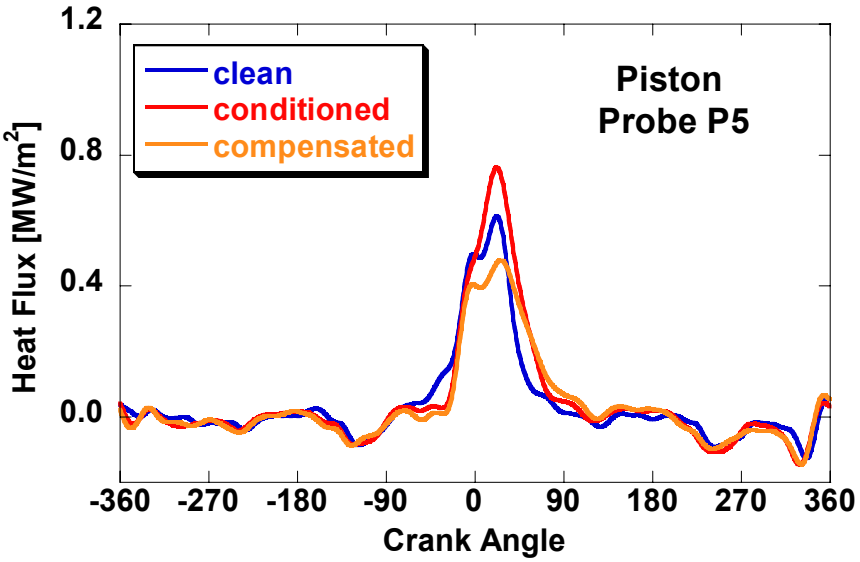

Figure 7.15 – Measured clean heat flux profile compared to the calculated deposit layer surface temperatures for piston location P5

Head Average Heat Flux

Most of the major features apparent in the average piston heat flux profiles apply to the case of the average head heat fluxes as well, as shown in Figure 7.16. The only significant difference is that there is less of a difference in heat flux during the intake stroke with deposits as compared to the average piston heat flux. This is most likely due to the piston surface's interaction with the intake charge compared to the head's. The other difference is that while peak heat flux levels are again reduced with a CCD layer, the absolute levels are consistently higher in the head than for the piston. This is because the average head side temperatures are cooler than the piston because of the direct influence of coolant flow.

It should be noted that the surface area considered in the calculations of the heat flux to the head side do not include the valves faces. These surfaces stayed clean throughout testing due to their elevated temperatures compared to the other surfaces of

the head. For this same reason, it is assumed that heat loss to the valves scaled with burn rates and was not affected by conditioning of the rest of the chamber.

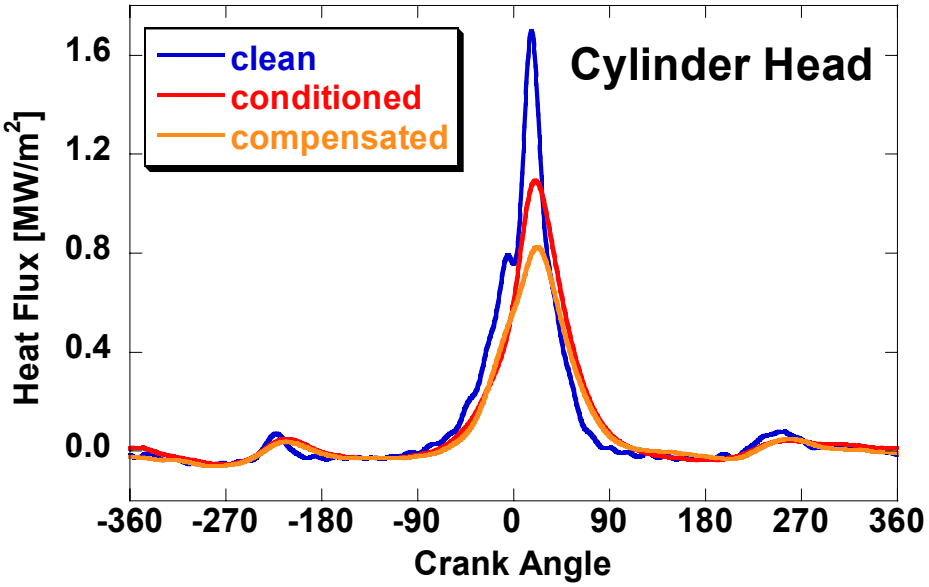

Figure 7.16 – Average heat flux profile representing all probe locations in the head

Total Chamber Heat Flux

Figure 7.17 is a plot of the representative total heat flux for all of the combustion chamber surfaces, including both the head and piston surfaces. It is a weighted average of the heat flux profiles shown in Figure 7.13 and Figure 7.16 based on the differences in surface area of the piston and head. These average heat flux profiles will be included in a quantitative comparison of the clean and conditioned cases of the chamber for determining the specific effect of CCD on heat loss.

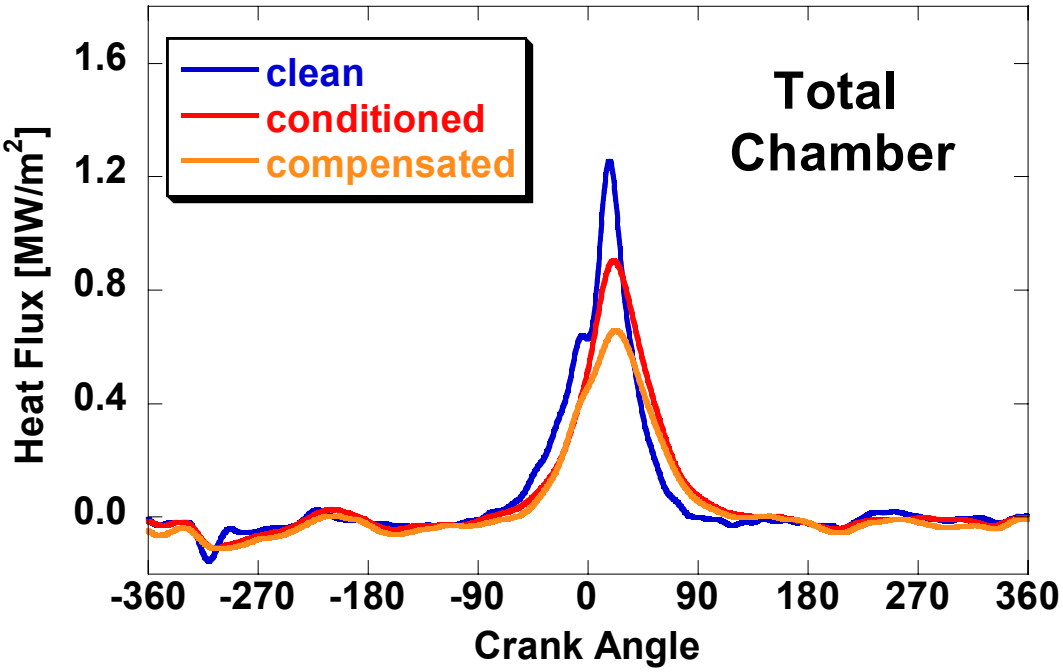

Figure 7.17 – Plot of the average heat flux profile representing all probe locations in the combustion chamber, with all probes weighted according to the surface area they represent.

Figure 7.17 shows that all the main features from the previous plots of the average head and piston plots are maintained. Notice that the heat flux profiles for the two cases with deposits (conditioned and compensated), are almost the same for most of the cycle. The only time at which there is any significant difference is during heat release. The purpose of lowering the intake temperature was to match burn rates of a clean chamber during heat release, and for this reason every other part of the cycle does not have a reason to show tremendously varying heat flux levels, because the wall conditions are the same. A closer look will actually indicate that during the intake stroke, while the profile shapes are the same, the absolute heat flux for the lowered intake case is a little less than the conditioned case. This is a result of a little more heat flux reversal into the chamber from the wall due to the 20°C less gas temperature. This becomes clearer in the next plot.

Figure 7.18 is a cumulative integration of the heat flux profiles from Figure 7.17 above. In this form, it is easier to see at which part of the cycle the deposits have the greatest effect on heat flux. As mentioned in the previous paragraph, in the case of reduced intake temperature, intake charge heating is greater than in the two other cases due to the greater temperature difference between the wall and gas. This is clearly seen in the first 360° of the cycle.

Comparing the clean and conditioned cases during the compression and heat release intervals of the cycle, confirms our main assumptions. With deposits there is less heat loss during compression, as the layer stores heat and increases in temperature compared to the clean metal wall. After the main heat release event, this stored heat eventually makes its way into the chamber wall, so at the end of the cycle the net heat loss between the clean and conditioned cases is actually the same. However, increased instantaneous surface temperatures during critical stages of HCCI combustion produce a very tangible effect.

A final note, clearly the cumulative heat loss in the compensated case is much lower than the clean and conditioned cases. Since the intake temperature was reduced by 20°C there is an additive effect of a cooler charge and the deposits to limit heat loss during combustion.

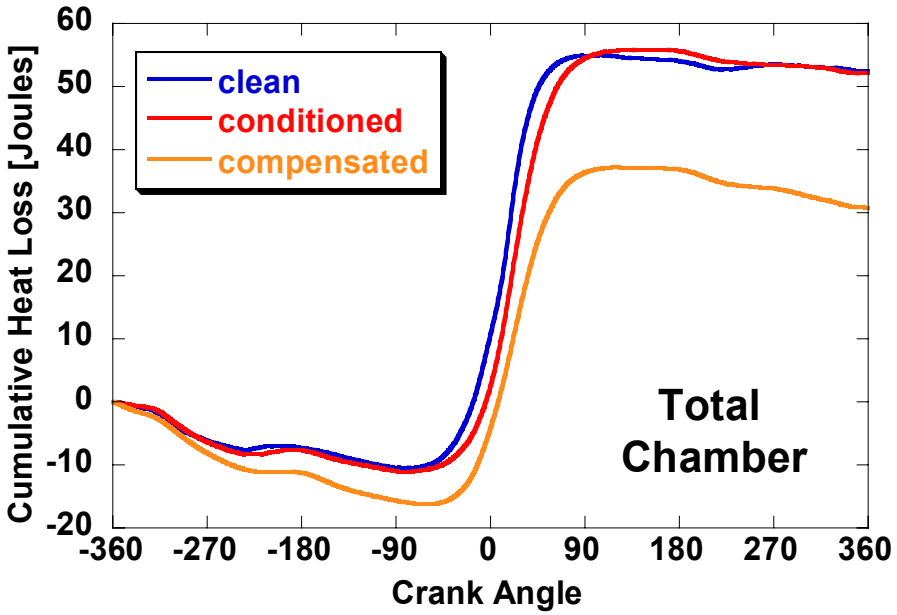

Figure 7.18 – Cumulative heat loss for the complete cycle for the three analysed cases

Based on these results, it is clear how important the thermal properties of the deposit material are compared to the aluminum wall. Specifically, the thermal capacitive versus conductive properties (by definition: thermal diffusivity), are what account for the changes in the shape of the heat flux profile with deposits. During the intake and exhaust strokes, the absolute temperature difference levels between the gas and wall are small, and there are no real differences in heat loss, despite the CCD layer. But during compression and heat release, where temperature differences levels between the gas and wall are high, the deposit layer is clearly inhibiting heat loss levels, or at least slowing them down. In effect, the deposit layer acts as a thermal capacitor.

Quantitative Heat Loss

Figure 7.19 is a plot of the clean and conditioned heat flux profiles split into the four stroke of the engine cycle (the compensated case is not plotted here for clarity). The differences between the three states (clean, conditioned, compensated) for each cycle are then integrated and quantified in Table 7.4. A better understanding of the effects of

deposits can be gleaned from analysis of the differences in loss for each individial stoke of the cycle.

As mentioned before, during the intake and exhaust strokes the heat loss levels between the clean and conditioned cases do not vary much because of low temperature differences between the gas and wall resulting in a low heat loss gradient.

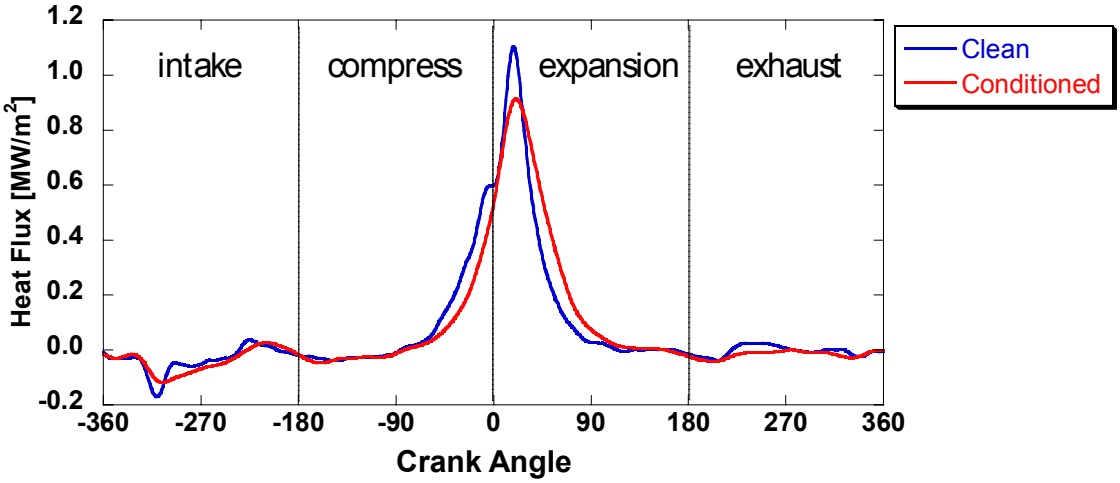

Figure 7.19 - Plot of the heat flux profiles for the clean and conditioned case separated into the four engine strokes.

The main differences between the clean and conditioned cases are first evident during the compression stoke. Heat loss leading up to TDC is almost halved with the CCD layer present. Then heat loss during the expansion stroke is almost 20% higher in the case of the deposit layer. This extra heat comes from what the deposit layer stored up during compression as well as the higher burn rates in the conditioned case leading to greater temperature gradients between the combustion gases and the walls. Again note that the decreased heat loss in the case of the deposit layer during compression is offset by the extra heat loss during heat release resulting in no net difference in heat loss for the cycle.

Table 7.4 – Comparison of the distribution of cycle heat loss for each stroke of the cycle

[Joules]	intake	compress	expansion	exhaust	Total
Clean	-7.3	17.7	43.7	-1.6	52.5
Conditioned	-7.7	9.9	53.5	-3.5	52.2
Conditioned (Tint=70)*	-11.2	6.9	41.3	-6.0	30.8

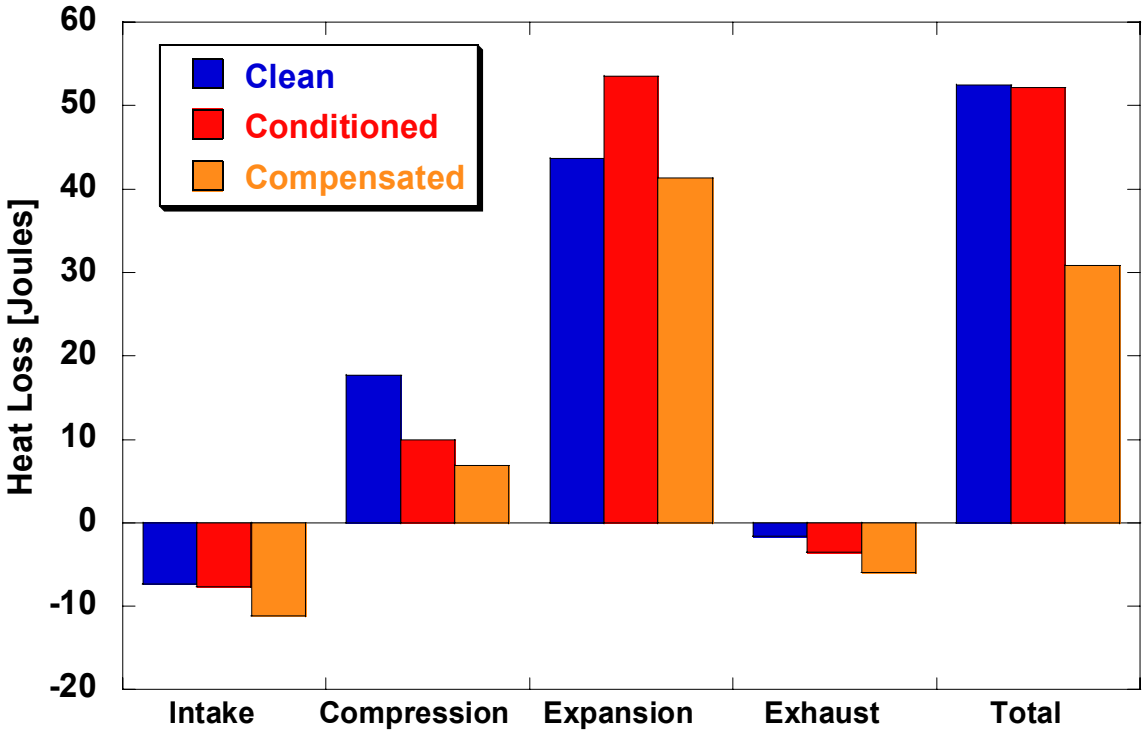

Figure 7.20 – The averge cycle heat flux for the combustion chamber is split up into the four strokes of the cycle. The integrated heat flux are quantified in Table 7.4.

A closer look at the decreased intake temperature case in Figure 7.20 gives a little better understanding of the effect of the deposit layer, when effects on burn rates are decoupled. During the intake stroke, intake charge heating is greater because of the greater temperature difference between the gas and wall. Keep in mind that one of the

most important factors affecting HCCI ignition timing is the gas temperature at intake valve closing (T_{IVC}) [114]. Then there is less heat loss during the compression stroke for the lowered intake temperature case. Since the ignition timing is the same, then leading up to the end of the compressions stroke (the first engine revolution of the cycle), the differences in heat loss between the two cases are the effects if the CCD layer offsetting the lowered intake temperature. Since burn rates are equal for the rest of the cycle, any differenes in heat loss during the expansion and exhaust strokes are due soley to the effect of the CCD layer. Specifically, the total heat loss during the expansion stroke for the clean and compensated cases are the same. Since burn rates are matched, the driving parameter for heat loss is the same. The only difference is that the heat loss occurs later in the stroke for the compensated case, as previously demonstrated.

7.4 Chapter Summary

This chapter analyses the results of applying the Lead-Corrector method to temperature measurements taken from different locations in the head and piston before and after a coating of combustion chamber deposits was present. The change in local heat flux at a few individual locations was shown in a comparison of a clean and conditioned combustion chamber. Then heat flux profiles from certain regions of the chamber were weighted on a surface area basis and averaged together for easier comparison between the clean and conditioned cases.

It was demonstrated that the layer of CCD did have a significant effect on wall heat flux, particularly during the critical intervals of the cycle. Heat loss during compression was reduced with a deposit layer present. This resulted in higher layer surface temperature swings and an advance in combustion ignition timing and phasing. It was shown that heat stored up in the deposit layer leading up to combustion did

eventually diffuse out of the chamber later in the expansion stroke. The effects of deposit coverage on bulk burning and hydrocarbon emissions can be attributed to this.

Due to the higher burn rates and thus higher peak gas temperatures with the deposit layer present, higher temperature gradients during combustion lead to greater net heat loss in the expansion stroke for the conditioned case, compared to the clean. But this just offsets the decreased heat loss with CCD during compression. The result is that the net heat loss into the head and piston surfaces for the complete cycle does not change with the deposit layer present even though burn rates are much earlier and faster.

In summary two separate effects imparted by the CCD layer are relevant. The first is heating of the incoming charge and to reduce heat loss during compression, as is most clearly demonstrated by the comparison of trends observed in the engine with clean walls and those found in the conditioned engine running with the same burn rates (compensated). This results in a higher gas temperature near TDC and thus earlier ignition timing. The second effect is clear from examination of the conditioned case without the reduced intake temperature. During heat release, near TDC, the deposit layer absorbs the heat from combustion, resulting in higher wall temperature swings and reduced peak heat flux levels. This can be attributed to the decrease in bulk burning time of the periphery of the air/fuel charge, as demonstrated in Chapter 4.

CHAPTER 8

EFFECT OF CCD ON THE OPERABILITY LIMITS OF HCCI COMBUSTION

8.1 Introduction

Up to this point it has been clearly indicated that combustion chamber deposits, regardless of how they are formed, have a significant effect on instantaneous wall heat transfer and thus affect HCCI combustion. As discussed in the opening chapter, practical application of the HCCI cycle to vehicular engines faces a few obstacles. The two main issues to contend with are its lack of discrete controllability and size of load range operability.

A gasoline-fueled SI engine triggers combustion with a spark discharge near TDC and a diesel fueled CI engine triggers it with fuel injection near TDC. HCCI ignition is dependent on suitable thermo-kinetic prerequisites for auto-ignition of the fuel/air mixture. The ability to accurately control combustion phasing is highly dependent on having prepared the correct air/fuel mixture conditions at the time of intake valve closure. Adding in the variability that deposits possess only serves to further complicate the process, but it seems that if the degree of CCD formation present can be tracked or if some form of indication based feedback control is utilized than accounting for the presence of deposits and their effects on combustion is a not a huge problem.

8.1.1 Background on HCCI operability limits

The second problem of HCCI load range operability is one that may prove to be a little more difficult to solve. In order to realize the potential benefits that HCCI is able to

provide at the vehicle level, in terms of fuel economy and emissions, it will need to be utilized for as much of the driving cycle as possible. This means that HCCI operability needs to be extended beyond what is possible for the state of the art today. The physics behind HCCI combustion to occur introduce inherent limits to the load levels at which it is able to operate. In order understand how deposits will affect this operating range the limits need to be understood.

High Load Limit

In the purest case of HCCI combustion, the fuel/air mixture is prepared homogeneously so that when auto-ignition does occur the whole charge ignites simultaneously. This is in contrast to a travelling flame front on SI combustion and a mixing controlled burning process for CI combustion. As a result, HCCI combustion duration is short and peak pressure as well as peak pressure rise rates are very high for a given load compared to conventional combustion modes. So any operation higher than typical mid-load leads to excessively noisy and potentially damaging pressure rise gradients in the engine [44]. For this reason, methods are being studied to tame the high heat release rates associated with HCCI, such as cooling, charge stratification, and super-charging [11,34, 42,53].

When taking into consideration the effects of deposits on HCCI combustion it is clear that the high load limit may be further affected. Deposits have the effect of advancing ignition and combustion phasing for given operational parameters. This naturally leads to higher burn rates when combustion timing is phased closer to TDC.

Low Load Limit

Because of minimum thermal requirements needed to promote auto-ignition of the fuel/air mixture, the degree of possible low load operation is controlled by the ability to

maintain enough thermal energy in the charge to sustain continued operation. For this reason idle operation and very low loads are problematic. Ultimately, the fueling rate needs to be high enough, with a certain fraction of the fuel energy being passed onto the piston, head, and cylinder walls as heat, so that successive cycles have enough of a local thermal energy sink in the chamber walls to maintain the minimum requirements for auto-ignition to occur. If the minimum thermal conditions are not met then high combustion instability, and also misfires, is the result.

When considering the overall effect of being able to utilize HCCI for portions of the driving cycle for the purpose of improving vehicle gas mileage, the nature of SI operation at low and mid loads needs to be considered. Conventional spark-ignition engines are required to operate at stoichiometric air/fuel ratios. For this reason, at part load operation the engine is throttled. This is one of the biggest deficiencies of SI engines and accounts for much of the fuel economy issue related to gasoline fueled engines. For this reason, any extension of the operability range that can be made for HCCI operation at low loads is a tremendous benefit to overall engine efficiency, even compared to gains made at the high load range of HCCI operability, where throttle losses are not as great.

Where it would seem that CCD would further hinder the upper load limit of HCCI, the results from the previous chapter indicate that the insulating properties of deposits leading up to ignition could potentially aid in meeting the minimum thermal requirements for auto-ignition at lower loads.

8.1.2 Objective

In previous chapters it has already been shown that for a given set of operating parameters, deposit coverage significantly changes combustion characteristics during HCCI operation. The objective of this chapter is to demonstrate the effects of CCD coverage on the operability limits of HCCI combustion within a given engine speed

range. Specific criteria will be used to determine the limits of practically operability in HCCI mode.

8.2 Testing Plan

The purpose of this testing is to determine the effect that combustion chamber deposits have on the range of operability of HCCI combustion. Typically this is performed by finding the boundaries on a speed/load plot. The limits of operability will first be found while the engine is clean. Then the procedure for aggressively conditioning the chamber is performed such that combustion rates at our baseline operating point (2000rpm, 11mg fuel) are the same as those at the end of 40 hours of natural conditioning of the engine. Once this has been accomplished, the operability limits are checked again.

For this testing, the range of engine speed used is from 1200 to 2400 rpm at increments of 400 rpm. While this is only a 1200 rpm range, it is enough to provide insight into the effect of engine speed on HCCI combustion and deposits. There is a factor of two separating the lowest and highest speeds and this is potentially useful for determining the contribution of thermal storage effects in the deposit layer. Furthermore, because of the general effects of engine speed on engine heat loss and when also taking into consideration the importance of ignition time constants, HCCI has been found to be limited to engine speeds not much higher than these [115].

8.2.1 Load Limit Criteria

It should be made clear that the purpose of this testing is to determine only the effect of CCD on HCCI load limits. This is not an exercise in trying to extend the boundaries of operation for this engine as far as possible. This engine setup is not intended for and is not suited to very much operational flexibility. Most importantly, the valvetrain timing is fixed (no cam-phasing or switchable lift profiles) so there is no way

to optimize residual levels or effective compressions ratio in accordance with load. Secondly, nothing is gained in the understanding of the effects of CCD by trying to squeeze all possible performance out of the engine. The only control 'knob' used to explore the limits of this engine is fueling rate. All other operational parameters will be kept constant, including injection timing, exhaust back-pressure, swirl control, external EGR, and intake temperature. The engine is maintained at wide open throttle throughout testing so intake manifold pressure is 1 bar.

Low Load Limit

The low limit is determined by minimum combustion stability. At a given engine speed, fueling rates will be decreased until the coefficient of variance (CoV) of IMEP reaches a value of 3.0 %. The load at this speed and fueling rate is the lower limit.

It is important to mention that while no other parameters will be manually changed, the residual rates for a given engine speed are not the same between the clean and conditioned cases. Differences in combustion and different loads, even for the same engine speed, will slightly vary the exhaust pressure and the density of the cylinder contents. This results in slight differences in the actual residual mass that enters the chamber during rebreathing. This is treated as a direct function of the operating point and is considered in the analysis of results.

High Load Limit

The high load limit for a given engine speed is determine by gradually increasing the fueling rate until the pressure rise gradient is reached. This was determined previously to be 50 bar/msec. This is the point at which burn rates are fast enough to cause excessive 'ringing'. Exceeding this value of pressure rise rate is noisy and possible damaging to the engine.

8.3 Results

Figure 8.1 is a plot of the actual load boundaries attained versus speed for the two cases in question. The main general observation is that the region of operability shifted downward, from the clean to conditioned case. This result would be expected when considering the thermally insulating effects of combustion chamber deposits, as demonstrated in the previous chapter.

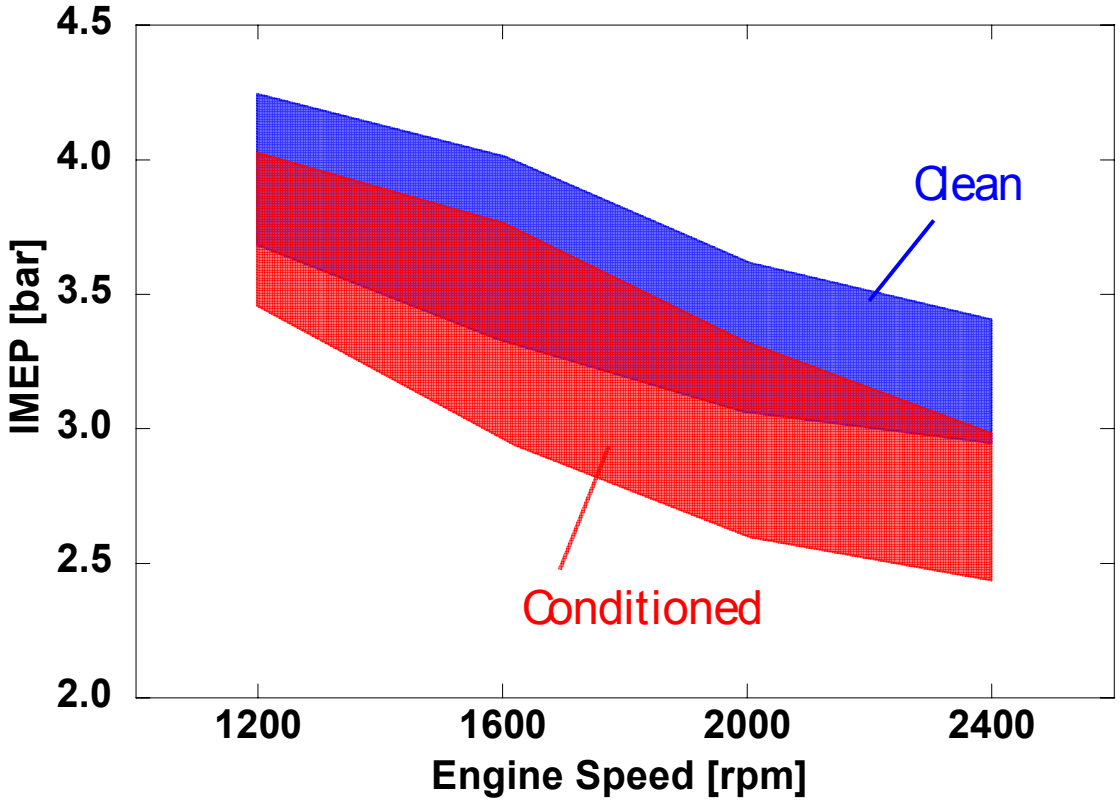

Figure 8.1 – Map of the operability limits of HCCI combustion for a clean combustion chamber compared to a conditioned combustion chamber. The upper limit is set by a maximum knock limit of 50 bar/ms and the lower limit is set by a maximum CoV of IMEP of 3%.

8.3.1 Dependence on Engine Speed

While the main trend for the speed/load map is a downwards shift with deposits, the amount of the shift is sensitive to engine speed. Figure 8.2 is a plot of the change in load between a clean and conditioned chamber as a function of engine speed, for both the low load and high load limits. Both cases show that there is an increase in influence of the deposits as engine speed increases. This is most likely due to the thermally diffusive properties of the deposit material compared to the metal wall, compared to the rate of heat loss from the chamber gases. It makes sense that with increased engine speed there is less actual time for heat transferred from the combustion gases to the walls to diffuse to the engine coolant. This will result in increased wall temperatures with speed, and less heat loss. Another important aspect to note is the relatively larger difference in the low load limit than the high.

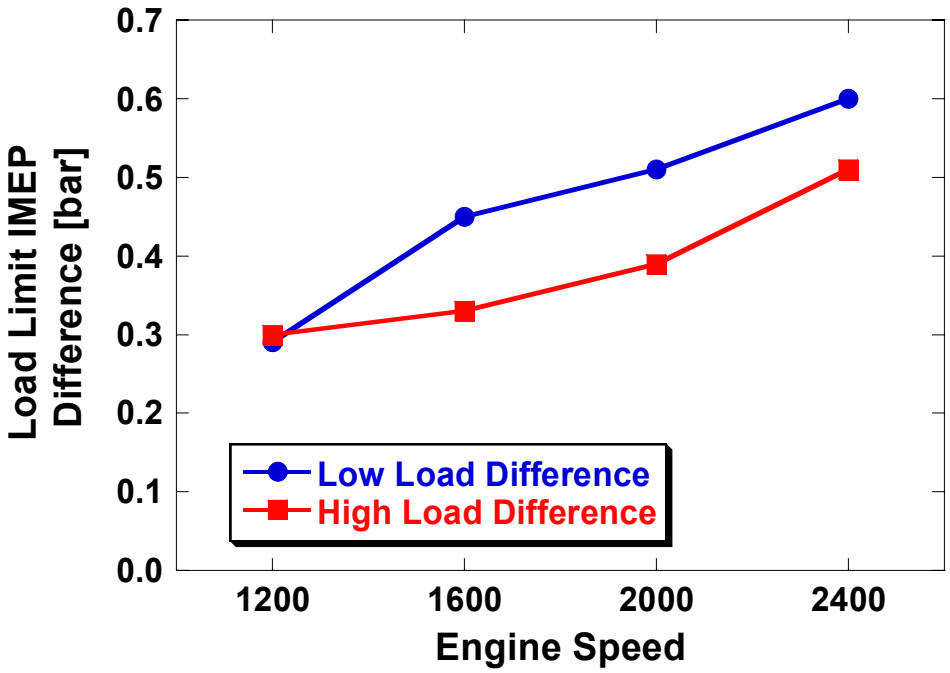

Figure 8.2 – Plot of the difference in load value at each of the lower and upper load limits of operability between a clean and conditioned chamber; showing the sensitivity of the change in limits to engine speed.

8.3.2 Low Load Limit

Table 8.1 lists the operating points for every engine speed tested at the low limit of operability for both the case of a clean combustion chamber and one covered in deposits. Care must be taken when comparing the same case of engine speed between the clean and conditioned points because they are not the same operating point. Specifically, the fueling rates are different, in accordance with the load point reached. In a later section of the chapter, a direct comparison of the same operating points as a function of engine speed will be made for a clearer understanding of the effect of CCD for the same operating parameters.

Table 8.1 – A comparison of operating parameters for a clean and conditioned combustion chamber at the respective low load limits for the four engine speeds tested.

LOW LOAD	Clean				CCD			
Speed (rpm)	**1200**	**1600**	**2000**	**2400**	**1200**	**1600**	**2000**	**2400**
IMEP (bar)	3.76	3.46	3.22	3.20	3.47	3.01	2.71	2.60
Fueling Rate (mg/cycle)	12.6	11.3	10.2	9.8	11.75	10.02	8.84	8.33
AFR (-)	17.2	17.3	18.9	20.8	17.1	18.7	20.7	21.6
RGF (%)	44.0	49.8	50.0	51.1	47.1	53.0	54.5	55.8
CoV IMEP (%)	3.17	3.21	3.16	3.24	3.01	3.02	3.07	3.22
Rmax (bar/ms)	12.67	17.09	22.08	22.18	13.10	17.47	20.04	19.49

At every engine speed the attainable load decreased after the chamber was conditioned, and as shown before as the engine speed increased the load difference was greater. At a given engine speed, as load (and fueling rate) is decreased, the average wall temperature decreases. Analogous to lowering coolant temperature in an HCCI engine, combustion ignition timing and phasing will retard and heat release rates will slow [7]. Eventually combustion stability will deteriorate and the CoV of IMEP will increase to the set limit of 3.0. As demonstrated in the previous chapter, deposits on the wall of the chamber will decrease heat loss during compression leading up to auto-ignition. This causes ignition timing and combustion phasing to advance, improving combustion stability, resulting in a lower CoV, compared to a clean engine. Thus the engine load can be decreased further. This will be more closely examined in a later section.

8.3.3 High Load Limit

Table 8.2 lists the operating points for every engine speed tested at the high limit of operability for both the case of a clean combustion chamber and one covered in deposits.

Table 8.2 - A comparison of operating parameters for a clean and conditioned combustion chamber at the respective high load limits for the four engine speeds tested.

HIGH LOAD	Clean				CCD			
Speed (rpm)	**1200**	**1600**	**2000**	**2400**	**1200**	**1600**	**2000**	**2400**
IMEP (bar)	4.32	4.13	3.80	3.65	4.02	3.80	3.41	3.14
Fueling Rate (mg/cycle)	14.6	13.1	11.7	11.0	13.7	12.4	10.8	9.7
AFR (-)	16.2	17.3	18.3	19.1	17.7	18.0	19.3	20.5
RGF (%)	41.2	45.2	48.4	50.3	41.2	46.9	50.5	52.8
CoV IMEP (%)	2.43	1.76	1.41	1.18	1.58	1.02	1.26	0.93
Rmax (bar/ms)	47.74	49.15	49.68	50.69	48.67	49.15	51.24	49.25

At every engine speed tested the maximum attainable load decreased after the combustion chamber was covered in deposits. Very much like the low limit cases, the difference in the max load increased with engine speed. Due to the insulating effects of the deposits, for a given fueling rate, combustion was more advanced and faster once the chamber was conditioned. Peak pressure gradients increase as combustion phasing advances closer to TDC, as demonstrated in Figure 8.3. As a result, with deposits the ringing limit of the engine is reached at a lower load.

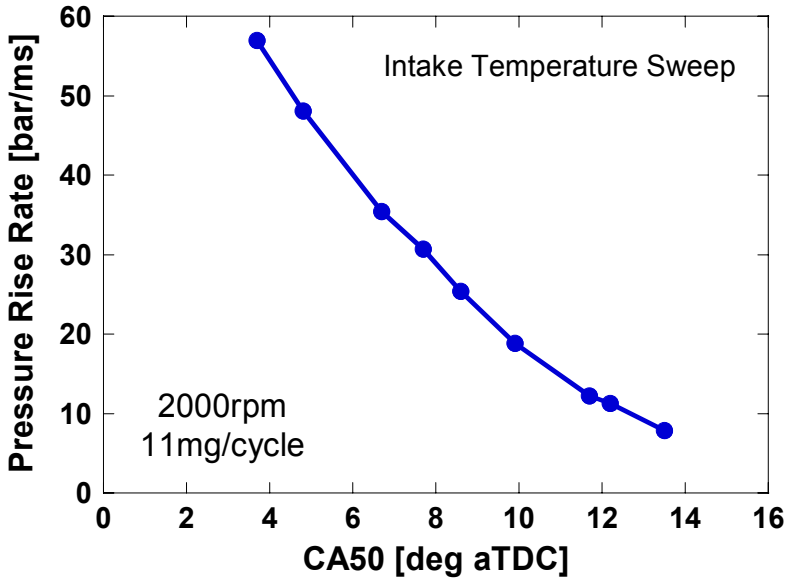

Figure 8.3 – Peak pressure rise rate versus combustion phasing for an intake temperature sweep at constant engine speed and load

8.3.4 Final note

The absolute range of operability is limited. For a given engine speed, the difference between the upper and lower load limits is on the order of half a bar in an engine with a fixed rebreathing cam, no external EGR and constant intake temperature. Recall that this engine is not setup or equipped for extended range of HCCI operability. A significantly greater range will ultimately be required for practical automotive use in a drive cycle. The purpose of this investigation is to understand the effect that deposits have on this range. It is presumed that if the engine was setup and able to operate at a more diverse spread of operating parameters, via the use of variable cam timing and other devices, the HCCI speed/load area will be wider, but the insight about the effect of deposits would still be applicable.

8.4 Direct Comparison

The previous section demonstrates how combustion chamber deposits cause the usable speed/load range for HCCI to decrease in load value. The span of operating points which this engine can run at in HCCI mode is different than when the engine is clean. In summary, operation points at lower loads can now be reached before the limit of CoV of IMEP is reached. The previous section compared HCCI at these new limits. But what is the effect of CCD at the same operating points? This section will provide a direct comparison between a clean and conditioned chamber for the same range of engine speeds. Specifically, after the engine was conditioned, it was operated at the same load points as the lower limit attainable when the engine is clean.

Figure 8.4 depicts the range of operating points being compared in this section for both the clean and conditioned chamber. All points to be compared lie along the clean low limit and are indicated by the yellow circles at each tested speed in the plot. The same points in the conditioned engine are roughly in the middle of the operability range.

An important clarification should be made. The points tested with the conditioned engine were run to match the *fueling rate* at the respective clean load. So while Figure 8.4 makes it seem as if the same load was used, it was actually the fueling rate at that load operating point.

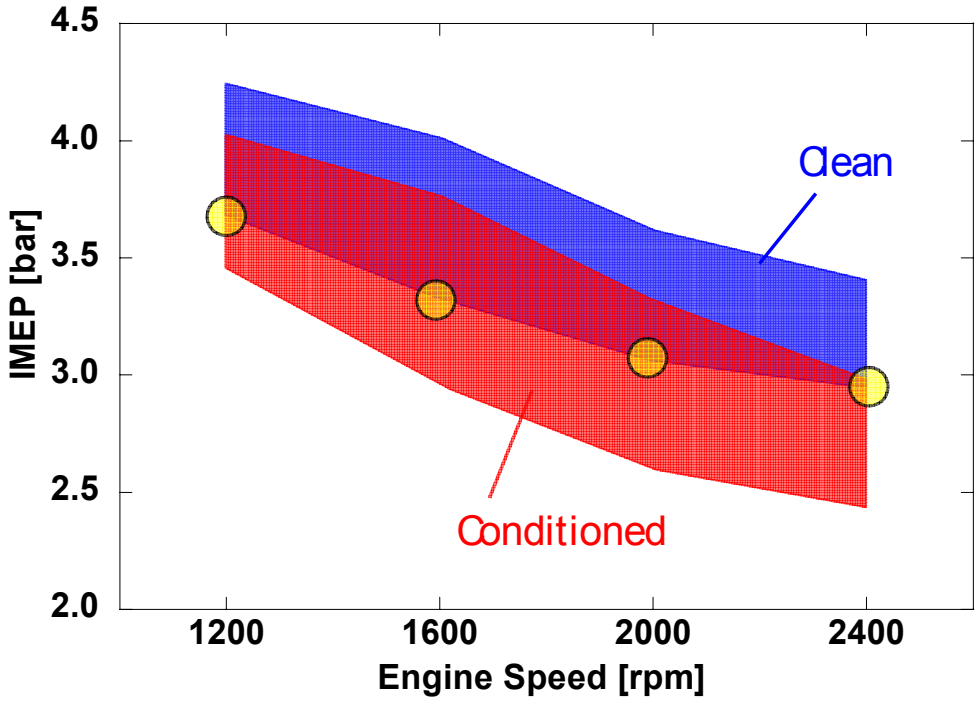

Figure 8.4 – The four circles on the map of speed/load operability indicate the points of direct comparison for the clean and conditioned cases. The points lie on the low load limit of clean operability and somewhere between the low and high load limits for the conditioned operation.

Table 8.3 lists the compared operating points along with several other important combustion parameters, such as emissions and heat release results. The results pertaining to the cases with the clean chamber are the same as those from the previous section which described the lower limit.

Take note that while the fueling rates for each engine speed match, the actual load does not, as previously noted. The load attained for the conditioned cases are a little higher for the same fueling rate, compared to the clean chamber.

Table 8.3 – Comparison of operation parameters and combustion performance figures for the four load/speed comparison points tested comparing a clean and conditioned combustion chamber.

	Clean				CCD			
Speed (rpm)	**1200**	**1600**	**2000**	**2400**	**1200**	**1600**	**2000**	**2400**
Fueling Rate (mg/cycle)	12.6	11.3	10.2	9.8	12.5	11.2	10.2	9.7
IMEP (bar)	3.76	3.46	3.22	3.20	3.89	3.58	3.29	3.24
AFR (-)	17.2	17.3	18.9	20.8	17.0	17.2	18.6	20.3
RGF (%)	44.0	49.8	50.0	51.1	45.3	50.6	52.7	53.2
CoV IMEP (%)	3.17	3.21	3.16	3.24	0.83	1.25	0.92	1.34
Rmax (bar/ms)	12.67	17.09	22.08	22.18	21.02	27.07	33.96	37.58
Isfc (g/kW-h)	219.5	214.1	206.1	201	211.0	204.4	201.3	196.6
CA10 (CA deg aTDC)	5.9	5.7	4.8	5.2	3.6	3.7	2.7	2.7
CA50 (CA deg aTDC)	12.4	11.5	10.3	10.7	8.6	8.5	7.3	7.4
Burn Duration (deg CA)	20.1	18.1	14.5	18.5	14.4	14.0	14.3	17.9
EI NO (g/kg fuel)	0.93	0.49	0.44	0.44	1.58	0.89	0.85	0.79
EI HC (g/kg fuel)	47.7	46.1	41.3	41.6	32.8	31.9	27.5	26.9
Combustion Efficiency (%)	94.75	95.24	95.22	95.46	95.83	96.08	96.82	96.36

8.4.1 Effect of CCD on Rate of Heat Release

In this section a direct comparison of the heat release rate trends will be performed for the data presented in the charts above. In addition, some plots show data of many other operating points from both a clean and conditioned combustion chamber. These are all inclusive points varying across engine speed (1200-2400rpm) and load (9-15 mg fuel/cycle). The purpose of these plots is to demonstrate general changes in the characteristics of HCCI combustion imposed by combustion chamber deposits.

Ignition

There is a clear general trend regarding the compared operating points. At every engine speed tested combustion is earlier and faster when the chamber is conditioned with deposits compared to when the chamber is clean. Figure 8.5 is a plot of the ignition timing (CA10) for all four engine speeds for both a clean and conditioned chamber. For all speeds, the ignition timing advanced an average of 2 degrees CA for the conditioned case. Figure 8.6 shows that combustion phasing has advanced with conditioned but this change is coupled to the change in ignition timing. This point is confirmed by Figure 8.7 which shows a similar graph but with many more operating points for both clean and conditioned operation. It is clear that all the points is question, clean and conditioned combined, follow one correlation indicating the strong dependence of combustion phasing on ignition. This indicates that deposits do not have any effect on the initial part of heat release apart from its effect on the ignition timing. In was demonstrated in the previous chapter how deposits reduced heat loss during compression resulting in higher gas temperatures near TDC, which accounts for the earlier ignition timing. Otherwise, there is no direct way for combustion chamber wall deposits to affect the core of the air/fuel mixture.

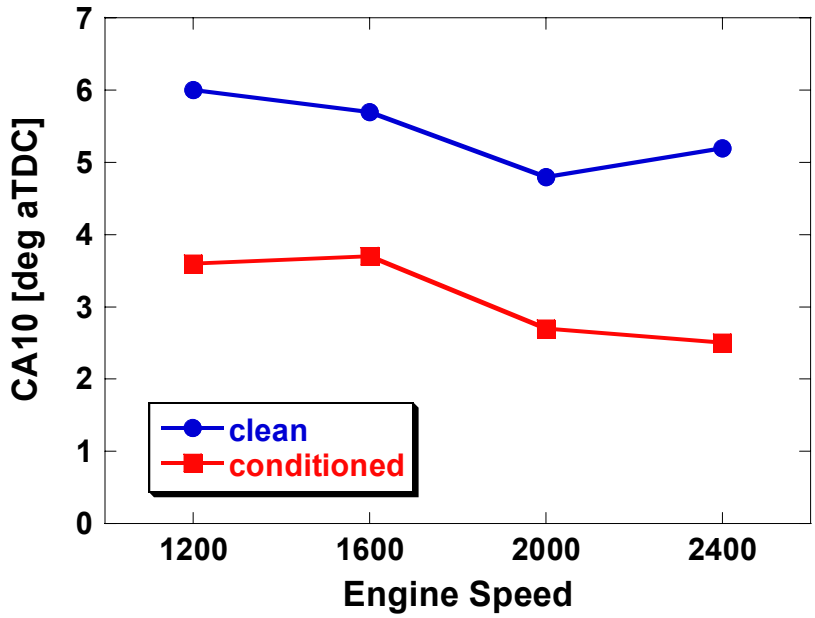

Figure 8.5 – Comparison of ignition timing (CA10) for a clean and conditioned combustion chamber.

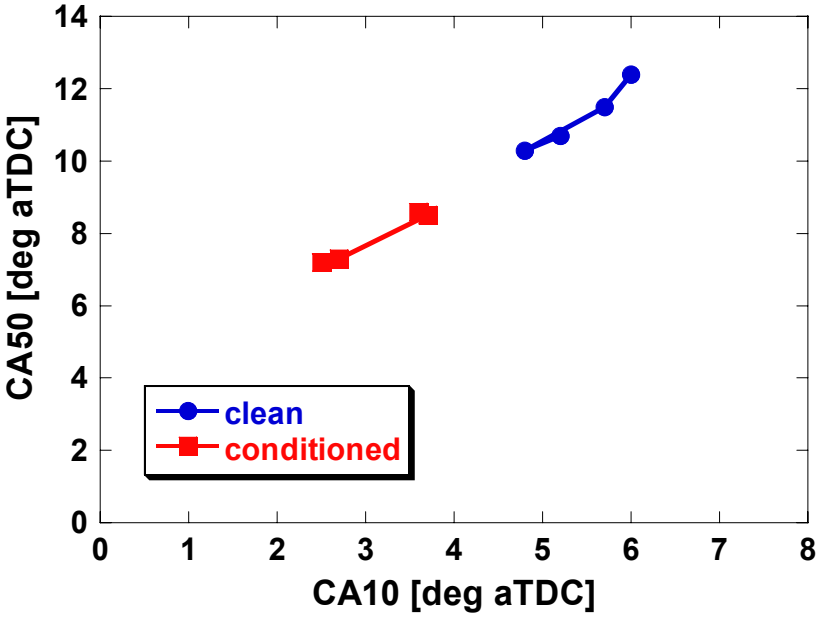

Figure 8.6 – Combustion phasing (CA50) versus ignition timing (CA10) for a clean and conditioned combustion chamber

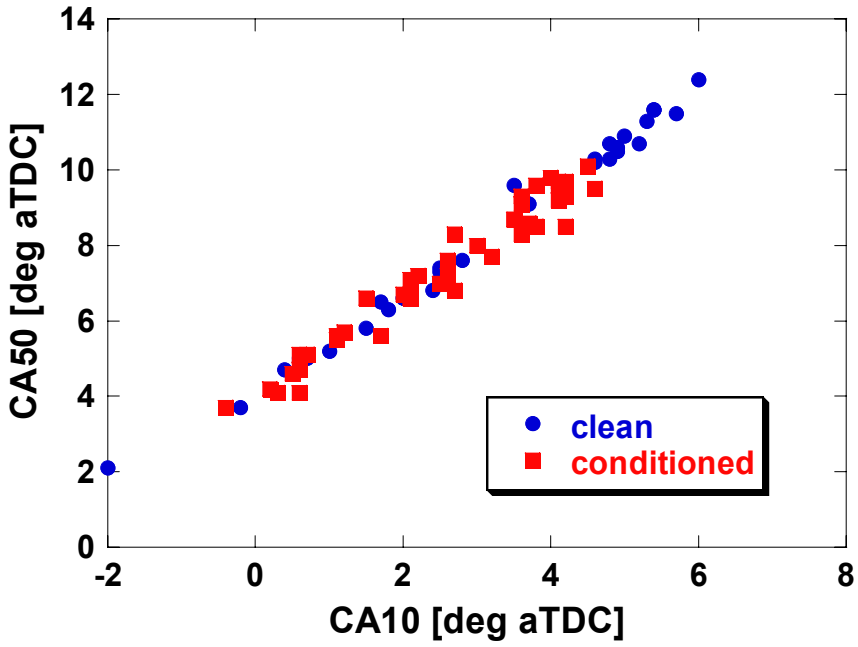

Figure 8.7 – Combustion phasing (CA50) versus ignition timing (CA10) for several operation points taken from operation with both a clean and conditioned combustion chamber.

Bulk Burn

The latter part of heat release is sometimes referred to as 'bulk burn'. The first half of release occurring as the first 50% of the fuel energy is release is mostly controlled by ignition processes as shown above in Figure 8.7. Though heat release in HCCI combustion is idealized as homogeneous and simultaneous everywhere in the chamber, there is still some degree of stratification present in the charge (reference), especially thermal stratification due to the cold combustion chamber walls and convection effects during compression. Furthermore, high levels of residual used for re-breathing, introduce another degree of stratification.

As HCCI ignition occurs first in hottest part of the fuel/air mixture, this typically is near of the core of the air/fuel mixture charge. The first 50% of heat release occurs in this core very rapidly. The second half of heat release, the 50-90% burn, encompasses the

periphery of the charge in the cylinder between the core and walls and takes longer to occur. This is the ‘bulk burn’. This is also the source of most unburned hydrocarbon emissions because of thermal quenching of the air/fuel mixture burn due to the quickly descending piston at this point in the stroke.

This is also the period of heat release in which near wall thermal conditions have a profound impact on reaction rates. Therefore, it is expected that deposits would have the greatest influence on this stage of combustion. Figure 8.8 confirms the expectation. For all the points tested, the duration of bulk burn (CA50-90) for the conditioned case, is much shorter with respect to combustion phasing, than the clean. Based on the blue points, corresponding to a clean chamber, the earlier combustion phasing (CA50) occurs, the faster the last half of heat release will occur, indicated by the CA50-90 decreasing as CA50 decreases. But when comparing the shift of the curves to the red conditioned cases, CA50-90 is shorter for a given phasing compared to the clean case.

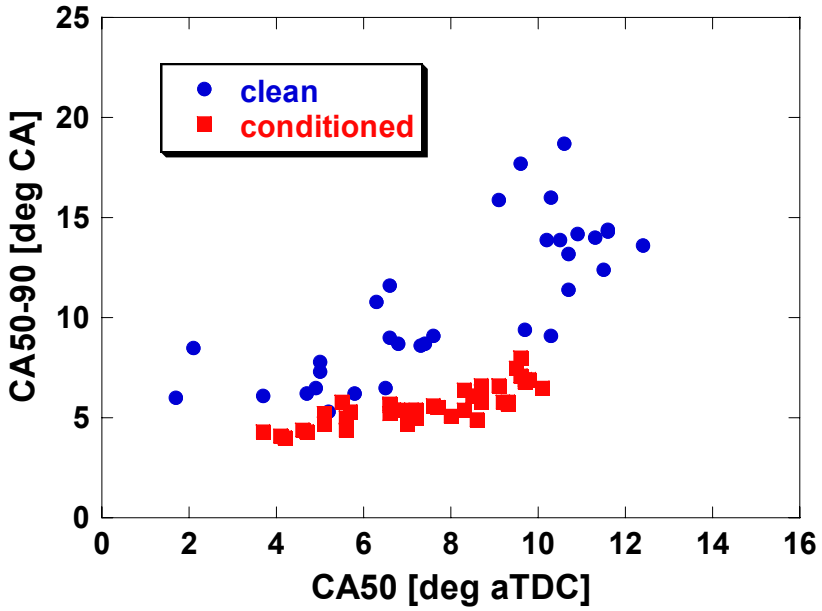

Figure 8.8 - CA50-90 burn duration versus combustion phasing (CA50) for several operation points taken from operation with both a clean and conditioned combustion chamber.

As shown in the previous chapter, the deposit layer causes the surface temperature swing to triple in some cases, compared to a clean chamber, resulting in higher peak wall temperatures during combustion. This extra heat stored at the wall surface is responsible for the differences in bulk burn demonstrated here. In general the outer periphery is maintained at higher temperatures, promoting the last phase of heat release.

Figure 8.9 shows conceptually how temperature gradients would exist in the air/fuel mixture. The red core region is where ignition occurs and, during the short combustion duration typically associated with HCCI combustion, heat release progresses towards the wall [37,55]. Of course this is nothing like a propagating flame as in SI combustion, as reactions start at multiple locations and progress at a fast rate. Nevertheless, it is reasonable to assume that thermal stratification slows down reactions near the wall as suggested by some CFD studies [11,55]. Even a small difference in near-wall conditions can have a large impact as thin layers on the periphery contain a lot of

mass (the area multiplying the average thickness is large). Based on the results shown here, deposits on the walls and their effect on transient heat flux and temperature history are capable of enhancing combustion in the lightest colored regions at the periphery of the chamber.

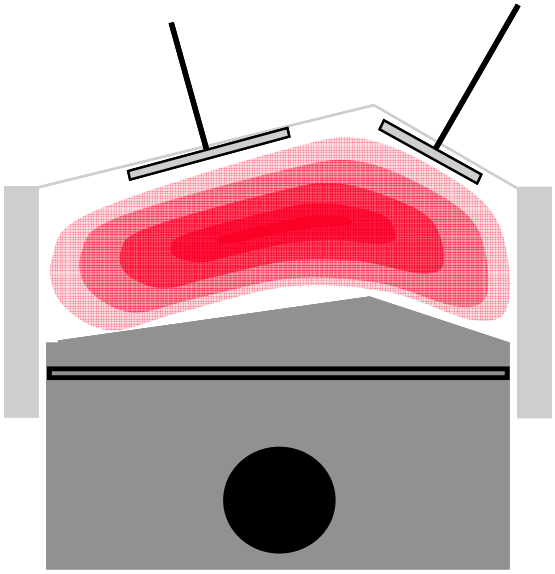

Figure 8.9 – A conceptual diagram of the contents of the combustion chamber leading up to ignition. Due to the colder chamber and piston surfaces the core of the air/fuel mixture is the hottest part of the charge, gradually decreasing in temperature in the boundary layer where the outer periphery of the charge is the coolest.

Unburned Hydrocarbons

As stated before, the periphery region is also responsible for most unburned hydrocarbon (HC) emissions. Based on the results from Table 8.3 it is clear that specific unburned hydrocarbon emissions are reduced when the chamber is conditioned, but this would be expected with advanced burn rates.

Figure 8.10 shows fuel specific unburned hydrocarbon emissions as a function of combustion phasing (ca50). As expected HC emissions decrease as combustion phasing

is advanced because the latter parts of heat release occur before the piston has descended as far down the cylinder and less quenching of the air/fuel mixture occurs. But it was not expected that the spread of points for the clean and conditioned points would lie on top of each other. It was thought that since most hydrocarbon emissions originate in the boundary layer near the wall, the extra thermal effects from deposits would reduce emissions, much like their effect on bulk burn duration. According to this result deposits themselves have no separate effect on HC emissions apart from their effect on combustion timing. It is possible that any reduction in HC emissions due to the thermal effects of CCD might be offset by physical effects of CCD, such as fuel absorption in the layer.

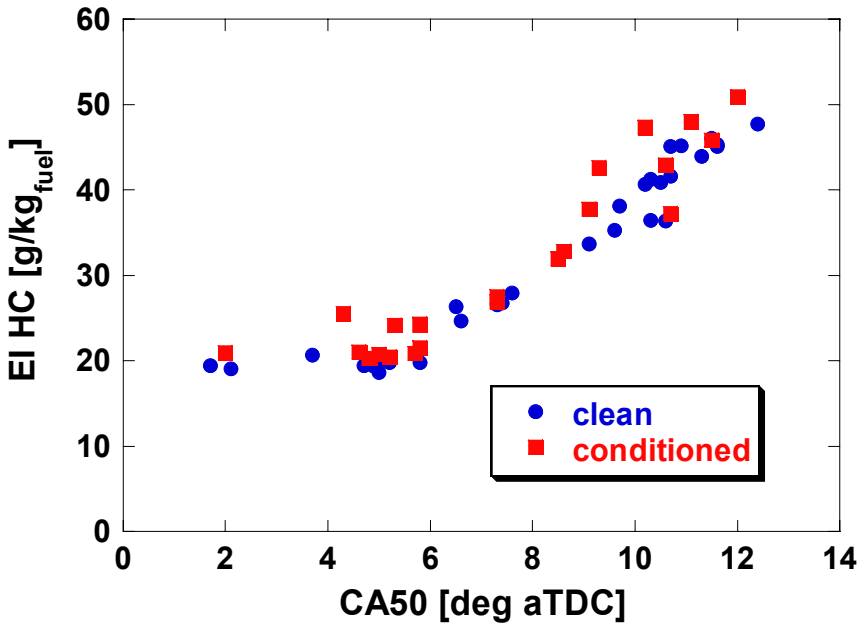

Figure 8.10 - A plot of end of unburned hydrocarbon emissions (EI HC) versus combustion phasing (CA50) for several operation points taken from operation with both a clean and conditioned combustion chamber.

Heat Loss

Figure 8.11 is a plot of calculated global heat loss for all the cases above (with equal fueling rates at each engine speed) as determined by heat release analysis of the pressure data. A modified version of Woschni's global heat transfer correlation is utilized for determining the convection coefficients [94]. The first plot is for all the clean cases and the second for the conditioned cases. At every engine speed heat loss is greater for the conditioned case. The calculation of heat loss uses an empirical correlation which is based on crank angle resolved gas temperature and pressure, among other factors. In the conditioned cases, heat release starts earlier and is faster, due to the effects of the deposits, so peak gas temperatures are higher. This results in higher heat loss during heat release. Since the heat loss correlation cannot take into account the state of the wall thermal conditions (apart from average wall temperatures, which do not change very much with deposits) combustion is the main driving factor for heat loss rates.

In actuality, as explained based on the results in Chapter 7, and specifically Figure 7.19, heat loss is in fact greater during the expansion stroke for the conditioned case compared to the clean because of the lower diffusive properties of deposits compared to metal. The shape of the heat loss profile calculated from heat release does not match the actual shape measured at the piston and head walls, but it does convey that the higher heat release rates with a conditioned chamber offset the insulating properties of the deposits themselves.

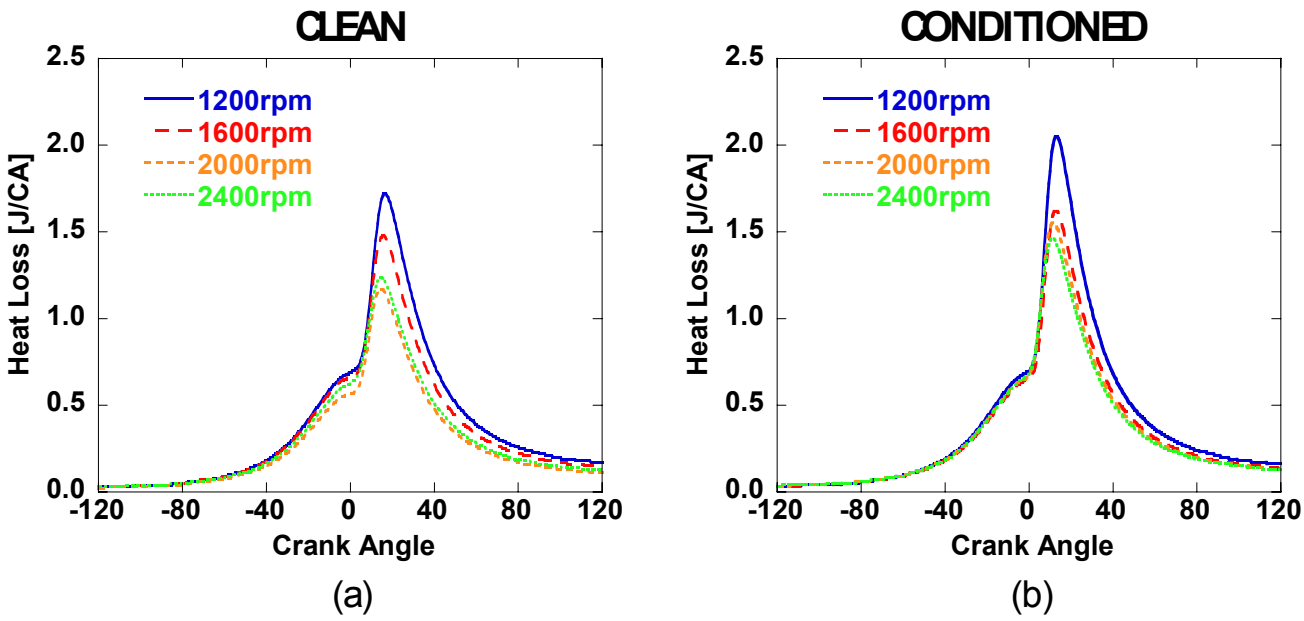

Figure 8.11 – Two plots of calculated global heat loss rates to the chamber walls for the clean (a) and conditioned (b) cases at the four engine speeds tested.

8.4.2 Effect of CCD on Thermal Efficiency

In work from the past related to thermal coatings, such as ceramics, they were used with the intent of decreasing the cycle net heat loss from the cylinder in order to increase thermal efficiency. When turbo-machinery was used with a diesel engine is when the highest potential for increasing exhaust energy through thermal insulation could be had, thus increasing the work that went to the compressor [116]. For this to be effective requires a net heat loss decrease for the cycle.

With the presence of combustion chamber deposits coating the walls, and considering the thermal properties of CCD material compared to metal, based on a historical review it is possible to presume that cycle heat loss will decrease and thermal efficiency will benefit.

Figure 8.12 is a plot of the indicated specific fuel consumption (ISFC) versus engine speed for the same operating points with a clean and conditioned engine compared with each other. From the plot it can be seen that at every engine speed there is a reduction in specific fuel consumption from the clean to the conditioned case. It would be natural to presume that the deposit layer in the chamber causes a reduction in heat loss and thus improves thermal efficiency for the cycle. But previously in Chapter 7 for the case of the baseline operation point at 2000rpm and 11mg fuel that was compared, it was shown that there is no significant different in net cycle heat loss, regardless of the presence of deposits. A further look at the other changes in combustion that combustion chamber deposits incur is required.

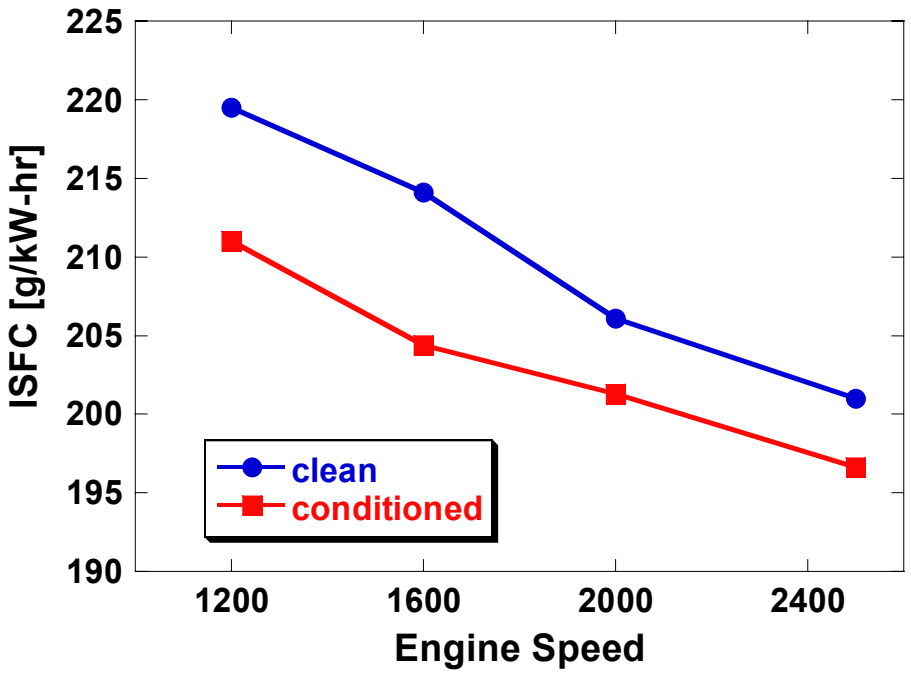

Figure 8.12 – Indicated specific fuel consumption (ISFC) plotted for the four tested engine speeds for a clean and conditioned combustion chamber

ISFC versus combustion phasing

Figure 8.13 is a conceptual plot of ISFC versus CA50 for any given engine operating any combustion type [66,67]. The solid line depicts the thermal efficiency of an ideal engine as a function of combustion phasing (CA50) where no heat loss occurs. Efficiency is maximized when the phasing of CA50 is at TDC. In an engine where there is no heat loss, the highest combustion efficiency would occur with combustion timing at TDC, due to the geometric pressure-volume relationship and maximizing the expansion work to movement of the piston [29]. However, in a real engine with heat transfer, if combustion is phased too close to TDC, then high peak cylinder pressures and temperatures result in extra heat transfer, thus a loss in thermal efficiency. Thus, varying levels of heat transfer would cause the curve to shift up and right moving the combustion point of peak thermal efficiency. The overall shape stays the same but the curve moves upward and to the right, towards more retarded combustion phasing. With no heat transfer, TDC phasing is ideal but in a real engine, the closer to TDC that combustion occurs, the higher the charge peak pressures and temperatures are. Thus heat transfer rates are higher, leading to reduce fuel efficiency. The greater the propensity for heat loss the more retarded the phasing must be for minimum specific fuel consumption.

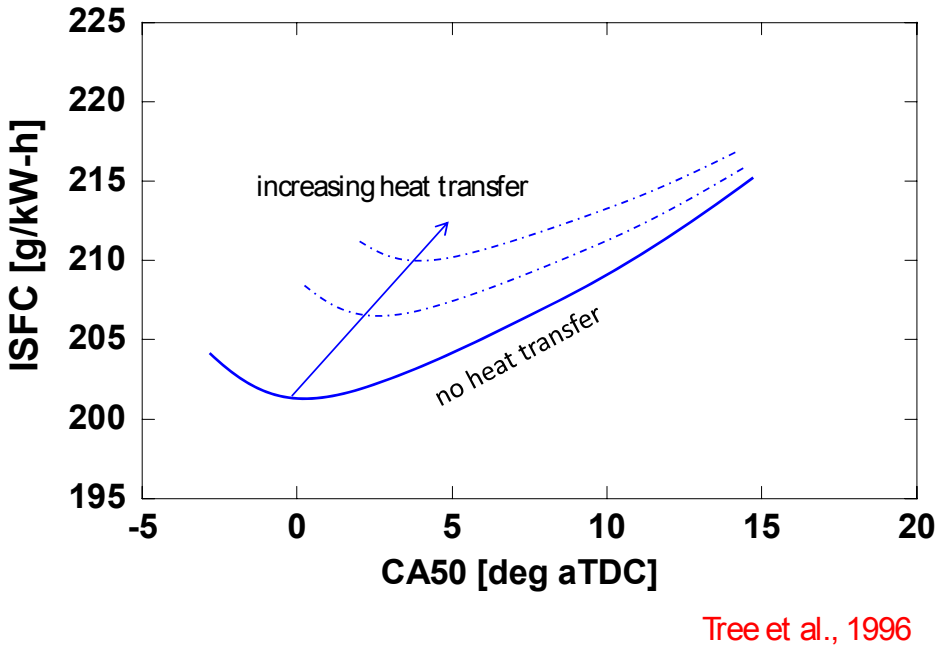

Figure 8.13 – A conceptual diagram of the effect of heat loss of thermal efficiency versus combustion phasing trend [66,67]

Figure 8.14 below is a plot of the indicated specific fuel consumption versus CA50 of several operating points run with the engine while the combustion chamber is clean and while it is coated in a deposit layer. These are the same collection of points shown in Figures 8.7, 8.8, and 8.10.

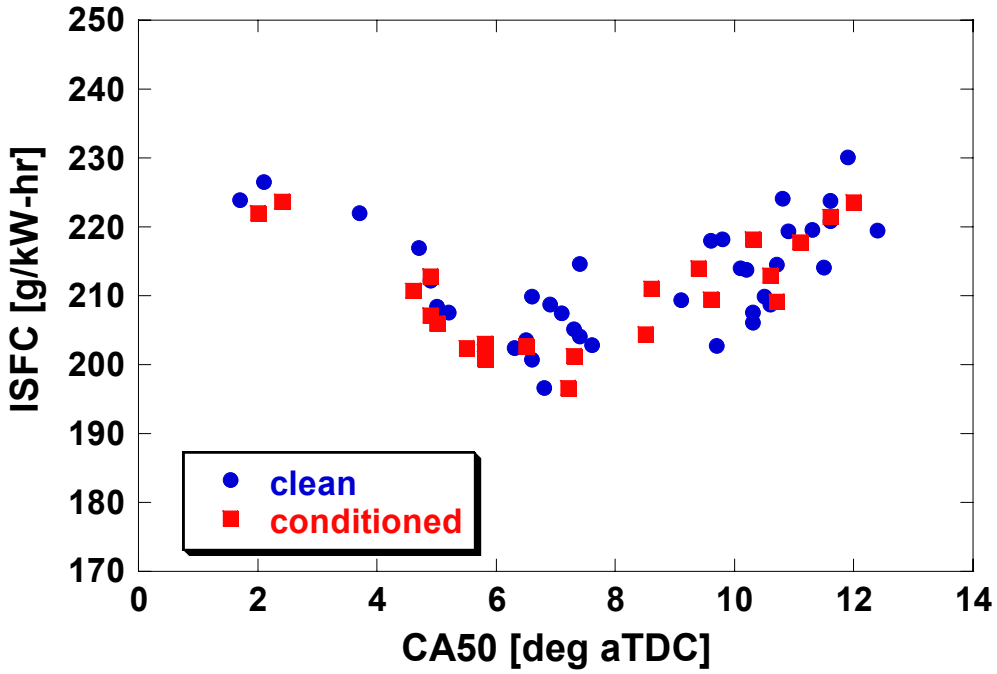

Figure 8.14 - A plot of indicated specific fuel consumption (ISFC) versus combustion phasing (CA50) for several operation points taken from operation with both a clean and conditioned combustion chamber.

In this case the plot of thermal efficiency versus combustion phasing for a clean combustion chamber lies over a plot for a conditioned combustion chamber. According to the results shown here, there is no indication that relative thermal efficiency changes as a function of combustion timing between a clean and conditioned chamber. In both cases the combustion phasing for minimum fuel consumption occurs at about 7-8 crank angle degrees after TDC. Also, at more advanced and retarded ca50 phasing, the points for ISFC line up going in either direction. In general, the scatter of plots line up with each other pretty closely.

This indicates that while deposits in the chamber cause a decrease in specific fuel consumption at a particular operating point, this decrease is only due to the change in combustion phasing. The same shift in combustion phasing in a clean engine would presumably bring about the same increase in efficiency. This confirms that efficiency

does not increase due to less heat loss imposed by the deposits. In fact, with the burn rates higher for a given operating point, it has already been shown that with deposits heat loss during the expansion stroke is actually higher. The added work that is extracted due to earlier combustion phasing outweighs this heat loss.

8.4.3 Combustion Stability

Figure 8.15 is a plot of the CoV of IMEP at the operating points in question for the clean and conditioned cases. Recall that the fueling rates for the respective cases are equal at each engine speed. Understanding the reasons behind the increase in combustion stability (decrease in CoV) with deposits in the chamber is important for understanding the effect of CCD on the HCCI operating limits for the engine. The low load limit is determined by the maximum allowable unstableness of combustion, in this case a CoV of 3.0 % is the maximum allowable for operation to be 'stable'. This is a practical limit set for the purpose of subjective perception of engine operation in a vehicle [12,117].

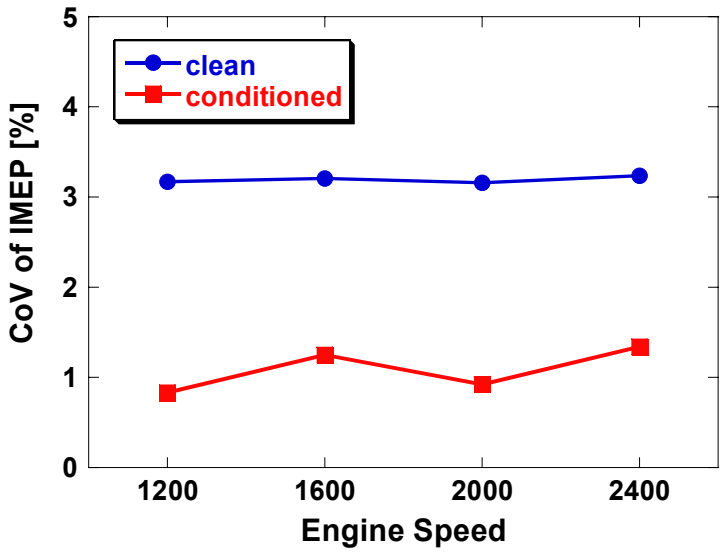

Figure 8.15 – A plot of the Coefficient of Variance of IMEP (CoV of IMEP) at the four tested engine speeds for a clean versus conditioned combustion chamber.

As demonstrated earlier in this chapter the low limit could be extended because of the decrease in CoV value for a given operating point when the chamber was conditioned. Figure 8.15 shows how combustion stability is significantly improved for the conditioned cases compared to the clean. But just as in the case of unburned HC emissions this could easily be attributable to the overall faster heat release rates associated with combustion while the chamber is conditioned. In order to understand if the deposits had a separate effect on combustion stability it is required to understand what aspect of HCCI combustion determines how stable steady state operation will be. It was hypothesized that some aspect of the magnitude or timing of heat release would be responsible with the CA50 timing and strength of the latter parts of heat release being reasonable possibilities.

Since the magnitude of heat release is so strongly coupled to phasing for HCCI combustion, whether auto-ignition occurs can easily be represented by ignition timing (CA10). But since it has already been shown that there is a strong relationship between CA50 and CA10, combustion stability versus phasing is shown in Figure 8.16 for the clean and conditioned cases over a broad range of operating points for each state. Both cases follow very similar trends indicating that combustion ignition timing and ultimately the phasing dictates combustion stability. In both cases CoV of IMEP decreases as phasing advances until a minimum at about 6-7 degrees aTDC. Then CoV starts to increase again with further phasing advance. At these extremely advanced combustion timings ringing is prevalent and because of pressure waves traversing the chamber, cycle-to-cycle IMEP values are not as steady, so stability decreases [117].

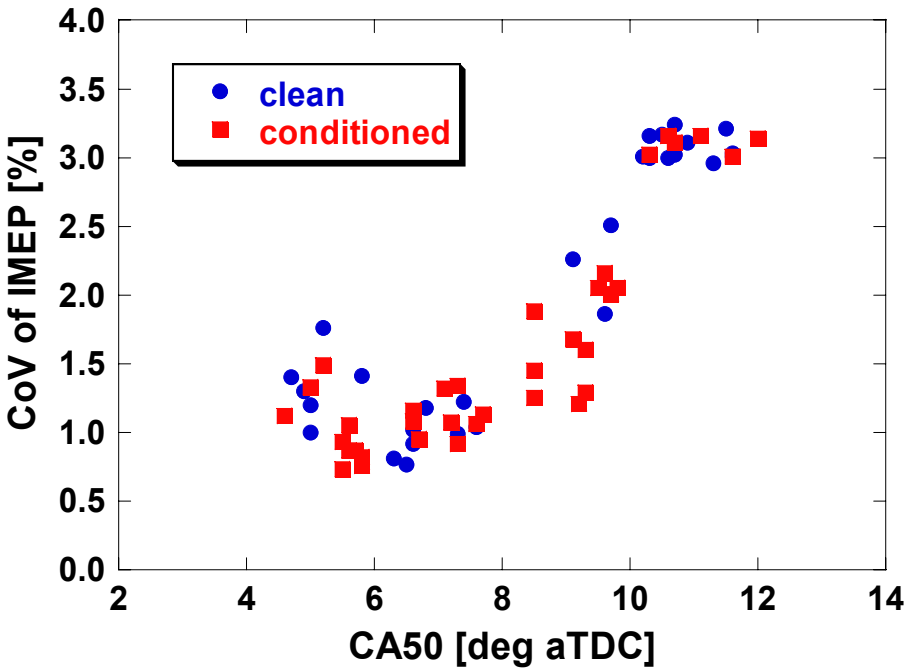

Figure 8.16 - A plot of the Coefficient of Variance of IMEP (CoV of IMEP) versus combustion phasing (CA50) for several operation points taken from operation with both a clean and conditioned combustion chamber.

Figure 8.17 shows that there does not seem to be a relationship between ca50-90 timing and CoV. This makes sense when it is considered that once half of the fuel charge has been consumed, the quality of heat release for the whole combustion event will have already been decided.

Based on these results, the reason that the low load limit for HCCI operation is extended with a conditioned chamber is due to the effects of deposits leading up to ignition. With CCD operating at the clean low load limits the CoV of IMEP is lower because decreased heat loss during compression causes ignition timing to occur earlier. Overall combustion phasing is advanced and with it stability increases (up to a point). At the same load point with lower CoV there is more room for decreasing the fueling rate before the stability limit is reached. Further investigation is likely required to understand the full characteristics and requirements for HCCI combustion stability. Only then can a

full assessment of the contribution of wall thermal coatings to the decrease in operating limit be made.

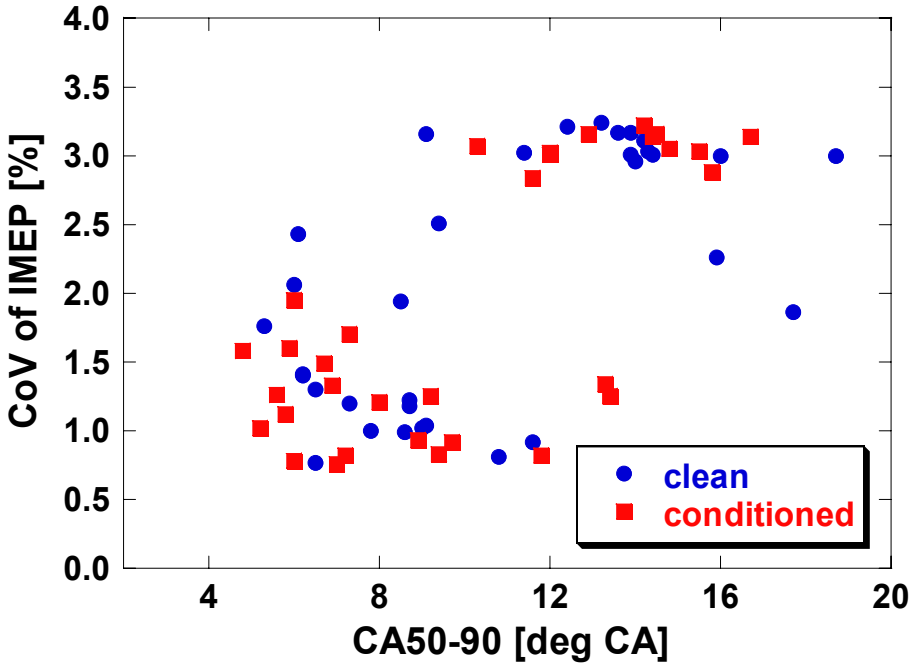

Figure 8.17 - Coefficient of Variance of IMEP (CoV of IMEP) versus the duration of bulk burn (CA50-90) for several operation points taken from operation with both a clean and conditioned combustion chamber.

For similar reasons the high load limit is reached at a lower limit with CCD. The ringing limit is reached at a lower load than with a clean chamber because the combustion phasing is advanced and thus peak heat release rates are higher for the same fueling rate

8.5 Chapter Summary

Having set criteria for the low and high load limits for HCCI operation, an operability map was made encompassing four engine speed with a clean combustion

chamber. When the chamber was conditioned by covering the walls with deposits both load limits decreased in value. The overall operating window shifted to lower loads.

In order to understand the differences imposed by CCD which lead to this shift in operability range, four operating points, at different engine speeds, at the low limit for a clean chamber were directly compared to the same operating points with a conditioned chamber. There are two main separable effects, analogous to the two separate effects discussed in the previous chapter; the effect of when auto-ignition occurs and the effect of bulk burn.

Confirmed by the surface heat fluxes calculated in Chapter 7 heat loss during the intake and compression strokes is reduced in a conditioned chamber compared to the clean. This leads to higher gas temperatures at the end of compression and results in advanced auto-ignition timings. Overall combustion phasing is advanced and peak heat release rates are higher. Several combustion parameters change with chamber conditioning but they are themselves directly dependent on combustion phasing and heat release rates only, which change because of CCD's effect on when ignition occurred. Thermal efficiency, unburned HC emissions, and combustion stability are dependent on phasing, and NOx emissions on peak gas temperatures. The deposits do not have a direct effect on these parameters.

The other separate effect of CCD's is to shorten the bulk burn duration of combustion. This is independent of the effect of deposits on combustion phasing but does not seem to be responsible for the extension of the low load limit.

The decrease in minimum load limit is due to the increased combustion stability associated with more advanced combustion phasing which deposits bring about. But for the same reason, excessive heat release rates are reached at lower loads in a conditioned chamber and high load limit is reduced as well.

CHAPTER 9

CONCLUSIONS AND FUTURE RECOMMENDATIONS

A comprehensive experimental study of the effect of combustion chamber deposits on homogeneous charge compression ignition combustion has been performed. A gasoline fueled single cylinder engine was used in conjunction with in-cylinder pressure measurements to quantify combustion and performance parameters to gain insight into combustion. Of equal importance were the use of crank angle resolved head and piston surface temperature and heat flux measurements. Combined with deposit thickness measurements, information about the thermal properties of deposits, as well as their effects on wall heat transfer was gained.

The research questions addressed start with understanding the dynamics of deposit formation and chamber 'conditioning' in a gasoline HCCI engine. This was followed by a characterization of the effects of combustion chamber deposits on HCCI combustion. Further in-depth analysis attempted to understand the influence of deposit coverage on measured instantaneous wall temperatures, with further insight gained regarding CCD thermal properties. Once the general influence of deposits on HCCI combustion was determined, a more detailed breakdown of the specific mechanism of the interactions between the deposit layer and chamber thermal boundary layer was performed, with emphasis placed on how this affects operating parameters and the limits of HCCI combustion.

9.1 Summary of Conclusions

The following list summarizes the major findings of this work:

1. The effect of CCD on HCCI combustion is much more significant than the influence on conventional combustion modes, due to the strong coupling between HCCI and heat transfer effects.
    a. A decrease in heat loss during compression results in advanced ignition timing and overall combustion phasing.
    b. Heat stored in the deposit layer leading up to ignition causes the periphery of the air/fuel charge to burn faster in the last half of the heat release event, also causing a reduction in unburned hydrocarbon emissions.
2. Combustion chamber deposits only have a transient effect on heat loss from the chamber.
    a. The insulating properties of CCD are offset by higher HCCI combustion rates associated with advanced phasing.
    b. Cycle net heat loss does not change with a conditioned combustion chamber so the only increase in thermal efficiency is due to the advanced phasing of combustion.
3. The thermal effects imparted by combustion chamber deposits cause a significant shift in the HCCI operability range compared to a clean combustion chamber.
    a. Advanced combustion phasing causes the ringing limit of combustion to be reached at a lower load.
    b. The transient thermal effects during compression and heat release allow minimum combustion stability to be maintained at lower loads.

4. There is a strong correlation between phasing shift of the measured instantaneous metal surface temperature profile below the deposit layer and the thickness of the deposit.
    a. This correlation allows in-situ tracking of deposit formations rates based on real-time instantaneous temperature measurements, assuming that changes in combustion phasing due to the presence of CCD are accounted for.
    b. This correlation can be extended to calculate the effective thermal diffusivity of the deposit layer, again ensuring that changes in combustion rates have been compensated for.

9.2 Summary of Accomplishments

The following list provides a summary of the accomplishments of the work regarding the effect of combustion chamber deposits on HCCI combustion.

- A full characterization of the changes in measured wall temperature and heat flux due to deposit coverage for an engine operating in HCCI mode was performed. This is important for understanding the thermal influence of CCD on HCCI combustion. As the deposit layer thickens over the location of the heat flux probe, there is a consistent characteristic change in the measured crank angle resolved temperature. This is caused by the burying of the thermocouple junction by a thickening insulating layer. Dependent on the thermal properties and thickness of the layer, heat transfer diffuses from the deposit surface down to the metal wall surface. This causes an overall dampening and retardation in phasing of the measured signal compared to a clean wall.

Another useful finding from this insight is that there is such a consistent relationship between the phasing of the measured temperature profile and the local deposit layer thickness that it is possible to track the deposit formation rates in a running

engine *in-situ*. Based solely on the shifting temperature profile measured in real time, the local thickness of the CCD layer can be estimated and possibly correlated to changes in other combustion parameters. Two separate relationships were found for deposits on the head and piston.

- A methodology to determine the effective thermal diffusivity of combustion chamber deposits for an engine operating in HCCI mode is developed. This is crucial for quantifying the changes in heat loss characteristics that CCD impose. Based on the characteristic retardation in phasing of the measured temperature profile below the CCD and a known local deposit thickness, it is possible to analytically calculate an effective thermal diffusivity value of the deposit layer. This requires a modification of the procedure developed by other researchers [72] for the specific case of HCCI combustion. The shift in measured cycle peak temperature phasing is a function of the thickness and the thermally diffusive properties of the layer and can be used to calculate the average thermal diffusivity of the deposit material. For the special case of HCCI, since heat release rates and the degree of CCD coverage are coupled, the change in combustion phasing is an additional factor in the measured change in temperature phasing. Thus in the particular case of an HCCI engine, phasing changes imparted by deposits are compensated for by a reduction in intake temperature until the phasing of the reference clean chamber is re-acquired. This modification to the original technique permits accurate results. The range of values of thermal diffusivity found varied from 0.8×10^{-7} to 1.5×10^{-6} m^2/s, depending on thickness and whether they were from the head or piston surfaces.
- A methodology was developed to calculate the crank angle resolved deposit layer surface temperature profile based solely on measurements from the engine. The Lead-Corrector method is a prediction-correction based process using finite-difference calculations to iteratively converge on a temperature profile for the surface of the deposit layer. Unlike previous work by other researchers, this methodology does not rely on global average gas temperature or convection coefficient estimates. The requirements are

measured temperature and heat flux profiles below the deposit layer, a known local deposit thickness, and the thermal properties of the deposit layer, which were determined previously. An iteratively corrected deposit surface temperature and the measured deposit/metal interface heat flux are used as spatial boundary conditions to calculate the temperature gradients within the CCD layer. These are checked next to the actual measured temperatures at the bottom of the deposit and the difference is used to correct the surface profile estimate. This procedure is continued until convergence of the calculated and measured profiles at the bottom of the layer. Once the temperature profiles throughout the layer are determined, the instantaneous surface heat flux may be calculated as well.

- The effects of combustion chamber deposits on HCCI combustion were determined. Contrary to conventional forms of combustion, such as SI and CI, deposits have primary influence on HCCI operation, due to the strong coupling of thermal effects and auto-ignition. It was found that deposits on the chamber walls have two separate general effects. The first is causing reduced heat loss to the chamber walls during the intake and compressions periods of the cycle. This causes the average gas temperatures to be higher leading up to TDC and results in earlier ignition timing and overall advanced phasing in heat release compared to a clean chamber. This advanced combustion phasing results in higher peak heat release rates and gas temperatures. The second effect is related to CCD's influence on the thermal boundary layer of the chamber near the walls. Higher temperature swings at the wall reduced heat loss during the main part of combustion resulting in a faster burn of the peripheral region of the air/fuel mixture. This decreases the overall burn duration on top of the decrease associated solely with advanced phasing. This extra heating of the chamber thermal boundary layer by the CCD layer is also thought to be responsible for a decrease in specific unburned hydrocarbon emissions.
- The changes in wall heat transfer imposed by combustion chamber deposits and how those are influenced by differences in combustion were quantified. The Lead-

Corrector method was used with measurements taken from two locations on the head surface and six locations on the piston surface. This allowed a direct comparison of the 'surface' temperature profile for locations in a clean chamber and one with a CCD layer. Also, a comparison of integrated heat flux for the two different cases provided specific insight into the change in heat loss characteristics caused by deposits. It was found that heat loss during compression and the peak heat release rate period was reduced. However, the heat stored in the CCD layer eventually diffuses into the chamber wall later in the expansion stroke, so that the net cycle heat loss with deposits is not significantly different than with a clean chamber. Thus the thermal effects of CCD in the HCCI engine are transient in nature and do not significantly change the overall heat loss characteristics of the engine. This was caused by an increase in the maximum temperature swing during the compression and heat release portion of the cycle from about 5°C at most locations in a clean chamber to 20°C at the surface of the deposit layer in a conditioned engine. This is due to the thermal properties of the CCD layer compared to those of the clean metal wall.

- Based on the changes in thermal response characteristics of the chamber walls and combustion imposed by deposits, an assessment of the effects on the limits of HCCI operability was performed. The low and high load limits at four engine speeds were determined with a clean chamber and then compared to those limits found with a conditioned combustion chamber. In general, the load limits of operability for HCCI decreased in value after the chamber was conditioned. In other words, the overall load-speed operating map shifted downwards. The insulating properties of deposit coverage causes ignition timing to advance which results in the ringing limit of the engine being reached at a lower fueling rate compared to a clean engine, causing the maximum load limit to decrease. The same heating effect at low loads decreases combustion instability because of the advanced overall phasing of combustion, which allows the fueling rate to be decreased further before the limits of stability are reached. In summary, the shift in

operability range is due to the effect of CCD on combustion phasing. Additionally, it was found that any increase in thermal efficiency found during operation with deposit coverage was due only to the advance in combustion phasing. Net heat loss for the cycle did not change with deposits because the higher heat release rates associated with advanced combustion were partially offset by an increase in peak heat loss rates.

9.3 Additional Notes

There are a few supplemental points which should be made regarding the findings in this work.

9.3.1 Nature of 'Deposits'

Recall that deposits were produced two different ways in this work. One way is to run the engine at a mid-load HCCI operating point for an extended period so that deposits naturally formed on the chamber walls over long-term operation, specifically about forty hours. This was referred to as 'passive conditioning'. The other method requires a few parameters of operation to be changed which results in smoke-producing operation. This requires about 2-3 hours of engine running to attain the same change in heat release rates as the first method, and is referred to as 'aggressive conditioning'. As stated before, even though the same changes in combustion are recorded, it would be a stretch to claim that the 'deposits' formed on the walls in each case had the same composition, porosity, etc. It is imperative to realize that this is only of secondary importance. The significance of this work is to determine the nature of the effect of any insulating wall coating on HCCI combustion, especially when considering the strong coupling between thermal effects (gas temperature, wall temperature, etc) and HCCI. From engine to engine, from driving cycle to driving cycle, the nature and composition of deposits in an engine are going to vary greatly. Clearly there is no way to account for all possibilities. What is important

here is the strong coupling of changes in wall heat transfer characteristics imposed by deposits (of any variety) and the nature of heat release for an auto-ignition cycle which is so dependent on the thermal history of the air/fuel charge. These findings can serve as a guideline for understanding the effects in any HCCI-type engine when changes in effective wall thermal properties are involved.

9.3.2 Magnitude of Conditioning

Another important point to be considered is the magnitude of deposit coverage in this testing. This is especially important when considering the finding that the net cycle heat loss did *not* change with the presence of deposits. That is not to say that this would be the case for a combustion chamber with a varying coverage of deposits. The thickness of the deposit layer over a heat flux probe was never greater than 100 microns. It may be possible that with thicker CCD layers of different thermal properties the effects on peak temperatures and heat flux would be magnified. This would result in a much stronger influence on heat transfer between the gas and walls, potentially changing net cycle heat loss and thus more significantly changing overall thermal efficiency. Detrimental effects on volumetric efficiency would likely arise as well. This would have further repercussions on the range of stable HCCI operation.

9.3.3 Long-Term Variability

There is one other important factor to take into consideration regarding the deposits in an HCCI engine. It had been shown how strongly coupled burn rates are to the level of CCD formation in the chamber, particularly when considering the long-term deposits formation testing discussed in Chapter 4. With other combustion modes, SI and CI, CCD have only a secondary effect. Octane requirement increase and fuel absorption are a couple of persistent issues. However, with HCCI the effects of deposits are much

more critical since over a short time period, depending on the nature of driving and environmental conditions, CCD coverage can vary greatly. As a result, deposits in an HCCI engine introduce another control variability which must be accounted for. Robust control of auto-ignition timing is already a major issue facing implementation of HCCI in a production vehicle; deposits will only add further complexity. In the best case, compensating for the effect of deposits will be handled by feedback-based control provided by in-cylinder pressure measurements that successful HCCI operation at the vehicle level will likely require.

9.4 Recommendations for Future Work

As with any body of work, there will always be more questions to ask once the work is completed. Most of the new questions are due to the natural cycle of needing to understand more about the new insights gained and how to utilize them. There are a host of additional issues to address regarding this work in deposits as a result of the findings discussed. There are also clearly new avenues to investigate in order to support and further illuminate certain details. Those are reviewed in this section.

Firstly there are a series of topics to further investigate as a clear continuation of the findings of this work:

- Would there be any characteristic differences in the effects of CCD on heat transfer and HCCI if the deposit levels were significantly thicker or of varying properties? As discussed, a significantly thicker deposit could have a much more obtrusive effect on cycle net heat loss and thus cause a measurable increase in cycle average wall temperatures. This could lead to much more significant effects on HCCI combustion as well as the operating limits.
- How much significance is there in the spatial variety of deposit coverage? It is hypothesized that CCD coverage on the piston has more influence on the recorded

changes in combustion than those on the head. Some initial testing was performed but no clear conclusions were drawn. If the piston does have a greater influence, is one part of the crown more effective than another? It is thought that deposits in the bowl may have a greater effect on heating the core gas, thus affecting ignition timing, while deposits on the crown periphery have more influence on the latter parts of the heat release event.

There are also a few topics which would require a whole different series of testing in order to perform:

- It would be very useful to confirm the thermal properties used in this work. Specifically the conductivity and diffusivity. Work on these topics is already in progress. In order to calculate the deposit thermal conductivity, a known steady heat flux source is required. Furthermore a separate method to physically determine the steady deposit surface temperature is needed. Currently in development is an oven which utilizes resistance heating to produce a radiation heat source on the order of the peak heat flux levels in an engine. The instrumented piston from the engine and the head heat flux probes can be mounted in this oven in such a way that a known heat source is applied to the deposit layer. Combined with infrared measurements, the conductivity can be calculated. This could be used to improve the LC-method based calculations and to confirm the magnitude of the thermal influence of the deposits.
- Recall that the determined thermal diffusivity values were ‘effective’ values, meaning representative average values for the entire layer. This is because the deposit layer is highly porous and likely affected by physical interactions with air and fuel. The previously described oven could also be used to separate out the effects of air and fuel on the apparent properties of the deposit layer. By using a transient heat source in the oven (chopping wheel) the thermal diffusivity of the layer could be determined independent of the effects of air, fuel, and other complications of doing the measurements in an engine

(the oven is operated in a nitrogen environment). This would be useful for further characterization of the deposit material itself.

Some other useful avenues to investigate would be:

- The effect of CCD on transients under HCCI operation
- The effect of CCD on HCCI cold-starts. It is hypothesized that the insulating effects of deposits will likely make cold-starts a little more plausible under HCCI operation. The problem with starting in HCCI mode with a rebreathing engine is that there is no source of hot residual to help promote auto-ignition. Perhaps a hybrid spark-assisted based starting procedure could be aided by the thermal effects of deposits.

APPENDIX

Determination of CCD Layer Thermal Diffusivity

First a solution will be found of the temperature distribution in the deposit layer with the temperature profile represented by Fourier series approximation. The solution is based on the problem of one-dimensional heat diffusion through a medium [72],

$$\frac{\partial^2 T(x,t)}{\partial x^2} = \frac{1}{\alpha}\frac{\partial T(x,t)}{\partial t} \tag{A1.1}$$

One method to solve the governing equation is by separation of variables,

$$T(x,t) = F(x)G(t) \tag{A1.2}$$

The particular solutions for each independent variable are,

$$F(x) = A_1 e^{+xi\sqrt{\lambda}} + A_2 e^{-xi\sqrt{\lambda}} + A_3 e^{+x\sqrt{\lambda}} + A_4 e^{-x\sqrt{\lambda}} \tag{A1.3}$$

$$G(t) = B_1 e^{+\alpha\lambda t} + B_2 e^{-\alpha\lambda t} \tag{A1.4}$$

With the general solution in the final form,

$$\begin{aligned} T(x,t) = {} & D_1 e^{\alpha\lambda t + xi\sqrt{\lambda}} + D_2 e^{\alpha\lambda t - xi\sqrt{\lambda}} + D_3 e^{\alpha\lambda t + x\sqrt{\lambda}} + D_4 e^{\alpha\lambda t - x\sqrt{\lambda}} \\ & + D_5 e^{-\alpha\lambda t + xi\sqrt{\lambda}} + D_6 e^{-\alpha\lambda t - xi\sqrt{\lambda}} + D_7 e^{-\alpha\lambda t + x\sqrt{\lambda}} + D_8 e^{-\alpha\lambda t - x\sqrt{\lambda}} \end{aligned} \tag{A1.5}$$

A Fourier series is used to represent the deposit surface temperature profile,

$$T(x,t) = \sum_{n=1}^{\infty} \left\{ a_n \cos(n\omega_0 t) + b_n \sin(n\omega_0 t) \right\} = \sum_{n=-\infty}^{\infty} c_n e^{in\omega_0 t} \tag{A1.6}$$

with

$$\alpha\lambda = in\omega_0$$

This can be substituted into the main temperature solution to obtain the general form

$$T(x,t) = \sum_{n=-\infty}^{\infty} c_n e^{\pm\left(x\sqrt{\frac{n\omega_0}{2\alpha}}\right)} e^{i\left(n\omega_0 t \pm x\sqrt{\frac{n\omega_0}{2\alpha}}\right)} \tag{A1.7}$$

Full expansion of (A1.7) results in another form of the final solution with the temperature profile represented as a Fourier series,

$$T(x,t) = \frac{a_0}{2} + \left(\sum_{n=1}^{\infty} c_n e^{-\left(x\sqrt{\frac{n\omega_0}{2\alpha}}\right)}\right)\left[a_n \cos\left(n\omega_0 t - x\sqrt{\frac{n\omega_0}{2\alpha}}\right)\right] + \left(\sum_{n=1}^{\infty} c_n e^{-\left(x\sqrt{\frac{n\omega_0}{2\alpha}}\right)}\right)\left[b_n \sin\left(n\omega_0 t - x\sqrt{\frac{n\omega_0}{2\alpha}}\right)\right] \tag{A1.8}$$

The a_0 term in (A1.8) represents the profile average temperature, α is the material thermal diffusivity from the governing equation, and ω_0 is the cycle frequency, dependant on engine speed, where t_0 is the duration of a cycle in seconds.

$$\omega_0 = \frac{2\pi}{t_0}$$

Now produce a specific Fourier series which is representative of the general shape of the cycle temperature profile on the deposit surface,

$$T(0,t) = 2\cos\left(\frac{2\pi\left(t - \frac{t_0}{12}\right)}{t_0}\right) - \sin\left(\frac{4\pi\left(t - \frac{t_0}{12}\right)}{t_0}\right) \tag{A1.9}$$

A plot of (A1.9) is depicted below. It represents the main features of the temperature profile at the surface of the deposit layer with the peak cycle temperature phasing at 0° so

that retardation of the temperature profile phasing below the layer is on an absolute scale. The magnitude of the y-axis, which represents temperature, is unimportant.

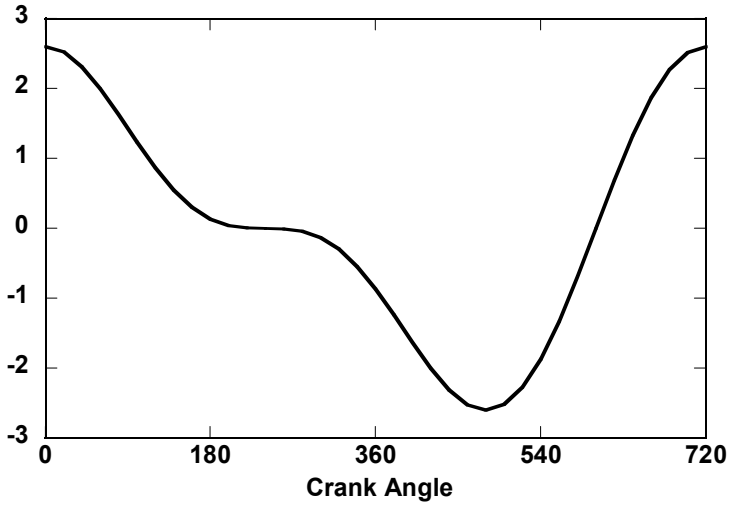

A.1 - Plot of Fourier series representation of general features of measured temperature profile

And substitute into the latest version of the solution, (A1.8). Note that the a_0 term has been set to zero because the absolute value of the temperature does not matter.

$$T(x,t) = 2\exp\left(-x\sqrt{\frac{\pi}{\alpha t_0}}\right)\cos\left(\frac{2\pi\left(t-\frac{t_0}{12}\right)}{t_0}-x\sqrt{\frac{\pi}{\alpha t_0}}\right) - \exp\left(-x\sqrt{\frac{2\pi}{\alpha t_0}}\right)\sin\left(\frac{4\pi\left(t-\frac{t_0}{12}\right)}{t_0}-x\sqrt{\frac{2\pi}{\alpha t_0}}\right) \quad \text{(A1.10)}$$

Since we are interested in the phasing shift of the cycle peak temperature, take the time derivative and set equal to zero. Now '*t*' represents the time for peak cycle temperature.

$$0 = -\frac{4\pi}{t_0}\exp\left(-x\sqrt{\frac{\pi}{\alpha t_0}}\right)\sin\left(\frac{2\pi\left(t-\frac{t_0}{12}\right)}{t_0}-x\sqrt{\frac{\pi}{\alpha t_0}}\right)$$
$$+\frac{4\pi}{t_0}\exp\left(-x\sqrt{\frac{2\pi}{\alpha t_0}}\right)\cos\left(\frac{4\pi\left(t-\frac{t_0}{12}\right)}{t_0}-x\sqrt{\frac{2\pi}{\alpha t_0}}\right) \tag{A1.11}$$

Combining terms and applying, $\cos(\varphi) = \sin(\pi/2+\varphi)$,

$$\exp\left(\left(1-\sqrt{2}\right)x\sqrt{\frac{\pi}{\alpha t_0}}\right)\sin\left(\frac{\pi}{6}+\frac{4\pi t_{peak}}{t_0}-x\sqrt{\frac{\pi}{\alpha t_0}}\right)=\sin\left(\frac{\pi}{6}-\frac{2\pi t_{peak}}{t_0}-x\sqrt{\frac{\pi}{\alpha t_0}}\right) \tag{A1.12}$$

since x, the thickness is small, the following applies,

$$\exp\left(\left(1-\sqrt{2}\right)\cdot x\sqrt{\frac{\pi}{\alpha t_0}}\right)\approx 1 \tag{A1.13}$$

Next, combine similar terms and applying trigonometric relations, leads to:

$$t = x\frac{\left(1+\sqrt{2}\right)}{6}\sqrt{\frac{t_0}{\pi\alpha}} \tag{A1.14}$$

And finally,

$$\alpha = \left(\frac{x}{t}\frac{\left(1+\sqrt{2}\right)}{6}\right)^2\frac{t_0}{\pi} \tag{A1.15}$$

Lead Corrector Method

The following are the governing equations describing the problem of heat flux into a deposit layer. In general terms, this is a one-dimensional transient heat diffusion problem.

$$\frac{\partial T}{\partial t} = \alpha \frac{\partial^2 T}{\partial x^2} \qquad \text{with, } T = T(x,t) \tag{A2.1}$$

Where 'T' is temperature, 't' is time, and 'x' is the spatial variable in the direction normal to the deposit or wall surface. The deposit layer is thin enough to assume that conductive heat flow is one-dimensional.

In order to solve this equation, three boundary conditions are required; one temporal and two spatial in x. Because this model represents a cyclic event, and the solution is iteratively determined, the temperature solution, T(x,t) at t=0 is set equal to the solution at $t=t_n$, with 'n' the duration of the cycle, so

$$T(x,t_0) = T(x,t_n) \tag{A2.2}$$

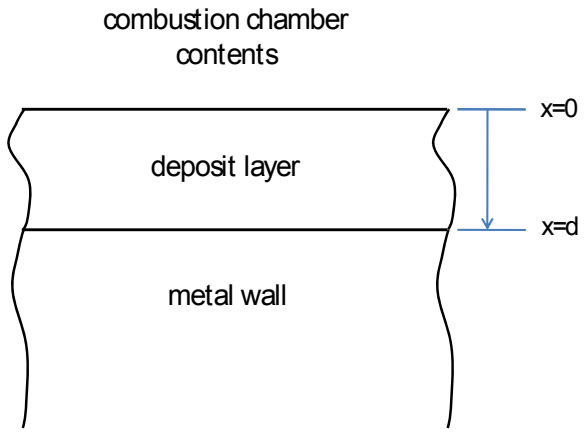

A.2 – Representation of x-direction referencing scheme

The top of the deposit surface boundary condition, at T(0,t), is equal to an iteratively corrected temperature profile, with '*c*' indicating the corrected temperature profile.

$$T(0,t) = T_c(0,t) \tag{A2.3}$$

The bottom of the deposit layer (at the CCD/metal wall interface), is the measured heat flux at the wall surface, with '*m*' indicting measured profile and '*d*' indicating the thickness of the deposit layer.

$$k\frac{\partial T}{\partial x}(d,t) = q_m(d,t) \tag{A2.4}$$

An implicit finite difference scheme will be used represent the problem described here. The 'Δx' interval was determined by testing different values until the maximum Δx value was found that would not result in a change in the final solution. This ended up being a value equal to the total thickness divided by 30 for the thickest CCD layer and was thus used thereafter for every deposit layer thickness. The 'Δt' interval is set as the measurements increment from the engine, 0.5 crank angles, converted to seconds. All data applied to the LC method was taken at 2000rpm with the number of temporal measurement intervals equal to 1440 (720 CAD @ 0.5 CA intervals). This is was the limiting factor for maintaining stability in an explicit finite difference scheme, but it caused final accuracy and convergence ability to suffer. For that reason an implicit scheme was ultimately used, permitting solution stability at any thickness interval chosen.

Figure A.3 below depicts how the finite difference scheme is setup with labeling format for the nodes in the x and t directions. Also indicated in the figure are the Δx and Δt intervals.

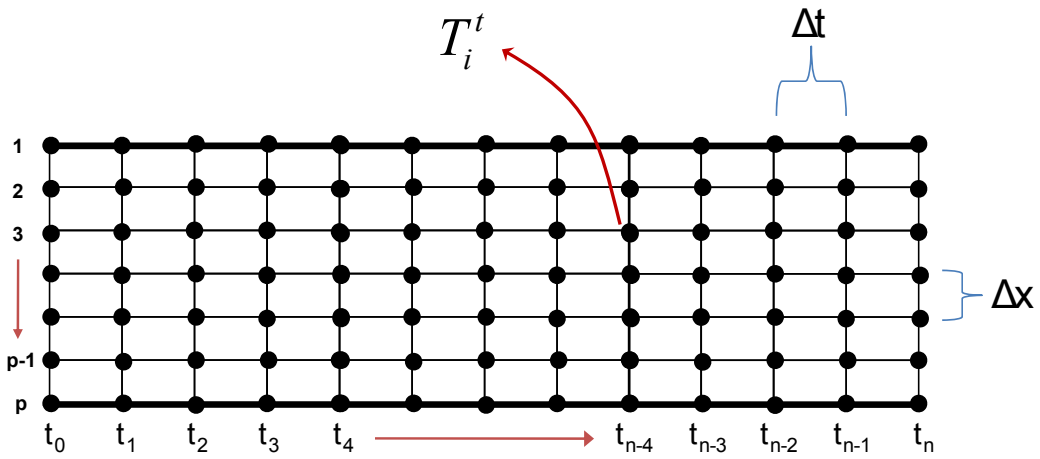

A.3 – Figure depicting the finite difference scheme representing the deposit layer

A first order in *t* and second order in *x* center-difference finite difference scheme with the pertinent boundary conditions was developed for all interior nodes:

$$\frac{\partial T}{\partial t} = \alpha \frac{\partial^2 T}{\partial x^2} \tag{A2.5}$$

$$\frac{T_i^{t+1} - T_i^t}{\Delta t} = \alpha \frac{\left(T_{i-1}^{t+1} - 2T_i^{t+1} + T_{i+1}^{t+1}\right)}{\Delta x^2} \tag{A2.6}$$

$$T_i^t = -rT_{i-1}^{t+1} + (1+2r)T_i^{t+1} - rT_{i+1}^{t+1} \tag{A2.7}$$

where, $r = \dfrac{\alpha \Delta t}{\Delta x^2}$

A similar formulation for the application of the heat flux boundary condition at the bottom of the CCD layer,

$$q_m'' + \frac{\partial T}{\partial t} = \alpha \frac{\partial^2 T}{\partial x^2} \tag{A2.8}$$

$$q''_m(t) + \frac{k\left(T_{p-1}^{t+1} - T_p^{t+1}\right)}{\Delta x} = \frac{\rho C(\Delta x)\left(T_p^{t+1} - T_p^{t}\right)}{2\Delta t} \tag{A2.9}$$

$$T_p^t = (1+2r)T_p^{t+1} - 2rT_{p-1}^{t+1} - 2q''_m(t)\frac{\alpha\Delta t}{k\Delta x} \tag{A2.10}$$

$$T_p^t = (1+2r)T_p^{t+1} - 2rT_{p-1}^{t+1} - 2rb_{q''} \tag{A2.11}$$

where $b_{q''} = \frac{\Delta x}{k} q''_m(t)$

Below is shown how the matrices for a deposit thickness consisting of 5 nodes would be set up for one instant in time. These matrices are solved for every 0.5 CA for the entire cycle.

$$\begin{bmatrix} 1 & 0 & 0 & 0 & 0 \\ -r & 1+2r & -r & 0 & 0 \\ 0 & -r & 1+2r & -r & 0 \\ 0 & 0 & -r & 1+2r & -r \\ 0 & 0 & 0 & -2r & 1+2r \end{bmatrix} \begin{bmatrix} T_1^{t+1} \\ T_2^{t+1} \\ T_3^{t+1} \\ T_4^{t+1} \\ T_5^{t+1} \end{bmatrix} = \begin{bmatrix} T_c^t \\ T_2^t \\ T_3^t \\ T_4^t \\ T_5^t + 2rb_{q''} \end{bmatrix}$$

The temperature calculated at the bottom of the deposit layer is then compared to the actual measured temperature profile using the fast response thermocouple. Based on the difference in the two profiles at every time interval (0.5 CA) a proportional correction is applied to the applied temperature profile for the surface of the deposit, T_c^t, for the next interval. This process is repeated until the calculated and measured temperature profiles at the bottom of the deposit layer match. The criteria for equal profiles are that the maximum difference in temperature anywhere in the cycle is 0.1°C.

BIBLIOGRAPHY

1. Institute for the Analysis of Global Security, www.iags.org/futureofoil.html.

2. Stanglmaier, R.H., Roberts, C.E., "Homogenous Charge Compression Ignition (HCCI): Benefits, Compromises, and Future Engine Applications," SAE 1999-01-3682, 1999.

3. Zheng, J., Yang, W., Miller, D.L., Cernansky, N.P., "A Skeletal Chemical Kinetic Model for the HCCI Combustion Process," SAE 2002-01-0423, 2002.

4. Flowers, D., Aceves, S., Smith, R., Torres, J., Girard, J., Dibble, R., "HCCI in a CFR Engine: Experiments and Detailed Kinetic Modeling," SAE 2000-01-0328, 2000.

5. Epping, K., Aceves, S., Bechtold, R., Dec, J., "The Potential of HCCI Combustion for High Efficiency and Low Emissions," SAE 2002-01-1923, 2002.

6. Shore, L., B., Ockert, K., F., "Combustion-Chamber Deposits – A Radiotracer Study," SAE Transactions, Volume 66, 1958.

7. Chang, J., Filipi, Z., Assanis, D., Kuo, T., Najt, P., Rask, R., "Characterizing the thermal sensitivity of a gasoline homogenous charge compression ignition engine with measurements of instantaneous wall temperature and heat flux," IMechE 2005 Volume 6, pp.289-309, 2005.

8. Cheng, S., Kim, C., "Effect of Engine Operating Parameters on Engine Combustion Chamber Deposits," SAE 902108, 1990.

9. Dec, J.E., Sjöberg, M. "Isolating the Effects of Fuel Chemistry on Combustion Phasing in an HCCI Engine and the Potential of Fuel Stratification for Ignition Control," SAE 2004-01-0557, 2004.

10. Onishi, S., Jo, S.H., Shoda, K., Jo, P.D., Kato, S., "Active Thermo-Atmosphere Combustion (ATAC) – A New Combustion Process for Internal Combustion Engine," SAE 790501, 1979.

11. Sjoberg, M., Dec, J.E., Babajimopoulos, A., Assanis, D.N., "Comparing Enhanced Natural Thermal Stratification Against Retarded Combustion Phasing for Smoothing of Hcci Heat-Release Rates," SAE 2004-01-2994, 2004.

12. Daw, C.S., Wagner, R.M., Green, J.B., "Modeling Cyclic Variability in Spark-Assisted HCCI," ASME ICEF2007-1685, 2007.

13. Ryan, T.W., Callahan, T., "Homogenous Charge Compression Ignition of Diesel Fuel," SAE 961160, 1996.

14. Takeda, Y., Keiichi, N., Keiichi, N., "Emission Characteristics of Premixed Lean Diesel Combustion with Extremely Early Staged Fuel Injection," SAE 961163, 1996.

15. Suzuki, H., Koike, N, Ishii, H., Odaka, M., "Exhaust Purification of Diesel Engines by Homogeneous Charge with Compression Ignition Part1: Experimental Investigation of Combustion and Exhaust Emission Behavior Under Pre-Mixed Homogeneous Charge Compression Ignition Method," SAE 970313, 1997.

16. Suzuki, H., Koike, N., Odaka, M., "Combustion Control Method of Homogenous Charge Diesel Engines," SAE 980509, 1998.

17. Suzuki, H., Odaka, M., Kariya, T., "Effect of start of injection on NOx and smoke emissions in homogenous charge diesel combustion," JSAE Review 2000-385-416, 2000.

18. Gray, A.W., Ryan, T.W., "Homogenous Charge Compression Ignition (HCCI) of Diesel Fuel," SAE 971676, 1997.

19. Mase, Y., Kawashima, J., Sato, T., Eguchi, M., "Nissan's New Multivalve DI Diesel Engine Series," SAE 981039, 1998.

20. Akagawa, H., Miyamoto, T., Harada, A., Sasaki, S., Shimazaki, N., Hashizume, T., Tsujimura, K., "Approaches to Solve Problems of the Premixed Lean Diesel Combustion," SAE 1999-01-0183, 1999.

21. Kalghatgi, G.T., Risberg, P., Angstrom, H., "Advantages of Fuels with High Resistance to Auto-Ignition in Late-injection, Low-temperature, Compression Ignition Combustion," SAE 2006-01-3385, 2006.

22. Stone, R., Introduction to Internal Combustion Engines, SAE, 1999.

23. Najt, P.M., Foster, D.E., "Compression-Ignited Homogenous Charge Combustion," SAE 830264, 1983.

24. Noguchi, M., Tanaka, Y., Tanaka, T., Takeuchi, Y., "A Study on Gasoline Engine Combustion by Observation of Intermediate Reactive Products during Combustion," SAE 790840, 1979.

25. Kong, S., Ayoub, N., Reitz, R.D., "Modeling Combustion in Compression Ignition Homogenous Charge Engine," SAE 920512, 1992.

26. Westbrook, C.K., "Chemical Kinetics of Hydrocarbon Ignition in Practical Combustion Systems," Proceedings of the Combustion Institute, Volume 28, pp. 1563-1577, 2000.

27. Aceves, S., Flowers, D.L., Westbrook, C.K., Smith, J.R., Pitz, W., Dibble, R., Christensen, M., Johansson ,B., "A Multi-Zone Model for Prediction of HCCI Combustion and Emissions," SAE 2000-01-0327, 2000.

28. Aceves, S.M., Martinez-Frias, J., Flowers, D.L., Smith, J.R., Dibble, R.W., "A Computer-Generated Reduced Iso-Octane Chemical Kinetic Mechanism Applied to Simulation of Hcci Combustion," SAE 2002-01-2870, 2002.

29. Heywood, J.B., Internal Combustion Engine Fundamentals, McGraw-Hill, New York, 1988.

30. Aoyama, T., Hattori, Y., Mizuta, J., Sato, Y., "An Experimental Study on Premixed-Charge Compression Ignition Gasoline Engine," SAE 960081, 1996.

31. Ishibashi, Y., Asai, M., "Improving the Exhaust Emissions of Two-Stroke Engines by Applying the Activated Radical Combustion," SAE 960742, 1996.

32. Kimura, S., Aoki, O., Ogawa, H., Muranaka, S., Enomoto, Y., "New Combustion Concept for Ultra-Clean and High-Efficiency Small Di Diesel Engines," SAE 1999-01-3681, 1999.

33. Glassman, I., Combustion, 3rd Edition, Academic Press, New York, 1996.

34. Christensen, M., Johansson, B., "Homogeneous Charge Compression Ignition with Water Injection," SAE 1999-01-0182, 1999.

35. Walter, B., Gatellier, B., "Development of the High Power NADI Concept Using Dual Mode Diesel Combustion to Achieve Zero NOx and Particulate Emissions," SAE 2002-01-1744, 2002.

36. Zheng, J., Yang, W., Miller, D.L., Cernansky, N.P., "A Skeletal Chemical Kinetic Model for the HCCI Combustion Process," SAE 2002-01-0423, 2002.

37. Dec, J.E., Hwang, W., Sjoberg, M., "An Investigation of Thermal Stratification in HCCI Engines Using Chemiluminescence Imaging," SAE 2006-01-1518, 2006.

38. Shen, Y., "Influences of Intake Charge Preparations on HCCI Combustion in a Single Cylinder Engine with Variable Valve Timing and Gasoline Direct Injection," SAE 2006-01-3274, 2006.

39. Allen, J., Law, D., "Variable Valve Actuated Controlled Auto-Ignition: Speed Load Maps and Strategic Regimes of Operation," SAE 2002-01-0422, 2002.

40. Christensen, M., Johansson, B., Einewall, P., "Homogenous Charge Compression Ignition (HCCI) Using Isooctane, Ethanol and Natural Gas – A Comparison with Spark Ignition Operation," SAE 972874, 1997.

41. Christensen, M., Johansson, B., "Influence of Mixture Quality on Homogenous Charge Compression Ignition," SAE 982454, 1998.

42. Kaneko, N., Ando, H., Ogawa, H., Miyamoto, N., "Expansion of the Operating Range With In-Cylinder Water Injection in a Premixed Charge Compression Ignition Engine," SAE 2002-01-1743, 2002.

43. Kakuho, A., Nagamine, M., Amenomori, Y., Urushihara, T., Itoh, T., "In-Cylinder Temperature Distribution Measurements and Its Application to HCCI Combustion," SAE 2006-01-1202, 2006.

44. Eng, J.A., "Characterization Of Pressure Waves in HCCI Combustion," SAE 2002-01-2859, 2002.

45. Thring, R.H., "Homogenous-Charge Compression-Ignition (HCCI) Engines," SAE 892068, 1989.

46. Zhao, H., Li, J., Ma, T., Ladommatos, N., "Performance and Analysis of a 4-Stroke Multi-Cylinder Gasoline Engine with CAI Combustion," SAE 2002-01-0420, 2002.

47. Hultqvist, A., Christensen, M., Johansson, B., Franke, A., Richter, M., Alden, M., "A Study of the Homogenous Charge Compression Ignition Combustion Process by Chemiluminescence Imaging," SAE 1999-01-3680, 1999.

48. Pucher, G.R., Gardiner, D.P., Bardon, M.F., Battista, V., "Alternative Combustion Systems for Piston Engines Involving Homogenous Charge Compression Ignition Concepts – A Review of Studies using Methanol, Gasoline, and Diesel Fuel," SAE 962063, 1996.

49. Chen, Z., Konno, M., Oguma, M., Yanai, T., "Experimental Study of CI Natural-Gas/DME Homogeneous Charge Engine," SAE 2000-01-0329, 2000.

50. Aroonsrisopon, T., Foster, D., Morikawa, T., Iida, M., "Comparison of HCCI Operating Ranges for Combinations of Intake Temperature, Engine Speed, and Fuel Composition," SAE 2002-01-1924, 2002.

51. Shibata, G., Oyama, K., Urushihara, T., Nakano, T., "Correlation of Low Temperature Heat Release with Fuel Composition and HCCI Engine Combustion," SAE 2005-01-0138, 2005.

52. Kalghatgi, G.T., "Auto-Ignition Quality of Practical Fuels and Implication for Fuel Requirements of Future SI and HCCI Engines," SAE 2005-01-0239, 2005.

53. Christensen, M., Johansson, B., Amneus, P., Mauss, F., "Supercharged Homogenous Charge Compression Ignition," SAE 980787, 1998.

54. Christensen, M., Johansson, B., "The Effect of In-Cylinder Flow and Turbulence on Hcci Operation," SAE 2002-01-2864, 2002.

55. Flowers, D.L., Aceves, S.M., Babajimopoulos, A., "Effect of Charge Non-uniformity on Heat Release and Emissions in PCCI Engine Combustion," SAE 2006-01-1363, 2006.

56. Iwabuchi, Y., Kawai, K., Shoji, T., Takeda, Y., "Trial of New Concept Diesel Combustion System – Premixed Compression-Ignited Combustion," SAE 1999-01-0185, 1999.

57. Van Blarigan, P., Paradiso, N., Goldsborough, S., "Homogenous Charge Compression Ignition with a Free Piston: A New Approach to Ideal Otto Cycle Performance," SAE 982484, 1998.

58. Chang, J., "Thermal Characterization and Heat Transfer Study of a Gasoline Homogenous Charge Compression Ignition Engine via Measurements of Instantaneous Wall Temperature and Heat Flux in the Combustion Chamber," PhD Dissertation, University of Michigan, Ann Arbor, 2004.

59. Kalghatgi, G.T., "Deposits in Gasoline Engine – A Literature Review," SAE 902105, 1990.

60. Nakic, D.J., Assanis, D.N., White, R.A., "Effect of Elevated Piston Temperature on Combustion Chamber Deposit Growth," SAE 940948, 1994.

61. Kalghatgi, G.T., McDonald, C.R., Hopwood, A.B., “An Experimental Study of Combustion Chamber Deposits and Their Effects in a Spark-Ignition Engine,” SAE 950680, 1995.

62. Cheng, S., “The Impacts of Engine Operating Conditions and Fuel Compositions on the Formation of Combustion Chamber Deposits,” SAE 2000-01-2025, 2000.

63. Ishii, H., Emi, M., Yamada, Y., Kimura, S., Shimano, K., Enomoto, Y., “Heat Loss to the Combustion Chamber Wall with Deposit Adhering to The Wall Surface in D.I. Diesel Engine,” SAE 2001-01-1811, 2001.

64. Woschni, G., Huber, K., “The Influence of Soot Deposits on Combustion Chamber Walls on Heat Losses in Diesel Engines,” SAE 910297, 1991.

65. LaVigne, P.A., Anderson, C.L., Prakash, C., “Unsteady Heat Transfer and Fluid Flow in Porous Combustion Chamber Deposits,” SAE 860241, 1986.

66. Tree, D.R., Wiczynski, P.D., Yonushonis, T.M., “Experimental Results on the Effect of Piston Surface Roughness and Porosity on Diesel Engine Combustion,” SAE 960036, 1996.

67. Tree, D.R., Oren, D.C., Yonushonis, T.M., Wiczynski, P.D., “Experimental Measurements on the Effect of Insulated Pistons on Engine Performance and Heat Transfer,” SAE 960317, 1996.

68. Overbye, V.D., Bennethum, J.E., Uyehara, O.A., Myers, P.S., “Unsteady Heat Transfer in Engines,” SAE Transactions, Volume 69, 1961.

69. Anderson, C.L., “An In-Situ Technique for Determining the Thermal Properties of Combustion Chamber Deposits,” PhD Dissertation, University of Wisconsin, Madison, 1980.

70. Nishiwaki, K., Hafnan, M., “The Determination of Thermal Properties of Engine Combustion Chamber Deposits,” SAE 2000-01-1215, 2000.

71. Anderson, C.L., Prakash, C., "The Effect of Variable Conductivity on Unsteady Heat Transfer in Deposits," SAE 850048, 1985.

72. Hopwood, A.B., Chynoweth, S., Kalghatgi, G.T., "A Technique to Measure Thermal Diffusivity and Thickness of Combustion Chamber Deposits In-Situ," SAE 982590, 1998.

73. Hayes, T.K., "Thermal Properties of Combustion Chamber Deposits and Their Effect on Engine Heat Transfer and Octane Requirement Increase," PhD Dissertation, University of Illinois, Urbana-Champaign, 1991.

74. Hultqvist, A., Christensen, M., Johansson, B., "The Application of Ceramic and Catalytic Coatings to Reduce the Unburned Hydrocarbon Emissions from a Homogenous Charge Compression Ignition Engine," SAE 2000-01-1833, 2000.

75. Chang, K., Babajimopoulos, A., Lavoie, G.A., Filipi, Z.S., Assanis, D., "Analysis of Load and Speed Transitions in an HCCI Engine Using 1-D Cycle Simulation and Thermal Networks," SAE 2006-01-1087, 2006.

76. Lee, C.S., "Characterization of a Single Cylinder Direct Injection Spark Ignition Engine and Comparison with Single Cylinder Port Fuel Injection SI Engine," M.S. Thesis, University of Michigan, Ann Arbor, 2001.

77. Lavy, J., Dabadie, J, Angelberger, C., Duret, P., Willand, J., Juretzka, A., Schäflein, J., Ma, T., Lendresse, Y., Satre, A., Schulz, C., Krämer, H., Zhao, H., Damiano, L., "Innovative Ultra-low NOx Controlled Auto-Ignition Combustion Process for Gasoline Engines: the 4-SPACE Project," SAE 2000-01-1837, 2000.

78. Oakley, A., Zhao, H., Ladommatos, N., Ma, T., "Dilution Effects on the Controlled Auto-Ignition (CAI) Combustion of Hydrocarbon and Alcohol Fuels," SAE 2001-01-3606, 2001.

79. Güralp, O.A., "Development and Application of a Telemetry System for Piston Surface Temperature Measurements in a Homogeneous Charge Compression Ignition Engine," MS Thesis, University of Michigan, Ann Arbor, 2004.

80. Bird, L.E., Gartside, R.M., “Measurement of Bore Distortion in a Firing Engine,” SAE 2002-01-0485, 2002.

81. Syrimis, M., “Characterization of Knocking Combustion and Heat Transfer in a Spark-Ignition Engine,” PhD Dissertation, University of Illinois, Urbana-Champaign, 1996.

82. Assanis, D., Badillo, E., “Evaluation of Alternative Thermocouple Designs for Transient Heat Transfer Measurements in Metal and Ceramic Engine,” SAE 890571, 1989.

83. Ishii, A., Nagano, H., Adachi, K., Kimura, S., Koike, M., Iida, N., Ishii, H., Enomoto, Y., “Measurement of Instantaneous Heat Flux Flowing into Metallic and Ceramic Combustion Chamber Walls,” SAE 2000-01-1815, 2000.

84. Klell, M., “Measurement of Instantaneous Surface Temperatures and Heat Flux in Internal Combustion Engines and Comparison with Process Calculations,” Institute for Internal Combustion Engines and Thermodynamics, 2000.

85. Takamatsu, H., Kanazawa, T., “Piston temperature measurement method for high-speed gasoline engines,” JSAE Review 20-259-279, 1999.

86. Woschni, G., “A Universally Applicable Equation for the Instantaneous Heat Transfer Coefficient in the Internal Combustion Engine,” SAE 670931, 1967.

87. Enomoto, Y., Furuhama, S., Minakami, K., “Heat Loss to Combustion Chamber Wall of 4-Stroke Gasoline Engine,” JSME Volume 28, Number 238, April 1985.

88. Assanis, D., Friedmann, F., “A Telemetry System for Piston Temperature Measurements in a Diesel Engine,” SAE 910299, 1991.

89. Fischer Technology, Inc, www.helmut-fischer.com.

90. Gatowski, J.A., Balles, E.N., Chun, K.M., Nelson, F.E., Ekchian, J.A., Heywood, J.B., “Heat Release Analysis of Engine Pressure Data,” SAE 841359, 1984.

91. Shayler, P.J., Wiseman, M.W., Ma, T., "Improving the Determination of Mass Fraction Burnt," SAE 900351, 1990.

92. Grimm, B.M., Johnson, R.T., "Review of Simple Heat Release Computations," SAE 900445, 1990.

93. Brunt, M., Rai, H., Emtage, A.L., "The Calculation of Heat Release Energy From Engine Cylinder Pressure Data," SAE 981052, 1998.

94. Chang, J., Güralp, O., Filipi, Z., Assanis, D., Kuo, T.W., Najt, P., Rask, R., "New Heat Transfer Correlation for an HCCI Engine Derived from Measurements of Instantaneous Surface Heat Flux," SAE 2004-01-2996, 2004.

95. Holman, J.P., Experimental Methods for Engineers, Sixth Edition, McGraw-Hill, 1994.

96. Cho, K., "Characterization of Combustion and Heat Transfer in a Direct Injection Spark Ignition Engine Through Measurements of Instantaneous Combustion Chamber Surface Temperature," PhD Dissertation, University of Michigan, Ann Arbor, 2003.

97. Alkidas, A.C., "Heat Transfer Characteristics of a Spark-Ignition Engine," ASME Volume 102, pp.189-193, 1980.

98. The Temperature Handbook, Vol.29, Omega Engineering, Inc, 1995.

99. Medtherm Bulletin, Medtherm Corporation, Huntsville, Al, Bulletin 500.

100. Richter, M., Engström, J., Franke, A., Aldén, M., Hultqvist, A., Johansson, B., "The Influence of Charge Inhomogeneity on the HCCI Combustion Process," SAE 2000-01-2868, 2000.

101. Mackney, D.W., Calder, R.M., Macduff, M.G.J., Wolfle, M., Walter, D., Katers, D., Vietzen, R., "Reducing Deposits in a Disi Engine," SAE 2002-01-2660, 2002.

102. Owrang, F., Mattsson, H., Nordlund, A., Olsson, J., Pedersen, J., "Characterization of Combustion Chamber Deposits from a Gasoline Direct Injection SI Engine," SAE 2003-01-0546, 2003.

103. Enomoto, Y., Furuhama, S., "Study on Thin Film Thermocouple for Measuring Instantaneous Temperature on Surface of Combustion Chamber Wall in Internal Combustion Engine," JSME Volume 28, Number 235, 1985.

104. Alkidas, A.C., Myers, J.P., "Transient Heat-Flux Measurements in the Combustion Chamber of a Spark-Ignition Engine," ASME Volume 104, pp.62-66, 1982.

105. Hayes, T.K., White, R.A., Peters, J.E., "Combustion Chamber Temperature and Instantaneous Local Heat Flux Measurements in a Spark Ignition Engine," SAE 930217, 1993.

106. Annand, J.D., "Heat Transfer in the Cylinders of Reciprocating Internal Combustion Engines," Proc Instn Mech Engrs Volume 177, Number 36, 1963.

107. Hohenberg, G.F., "Advanced Approaches for Heat Transfer Calculations," SAE 790625, 1979.

108. Douaud, A.M., Eyzat, P., "Four-Octane-Number Method for Predicting the Anti-Knock Behavior of Fuels and Engines," SAE 780080, 1978.

109. Incropera, F.P., DeWitt, D.P., Introduction to Heat Transfer, Third Edition, John Wiley & Sons, 1996.

110. Babjimopoulos, A., "Development of Sequential and Fully Integrated CFD/Multi-Zone Models with Detailed Chemical Kinetics for the Simulation of HCCI Engines," PhD Dissertation, University of Michigan, Ann Arbor, 2005.

111. Özışık, M.N., Finite Difference Methods in Heat Transfer, CRC Press, Boca Raton, Fl, 1994.

112. Tannehill, J.C., Anderson, D.A., Pletcher, R.H., Computational Fluid Mechanics and Heat Transfer, Second Edition, Taylor & Francis, 1997.

113. Kaviany, M., Principles of Heat Transfer, John Wiley & Sons, Inc, New York, 2002.

114. Sjoberg, M., Dec, J.E., "An Investigation of the Relationship Between Measured Intake Temperature, BDC Temperature, and Combustion Phasing for Premixed and DI HCCI Engines," SAE 2004-01-1900, 2004.

115. Yang, J., Culp, T., Kenney, T., "Development of a Gasoline Engine System Using HCCI Technology – The Concept and the Test Results," SAE 2002-01-2832, 2002.

116. Morel, T., Wahiduzzaman, S., Fort, E.F., Tree, D.R., DeWitt, D.P., Kreider, K.G., "Heat Transfer in a Cooled and an Insulated Diesel Engine," SAE 890572, 1989.

117. Li, H., Neill, S., Chippior, W., Taylor, J.D., "An Experimental Investigation of HCCI Combustion Stability Using N-Heptane," ASME ICEF2007-1757, 2007.

118. Cheng, S., "A Micrographic Study of Deposit Formation Processes in a Combustion Chamber," SAE 962008, 1996.

119. Choi, G.H., Choi, K.H., Lee, J.T., Song, Y.S., Ryu, Y., Cho, J.W., "Analysis of Combustion Chamber Temperature and Heat Flux in a DOHC Engine," SAE 970895, 1997.

120. Fiveland, S.B., Assanis, D.N., "A Four-Stroke Homogenous Charge Compression Ignition Engine Simulation for Combustion and Performance Studies," SAE 2000-01-0332, 2000.

121. Flowers, D., Aceves, S., Smith, R., Torres, J., Girard, J., Dibble, R., "HCCI in a CFR Engine: Experiments and Detailed Kinetic Modeling," SAE 2000-01-0328, 2000.

122. Mruk, A., Jordan, W., Taler, J., Lopata, S., Weglowski, B., "Heat Transfer Through Ceramic Barrier Coatings Used in Internal Combustion Engines," SAE 941779, 1994.

123. Myers, J.P., Alkidas, A.C., “Effects of Combustion Chamber Surface Temperature on the Exhaust Emissions of a Single-Cylinder Spark-Ignition Engine,” SAE 780642, 1978.

124. Sihling, K., Woschni, G., “Experimental Investigation of the Instantaneous Heat Transfer in the Cylinder of a High Speed Diesel Engine,” SAE 790833, 1979.

125. Sjoberg, M., Dec, J.E., “Combined Effects of Fuel-Type and Engine Speed on Intake Temperature Requirements and Completeness of Bulk-Gas Reactions for HCCI Combustion,” SAE 2003-01-3173, 2003.